NÚMERO: 425/2010
UNIVERSIDADE ESTADUAL DE CAMPINAS
INSTITUTO DE GEOCIÊNCIAS
PÓS-GRADUAÇÃO EM GEOCIÊNCIAS
ÁREA DE GEOLOGIA E RECURSOS NATURAIS

WAGNER DA SILVA AMARAL

ANÁLISE GEOQUÍMICA, GEOCRONOLÓGICA E TERMOBAROMÉTRICA DAS ROCHAS DE ALTO GRAU METAMÓRFICO, ADJACENTES AO ARCO MAGMÁTICO DE SANTA QUITÉRIA, NW DA PROVÍNCIA BORBOREMA

Tese de Doutorado apresentada ao Instituto de Geociências como parte dos requisitos para a obtenção do título de Doutor em Geociências, Área de Geologia e Recursos Naturais.

Orientador: Prof. Dr. Ticiano José Saraiva dos Santos

CAMPINAS - SÃO PAULO

Dezembro-2010

FICHA CATALOGRÁFICA ELABORADA PELO
Sistema de Bibliotecas da UNICAMP /
Diretoria de Tratamento da Informação
Bibliotecário: Helena Joana Flipsen – CRB-8ª / 5283

Amaral, Wagner da Silva.
Am13a Análise geoquímica, geocronológica e termobarométrica das rochas de alto grau metamórfico, adjacentes ao arco magmático de Santa Quitéria, NW da Província Borborema / Wagner da Silva Amaral. -- Campinas, SP : [s.n.], 2011.

Orientador: Ticiano José Saraiva dos Santos.
Tese (doutorado) - Universidade Estadual de Campinas, Instituto de Geociências.

1.Geoquímica – Brasil, Nordeste. 2. Geocronologia. 3. Granulitos - Província Borborema (CE). I. Santos, Ticiano José Saraiva dos. II. Universidade Estadual de Campinas. Instituto de Geociências. III. Título.

Título e subtítulo em inglês: Geochemical, geochronological and thermobarometrical analyse of high-grade metamorphic rocks proximal to the Santa Quitéria magmatic arc, NW Borborema Province.

Palavras-chave em inglês (Keywords): Geochemistry – Brazil, Northeast; Geochronology; Granulite - Borborema Province (CE).

Área de Concentração: Geologia e Recursos Naturais.

Titulação: Doutor em Ciências.

Banca examinadora: Reinhardt Adolfo Fuck, Elson Paiva de Oliveira
Lena Virginia Soares Monteiro, Maria da Glória Motta Garcia

Data da Defesa: 22-12-2010

Programa de Pós-Graduação em Geociências.

UNICAMP

UNIVERSIDADE ESTADUAL DE CAMPINAS
INSTITUTO DE GEOCIÊNCIAS
PÓS-GRADUAÇÃO EM GEOCIÊNCIAS NA
ÀREA DE GEOLOGIA E RECURSOS NATURAIS

AUTOR: Wagner da Silva Amaral

"Análise geoquímica, geocronológica e termobarométrica das rochas de alto grau metamórfico adjacentes ao arco magmático de Santa Quitéria, NW da Província Borborema".

ORIENTADOR: Prof. Dr. Ticiano José Saraiva dos Santos

Aprovada em: 22/12/2010

EXAMINADORES:

Prof. Dr. Ticiano José Saraiva dos Santos _____ - Presidente

Prof. Dr. Reinhardt Adolfo Fuck _____

Prof. Dr. Élson Paiva de Oliveira _____

Profa. Dra. Lena Virginia Soares Monteiro _____

Profa. Dra. Maria da Glória Mota Garcia _____

Campinas, 22 de dezembro de 2010.

Aos meus pais Maria Inês e Gilberto,
à minha companheira Carolina,
ao meu irmão Luis Henrique, Simone
e as minhas queridas sobrinhas Laís e Lara.
É para vocês que dedico este trabalho...
...pela ausência em muitos momentos.

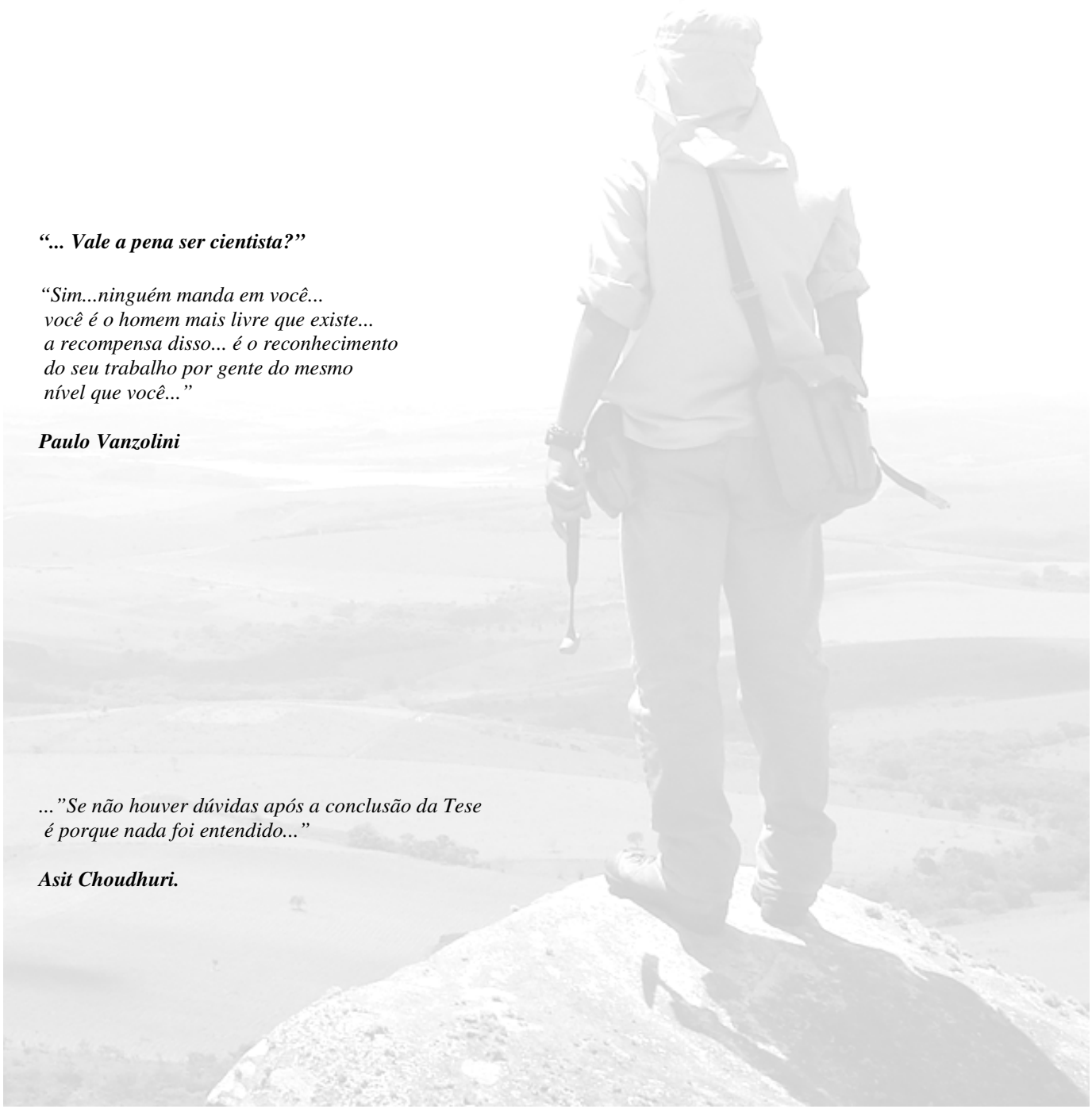

"... Vale a pena ser cientista?"

"Sim...ninguém manda em você...
você é o homem mais livre que existe...
a recompensa disso... é o reconhecimento
do seu trabalho por gente do mesmo
nível que você..."

Paulo Vanzolini

..."Se não houver dúvidas após a conclusão da Tese
é porque nada foi entendido..."

Asit Choudhuri.

AGRADECIMENTOS

Deixo aqui registrado os meus sinceros agradecimentos a todas as pessoas que de alguma maneira me ajudaram nessa longa jornada. Aqui a gente percebe realmente quanto o tempo passou, por isso não me lembrarei de todos e desde já peço desculpas àqueles que não forem citados nestas breves palavras.

Primeiramente agradeço a Deus por me permitir a cada dia viver bem e com saúde na busca pelo conhecimento e pelo crescimento humano. Aos meus pais Gilberto Batista do Amaral e Maria Inês da Silva Amaral por todo amor e pelo total apoio durante toda minha vida. À minha doce companheira de vida, Carolina Moreto, sempre presente e sempre me incentivando a fazer o certo e o melhor.

Ao Prof. Dr. Ticiano José Saraiva dos Santos, por ter me orientado novamente. Acho que aprendemos muito um com o outro, principalmente nos trabalhos de campo, obrigado por acreditar e levar a diante mais este projeto.

Ao amigo e mestre Eberhard Wernick, pelos dias que passamos discutindo o trabalho e aprendendo sobre diversas coisas, inclusive geologia. Devo muito a você e a sua esposa Anne que juntos me acolheram carinhosamente em sua agradável casa.

Ao Prof. Elton Luiz Dantas e a todos do Laboratório de Geocronologia da UnB: Prof. Massimo, Prof. Bernhard, Nathália, Bárbara, Denílson, Giana, Jaqueline, Jô, Emília, Sérgio e ao grande parceiro Jonas, foi muito bom conviver com vocês.

Aos professores, técnicos e colegas da USP: Profa. Maria da Glória, Profa. Gianna Garda, Prof. Caetano Juliani, Marcos (Microsonda) e a Thais Hyppólito pela ajuda no tratamento dos dados termobarométricos.

Aos brothers da "geologia roots" meus amigos Carlos Eduardo-Caê (Isopor), Felipe Grandjean (Creisson) e Ignácio Torresi (Fino) pelas longas e loucas discussões geológicas, espero que elas nunca acabem...

Aos colegas da pós-graduação e àqueles que ainda restaram na graduação (Carol, Aloísio, Bairral, Bienvenido, Emílio, Lenita, Patrícia, Veridiana, Juliano, Alexis, Cleyton, Lucíola, Marquinhos, Mariana, Liminha, Sam, Juliana, Zé Henrique, Matheus, Téo, Rodrigo e Amarildo) não só pelo café e pelas cervejas, mas também pelo bom convívio e pela amizade.

Aos boêmios e parceiros do Subducsamba (Roy, Manicômio, Puff, et al.,)... O samba agonizou, mas não morreu...

Aos professores Lena Virgínia Soares Monteiro, Jacinta Enzweiler, Asit Choudhuri, Carlos Roberto de Souza Filho, Elson Paiva de Oliveira, Bernardino Ribeiro de Figueiredo, Alvaro Crósta Penteado e Wanilson Luiz Silva, que sempre deram aquela força.

Aos funcionários do Instituto de Geociências, em especial ao Cristiano (Laminação), Dailto (Microscopia), Rosane (MEV), Lúcia (Química), Ricardo (Informática), Seu Aníbal e Guerreiro (Manutenção). As queridas secretárias da pós-graduação, Valdirene e Gorete pela eficiência, paciência, carinho e dedicação com todos os alunos!

Ficam também registrados meus sinceros agradecimentos aos Professores da UFC: Zeca, Christiano e Afonso, por facilitarem o apoio logístico referente ao transporte para as atividades de campo e ao envio das amostras; Ao grande mestre Prof. Michel Arthaud (in memoriam), pela amizade, paciência e total apoio aqueles que se interessaram pela fantástica geologia do Ceará, e ao incansável e destemido Prof. Renaud Caby pelos dias de campo e seus comentários nos artigos.

Aos membros da banca examinadora desta Tese, por aceitarem o convite de participação, contribuindo assim com críticas e sugestões para aprimorar o trabalho.

Por fim agradeço ao Conselho Nacional de Desenvolvimento Científico e Tecnológico (CNPq), pela bolsa de estudos e taxa de bancada; ao Projeto do Instituto do Milênio CNPq/MCT (Proc. 42.0222/2005-7) pelo auxílio financeiro para parte dos trabalhos de campo e a Fundação de Amparo à Pesquisa do estado de São Paulo (FAPESP Proc. 07/58535-6) pelo auxílio financeiro para os trabalhos de laboratório e campo.

Súmula Curricular

Wagner da Silva Amaral

Geólogo (2005), Mestre (2007) e Doutor (2010) pela Universidade Estadual de Campinas - UNICAMP. Possuo experiência na área de Geociências, com ênfase em geologia de campo, geologia estrutural e integração de dados geológicos e aerogeofísicos. Trabalhei em 2006 no sul do Cráton Amazônico como geólogo de exploração mineral na prospecção de ouro.

Realizei o Mestrado (2005-2007) com processamento de dados aerogeofísicos e mapeamento geológico no noroeste da Província Borborema, o que me rendeu diversas publicações em congressos e simpósios nacionais e internacionais e a publicação de um artigo na ***Brazilian Journal of Geophysics (2008).***

Também realizei o Doutorado (2007-2010) na Província Borborema, no Domínio Ceará Central, onde tive a oportunidade de trabalhar com geocronologia, geoquímica e geotermobarometria, com o objetivo de estudar rochas ígneas e metamórficas de alto grau. Neste período, publiquei mais de uma dezena de resumos nos principais congressos e simpósios no Brasil e no exterior. Publiquei ainda dois artigos em periódicos internacionais, um no ***Gondwana Research (2009)*** e outro no ***Geological Journal (2010)***. Outros três artigos que tratam o tema desta Tese também serão submetidos em breve.

SUMÁRIO

1. ASPECTOS INTRODUTÓRIOS 01

1.1. Apresentação do Trabalho e Motivação 01
1.2. Justificativa 02
1.3. Objetivos 05

2. ARCABOUÇO TECTÔNICO DA PROVÍNCIA BORBOREMA 07

2.1. Domínio Ceará Central-DCC 09
2.2. Núcleo Arqueano 10
2.3. Embasamento gnáissico Paleoproterozóico 10
2.4. Supracrustais Neoproterozóicas 11
2.5. Complexo Tamboril-Santa Quitéria 12

3. MATERIAIS, MÉTODOS E ORGANIZAÇÃO DA TESE 15

5.1. Análises de química mineral e geotermobarometria 15
5.2. Análises geoquímicas 16
5.3. Análises geocronológicas 16

4. APRESENTAÇÃO DOS RESULTADOS 17

5. SÍNTESE DAS DISCUSSÕES DOS ARTIGOS E CONCLUSÕES 19

6. EVOLUÇÃO GEODINÂMICA DO DOMÍNIO CEARÁ CENTRAL 23

7. REFERÊNCIAS BIBLIOGRÁFICAS 29

ANEXO 01 37

Amaral, W.S., Nogueira Neto, J.A., Santos, T.J.S., Wernick, E., Dantas, E.L., Matteini, M.,. (*Submitted*). **High-pressure granulites from Cariré, NW of the Borborema Province-Brazil: tectonic setting, geothermobarometry and U-Pb, Lu-Hf, Sm-Nd geochronology.** *Gondwana Research* (Submetido) 39

ABSTRACT 39

1. INTRODUCTION 39

2. GEOLOGICAL SETTINGS 41

2.1. Médio Coreaú Domain 41

2.2. Granja Granulite Complex 44

2.3. Ceará Central Domain 44

2.4. The Forquilha Eclogite Zone 45

2.5. The Cariré Granulite Region 45

3. PETROGRAPHY 47

4. MINERAL CHEMISTY 50

5. P-T CONDITIONS 56

U-Pb, Sm-Nd and Lu-Hf GEOCHRONOLOGY 58

6. ANALYTICAL PROCEDURE 58

RESULTS 60

7. U-Pb ZIRCON ANALYSES 60

8. Lu-Hf ANALYSES OF ZIRCON 66

9. WHOLE ROCK Sm-Nd DATA 66

10. DISCUSSION AND CONCLUSION 68

AKNOWLEDGEMENTS 71

REFERENCES 71

ANEXO 02 81

Amaral, W.S., Santos, T.J.S., Wernick, E. 2010. **Occurrence and geochemistry of metamafic rocks from the Forquilha Eclogite Zone, central Ceará (NE Brazil): Geodynamic implications.** *(Special Issue) Geological Journal* (DOI: 10.1002/gj.1224) 83

ABSTRACT 83

1. INTRODUCTION 84

2. GEOLOGICAL SETTING 86

3. FIELD OCCURRENCE AND SAMPLE DESCRIPTION 88

4. GEOCHEMISTRY 92

5. DISCUSSION 103

6. CONCLUSIONS 107

AKNOWLEDGEMENTS 108

REFERENCES 108

ANEXO 03 117

Amaral, W.S., Santos, T.J.S., Dantas, E.L. *(In prep.)* **Sm-Nd and LA-MC-ICP-MS U-Pb, Lu-Hf zircon geochronology of high pressure rocks from the Forquilha Eclogite Zone, Borborema Province, NE-Brazil: an evidence for the break-up of Columbia supercontinent.** (Em preparação) 119

ABSTRACT 119

1. INTRODUCTION 119

2. GEOLOGICAL SETTING 120

3. U-Pb, Lu-Hf and Sm-Nd GEOCHRONOLOGY 123

4. ANALYTICAL PROCEDURE 123

U-Pb ZIRCON ANALYSES RESULTS 126

5. METAMAFIC ROCKS 126

6. PARA-DERIVED HOST ROCKS 140

6.1. Migmatitic Kinzigite 140

6.2. Sillimanite-garnet-biotite gneiss 145

6.3. Calc-silicate rocks 148

7. WHOLE ROCK Sm-Nd RESULTS 153

8. DISCUSSION AND CONCLUSIONS 155

9. REFERENCES 161

ANEXO 04 167

Química mineral e Geotermobarometria das rochas metamáficas e metassedimentares da Faixa Eclogítica de Forquilha 167

1. APRESENTAÇÃO 169

2. MATERIAIS E MÉTODOS 169

3. GRANADA ROCHAS METAMÁFICAS 172

3.1. Amostra WT8-302: Retroeclogito (setor centro-sul) 173

3.2. Amostra TJF5-335: Granada-clinopiroxênio anfibolito (setor sul) 173

4. GRANADA ROCHAS METASSEDIMENTARES 178

5. PIROXÊNIO 182

6. ANFIBÓLIO 184

7. PLAGIOCLÁSIO 188

8. FELDSPATO 189

9. BIOTITA 190

10. GEOTERMOBAROMETRIA 191

10.1. Geotermobarometria metamáficas (PTMAFIC 2.0) 194

10.2. Estimativa do "pico metamórfico" 195

11. DISCUSSÕES E CONCLUSÕES SOBRE A TERMOBAROMETRIA E IMPLICAÇÕES TECTÔNICAS 197

12. REFERÊNCIAS BIBLIOGRÁFICAS 201

APÊNDICES 205

TABELAS DAS ANÁLISES DE QUÍMICA MINERAL 205

TABELA DAS ANÁLISES GEOCRONOLÓGICAS (U-Pb) 235

LISTA DE FIGURAS

Figura 1: Mapa de localização e principais vias de acesso das áreas investigadas. Topografia gerada a partir do modelo digital do terreno (SRTM)..... 03

Figura 2: Principais unidades crustais do paleocontinente Gondwana ocidental..... 08

Figura 3: Esboço geológico regional da porção setentrional da Província Borborema e dos arredores do lineamento Patos. LTB = lineamento Transbrasiliano; ZCSP = Zona de Cisalhamento Senador Pompeu; ZCPa = Zona de cisalhamento Patos; CC = Complexo Cruzeta; MSJC = Maciço São José do Campestre; CG = Complexo Granjeiro 09

Figura 4: Mapa geológico regional da porção NW do Domínio Ceará Central. No detalhe, a área de estudo 13

Figura 5: Modelo tectônico da evolução geodinâmica do Domínio Ceará Central..... 27

ANEXO 01: Amaral, W.S., Nogueira Neto, J.A., Santos, T.J.S., Wernick, E., Dantas, E.L., Matteini, M.,. (Submitted). **High-pressure granulites from Cariré, NW of the Borborema Province-Brazil: tectonic setting, geothermobarometry and U-Pb, Lu-Hf, Sm-Nd geochronology**

Figure 1: Geological map of the northern block of the Borborema Province, showing the three main domains and Brasiliano granitic plutons situated north of the Patos Lineament (PaL): Cruzeta Complex (CC); São José do Campestre Massif (SJCM); Granjeiro Complex (GC); Transbrasiliano Lineament (TBL); Senador Pompeu Lineament (SPL); Médio Coreaú Domain (MCD); Ceará Central Domain (CCD); Rio Grande do Norte Domain RGND) 41

Figure 2: Geological map of the Médio Coreaú (MCD) and Central Ceará Domains (CCD). Legend: 1. Alluvial cover; 2. Parnaíba basin; 3. Jaibaras basin; 4. Brasiliano granites and monzogranites; 5. Cariré granulites; 6. Forquilha retrograded eclogites; 7. Ubajara basin; 8. Santa Quitéria magmatic arc; 9. Martinópole Group; 10. Ceará Group; 11. Canindé Complex; 12. Granja Granulites; 13. Basement migmatites and gneisses. Detail: see Figure 3..... 43

Figure 3: Geologic map of the Cariré region adjacent to the Transbrasiliano Lineament 47

Figure 4: Field and petrographic characteristics of the Cariré granulites: A) An approximately 2m-thick felsic granulite belt sub-concordant with the mylonitic orthogneisses foliation. B) Detail of an enderbite sample showing well-delineated bands of biotite and orthopyroxene. C) Photomicrograph showing well-defined mafic (Opx + Bt) and felsic (Qtz + Pl) bands. D) Mafic granulite lens hosted in sheared granodiorite. E) The detail shows the mineral association common in the mafic granulites: garnets up to 3 cm in diameter, rimmed by plagioclase in a matrix of amphibole and clinopyroxene. F) Photomicrograph of xenoblastic and poikiloblastic garnet with ilmenite and hornblende inclusions. G) Garnet crystals with well-defined Pl and Hbl aureoles. H) Detail of quartz inclusions in garnet with radial fractures. 49

Figure 5: Mineral chemistry diagrams for felsic granulites (blue square) and mafic granulites (red triangles). a) garnet composition in the Almandine-Grossular-Pyrope diagram. b) Chemical classification of pyroxenes (Morimoto *et al.* 1988). c) Chemical classification of biotite in felsic granulites. d) Chemical classification of amphiboles showing variation from edenitic hornblende to Fe-pargasitic hornblende, whereas e) compositions vary from Fe-hornblende to Fe-tschermakite in hornblende from metabasic rocks (Leake *et al.* 1997). f) Chemical classification of plagioclase 55

Figure 6: Reactions according to TWEEQU for felsic granulites (a and b) and mafic granulites (c and d). a) P = 8.8 ± 0.55 kbar and T = 826 ºC (sample ZC11-b); b) P ~ 9.36 kbar and T ~ 867 ºC (sample ZC30-2); c) P ~10.23 kbar and T ~ 750 ºC (sample ZC-56b-1; d) P ~ 13.60 kbar and T ~ 911 ºC (sample ZC-56b-2)..... 57

Figure 7: Cathodoluminescence image (CL) of zircon analyzed by LA-MC-ICPMS (mafic granulite sample WT7-3A). A) Larger and more elongated zircon from the first population (Z15: 619± 6.4 Ma). B) Oval zircon from the first population, showing inherited core rimmed by a highly luminescent overgrowth (Z3: 621 ± 6.4 Ma). C) Oval zircon from the first population rimmed by a thin, oscillatory chaotic layer. Its core yielded the oldest age for the mafic granulites (Z14: 628.6±6.6 Ma). D) Slightly elongated zircon, preserving some external euhedral faces (Z4: 617 ± 6.4 Ma). E) A more homogeneous zircon from the second population, lacking well-defined faces and a homogeneous core (Z8: 602± 6.2 Ma). F) "Soccer ball" grain preserving a single homogeneous core rimmed by a discrete overgrowth (Z13: 612.3 ± 6.3 Ma). G) Sub-euhedral, ovoid zircon from the second population with chaotic core (Z1: 613± 6.3 Ma). Zircon grains from the second population show all the characteristics of the metamorphic zircon and recorded the same or similar ages to those obtained by the concordia diagram. 61

Figure 8: Back-scattered electron image of zircon grains from granodiorite sample WT9-06. Elongated grains show intergrowth evidences and fracturing at the rims. 30 µm-sized spots analyzed by the U-Pb method using LA-ICP-MS..... 61

Figure 9: Concordia plot for LA-ICP-MS analyses of zircon grains from the Cariré Granulite Region: A) mafic granulite (sample WT7-3A); B) mafic granulite (sample WT7-3B); C) mylonitic granodiorite (sample WT7-02); D) granodiorite (WT9-06); E) Lower intercep of the sample (WT9-06); F) ID-TIMS analyses of zircon grains from a felsic granulite (ZC-11Z) (Fetter, 1999) 65

Figure 10: Diagram ε_{Nd} versus time showing evolutionary tendency for mafic and felsic granulites from the Cariré Region Ceará Central Domain. Also shown is the isotopic evolution for the basement gneisses from the Ceará Central Domain (Fetter, 1999) 67

ANEXO 02: Amaral, W.S., Santos, T.J.S., Wernick, E. 2010. **Occurrence and geochemistry of metamafic rocks from the Forquilha Eclogite Zone, central Ceará (NE Brazil): Geodynamic implications.** (Special Issue) Geological Journal (DOI: 10.1002/gj.1224) (Publicado)

Figure 1: The Borborema Province in the context of the Western Gondwana supercontinent (modified after Caby, 1989 and Arthaud et al. ,2008)..... 87

Figure 2: Simplified geologic map of the Médio Coreaú Domain and the Ceará Central Domain in the NW part of the Borborema Province. The locations of the samples collected for this study are: 1) TJF6-296; 2) RM-220, 3) WT8-53E, 4) W8-10 (A-F), 5) WT7-53D, 6) VC-57 (E-G-g), 7) RM-

120A, 8) RM-107 (C-D), 9) RM-182, 10)VC-60, 11) RM-179, 12) TJF5-181, 13) TJF6-302, 14) TJF6-335 (A-D), 15) VC-4 (A-B), 16) WT7-25 89

Figure 3: a) Most common lenticular form of occurrence of metamafic rocks; b) detail of the lenticular form of an retrograde eclogite; c) detail of a representative sample of garnet amphibolites, where garnets form coronas and hornblende is the main mineral; d) garnets with inclusions of drop-shaped quartz and plagioclase aureoles in hornblende (Hbl); e) mesoscopic sample of a retrograded eclogite with oriented amphiboles and pyroxenes; f) microphotograph of a sample representative of retrograde eclogites: garnet (Grt), clinopyroxene (Cpx), apatite (Ap), ilmenite (IL), rutile (Rt) and clinopyroxene + plagioclase (Pl) ± quartz (Qtz) symplectites; g) diopside-rich sample representative of clinopyroxene garnet amphibolites; h) microphotograph of a cpx-garnet amphibolite, where symplectites of Cpx+ Pl and narrow amphibole (Amp) rim surrounding the garnets 91

Figure 4: Fenner diagram for a) SiO_2; b) CaO; c) Al_2O_3; d) Fe_2O_3*; e) TiO_2; f) Na_2O; g) Zr; h) Ni 93

Figure 5: Plots for the Forquilha Eclogite Zone samples in the: a) Zr/Nb *vs*. Y/Nb, b) Zr/Nb *vs.* Zr/Y, c) Y_{PM} *vs.* Zr_{PM}, d) Nb_{PM} *vs.* La_{PM}, e) Y_{PM} *vs.* Ti_{PM} and f) La_{PM} *vs.* La/Lu diagrams. 95

Figure 6: a) Nb/Y *vs.* (Zr/TiO_2 * 0.0001) diagram, fields from Winchester and Floyd (1977); b) FeO_T:(Na_2O+K_2O):MgO diagram, fields from Irvine and Barragar (1971); c) Zr/(10000 P_2O_5) *vs.* Nb/Y diagram, fields from Floyd and Winchester (1975). 97

Figure 7: a) Zr *vs*. Y diagram, fields after Le Roex (1987); b) Zr *vs.* Nb diagram, fields after Le Roex (1987); c) Nb/Yb *vs.* Th/Yb diagram, composition of N-MORB, E-MORB, OIB, Upper Continental Crust (UCC), Lower Continental Crust (LCC) are from Sun and McDonough (1989) and Taylor and McLennan (1985); d) La/Ta *vs.* Tb/Ta diagram, modified from Cabanis and Lècolle (1989); primordial mantle from Wood *et al.* (1979) 98

Figure 8: a) Ti/1000 *vs.* V diagram; fields after Shervais (1982); b) Sr/Ce *vs*. Sm/Ce diagram, fields after Kampunzu and Mohr (1991); c) La/Yb *vs.* Th/Ta diagram; internal geotectonic units after Condie (2001); d)Y-La-Nb diagram; fields after Cabanis and Lècolle (1989) 99

Figure 9: a) REE_{PM} pattern for a) Group 1; b) Group 2; c) Group 3; d) La_{PM} *vs.* $(Eu/Eu^*)_{PM}$ plot, Primitive Mantle and N-MORB Standard from Sun and McDonough (1989); Mafic Lower Crust from Rudnick and Fountain (1995) 101

Figure 10: $(SPIDER)_{PM}$ pattern for Group 1 (a); Group 2 (b); Group 3 (c); d) Nb/La plot, Primitive Mantle and N-MORB (dashed line) from Sun and McDonough (1989); Mafic Lower Crust from Rudnick and Fountain (1995) 103

ANEXO 03: Amaral, W.S., Santos, T.J.S., Dantas, E.L. *(In prep.)* **Sm-Nd and LA-MC-ICP-MS U-Pb, Lu-Hf zircon geochronology of high pressure rocks from the Forquilha Eclogite Zone, Borborema Province, NE-Brazil: an evidence for the break-up of Columbia supercontinent.** (Em preparação)

Figure 1: North block of the Borborema Province, showing the main tectonic features and Brasiliano granitic plutons situated north of the Patos shear zone (PaSZ): Cruzeta Complex (CC); SJCM (São José do Campestre Massif; Granjeiro Complex (GC); Transbrasiliano Lineament

(TBL); Senador Pompeu shear zone (SPSZ); Médio Coreaú Domain (MCD); Ceará Central Domain (CCD); Rio Grande do Norte Domain (RGND) (After Santos *et al.,* 2009). In detail, the study area in the CCD context.) 121

Figure 2: Geological map of the northwestern part of the Forquilha Eclogite Zone, after Ancelmi (2008) samples WT7-25, WT8-12F and WT7-21B are not shown here..... 125

Figure 3: Back-scattered electron image of representative zircon grains from the pyroxene-bearing garnet amphibolite WT7-25. The elongated grains do not show evidence of intergrowth and contain a few oxide inclusions. Note spot analyzed by the U/Pb (raster) and Lu/Hf (spot size = 30 µm) methods with the respective $^{235}U/^{207}Pb$ ages, T_{DM} and ε_{Hf}..... 127

Figure 4: U/Pb concordia diagram (LA-ICPMS) for sample WT7-25 zircon grains, depicting a concordant population around 1.5Ga and a population showing Pb loss..... 128

Figure 5: Evolution diagram showing ε_{Hf} values calculated for a crystallization age of 1566 Ma. Strongly positive ε_{Hf} values stand out 128

Figure 6: Characterization at different scales of sample WT8-12F: a) Outcrop where the sample was collected, showing low-angle dip (~35°) towards E-SE; b) arrangement of slightly oriented minerals, such as pyroxene (green), garnet (pink) and amphiboles (black); c) detail of a polished thin section (10x) showing the main mineral phases: clinopyroxene (Cpx), garnet (Grt), hornblende (Hbl), plagioclase (Pl) and quartz (Qtz). Note the destabilization of Cpx in Hbl + Pl ± Qtz; d) Garnet containing a large number of inclusions, such as zircon (Zr), rutile (Rt) and apatite (Ap) 129

Figure 7: Back-scattered electron image of representative zircon grains from the clinopyroxene-garnet amphibolite WT8-12F. The grains are in part elongated (4x1) and sub-rounded (3x2) and show no intergrowths; Circles spots analyzed by the U/Pb method (30 and 25 µm-sized spots) and corresponding $^{235}U/^{207}Pb$ ages 130

Figure 8: U/Pb Concordia diagram (LA-ICPMS) for sample WT8-12F zircon grains 131

Figure 9: Sample WT8-53E: a) Outcrop in the shape of a meter-sized "lens" intercalated with para-derived migmatites, where sample WT8-53E was collected; b) hand specimen, abundant garnet, pyroxene and amphibole 131

Figure 10: Zircon grains from the mesocratic clinopyroxene-garnet amphibolite WT8-53E. The grains are elongated, subhedral, some showing luminescent cores and internal fracturing. Circles indicate spots by the U/Pb method (30 and 25 µm-sized spots) and corresponding $^{235}U/^{207}Pb$ ages..... 132

Figure 11: Concordia diagram for U/Pb analyses (LA-ICPMS) of the mesocratic clinopyroxene-garnet amphibolite WT8-53E, showing a concordant age of 1559 ± 70 Ma 133

Figure 12: Detail of leucosomes from where zircon grains were extracted for analysis. These melts are mainly composed of plagioclase, quartz, garnet and amphibole. Accessory minerals are zircon, apatite and rutile..... 133

Figure 13: Back-scattered electron images of the representative zircon crystals from sample WT8-53X. The grains are elongated, sub-euhedral, and contain punctual inclusions and a few fractures. Inset: regions analyzed by the U/Pb method (30 and 25 µm-sized spots) and corresponding $^{235}U/^{207}Pb$ ages. 134

Figure 14: Concordia diagram for the U/Pb analyses (LA-ICPMS) of the leucocratic portion of sample WT8-53X, showing an age of the upper intercept of 1615 ± 40 Ma. The loss of radiogenic Pb is conspicuous. 135

Figure 15: Characterization at different scales of sample TJF6-302: a) block of approximately 50 kg collected for geochronologic studies; b) strong mineral orientation outlined in hand specimen; c) photomicrograph of thin section showing stretched garnet (grt) and pseudomorphs filled by vermiform intergrowths of clinopyroxene (cpx) + plagioclase (pl) ± quartz (qtz); d) back-scattered electron image showing a large quantity of symplectites and accessory minerals such as zircon (zr) inclusions in garnet, rutile (rt), apatite (ap) and ilmenite (il). 135

Figure 16: Back-scattered electron images of representative zircon crystals from retrogressed eclogite (sample TJF6-302). 137

Figure 17: Concordia diagram for U/Pb analyses (LA-ICPMS) of retrogressed eclogite zircons (sample TJF6-302). 137

Figure 18: Sample TJF6-335: a) blocks of approximately 30 kg collected for geochronologic studies; b) the predominance of garnet and clinopyroxene is observed in hand specimen 138

Figure 19: Concordia diagram for U/Pb analyses (LA-ICPMS) of sample TJF6-335 139

Figure 20: Concordia diagram using U-Pb concordant ages (LA-ICPMS) obtained for zircon crystals from sample TJF6-335. 139

Figure 21 : Characterization of samples WT8-53MM and WT8-53ML: a) low-angle (~30°SE) dipping slab-shaped outcrop; b) banding defined by alternating biotite- and garnet-rich melanocratic layers and garnet-, sillimanite-, feldspar- and quartz-rich leucocratic layers; c) centimeter-sized kyanite clustered in biotite and garnet aggregates; d) leucosome sample used for zircon and monazite separation 141

Figure 22: Back-scattered electron images of representative zircon crystals from sample WT8-53MM melanosome. Circles indicate analyzed spot by the U-Pb method (spot size = 30 µm) and corresponding $^{235}U/^{207}Pb$ ages.. 141

Figure 23: Back-scattered electron images of representative zircon crystals from sample WT8-53ML leucosome. Two populations were identified: one containing elongated grains (Z10 and Z12) and another with ovoid and rounded grains (Z7, Z9, Z11 and Z14). Circles regions analyzed by the U/Pb method (spot size = 25 µm), mostly grain rims, with corresponding $^{235}U/^{207}Pb$ ages 143

Figure 24: Back-scattered electron images of representative monazite crystals from sample WT8-53ML leucosome. Circles regions analyzed by the U/Pb method (spot size = 30 μm) with corresponding $^{235}U/^{207}Pb$ ages 143

Figure 25: Frequency histogram for the U/Pb analyses of melanosome zircon (sample WT8-53MM) 144

Figure 26: Concordia diagram for U/Pb analyses (LA-ICPMS) of leucosome zircon from host migmatites (sample WT8-53ML). 144

Figure 27: Diagram of weighted mean U/Pb values for leucosome monazite from host migmatites (sample WT8-53ML). 145

Figure 28: Outcrop along Highway BR-222, where samples WT7-21A (leucogranite) and WT7-21B (sillimanite-garnet-biotite gneiss) were collected. a) Outcrop dipping SE at low-angles (~35°), showing a leucogranite injection (garnet, quartz, feldspar), sampled for monazite dating; b) metasediment sampled for zircon dating. 146

Figure 29: Concordia diagram for U/Pb analyses of monazite from leucogranite sample WT7-21A 147

Figure 30: Back-scattered electron images of representative zircon crystals from the sillimanite-garnet-biotite gneiss (sample WT7-21B). Circles regions analyzed by the U-Pb method (raster) with the corresponding $^{235}U/^{207}Pb$ ages 147

Figure 31: Frequency histogram for the U/Pb analyses of zircon from the sillimanite-garnet-biotite-gneiss sample WT7-21B 148

Figure 32: Outcrop of calc-silicate rock, easily recognized by its typical greenish color and karst-like alteration surface. Inset: block sampled for geochronologic studies.. 149

Figura 33: Back-scattered electron images of representative zircon crystals from sample TJF4-7. Circles and rectangles analyzed spot by the U/Pb (raster) and Lu/Hf (spot size = 30 μm) methods with corresponding $^{235}U/^{207}Pb$, T_{DMHf} and ε_{Hf} values. 150

Figure 34: Frequency histogram for U/Pb analyses of sample TJF4-7 zircon. 151

Figure 35: Concordia diagram age for U/Pb analyses (LA-ICPMS) of sample TJF4-7. 152

Figure 36: Evolution diagram showing ε_{Hf} values calculated to 2150 and 600 Ma. 152

Figure 37: T_{DM} *versus* ε_{Nd} diagram representing the isotopic evolution fields for the Forquilha Eclogite Zone metamafic rocks. 154

ANEXO 04: Química mineral e Geotermobarometria das rochas metamáficas e metassedimentares da Faixa Eclogítica de Forquilha.

Figura 1: Mapa geológico da Faixa Eclogítica de Forquilha. Com exceção da amostra WT7-25 situada a norte do granito Serra da Barriga, as amostras analisadas nesse estudo estão assinaladas: (estrela) metamáficas e (**Circulo**) granulitos encaixantes (adaptado de Ancelmi, 2009)... 171

Figura 2: Imagem de elétrons retro-espalhados obtida em MEV: a) granada com borda idioblástica circundada por plagioclásio e clinopiroxênio Esse último também presente como simplectito na parte central da granada; b) granada parcialmente desestabilizada formando textura em atol, com um núcleo envolto por simplectito de clinopiroxênio e plagioclásio. Destaque para uma pequena inclusão de ouro no centro (Amostra TJF5-335)... 174

Figura 3a: Imagem de elétrons retro-espalhados mostrando a granada e os respectivos pontos analisados em EDS no MEV (Modificado de Reginato, 2009) 175

Figura 3b: Gráfico mostrando a distribuição do número de íons de Fe, Ca e Mg para cada ponto analisado na granada pelo método semi-quantitativo. Há uma tendência ao aumento de piropo em direção as bordas do mineral, ilustrada pelo aumento do número de Mg em detrimento do Fe e do Ca... 176

Figura 4a: Imagem de elétrons retro-espalhados obtida em granada com seu respectivo perfil analisado. Notar a presença de quartzo sob a forma de inclusões retilíneas marcando o pseudomorfo da granada reliquiar da 1° geração (Modificado de Reginato, 2009). 176

Figura 4b: Gráfico mostrando a distribuição do número de íons de Fe, Ca e Mg para cada ponto analisado na granada pelo método semi-quantitativo. As linhas tracejadas marcam as composições nas bordas da granada.(M1: primeiro evento metamórfico de geração da granada; M2 segundo evento) 177

Figura 5: Imagem microscópica de granada (amostra TJF5-335) com os pontos do perfil analisado em microssonda eletrônica. Em grande parte dos cristais de granada observa-se a dupla textura coronítica que envolve os cristais com anfibólios e plagioclásio.. 177

Figura 6: Perfil composicional do porfiroblasto de granada da amostra TJF5-335. Embora a quantidade de pontos seja relativamente pequena, é possível observar a tendência ao aumento de piropo em direção as bordas do mineral.. 178

Figura 7: Imagem de granada (amostra WT8-07) com os pontos em perfil analisados em microssonda eletrônica. Destaque para a inclusão com fraturamento radial típica feição de quartzo β. 179

Figura 8: Perfil composicional de granada da amostra WT8-07. É possível observar claramente que as proporções de almandina e piropo são inversamente proporcionais. Os pontos 11 e 12 posicionados na parte central docristal revelam os maiores teores de piropo, enquanto em direção para as bordas as proporções de piropo diminuem e de almandina tende a aumentar... 180

Figura 9: Classificação da granada analisada: a) granada representativa das rochas metamáficas, com tendência de enriquecimento em piropo nas amostras coletadas no sul da área investigada; b) Relação entre XFe *vs.* XMg mostrando, mais uma vez, a tendência de enriquecimento em Mg nas granadas das rochas metamáficas na parte sul; c) granada representativa das rochas encaixantes. Notar uma leve tendência de enriquecimento em grossulária para as granadas da amostra WT8-07; d) Tendências da correlação XFe *vs.* XMg observada nas rochas encaixantes..... 181

Figura 10: Diagramas de classificação para piroxênio: a) Variação composicional em função dos componentes **Wo** ($Ca_2Si_2O_6$), **En** (Mg_2Si2O_6) e **Fs** ($Fe_2Si_2O_6$), 99% dos clinopiroxênios foram classificados como diopsídio (Morimoto *et al.* 1988); b) Diagrama Jd *vs.* Na_2O mostrando o aumento do componente Jd nas amostras do setor sul; c) Diagrama ternário de classificação dos piroxênios ricos em Na, evidenciando um *trend* linear em direção ao campo da onfacita (Morimoto *et al.* 1988); d) Diagrama MgO *vs.* Na_2O onde é possível a definir duas tendências (I): para as rochas da porção Norte/Central e (II): para as amostras da região sul (TJF5-335, TJF5-335A, TJF5-335B e TJF6-302) 183

Figura 11: Diagramas classificatórios para anfibólio: a) Classificação em termos de Ca (C), Na (N) e Mn + Fe + Mg (FM) no sítio M4 (Robinson *et al.,* 1982) b) Classificação geral dos quatro principais grupos de anfibólio (Leake *et al.* 1997); c) Classificação segundo ($Ca > 1.5$; $(Na + K)_A < 0.5$ e $Ti < 0.5$); d) Diagrama classificatório ($Ca_B > 1.5$; $(Na + K)_A > 0.5$; $Ti < 0.5$ e $Al_C > Fe^{3+}$)..... 187

Figura 12: Variação composicional do feldspato, segundo os componentes moleculares albita (Ab), anortita (An) e ortoclásio (Or): a) rochas metamáficas o plagioclásio ocupa predominantemente os campos do oligoclásio e andesina; b) granulitos aluminosos encaixantes predomínio de ortoclásio e oligoclásio..... 189

Figura 13: Classificação da biotita dos granulitos aluminosos conforme os extremos da solução sólida anita-flogopita-eastonita-siderofilita, notar a tendência para a composição da flogopita 191

Figura 14: Diagramas P-T obtidos para a amostra TJF5-335 com o programa TWQ (1.02), utilizando as seguintes associações: a) piropo + onfacita (jadeíta) + albita + quartzo; b) granada + onfacita + tschermakita + albita + rutilo + titanita + quartzo, com $X_{H2O} = 0,8$ e $X_{CO2} = 0,2$..... 196

UNIVERSIDADE ESTADUAL DE CAMPINAS
INSTITUTO DE GEOCIÊNCIAS
PÓS-GRADUAÇÃO EM GEOCIÊNCIAS
ÁREA DE GEOLOGIA E RECURSOS NATURAIS

Análise geoquímica, geocronológica e termobarométrica das rochas de alto grau metamórfico, adjacentes ao arco magmático de Santa Quitéria, NW da Província Borborema

RESUMO

Tese de Doutorado

Wagner da Silva Amaral

A aglutinação de massas continentais durante a formação do Gondwana ocidental desencadeou o fechamento de oceanos em zonas de subducção e a geração de arcos magmáticos. Em geral, os limites da colisão dos diferentes blocos crustais são representados por um cinturão de rochas de alto grau associadas ou não a lascas ofiolíticas. No noroeste do Domínio Ceará Central (porção norte da Província Borborema), na borda oeste do arco magmático de Santa Quitéria – AMSQ, e ao longo do lineamento Transbrasiliano, ocorrem rochas com paragêneses de alta pressão (retroeclogitos) e alta temperatura (granulitos máficos, félsicos) nas regiões de Forquilha e Cariré, respectivamente. Os retroeclogitos de Forquilha definem uma faixa N-S de aproximadamente 30 km de comprimento por 4 km de largura, de corpos métricos lenticulares denominados Faixa Eclogítica de Forquilha - FEF representados por conjunto descontínuo de corpos com comprimentos médios de 5 a 300 metros de extensão. Essas rochas estão encaixadas em paragnaisses, quartzitos, mármores e rochas cálcio-silicáticas. Em Cariré os granulitos estão alongados na direção NE-SW e hospedados em granodioritos cisalhados. Em ambas as áreas a foliação (Sn) com mergulho de baixo ângulo para E-SE aumenta de intensidade exibindo mergulhos sub-verticalizados na região de Cariré. A lineação (Lx) definida por sillimanita e cianita é *downdip* e torna-se oblíqua para S-SE à medida que se avança para W. Dados de geotermobarometria para os granulitos de Cariré revelaram condições de P-T de 8,3-9,4 kbar e 804-870°C para granulitos félsicos e de 10,2-13,6 kbar e 750-910°C para granulitos máficos. Por outro lado, na região de Forquilha as condições de P-T situam-se em 11,2-22,0 kbar e 495-840°C para as rochas metamáficas e 9,9-11,0 kbar e 734-851 °C para as rochas metassedimentares encaixantes. Esses valores indicam a existência de granulitos de alta pressão em Cariré e rochas eclogíticas/granulíticas na FEF. Análises petrográficas e geoquímicas permitiram a individualização de três grupos de rochas metamáficas na FEF: i) Granada anfibolitos, com padrão Elementos Terras Raras-ETR plano e anomalias negativas de Rb, Th, Nb, Zr e Ta, no diagrama multielementar, indicam similaridades com basaltos de arco de ilha, tipo IAT; ii) Retroeclogitos com padrão (ETR) plano e estreito e similaridades com o padrão N-T-MORB compatíveis com basaltos de ambiente extensional tipo cadeia meso-oceânica ou *back-arc* de arcos intra-oceânicos.; iii) Clinopiroxênio-granada anfibolitos possuem o padrão (ETR) mais inclinado, com razão (La/Yb) entre 2.63 e 7.32, o que sugere leve fracionamento. É o grupo mais enriquecido em termos de álcalis e elementos traços incompatíveis, similar a rochas alcalinas e basaltos continentais. Dados geocronológicos (Sm-Nd em rocha total e U-Pb, Lu-Hf em zircão e monazita) denotam dois episódios magmáticos, um paleoproterozóico, registrado nos granodioritos de Cariré ao redor de 2,1 Ga. E outro mesoproterozóico definido por U-Pb em zircão das rochas metamáficas da FEF, situado entre 1455 e 1618 Ma. Dados Lu-Hf em zircão (T_{DMHf} = 1,57 - 1,80 Ga e $\varepsilon_{Hf\ (1500)}$ = +7,46 e +9,63) e isótopos de Nd (T_{DMNd} = 1,57 - 2,81 Ga e $\varepsilon_{Nd\ (1500)}$ = +4,11 e +4,33), revelam valores de fontes próximos à idade de cristalização com valores de épsilon positivos. Análises U-Pb em bordas de zircão e em cristais com texturas metamórficas com baixas razões Th/U possibilitaram a caracterização de dois estágios metamórficos: i) entre 640 – 650 Ma obtido em rochas paraderivadas encaixantes dos retroeclogitos na FEF e correlato ao metamorfismo colisional de fácies eclogíto; ii) entre 590 e 615 Ma registrado nos granulitos de Cariré e do sul de Forquilha. Datação em zircão detrítico de quatro rochas metassedimentares ao longo da FEF revelaram proveniência principal de fontes paleoproterozóicas (Riaciano/Orosiriano) e idades máximas de deposição ao redor de 1,65-1,80 Ga. Neste cenário, o modelo de *Slab-breakoff* é proposto.

UNIVERSIDADE ESTADUAL DE CAMPINAS
INSTITUTO DE GEOCIÊNCIAS
PÓS-GRADUAÇÃO EM GEOCIÊNCIAS
ÁREA DE GEOLOGIA E RECURSOS NATURAIS

Geochemical, geochronological and thermobarometrical analyse of high-grade metamorphic rocks proximal to the Santa Quitéria magmatic arc, NW Borborema Province

ABSTRACT

PhD Dissertation

Wagner da Silva Amaral

The amalgamation of continental blocks during the development of the Western Gondwana led the closure of oceans in subduction setting and the formation of magmatic arcs. The boundaries of the collision of different crustal blocks are typically represented by a high-grade rock belts associated or not with ophiolitic sequence. In the northwestern part of the Ceará Central Domain (northern portion of the Borborema Province), in the western border of the Santa Quitéria Magmatic Arc, within the Transbrasiliano Lineament, high-pressure (retrograded eclogites) and high-temperature rocks (mafic and felsic granulites) were described near the Forquilha and Cariré regions, respectively. The retrograded eclogites of the Forquilha region define a N-S strike belt (ca. 30 km long and 4 km wide) of lenticular discontinuous metric bodies (5 to 300 meters) called Forquilha Eclogite Zone (FEZ). These rocks are hosted by paragneiss, quartzites and calc-silicate rocks. In the Cariré region the granulites are elongated along the NE-SW strike and hosted by sheared granodiorites. In both areas the foliation (Sn) has low-angle E-SE dip that grades to sub-vertical dip towards the Cariré region. The mineral lineation (Lx) is defined by sillimanite and kyanite and may be down-dip, becoming oblique (S-SE strike) towards west. The geothermobarometrical data for the granulites of Cariré reveals P-T conditions between 8.3-9.4 kbar and 804-870°C for the felsic granulites and between 10.2-13.6 kbar and 750-910°C for the mafic granulites. In the Forquilha region, the P-T conditions range from 11.2 to 22.0 kbar and 495 to 840°C for the metamafic rocks and from 9.9 to 11.0 kbar and 734 to 851 °C for the metasedimentary host rocks. These data indicate the existence of high-pressure granulites in the Cariré region and eclogitic/granulitic rocks in the FEZ. The petrography and geochemistry allowed the identification of three groups of metamafic rocks in the FEZ: i) Garnet amphibolites, with flat REE pattern, negative anomalies of Rb, Th, Nb, Zr e Ta and similarities with island arc basalts, IAT-type (SPIDER diagram); ii) Retrograded eclogites with flat narrow REE pattern that show similarities with N-T-MORB pattern, similar to basalts from extensional setting, like mid ocean ridge or back-arc from intra ocean arcs; iii) Clinopyroxene-garnet amphibolites with greater slope in the REE pattern, with La/Yb ratio between 2.63 to 7.32, that suggest slightly fractionation. This group has an enrichment in alkalis and in incompatible trace elements, similar to alkaline rocks and continental basalts. The geochronological data (whole-rock Sm-Nd and zircon and monazite U-Pb and Lu-Hf) indicate two magmatic episodes. The first is paleoproterozoic and registered by the 2.1 Ga granodiorites from Cariré region. The second is mesoproterozoic and recorded by the 1455 and 1618 Ma zircons from the metamafic rocks from FEZ. The zircon Lu-Hf data (T_{DMHf} = 1.57 – 1.80 Ga and $\varepsilon_{Hf\ (1500)}$ = +7.46 e +9.63) and Nd isotopes (T_{DMNd} = 1.57 – 2.81 Ga and $\varepsilon_{Nd\ (1500)}$ = +4.11 and +4.33) reveals sources values close to the crystallization ages with positive ε values. The U-Pb data in zircon rims and in crystals with metamorphic textures and low Th/U ratios, allowed the characterization of two metamorphic stages: i) 640 – 650 Ma, obtained in the metasedimentary host rocks of the retrograded eclogites from the FEZ and related to the collisional metamorphism in eclogite facies; ii) 590 to 615, registered by the granulites from the Cariré region and from south of Forquilha city. Dating of detrital zircon from four metasedimentary rocks along the FEZ, showed that the main source is Rhyacian/Orosirian paleoproterozoic with maximum depositional ages around 1.65 to 1.80 Ga. In this context, the Slab-breakoff model is proposed.

1. ASPECTOS INTRODUTÓRIOS

O documento apresentado é parte dos requisitos exigidos para a obtenção do título de Doutor em Geociências, área de concentração em Geologia e Recursos Naturais, junto ao curso de Pós-Graduação em Geociências do Instituto de Geociências (IG) da Universidade Estadual de Campinas (UNICAMP)

De acordo com as normas da Resolução 01/2008 do Programa de Pós-Graduação em Geociências do IG-UNICAMP, este documento é composto por 25 páginas introdutórias circunstanciando a pesquisa, objetivos, materiais e métodos, discussões e conclusões, quatro anexos onde constam três artigos, sendo um aceito e dois em correção, e as descrições petrográficas e os resultados das análises de química mineral e geotermobarometria.

O Desenvolvimento deste trabalho em suas diversas etapas contou com o subsídio do Conselho Nacional de Desenvolvimento Científico e Tecnológico (CNPq) no que se refere à concessão da bolsa de estudos, do Projeto do Instituto do Milênio CNPq/MCT (Proc. 42.0222/2005-7) com auxílio financeiro e logístico para parte dos trabalhos de campo; e da Fundação de Amparo à Pesquisa do Estado de São Paulo (FAPESP) com auxílio financeiro para os trabalhos de laboratório e campo (Proc. 07/58535-6).

1.1 Apresentação do trabalho e motivação

A motivação para a elaboração desta Tese se deu em 2006 no final do meu mestrado quando o Professor Ticiano e eu estávamos mapeando uma área a oeste do arco magmático de Santa Quitéria dentro do Projeto FAPESP (Proc. 03/07663-3) e começamos a encontrar algumas ocorrências de rochas metamáficas, ora *in situ*, ora como blocos dispersos. Eram granada anfibolitos, com auréolas de plagioclásio ao redor de granada e uma quantidade dominante de anfibólio, semelhante aos retroeclogitos descritos por Castro (2004), a leste do arco, região de Madalena. A partir da coleta de algumas amostras para petrografia, começamos a identificar algumas texturas microscópicas mais interessantes, tais como simplectitos formados por plagioclásio, quartzo e anfibólio ± diopsídio. Desde então, nas etapas subsequentes de campo, começamos a detalhar as regiões de ocorrência dessas rochas metamáficas. Os afloramentos foram mais explorados sempre com o objetivo de coletar as amostras menos

deformadas/cisalhadas, preferencialmente nas partes centrais dos afloramentos, na tentativa de encontrar minerais e paragêneses de alto grau metamórfico. A identificação de pseudomorfos de onfacita preenchidos por simplectitos de clinopiroxênio e plagioclásio sódico, em granada-clinopiroxênio anfibolitos e estudos termobarométricos iniciais levaram à caracterização de rochas da fácies eclogito na região de Forquilha (Santos *et al.,* 2009). A partir disto, alguns questionamentos começaram a ser formulados: 1) Qual seria a abrangência dessas rochas nesta região? 2) Qual a natureza geoquímica dos protólitos? 3) Quais as condições de pressão e temperatura máxima das metamáficas e suas encaixantes? 4) E as idades de cristalização e do metamorfismo? Na extremidade NW do Domínio Ceará Central, próximo ao lineamento Transbrasiliano, na região de Cariré (distante aproximadamente 35 km a sudoeste de Forquilha - Figura 1), Nogueira-Neto (2000) descreve a ocorrência de granulitos máficos e félsicos com associações de alta pressão. Seria possível que, a exemplo do que ocorre na borda leste do Cráton Oeste Africano, estas associações de rochas de alto grau metamórfico que afloram a oeste do arco magmático de Santa Quitéria e próximo ao lineamento Transbrasiliano constituem uma importante zona de sutura? Esse cenário geotectônico e a busca pelas respostas aos questionamentos centrais foram a grande motivação para a execução desta Tese. Este trabalho também foi extremamente instigante e progressivamente aumentou o meu conhecimento em diversas áreas das Geociências.

1.2. Justificativa

A aglutinação de massas continentais durante a formação do supercontinente Gondwana ocidental desencadeou o fechamento de oceanos em zonas de subducção e a consequente geração de arcos magmáticos no Brasil (Pimentel & Fuck, 1992, Pedrosa-Soares *et al.,* 2001, Paixão *et al.,* 2008, Tohver *et al.,* 2010)

Considerando a Província Borborema (PB) e sua continuidade do lado africano, o conhecimento atual mostra que as principais zonas de sutura associadas a processos de subducção são registradas pelas ocorrências de lascas ofiolíticas e rochas máficas com paragêneses de alto grau metamórfico (fácies granulito/eclogito) situadas nas bordas das grandes massas cratônicas (Affaton *et al.,* 1980; Bernard-Griffiths *et al.,* 1991; Agbossoumodé *et al.,* 2004; Duclaux *et al.,* 2006; Santos *et al.,* 2008, 2009). A continuidade das feições geológicas regionais da PB pode ser

seguida no lado africano na Província policíclica Camarões-Nigéria e nas faixas Dahomeyides e Hoggar, indicando que estas duas províncias correspondiam antes da instalação do oceano Atlântico, a uma vasta região intensamente afetada pela tectônica resultante da aproximação das referidas massas cratônicas durante o Neoproterozóico (Figura 2).

Figura 1: Mapa de localização e principais vias de acesso das áreas investigadas. Topografia gerada a partir do modelo digital do terreno (*SRTM*).

A extremidade norte da PB é limitada a sul pelo lineamento Patos, e subdividida nos domínios Médio Coreaú, Ceará Central e Rio Grande do Norte, delimitados pelos lineamentos Transbrasiliano e Senador Pompeu (Brito Neves *et al.,* 2000) (Figura 3). Do ponto de vista tectônico, o Domínio Ceará Central (DCC) constitui um dos mais importantes da PB. Dentre os diferentes terrenos deste domínio, destacam-se: um núcleo Arqueano; o embasamento Paleoproterozóico; supracrustais Paleo a Neoproterozóicas; o Complexo Tamboril-Santa Quitéria (arco magmático de Santa Quitéria – AMSQ, Fetter *et al.,* 2003) e diversos corpos graníticos sin- e pós-tectônicos. A caracterização isotópica das rochas ortoderivadas constituintes do AMSQ encontra-se relativamente bem estabelecida. Isto se deve à quantidade de dados obtidos pelos métodos U-Pb em zircão, titanita e monazita e Sm-Nd em rocha total (Fetter 1999; Fetter *et al.,*

2003; Santos *et al.,* 2004; Castro 2004), que forneceram idades de cristalização ao redor de 640 Ma, idades de metamorfismo entre 640 e 615 Ma e valores de $\varepsilon_{Nd\ (t=640)}$ positivos que sugerem a existência de materiais juvenis.

A partir da existência de uma marcante anomalia gravimétrica positiva no extremo noroeste da PB abaixo da bacia do Parnaíba, Fetter *et al.,* (2003) propuseram uma subducção com polaridade de NW para SE. Resquícios de crosta oceânica e de uma possível zona de sutura provavelmente estariam encobertos pelos sedimentos da bacia (Lesquer *et al.,* 1984; Trompette 1994; El-Hadj *et al.,* 1997; Fetter *et al.,* 2003). Por outro lado, Castro *et al.,* (2004) e Arthaud (2008) apontam uma outra interpretação para a evolução tectônica do DCC, com base na identificação de rochas de alta pressão, na borda leste do AMSQ. Estas rochas estão situadas na base das *nappes* de vergência para SE da área investigada, sugerindo que a zona de sutura correspondente ao fechamento do oceano existente entre os domínios Médio Coreaú e Ceará Central estaria situada a sudeste do arco magmático de Santa Quitéria (Figura 3).

Trabalhos de mapeamento sistemáticos em escala de detalhe e semi-detalhe realizados nas adjacências do AMSQ, mais especificamente na sua borda oeste, e ao longo do lineamento Transbrasiliano, têm evidenciado a presença de rochas máficas com associações minerais de alta pressão (retroeclogitos) e alta temperatura (granulitos máficos, félsicos e kinzigitos) nas regiões de Forquilha e Cariré, respectivamente (Nogueira-Neto, 2000, Santos *et al.,* 2008; Amaral *et al.,* 2008; Santos *et al.,* 2009).

Os retroeclogitos da região de Forquilha definem uma faixa N-S de aproximadamente 30 km de comprimento por 4 km de largura, representados por corpos lenticulares descontínuos com comprimentos que variam de 5 a 300 metros de extensão. Encontram-se encaixados em principalmente em xistos, gnaisses aluminosos, quantidades subordinadas de quartzitos, mármores e rochas cálcio-silicatadas. Apresentam associações e texturas minerais indicativas de desestabilização da fácies eclogito e de rochas que foram submetidas à alta pressão. Esta sequência de rochas foi denominada de Faixa Eclogítica de Forquilha (FEF) (Santos *et al.,* 2008, 2009; Amaral *et al.,* 2010). Dados termobarométricos indicam condições de pressão e temperatura, respectivamente de 17,3 kbar e 770ºC (Santos *et al.,* 2009).

Na região de Cariré, granulitos máficos (granada-clinopiroxênio anfibolitos) e félsicos (granulitos de composição tonalítica/enderbítica) afloram adjacentes ao lineamento Transbrasiliano (Fetter, 1999; Nogueira-Neto, 2000; Amaral *et al.,* 2008). Os granulitos ocorrem

frequentemente como blocos e matacões de dimensões métricas ou como lentes boundinadas de dimensões métricas (em média 10 x 3 metros) encaixados em rochas ortoderivadas de composição diorítica e granodiorítica, intensamente cisalhadas.

Neste contexto a caracterização de rochas metamórficas de alto grau no DCC fornece importantes subsídios para a confirmação de uma provável zona de subducção e da colisão continental nesta região da Província Borborema. São raras as informações geoquímicas e geocronológicas das rochas de alto grau descritas nas regiões de Forquilha e Cariré. Portanto, estabelecer a petrogênese desses litotipos e de suas encaixantes, obter a maior quantidade de dados termobarométricos que permitam estimar as condições de equilíbrio nos diferentes estágios do metamorfismo e contextualizar a cronologia de geração dos protólitos e do processo colisional/metamórfico, é tarefa fundamental para o entendimento da evolução geodinâmica do Domínio Ceará Central.

1.3 Objetivos

A principal meta desta Tese é caracterizar a evolução geodinâmica da porção noroeste do DCC, onde se inserem o AMSQ, o lineamento Transbrasiliano e rochas metamáficas de alta pressão e alta temperatura nas regiões de Forquilha e Cariré.

Como objetivos específicos, têm-se a:

i) Caracterização geoquímica das rochas metamáficas que ocorrem nas circum-vizinhanças do arco de Santa Quitéria e a determinação de seus ambientes de formação;

ii) Definição petrográfica e termobarométrica das associações minerais e texturais das rochas metamáficas e de suas encaixantes, situadas entre o AMSQ e o lineamento Transbrasiliano, nas regiões dos municípios de Forquilha e Cariré;

iii) Datação dos eventos de cristalização e metamorfismo das rochas metamáficas e suas encaixantes a partir de estudos geocronológicos (U-Pb, Lu-Hf e Sm-Nd) em zircão, monazita e rocha total;

iv) Discussão de um modelo tectônico evolutivo para o Domínio Ceará Central e suas implicações para a evolução crustal desta porção da Província Borborema.

2. ARCABOUÇO TECTÔNICO DA PROVÍNCIA BORBOREMA

A Província Borborema foi originalmente descrita e definida por Almeida (1977) e Almeida *et al.,* (1981) como uma complexa região de domínios tectono-estratigráficos, associada a eventos tectônicos de idade neoproterozóica. Esta província compreende uma área de aproximadamente 450.000 km^2 e foi estruturada a partir da convergência dos crátons Amazônico, São Luis – Oeste Africano e São Francisco, por volta de 600 Ma, na intitulada colagem brasiliana (Trompette, 1994, Brito Neves & Cordani, 1991) (Figura 2). Estudos isotópicos especialmente de proveniência em zircão detrítico, realizados por toda Província Borborema, têm auxiliado a configurar um quadro de evolução crustal mais preciso, envolvendo a colagem de diferentes terrenos tectono-estratigráficos, devido à atuação de distintos ciclos tectônicos (Oliveira *et al.,* 2006, Van-Schmus *et al.,* 2008 Arthaud, 2008, Neves *et al.,* 2009, de Araújo *et al.,* 2010a, Santos *et al.,* 2010)

A estruturação e os litotipos da Província foram desenvolvidos durante a evolução de dois ciclos tectônicos: i) orogênese Cariris Velhos (Brito Neves *et al.*, 1995, Santos *et al.,* 2010), que ocorreu desde o Mesoproterozóico Superior (~1,2 Ga) até o início do Neoproterozóico (1,0- 0,92 Ga); e ii) orogênese Pan-Africana/Brasiliana, desencadeada durante o Neoproterozóico Superior (~600 Ma) (Van Shumus *et al.,* 1995; Trompette, 1994; Brito Neves & Cordani, 1991). Adicionalmente, no embasamento da Província foram reconhecidas evidências de outros ciclos tectônicos atribuídos a importantes estágios de amalgamação continental durante o Paleoproterozóico (*e.g.* Hackspacher *et al.*, 1990, Fetter *et al.,* 2003, Martins *et al.,* 2009) e o Arqueano (*e.g.* Dantas *et al.,* 1998, 2004, Silva *et al.,* 2002).

O quadro pré-cambriano da Província caracteriza-se, ainda, pela existência de extensas zonas de cisalhamento dúctil transcorrente com orientações NE-SW, NNE-SSW e E-W (Figura 2), desenvolvidas no final da orogênese Brasiliana (Vauchez *et al.*, 1995, Monié *et al.,*1997) .

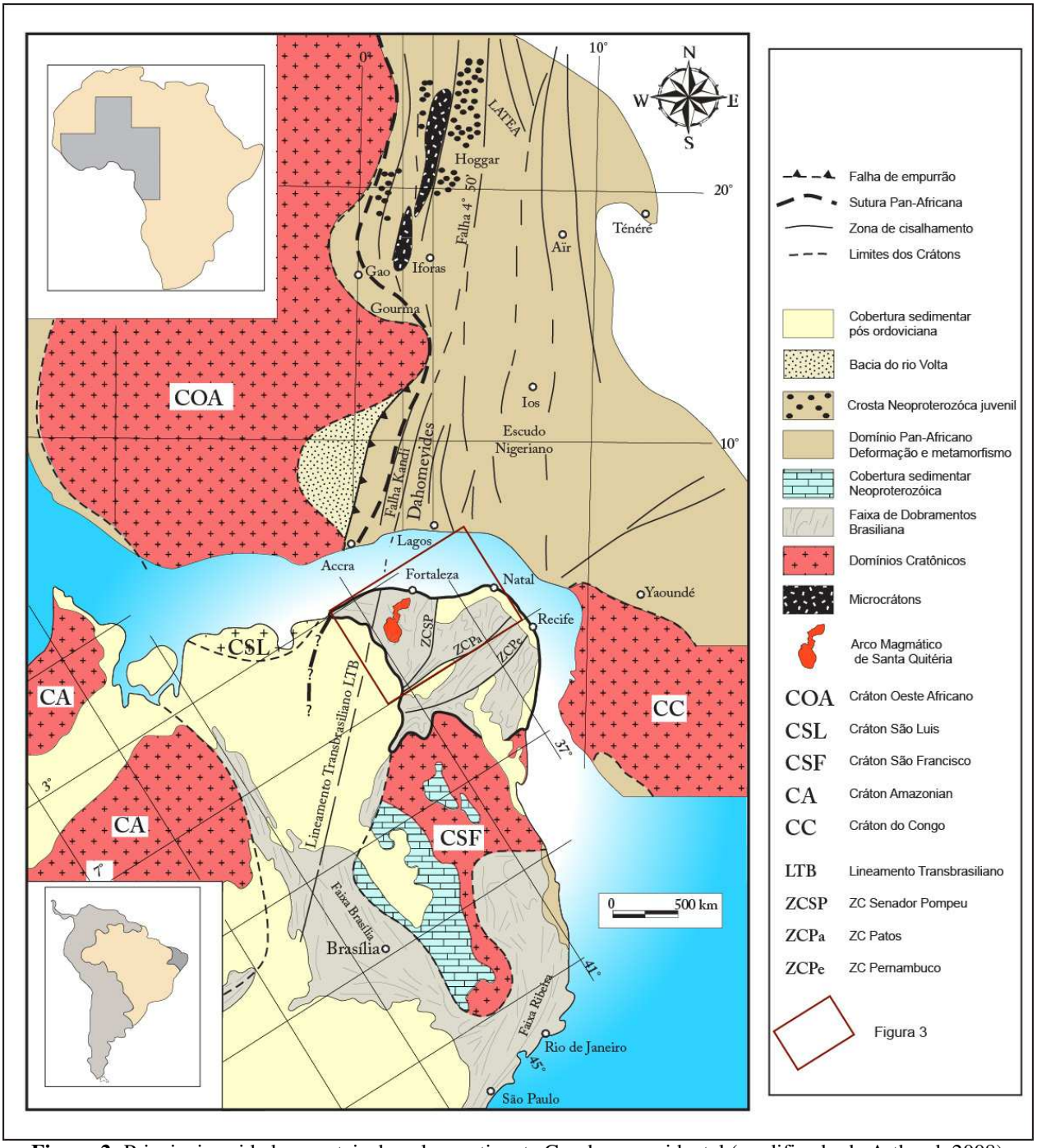

Figura 2: Principais unidades crustais do paleocontinente Gondwana ocidental (modificado de Arthaud, 2008)

A zona de cisalhamento Patos divide a PB em dois grandes blocos tectônicos, o Domínio Norte e o Domínio Sul (Van Schmus *et al.,* 1995). Com base em assinaturas crustais de Nd e diferenças de idades U-Pb em zircão, esses domínios foram ainda subdivididos em domínios crustais menores (Brito Neves *et al.,* 2000).

Os lineamentos Transbrasiliano e Senador Pompeu subdividem o Domínio Tectônico Norte em três unidades crustais conhecidas por Domínio Médio Coreaú, Domínio Ceará Central e Domínio Rio Grande do Norte. O Domínio Ceará Central será enfatizado por localizar as áreas investigadas neste estudo (Figura 3).

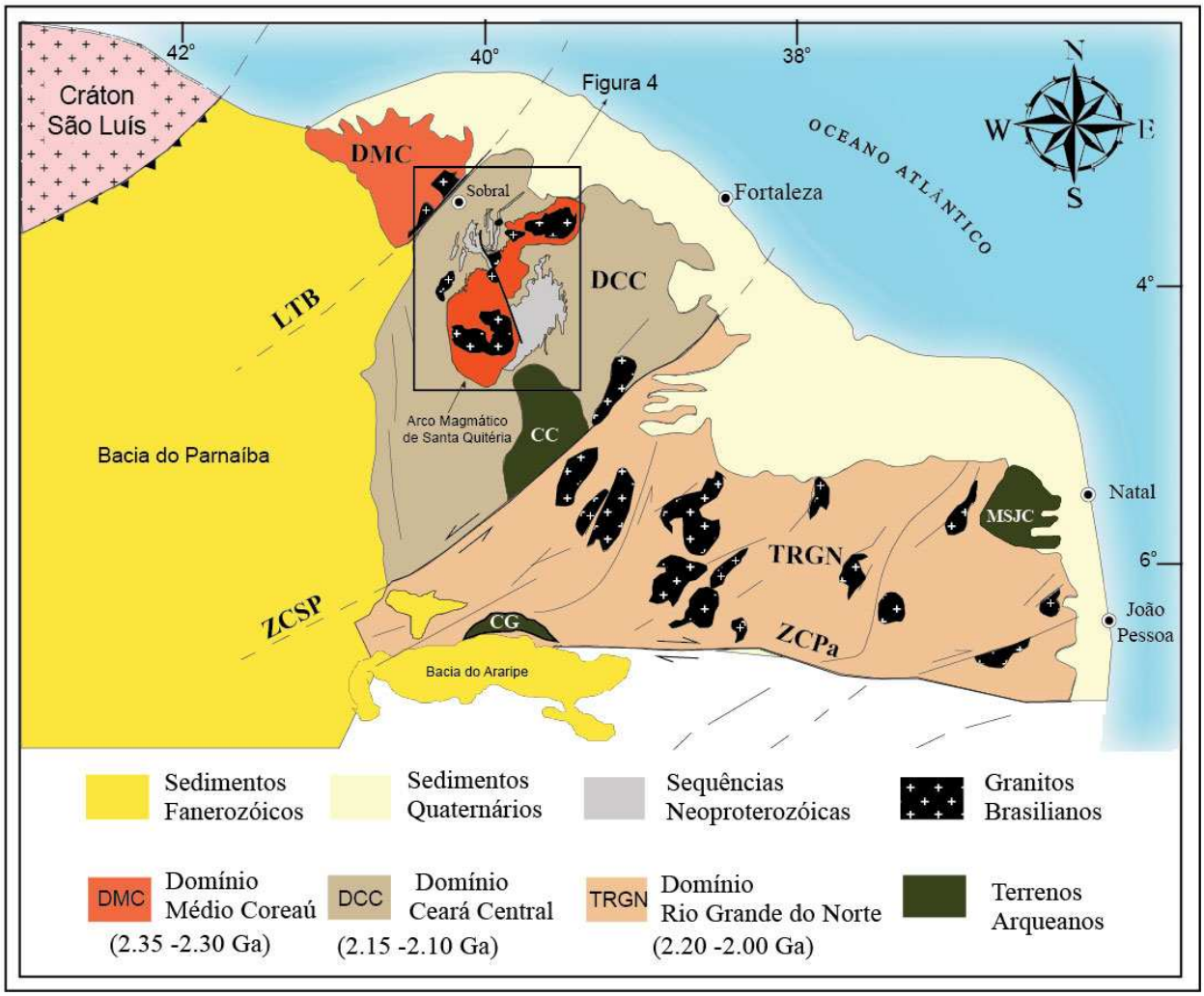

Figura 3: Esboço geológico regional da porção setentrional da Província Borborema e dos arredores do lineamento Patos. LTB = lineamento Transbrasiliano; ZCSP = Zona de Cisalhamento Senador Pompeu; ZCPa = Zona de cisalhamento Patos; CC = Complexo Cruzeta; MSJC = Maciço São José do Campestre; CG = Complexo Granjeiro (modificado de Van Schmus *et al.,* 1995).

2.1 Domínio Ceará Central - DCC

O DCC é a mais extensa unidade geotectônica da porção norte da Província Borborema e abrange quase a totalidade do Estado do Ceará. É delimitado a NW pela zona de cisalhamento

Sobral-Pedro II (lineamento Transbrasiliano) e a SE pela zona de cisalhamento Senador Pompeu (ZCSP), sendo encoberto a SW-W pelos sedimentos da Bacia do Parnaíba.

De acordo com Fetter *et al.,* 2000, o Domínio Ceará Central pode ser dividido em quatro unidades geotectônicas: (1) Núcleo Arqueano; (2) Embasamento gnáissico paleoproterozóico; (3) Supracrustais de idade neoproterozóica; e (4) Complexo Tamboril-Santa Quitéria.

2.2 Núcleo Arqueano

Representado por parte do Complexo Cruzeta (CC), o núcleo Arqueano aflora na porção sudeste do DCC e está balizado a leste pela zona de cisalhamento Senador Pompeu e a oeste e a norte pelos gnaisses do embasamento Paleoproterozóico (Figura 3). O complexo é seccionado pela zona de cisalhamento Sabonete-Inharé, que o divide em duas unidades litológicas distintas, intituladas unidades Mombaça a sudeste, e unidade Pedra Branca a noroeste, ambas de afinidade TTG.

Com base em análises isotópicas U-Pb e Sm-Nd, Fetter (1999) aponta uma assinatura juvenil para a Unidade Pedra Branca enquanto os litotipos da Unidade Mombaça apresentam indícios de retrabalhamento de fontes ligeiramente mais antigas. Similarmente, as idades de cristalização indicam que a unidade Pedra Branca é mais jovem (*ca.* 2,7 Ga) que a Unidade Mombaça (*ca.* 2,8 Ga). Entretanto, registro de crosta mais antiga foi reportado por Silva *et al.* (2002), utilizando determinações U-Pb SHRIMP em zircão de gnaisses tonalíticos localizados a sudoeste de Boa Viagem. As análises indicaram idade de 3270 ± 5 Ma e uma borda sobrecrescida datada em 2084 ± 14 Ma.

2.3 Embasamento gnáissico Paleoproterozóico

As rochas do embasamento que afloram na região de Madalena até Choró são representadas por gnaisses, por vezes migmatíticos, de composição diorítica a tonalítica e por terrenos TTG (Figura 4).

Martins (2000) agrupou estas rochas na Suíte Metamórfica Algodões-Choró e constatou a existência de uma associação de paragnaisses e anfibolitos intrudidos por ortognaisses de composição tonalítica a diorítica. A partir de dados geocronológicos (U-Pb e Sm-Nd) Fetter

(1999) e Fetter *et al.*(2003) sugeriram para a região um regime de sucessivas colagens de arcos de ilha em torno do núcleo Arqueano.

Castro (2004) obteve em ortognaisses de composição quartzo-diorítica a tonalítica, da região de Madalena idades U-Pb em zircão de 2,1 Ga e idades-modelo (T_{DM}) entre 2,3 e 2,1 Ga, similares às idades obtidas por Fetter (1999) e Martins (2000) em ortognaisses da mesma suíte.

Martins *et al.,* (2009), utilizando dados geoquímicos e geocronológicos constataram que os anfibolitos da suíte Algodões possuem similaridades com platôs oceânicos e basaltos gerados em ambientes de *back-arc*. Uma idade isocrônica Sm-Nd de *ca.* 2,23 Ga foi interpretada como a idade mínima do protólito, enquanto ortognaisses tonalíticos forneceram a idade U-Pb em zircão de 2,13 Ga.

Ocorre ainda no Domínio Ceará Central uma série de associações gnáissicas migmatíticas, representativas do embasamento das supracrustais neoproterozóicas agrupadas no Complexo Canindé (Torres *et al.,* 2010). Estas associações compreendem ortognaisses de composição tonalítica a granodiorítica, geralmente metamorfizados em fácies anfibolito de alta temperatura, com condições variáveis de migmatização (Cavalcante *et al.*, 2003). Idades U-Pb para essa associação situam-se entre 2,11 e 2,19 Ga com idades modelo T_{DM} entre 2,42 e 2,48 Ga (Hackspacher *et al.* 1990; Fetter, 1999, Castro, 2004). A contraparte sedimentar deste complexo é composta por biotita gnaisses, granada-biotita gnaisses e localmente sillimanita-granada-biotita gnaisses e apresentam fontes com picos de zircão detrítico ao redor de 1,8 Ga e 2,1-2,2 Ga (Amaral *et al.,* 2010b).

2.4 Supracrustais Neoproterozóicas

As sequências supracrustais do DCC ocorrem principalmente bordejando o arco magmático de Santa Quitéria (AMSQ). Estas sequências apresentam, frequentemente, paragêneses de alta pressão e alta temperatura (Castro 2004, Garcia & Arthaud 2004, Arthaud *et al.,* 2008, Santos *et al.,* 2009) associada a uma tectônica de baixo ângulo (Figura 4). No mapa geológico do estado do Ceará (Cavalcante *et al.,* 2003) estas unidades foram incluídas no Complexo ou Grupo Ceará.

O Complexo Ceará é caracterizado pela ocorrência de rochas essencialmente metapelíticas e metapsamíticas, representadas por cianita-muscovita-biotita gnaisse, sillimanita-

granada gnaisse, quartzitos, anfibolitos, mármores, rochas cálcio-silicáticas e metariolitos (Cavalcante *et al.,* 2003, Fetter *et al.,* 2003, Arthaud, 2008).

Estudos de proveniência em metapelitos e idades de cristalização U-Pb em zircão obtidas em rochas metamáficas intercaladas no Complexo Ceará, sugerem que a sedimentação dessa unidade teve início ao redor de 750 Ma a partir do rifteamento do embasamento arqueano/paleoproterozóico (Arthaud, 2008). Fetter (1999) obteve a idade U-Pb de 772 ± 31 Ma em metariolito próximo à localidade de Independência. O mesmo autor sugere que os sedimentos que deram origem às rochas metassedimentares do Complexo Ceará foram depositados em uma bacia do tipo retro-arco relacionada ao AMSQ.

A distinção entre os litotipos representados pelo Complexo Canindé nem sempre é fácil e variações na proveniência dos detritos que compõem ambos complexos podem indicar uma sobreposição de bacias mais jovens *versus* bacias mais antigas ou, alternativamente mudança das condições tectônicas que poderiam influenciar em variações bruscas na proveniência dessas rochas.

Castro (2004) engloba as rochas do Complexo Ceará na sequência Supracrustal Rio Curu-Itataia-Independência, composta por gnaisses migmatíticos aluminosos, rochas carbonáticas e vulcânicas, com idades modelo $T_{(DM)}$ em torno de 2,4 Ga, indicando que fontes mais antigas contribuíram para a deposição desta sequência.

Idades modelo $T_{(DM)}$ antigas, como as reportadas por Castro (2004), também foram obtidas por Santos *et al.* (2003), em torno de 2,25 Ga., mostrando que a contribuição do embasamento Paleoproterozóico, como área fonte para a geração das rochas metassedimentares, é dominante nesta sequência.

Ainda dentro do contexto das rochas supracrustais do DCC, o Grupo Novo Oriente, constituído por metapelitos distais e metapsamitos proximais, vem sendo interpretado como parte de uma margem passiva com idade máxima de *ca.*1.3 Ga (de Araujo *et al.*, 2010a).

2.5 Complexo Tamboril-Santa Quitéria

O Complexo Tamboril-Santa Quitéria (Figura 4) corresponde a um complexo anatético-ígneo formado principalmente por diatexitos e metatexitos, preservando mega-enclaves de rochas

cálcio-silicáticas e anfibolitos. Esses migmatitos foram intrudidos por grande volume de magmas tonalíticos a graníticos (Fetter *et al,* 2003, Castro 2004, Arthaud, 2008).

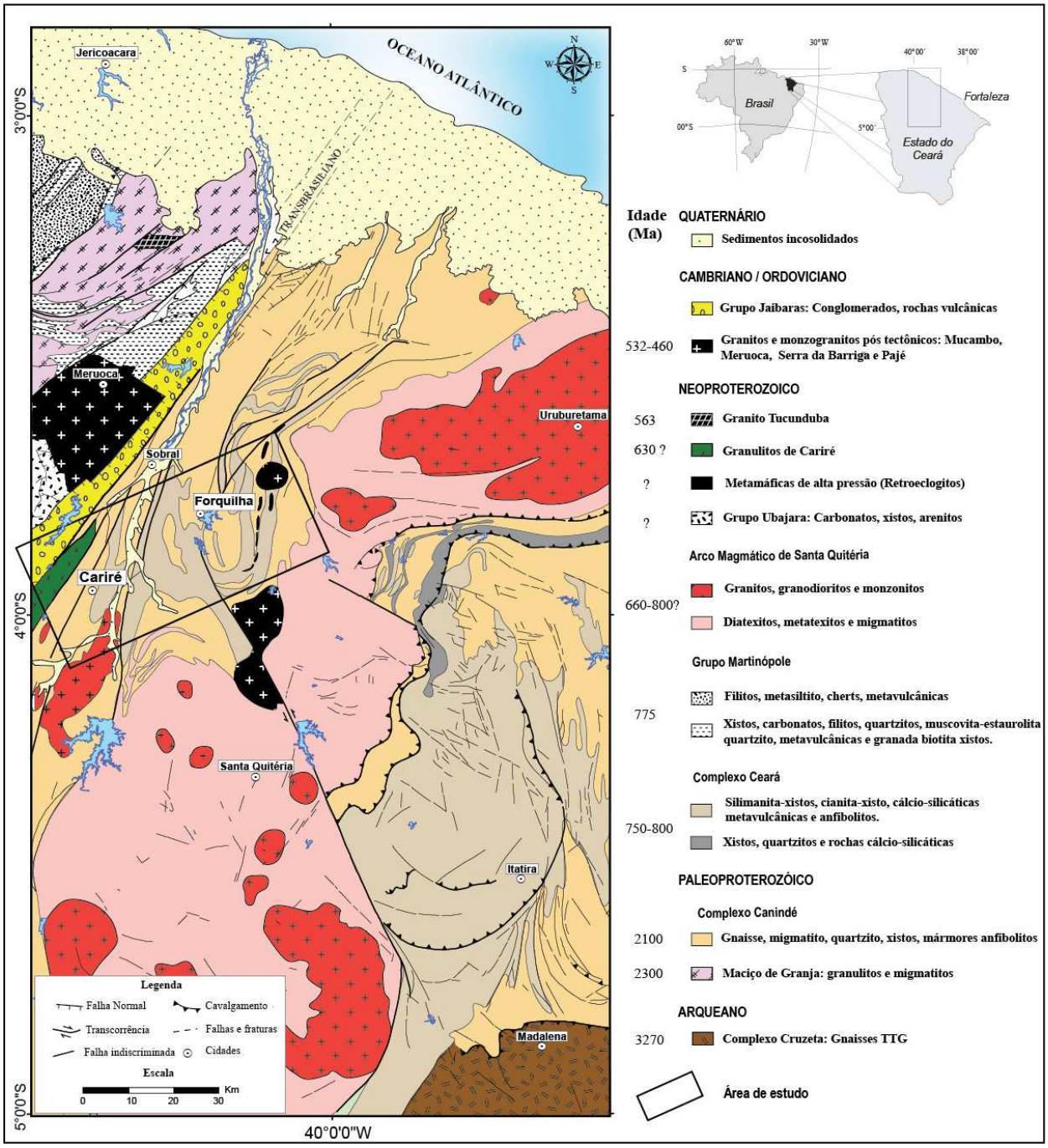

Figura 4: Mapa geológico regional da porção NW do Domínio Ceará Central. O retângulo indica a área de estudo (modificado de Cavalcante *et al.,* 2003).

As idades U-Pb em zircão dos granitóides desse complexo variam entre 660 e 614 Ma (Fetter *et al.,* 2003; Brito Neves *et al.,* 2003) e 620 e 611 Ma (Castro 2004). As idades modelo

T_{DM} são geralmente meso a neoproterozóicas, com ε_{Nd} (600) levemente negativos a positivos, variando entre -3 e +3 (Fetter *et al.,* 2003). Com base nesses dados e em aspectos petrográficos, Fetter *et al.,* (2003) sugeriram um ambiente de arco magmático continental para essa unidade - AMSQ.

Recentemente, de Araujo *et al.,* (2010b) propuseram ambiente colisional para grande parte das linhagens magmáticas representadas pelo AMSQ. Os mesmos autores reportam uma idade Pb-Pb em zircão de 795 Ma em gnaisses granodioríticos na borda leste do complexo, sugerindo que possam representar a fase cordilherana (pré-colisional), ou mesmo registro de arcos intraoceânicos associados à orogênese Pan-Africana/Brasiliana.

A região de ocorrência do AMSQ está associada a um sistema de *nappes,* que afetou o embasamento e as rochas supracrustais, com vergência predominante para SSE (Caby & Arthaud 1986; Arthaud *et al.,* 2008). A idade para o metamorfismo regional foi estabelecida ao redor de 600 Ma por Castro (2004) pelo método U-Pb em monazita.

A caracterização de retroeclogitos e granada anfibolitos na borda leste deste arco nos arredores de Itataia e Pentecostes, respectivamente (Castro 2004; Garcia & Arthaud 2004; Amaral & Santos 2008) contribuiu para uma interpretação divergente da discutida por Fetter *et al.,* (2003), em relação à polaridade da zona de subducção que teria dado origem ao AMSQ. Com base nos retroeclogitos descritos, Castro (2004) sugeriu o sentido NNW para o fechamento oceânico. Por outro lado, Fetter *et al.,* (2003), com base na posição atual do AMSQ e nas anomalias gravimétricas positivas no extremo NW da PB (Lesquer *et al.,* 1984, Trompette 1994; El-Hadj *et al.,* 1997), propuseram o sentido SE para o processo de subducção. Santos *et al.*(2009) corroboram com polaridade para SE devido à descoberta de uma faixa N-S de rochas metamáficas de alto grau (P~17.4 kbar e T~750 °C) na borda oeste do AMSQ, o que não invalida a existência de mais de uma zona de sutura neste domínio, com idades distintas.

Adicionalmente, deve ser ressaltado a expressiva granitogênese (Figura 4). O primeiro episódio (Tardi-Proterozóico) é representado pelas suítes Quixadá-Quixeramobim, com idades U-Pb de 585 Ma (Fetter, 1999). O segundo, e mais jovem episódio (Cambro-Ordoviciano), é representado por uma série de corpos, no qual se destacam os granitos Mucambo, Meruoca, Serra da Barriga, Pagé, Serrote São Paulo e Complexo Anelar Quintas com idades U-Pb variando entre 535 e 480 Ma (Texeira, 2006, Castro, 2004, Fetter, 1999).

3. MATERIAIS, MÉTODOS E ORGANIZAÇÃO DA TESE

Para alcançar os objetivos propostos no projeto de Tese, foram realizadas seis etapas de campo com média de duas semanas de duração cada uma, totalizando trezentos afloramentos descritos e a coleta de aproximadamente uma tonelada de amostras para petrografia, geoquímica e geocronologia. As informações obtidas em campo e todos os resultados das análises geoquímicas e geocronológicas foram integrados em sistema de informações geográficas (SIG), o que facilitou tanto o planejamento quanto a execução dos objetivos propostos.

Foram confeccionadas 155 lâminas delgadas e polidas, visando a caracterização dos diversos litotipos das regiões de Forquilha e Cariré. Finalizada a etapa de descrição petrográfica, classificou-se as rochas metamáficas em três grupos: granada anfibolitos, retroeclogitos e clinopiroxênio-granada anfibolitos. Essa classificação petrográfica foi, posteriormente, confirmada com a litoquímica. Os granulitos da região de Cariré foram classificados como máficos e félsicos. O principal critério utilizado para tal divisão baseou-se na porcentagem de minerais quartzo-feldspáticos, nas paragêneses e associações minerais e nas texturas metamórficas e ígneas observadas. Para melhor caracterização dos minerais acessórios e das inclusões, foram confeccionadas seções delgadas polidas para investigação ao microscópio de varredura eletrônica (MEV), com a geração de imagens de elétrons retro-espalhados (*backscattered electrons* - BSE).

3.1 Análises de Química mineral e Geotermobarometria

Com o objetivo de determinar a química mineral e as condições de equilíbrio termobarométricas na Faixa Eclogítica de Forquilha, nove amostras de rochas metamáficas e três metassedimentares encaixantes foram selecionadas ao longo do *trend* estrutural da faixa. As análises foram realizadas no Instituto de Geociências da Universidade de São Paulo-USP. Detalhes da metodologia e resultados são apresentados no Anexo 4.

3.2 Análises Geoquímicas

Foram selecionadas sessenta amostras de rochas metamáficas que ocorrem nos arredores de Forquilha e Cariré para análises geoquímicas de elementos maiores e traços. As análises foram realizadas no Instituto de Geociências da Universidade Estadual de Campinas UNICAMP e também no ACME Labs. (Canadá). Para maiores detalhes sobre a metodologia aplicada, discussões e resultados, ver o Anexo 2.

3.3 Análises Geocronológicas

Foram obtidas oito análises U-Pb em zircão de rochas metamáficas e seis análises U-Pb em zircão e monazita de rochas encaixantes (metassedimentares, granodioritos e cálcio-silicáticas). Adicionalmente, foram obtidas três análises Lu-Hf em zircão de rochas metamáficas e cálcio-silicáticas e vinte e uma análises de Sm-Nd (rocha total) nas rochas metamáficas. Todas essas análises foram realizadas no Laboratório de Geocronologia da UnB, sob a orientação do Prof. Dr. Elton Luis Dantas durante o período de intercâmbio com o Laboratório. Resultados e detalhes da metodologia são apresentados nos anexos 1 e 3.

4. APRESENTAÇÃO DOS RESULTADOS

Todos os objetivos propostos para o desenvolvimento desta Tese foram alcançados e os resultados estão apresentados sob a forma de três artigos originais submetidos a revistas arbitradas e inclusos como anexos neste documento. Os Anexos 1 e 3 são passíveis de alterações uma vez que estão em fase de correções e análise pelo corpo editorial do periódico para o qual foram submetidos. O Anexo 4 está organizado como capítulo, pois não houve tempo hábil para a organização na forma de artigo, tendo em vista que as análises em microssonda eletrônica foram realizadas na última etapa desta Tese.

Além dos artigos completos gerados, o desenvolvimento deste trabalho também resultou em um resumo expandido (Amaral *et al.,* 2010) apresentado no VII-*South American Symposium on Isotope Geology* e sete resumos (Amaral *et al.,* 2010a, Amaral *et al.,* 2010b, Amaral *et al.,* 2009a, Amaral *et al.,* 2009b, Amaral *et al.,* 2009c, Amaral *et al.,* 2008a, Amaral *et al.,* 2008b) apresentados, respectivamente no 45° Congresso Brasileiro de Geologia, XXIII-Simpósio de Geologia do Nordeste, XI-Simpósio de Geologia do Centro-Oeste, XII-Simpósio Nacional de Estudos Tectônicos e 44° Congresso Brasileiro de Geologia.

O artigo apresentado no primeiro anexo trata exclusivamente das rochas granulíticas e suas encaixantes da região de Cariré, enquanto os outros três anexos abordam a geoquímica, a geocronologia e a geotermobarometria das rochas que compõem a Faixa Eclogítica de Forquilha.

O Anexo 1 contém a seguinte referência: "Amaral, W.S., Nogueira Neto, J.A., Santos, T.J.S., Wernick, E., Dantas, E.L., Matteini, M.,. 2010. **High-pressure granulites from Cariré, NW of the Borborema Province-Brazil: tectonic setting, geothermobarometry and U-Pb, Lu-Hf, Sm-Nd geochronology.** *Gondwana Research* (Submetido)". Neste trabalho os autores abordam as relações de campo das rochas de alto grau metamórfico que ocorrem na Faixa Granulítica de Cariré, as condições de equilíbrio termobarométrico dos granulitos presentes nessa Faixa e as idades U-Pb, Lu-Hf e Sm-Nd obtidas em zircão tanto dos granulitos quanto das rochas encaixantes. Este é um tema de grande relevância para entendimento geodinâmico do Domínio Ceará Central no contexto de amalgamação do supercontinente Gondwana devido à proximidade do lineamento Transbrasiliano, e similaridades químicas e cronológicas com seus análogos na contra parte africana.

O Anexo 2 aborda os resultados obtidos por meio da caracterização geoquímica e petrográfica de 30 amostras metamáficas da Zona Eclogítica de Forquilha (ZEF) e as implicações geotectônicas decorrentes. "Amaral, W.S., Santos, T.J.S., Wernick, E. 2010. **Occurrence and geochemistry of metamafic rocks from the Forquilha Eclogite Zone, central Ceará (NE Brazil): Geodynamic implications.** *(Special Issue) Geological Journal* (DOI: 10.1002/gj.1224).

No Anexo 3 são apresentados os resultados geocronológicos dos diversos métodos utilizados (Sm-Nd, U-Pb, Lu-Hf) para as rochas metamáficas e metassedimentares que compõem a Faixa Eclogítica de Forquilha: **Amaral, W.S., Santos, T.J.S., Dantas, E.L.** ***(In prep.)*** Sm-Nd and LA-MC-ICP-MS U-Pb, Lu-Hf zircon geochronology of high pressure rocks from the Forquilha Eclogite Zone, Borborema Province, NE-Brazil: an evidence for the break-up of Columbia supercontinent (*Em preparação)"*

No Anexo 4 são apresentados as descrições petrográficas, os gráficos de classificação mineral e os cálculos termobarométricos dos dados obtidos com microssonda eletrônica em rochas da região de Forquilha. Este anexo será transformado posteriormente em artigo e submetido a um periódico específico internacional.

5. SÍNTESE DAS DISCUSSÕES DOS ARTIGOS E CONCLUSÕES

O Anexo 1 aborda exclusivamente as relações de campo, e a caracterização petrográfica/termobarométrica e geocronológica dos granulitos e de suas encaixantes (granodioritos milonitizados) que ocorrem nos arredores de Cariré, situada na porção NW do Domínio Ceará Central.

A trama estrutural descrita em campo inclui a fase inicial de deformação contracional com vergência para NW, responsável pela exumação dos granulitos da infraestrutura, seguida da fase de transcorrências NE-SW em regime dúctil e prosseguindo em alguns casos em transtração e a subsequente colocação de granitos.

Os granulitos félsicos e máficos são constituídos, respectivamente, pelas paragêneses: hiperstênio + diopsídio + plagioclásio + quartzo ± hornblenda ± granada ± biotita e diopsídio + plagioclásio + granada + hornblenda ± quartzo ± rutilo. As condições de pressão e temperatura mais elevadas obtidas foram de 8,3 – 9,4 kbar e 804 – 870°C em granulitos félsicos e de 10,2 – 13,6 kbar e 750 – 910°C em granulitos máficos. Esses valores de P-T convergem no sentido de granulitos de alta pressão (O´Brien & Rötzler, 2003; Pattison, 2003). É debitada a falhas de empurrão de idade brasiliana a colocação dos granulitos nos granodioritos, configurando discordância local em termos de P-T.

Foram realizadas quatro análises U-Pb em zircão de dois granodioritos encaixantes e dois granulitos máficos. Também foram obtidas uma análise Lu-Hf em zircão do granulito máfico e cinco análises Sm-Nd, sendo três em granulitos máficos e duas em félsicos. Esses dados isotópicos, somados aos trabalhos anteriores, permitiram o reconhecimento de dois eventos magmáticos nesta faixa granulítica, sendo um mesoproterozóico e outro regional, paleoproterozóico, ambos com registro de metamorfismo neoproterozóico.

Dados U-Pb em zircão indicam idades de cristalização de 2044 e 2157 Ma nos granodioritos. Os granulitos félsicos também forneceram uma idade de cristalização paleoproterozóica em zircão de 2110 Ma (Fetter, 1999). Nos granulitos máficos foram obtidas duas idades concordantes em 590 e 613 Ma. Esses valores registrados em grãos de zircão arredondados, com textura *soccer ball*, e razões Th/U muito baixas (*ca*. 0,01-0,03) foram interpretados como sendo metamorfismo de alto grau. Não foi possível identificar a idade de cristalização dessas rochas uma vez que o metamorfismo de alta temperatura pode ter afetado e

reequilibrado o sistema isotópico do zircão. Idades de 587 e 573 Ma também foram registradas nos interceptos inferiores das concórdias dos granodioritos e granulitos félsicos (Fetter, 1999).

Idades T_{DM-Nd} e T_{DM-Hf} semelhantes (entre 1,28-1,61 Ga) e valores de ε_{Nd} e ε_{Hf} positivos sugerem que os granulitos máficos podem ter sido derivados de uma crosta juvenil mesoproterozóica. Por outro lado, as idades T_{DM-Nd} tanto dos granulitos félsicos quanto dos granodioritos apresentam valores próximos às idades de cristalização U-Pb (*ca.* 2200 Ma), o que, aliado a valores ε_{Nd+}, indica fonte mantélica paleoproterozóica para ambos.

No Anexo 2 são apresentados dados petrográficos e geoquímicos exclusivos da Faixa Eclogítica de Forquilha. Os resultados permitiram a individualização de três grupos de rochas: granada anfibolitos, retroeclogitos e granada clinopiroxênio anfibolitos.

O grupo 1 apresenta padrão de Elementos Terras Raras normalizado $(ETR)_N$ relativamente plano, porém o segmento $(La\text{-}Nd)_N$ tem tendência levemente decrescente, oposta ao do padrão N-MORB. Somente neste grupo ocorrem rochas mais evoluídas – andesitos. O padrão $(SPIDER)_N$ contém anomalias negativas, principalmente de Rb, Th, Nb, Zr e Ta. As anomalias de Nb são mais acentuadas em relação aos padrões N-MORB e da Crosta Máfica Inferior. Variações nos teores de Eu e Sr sugerem processos discretos de acúmulo ou fracionamento de plagioclásio. A baixa relação Nb/La é típica para este grupo. Assim, os dados indicaram similaridades das rochas desse grupo com basaltos de arco de ilha, tipo IAT. Essa hipótese é corroborada pelos diagramas Ti/1000 vs. V, Sr/Ce vs. Sm/Ce e Y-La-Nb (Figura 8 - Anexo2).

O estreito padrão $(ETR)_N$ do grupo 2 é plano, parecido com o grupo 1, no entanto são ausentes as anomalias de Eu. É caracterizado também por baixas e variáveis relações Nb/La típica entre N- e T-MORB. Além disso, as rochas desse grupo apresentam as maiores razões Zr/Nb (15-22) e valores de Tb/Ta próximos aos do manto primitivo. O padrão $(SPIDER)_N$ contém anomalias positivas de Ba, Ta e Sr e negativas de Rb e P. As razões $(La/Yb)_N$ variam entre 1,38 e 3,06. Deste modo, as características geoquímicas dos retroeclogitos deste grupo são compatíveis com basaltos de cadeia meso-oceânica ou *back-arc* de arcos intra-oceânicos. Esta correlação é também suportada por numerosos diagramas, tais como Zr vs. Y, Nb/Yb vs. Th/Yb, Ti/1000 vs. V, La/Yb vs. Th/Ta (Figura 7 - Anexo 2).

O terceiro grupo apresenta o padrão $(ETR)_N$ mais inclinado, com razão $(La/Yb)_N$ entre 2,63 e 7,32, o que sugere leve fracionamento. Trata-se do grupo geoquimicamente mais enriquecido em termos de álcalis e elementos traços incompatíveis, ambos semelhantes a basaltos alcalinos. A razão Nb/Yb vs. Th/Yb situa essas rochas nas proximidades do padrão E-MORB, feição suportada por altos valores de Nb (8,10-24,50 ppm). No padrão $(SPIDER)_N$ ressaltam anomalias negativas pronunciadas de Ba e Sr. Diversos diagramas mostram indícios evidentes de fracionamento, como indicam as baixas razões Zr/Nb, K/Ba e Y/Nb. Muitas feições geoquímicas são compatíveis com rochas alcalinas tipo *ocean island basalts* (OIB), plumas ou basaltos continentais enriquecidos. Essa diversidade de vinculação geotectônica é observada também nos diagramas Nb/Yb vs. Th/Yb, La/Yb vs. Th/Ta e Y-La-Nb (Figura 8 - Anexo2).

Assim, as principais conclusões do artigo indicam a vinculação petrológica/geoquímica das rochas metamáficas de Forquilha com crosta oceânica, geradas respectivamente em ambientes tectônicos de arco intra-oceânico, dorsal meso-oceânica ou *back-arc* e basaltos alcalino-continentais.

O Anexo 3 é apresentado na forma de um artigo em fase final de preparação no qual constam os resultados geocronológicos das análises U-Pb e Lu-Hf em zircão e monazita de seis rochas metamáficas e quatro metassedimentares. Também são apresentados e discutidos os resultados das análises de dezoito amostras pelo método Sm-Nd em rocha total, sendo quatro de granada anfibolitos, treze de clinopiroxênio-granada anfibolitos (retroeclogitos) e uma de rocha cálcio-silicática. Todas as amostras foram coletadas ao longo da Faixa Eclogítica de Forquilha (FEF).

Os dados isotópicos obtidos permitiram a individualização de, pelo menos, dois importantes eventos ainda pouco conhecidos no Domínio Ceará Central, sendo um mesoproterozóico, registrado nas rochas metamáficas, e outro neoproterozóico, correlato ao metamorfismo de alto grau. O intervalo entre 2,0 e 2,2 Ga corresponde às principais fontes do zircão das sequências paraderivadas que ocorrem ao longo da FEF. O intervalo de idades Riaciano/Orosiriano é bem conhecido em todo DCC e representa a formação do embasamento paleoproterozóico deste domínio, juvenil em maior parte, mas com importantes indícios da presença de rochas arqueanas retrabalhadas (Fetter *et al.,* 2000; Castro, 2004; Arthaud, 2008; Martins *et al.,* 2009, Torres *et al.,* 2010).

Os principais resultados U-Pb, Lu-Hf e Sm-Nd estão sumarizados na Tabela 1.

Tabela 1: Síntese das principais idades obtidas por diferentes métodos

Amostra	*Litotipo*	*Idade (Ma)* Cristalizacão*	*Idade (Ga)* Proveniência*	*Idade (Ma)* Metamórfica*	*T_{DM}Hf* (Ga)*	*εHf*	*T_{DM}Nd (Ga)*	*εNd*
Rochas metamáficas								
WT7-25	Cpx-Grt Anfibolito	1566 ± 8,8	-	-	~1,57	+7,46/+9,63	-	-
WT8-12F	Cpx-Grt Anfibolito	1546 ± 37	-	-	-	-	1,60	+4,11
WT8-53E	Retroeclogito	1559 ± 70	-	-	-	-	-	-
WT8-53X	Banda félsica retroeclogito	1615 ± 40	-	-	-	-	-	-
TJF6-302	Retroeclogito	1455 ± 120	-	-	-	-	-	-
TJF6-335	Retroeclogito	-	-	614,9 ± 3,9	-	-	1,79	-
Rochas metassedimentares								
WT8-53M	Kinzigito	-	~2,1 Ga	-	-	-	-	-
WT8-53L	Kinzigito	-	~2,0 Ga	639 ± 10	-	-	-	-
WT7-21B	Sill-Grt Gnaisse	-	~2,2 Ga	-	-	-	-	-
TJF4-7	Calcio-silicatica	-	~2,1 Ga	650 ± 2.5	~2,44	-	2,24	-

** Idades obtidas em zircão*

As idades mesoproterozóicas (1566-1455 Ga) obtidas em núcleos de zircão prismáticos correspondem ao intercepto superior de quatro amostras metamáficas coletadas ao longo da FEF. Idades modelo obtidas pelo método Lu-Hf nos mesmos grãos de zircão (amostra WT7-25), forneceram $T_{DM\text{-}Hf}$ entre 1570 e 1810 Ma com valores de ε_{Hf} (t=1566 Ma) positivos, variando entre+7,46 e +9,63. Valores de Sm-Nd em rocha total forneceram $T_{DM\text{-}Nd}$ entre 1,57 e 2,28, com valores de ε_{Nd} (t=1566 Ma) também positivos, variando entre +4,08 e +4,11. Esses valores sugerem uma fonte a partir de magma juvenil. Os resultados geocronológicos também se coadunam coerentemente com os dados geoquímicos que demonstram afinidade N-T-MORB para o protólito dessas rochas gerados em ambientes extensionais (Anexo 2).

A idade do metamorfismo de mais alto grau (fácies eclogito) foi determinada em duas populações de zircão presentes em rochas paraderivadas de alto grau metamórfico (amostras WT8-53ML e TJF4-7). As idades obtidas para esse evento foram de 639 ± 10 Ma e 650 ± 2,5 Ma, respectivamente. Os cristais de zircão que definiram essas idades foram visivelmente modificados durante o evento metamórfico. No caso do sillimanita gnaisse (WT8-53ML), os

grãos apresentam núcleo interno de origem ígnea e borda de sobrecrescimento bem definida, sobre os quais foram direcionadas as análises pontuais. A rocha cálcio-silicática (TJF4-7) apresentou, ao menos, duas populações de zircão bem definidas, sendo uma euedral em *ca.* 2,1 Ga e outra arredondada *ca.* 0,65 Ga.

Idades modelo obtidas pelo método Lu-Hf nos mesmos cristais analisados pelo método U-Pb, foram calculadas para os grãos concordantes neoproterozóicos e paleoproterozóicos. Os primeiros apresentaram T_{DMHf} entre 2,44 e 2,62 Ga com valores de ε_{Hf} (t=650 Ma), negativos, variando entre -17,91 e -21,36, indicando metamorfismo. Os cristais de zircão paleoproterozóicos definiram T_{DMHf} entre 1,92 e 2,45 Ga com valores de ε_{Hf} (t=2100 Ma) positivos, variando entre +1,39 e +10,88.

Cristais de zircão límpidos, levemente arredondados, inferiores ao tamanho médio de 100 µm e com baixa razão Th/U (<0.03) encontrados nas rochas metamáficas (TJF6-335 e WT7-3A) são típicos de rochas granulíticas de alta pressão (Corfu *et al.,* 2003). As idades de 614 ± 3,9 Ma e 612,9 ± 3,3 Ma obtidas em retroeclogitos do setor sul da FEF e em granulitos máficos da região de Cariré (Anexo 1), respectivamente, são interpretadas como o registro metamórfico de alta temperatura (Fácies granulito) caracterizado principalmente nas rochas metamáficas das duas áreas investigadas.

6. EVOLUÇÃO GEODINÂMICA DO DOMÍNIO CEARÁ CENTRAL

A partir dos dados gerados nesta Tese e das referências disponíveis na literatura, propõem-se a seguinte evolução geológica para o Domínio Ceará Central e adjacências (Figura 5):

A) ESTÁGIO RIFTE (1,60-1,50 Ga): Dados geocronológicos e paleomagnéticos sustentam a teoria do supercontinente Paleo-Mesoproterozóico Colúmbia (1,9-1,6 Ga) que teria existido antes da amalgamação de Rodínia (Rogers & Santosh, 2002). Sua fragmentação teve início *ca.* 1,6 Ga, com rifteamentos seguidos de enxames de diques no norte da China, Zimbabwe, África do Sul, Austrália e América do Norte (Rogers & Santosh, 2002; Zhao *et al.,* 2004, Ernst *et al.,* 2008, Rogers and Santosh, 2009). No Brasil, no sul do Cráton Amazônico, são encontrados nas faixas Rio Negro-Juruena e Rondoniana-San Ignácio diversos pulsos anorogênicos e sequências de

rochas supracrustais máficas com idades ao redor de 1,5 Ga (Bettencourt *et al.* 1999, Matos *et al.,* 2004, Ruiz *et al.* 2004, Santos *et al.* 2008). No DCC, as rochas do final do Paleoproterozóico, ao redor de 1,8 Ga, estão relacionadas ao vulcanismo bimodal da faixa Orós (Sá *et al.*, 1997) e metariolitos da região de Bixopá e Itaiçaba (Cavalcante, 1999). Em zircão de sequências metassedimentares do Complexo Ceará, na região de Itatira, Arthaud (2008) obteve idades ao redor de 1,56 Ga. Este autor atribuiu como área fonte a Faixa Transversal da Província Borborema, onde é conhecido no terreno Rio Capibaribe a suíte gabro-anortosítica e granítica estateriana-calimiana com idades variando entre 1,6 e 1,7 Ga, e o granito anorogênico da Serra de Taquaritinga com idade de 1,52 Ga (Sá *et al.* 1997; Santos *et al.* 2009). Para a faixa de alta pressão de Forquilha, quatro amostras de rochas metamáficas forneceram idades U-Pb em zircão entre 1455 e 1615 Ma. Idades modelo obtidas pelo método Lu-Hf em zircão de um clinopiroxênio-granada anfibolito (WT7-25), forneceram $T_{DM(Hf)}$ entre 1570 e 1810 Ma, com valores de ε_{Hf} (t=1566 Ma) positivos, variando entre +7,46 e +9,63. Análises Sm-Nd em rocha total foram realizadas no intuito de comprovar a idade de extração mantélica dessas rochas. Embora muitas amostras não tenham fornecido resultados satisfatórios com a aplicação do método Sm-Nd, foram obtidos $T_{DM(Nd)}$ entre 1,57 e 1,61 Ga e valores de ε_{Nd} (t=1566 Ma) positivos variando entre + 4,08 e + 4,11. Esses valores são bem coerentes com os resultados obtidos pelos métodos U-Pb e Lu-Hf, confirmando a existência de rochas metamáficas com idades de cristalização mesoproterozóicas e derivação mantélica juvenil no DCC. Além dos dados isotópicos, dados geoquímicos detalhados no Anexo II, mostram que parte das rochas metamáficas possui assinatura de crosta oceânica gerada em ambientes extensionais.

B) ESTÁGIO PRÉ-COLISIONAL (800-660 Ma?): Não há, por enquanto, registro da Orogênese Greenviliana na porção norte da Província Borborema, consequentemente não é possível determinar com precisão os eventos tectônicos que atuaram no intervalo entre 1400 e 800 Ma. Diversos estágios de acresção e tafrogênese podem ter ocorrido neste intervalo, porém ainda não foram descritos. Por outro lado, o registro da orogenia Brasiliana é evidente em toda província. Com base em dados geoquímicos e isotópicos Fetter *et al.* (2003) interpretam o funcionamento do arco magmático de Santa Quitéria (AMSQ) no período entre 660-610 Ma. Entretanto, outros autores propõem um estágio pré-colisional associado a magmatismo juvenil com $\varepsilon_{Nd\ WR}$ (t=795) positivo +4,4 do tipo Andino ao redor de 800 Ma. Esses dados foram

registrados em zircão de ortognaisses metaluminosos de composição granodiorítica nas adjacências do AMSQ e em rochas metassedimentares do Complexo Ceará (de Araújo *et al.,* 2010b, Torres *et al.,* 2010). Este magmatismo também poderia representar o registro de um arco intra-oceânico (Amaral *et al.,* 2010a – Anexo 2) semelhante à evolução da faixa Brasília (Pimentel & Fuck, 1992) ou em Mali na África Central (Caby, 2003). Outros autores propõem a existência de um período extensional *ca.* 750 Ma, com base em datações U-Pb em zircão de metarriolitos (Fetter, 1999; Castro, 2004) e um único zircão em um granada anfibolito (Arthaud, 2008) na borda leste do AMSQ. Esses dados podem ser perfeitamente correlacionados à instalação de bacias marginais (*e.g.*retro-arco) com magmatismo bimodal nas adjacências do arco durante a sua evolução.

C) ESTÁGIO (CEDO) SIN-COLISIONAL (650-630 Ma): Período do início da colisão continental entre os domínios Médio Coreaú (2,3 Ga) e Ceará Central (2,1 Ga), registrado pelo metamorfismo de mais alta pressão (fácies eclogito). As idades obtidas no intervalo entre 650 e 630 Ma constituem o registro do metamorfismo mais antigo do Domínio Ceará Central. Na contraparte africana, na Província do Hoggar, idades U-Pb em zircão de batólitos cálcio-alcalinos (*Iskel magmatic arc*) sugerem que a subducção teve início em *ca.* 680 Ma (Caby, 2003). Na faixa Dahomeyides, os eclogitos Lato Hills estão situados no intervalo entre 650 e 595 Ma (Bernard-Griffiths *et al.,* 1991). A partir de análises U-Pb em granitóides do arco AMSQ, Fetter *et al.* (2003) definiram o intervalo entre 640 e 620 Ma como sendo o período do início da subducção com polaridade para sudeste. Por outro lado, a partir de determinações U-Pb convencional e U-Th-Pb em monazita e zircão de retroeclogitos paraderivados da região de Madalena e Itataia-CE, Castro (2004), definiu o intervalo entre *ca.* 640-630 Ma como sendo o período de desenvolvimento dos processos de subducção e metamorfismo até a fácies eclogito, registrado tanto nas sequências paraderivadas quanto nos granitóides mais antigos do arco magmático de Santa Quitéria. Para a Faixa Eclogítica de Forquilha, determinações U-Pb em zircão de duas rochas paraderivadas, sillimanita gnaisse e cálcio-silicática (WT8-53ML e TJF4-7, respectivamente), forneceram idades concordantes em 639 ± 10 Ma e 650 ± 2.5 Ma, respectivamente. Também nesta mesma Faixa, dados inéditos de Ancelmi *et al.,* (*submitted*) mostram idades U-Pb em grãos de zircão concordantes com baixas razões Th/U (0,00-0,03) ao

redor de 650 Ma, obtidas em duas amostras de alto grau metamórfico, um sillimanita-granada gnaisse e um cianita-granada gnaisse.

D) ESTÁGIO (TARDI) SIN-COLISIONAL (620-580 Ma): Para o grande pulso do magmatismo do AMSQ, Costa *et al.* (2010) propõem o modelo de *Slab Breakoff* (Davies & Blanckenburg, 1995), que causa a ruptura de parte da crosta oceânica e facilita desta maneira a ascensão da astenosfera, podendo causar distúrbio no manto litosférico sobrejacente e então produzir magmas ricos em potássio.Consequentemente, atua o metamorfismo de alta temperatura (fácies granulito) acompanhado da fusão parcial das rochas da base do AMSQ e a geração de migmatitos e diatexitos. Além disso, tem início a rápida exumação das rochas de alto grau metamórfico por falhamentos reversos, gerando as texturas de descompressão descritas nos retroeclogitos e nos granulitos máficos. Este estágio é bem registrado nas rochas granulíticas de Cariré (~613 Ma) e Forquilha (~615 Ma).

E) ESTÁGIO PÓS-COLISIONAL (580-480 Ma): Por fim, tem-se o período de instalação das principais zonas de cisalhamento transcorrentes (Monié *et al.* 1997; Fetter, 1999, Fetter *et al.,* 2003, Cunha, 2007) e a colocação da granitogênese pós-colisional (Plútons Meruoca, Mucambo, Serra da Barriga, Pajé e Taperuaba) (Fetter, 1999, Castro, 2004, Teixeira, 2005).

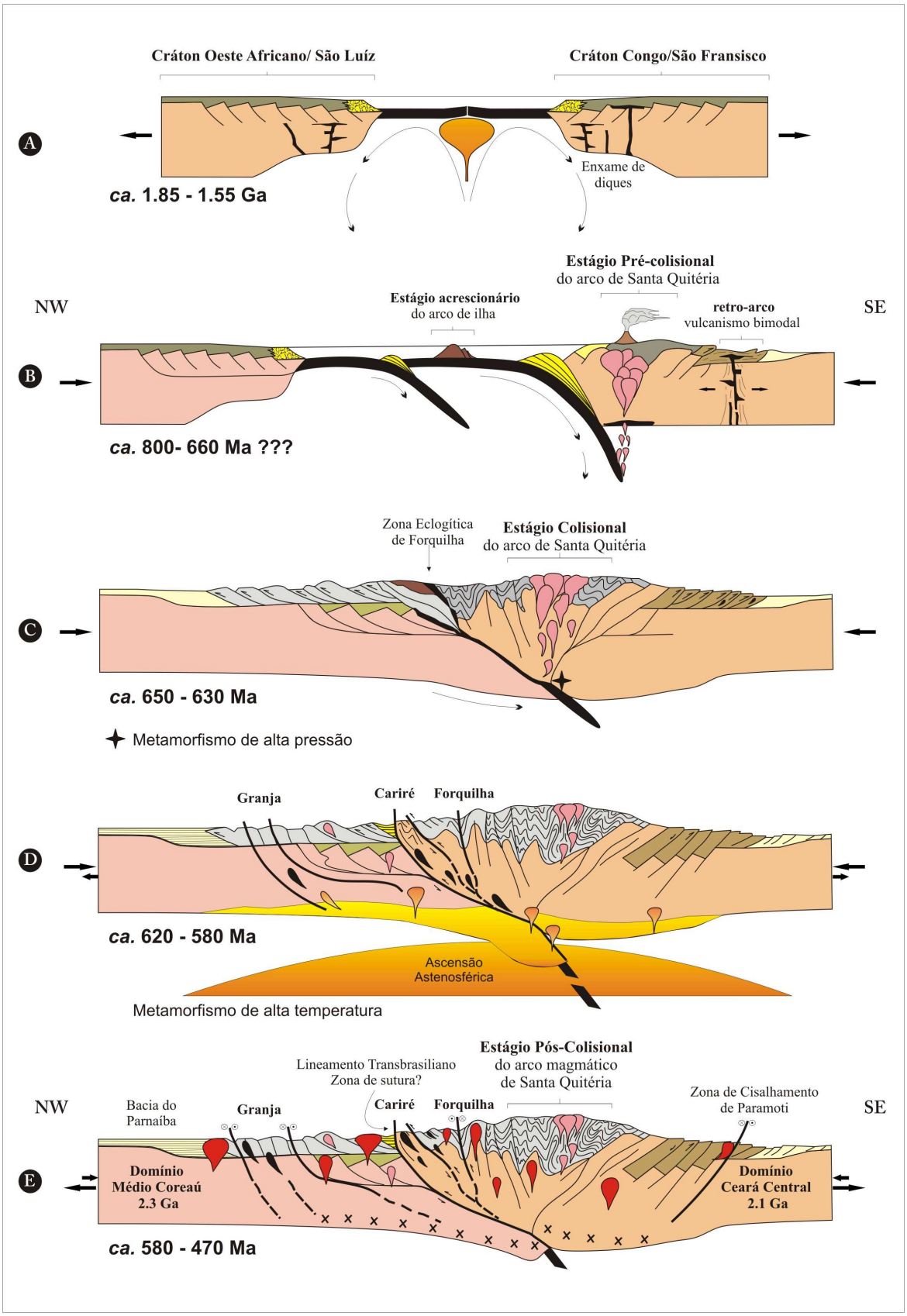

Figura 5: Modelo tectônico da evolução geodinâmica do Domínio Ceará Central.

7. REFERÊNCIAS BIBLIOGRÁFICAS

Affaton, P., Sougy, J., Trompette, R. 1980. The tectono-stratigraphic relationships between the Upper Precambrian and Lower Paleozoic Volta basin and the Pan African Dahomeyide orogenic belt (West Africa). *American Journal of Science,* **280:** 224-248.

Agbossoumondé, Y., Guillot, S., Menot, R.P. 2004. Pan-African subduction–collision event evidenced by high-P coronas in metanorites from the Agou massif (southern Togo) *Precambrian Research,* **135:** 1-21.

Almeida, F.F.M. 1977. *O Cráton do São Francisco*. *Revista Brasileira de Geociências,* **7:** 349-364.

Almeida, F.F.M., Hasui, Y., Brito Neves, B.B., Fuck, R.A. 1981. Brazilian Structural Provinces: an introduction. *Earth Sciences Reviews,* 17**:** 1-29.

Amaral, W.S., Santos, T.J.S. 2008. Airborne geophysical and tectonics of the Ceará Central Domain, eastern region of the Santa Quitéria magmatic arc, Borborema Province, NE Brazil. *Brazilian Journal of Geophysics,* **26:** 527-542.

Amaral, W.S., Nogueira Neto, J.A., Santos, T.J.S., Fetter, A.H., Arthaud, M.H. 2008. Faixa Granulítica de Cariré, Domínio Ceará Central (DCC): Idades Modelo Sm-Nd, Lu-Hf e U-Pb (zircões) e Contexto Geológico. *44° Congresso Brasileiro de Geologia*, Curitiba PR.

Amaral, W.S., Santos, T. J. S., Wernick, E. 2010a. Occurrence and geochemistry of metamafic rocks from the Forquilha Eclogite Zone, central Ceará NE Brazil: Geodynamic implications. *Geological Journal* (DOI: 10.1002/gj.1224).

Amaral, W. S. ; Santos, T. J. S. ; Wernick, E. ; Nogueira Neto, J. A. ; Matteini, M. ; Dantas, E. L. 2010b. Gênese e evolução dos granulitos de Cariré - NW do Domínio Ceará Central, Província Borborema. *45° Congresso Brasileiro de Geologia,* Belém-PA.

Amaral, W. S. ; Santos, T. J. S. ; Wernick, E. ; Matteini, M. ; Dantas, E. L. ; Moreto, C. P. N. 2010c. U-Pb, Lu-Hf and Sm-Nd geochronology of rocks from the Forquilha Eclogite Zone, Ceará Central Domain, Borborema Province, NE-Brazil. *VII-SSAGI South American Symposium on Isotope Geology,* Brasília-DF (CD-ROM).

Ancelmi, M.F., Santos, T.J.S., Amaral, W.S., Dantas, E.L. (Submetido) Sediment provenance based on detrital zircon of the metasedimentary country rocks of the retrograded eclogites of Forquilha - CE, NW Borborema Province. *Journal of south America* (submitted).

Arthaud, M.H. 2008. Evolução neoproterozóica do Grupo Ceará (Domínio Ceará Central, NE Brasil): da sedimentação à colisão continental brasiliana. Tese de Doutorado, Instituto de Geociências, Universidade de Brasília, Brasil.

Arthaud, M.H., Caby, R., Fuck, R.A., Dantas, E.L., Parente, C.V. 2008. Geology of the northern Borborema Province, NE Brazil and its correlation with Nigeria, NW Africa. In: *West Gondwana: Pre-Cenozoic Correlations Across the South Atlantic Region*, Pankhurst, R.J., Trouw, R.A.J., Brito Neves, B.B., de Wit, M.J. (eds). Geological Society of London, Special Publications, **294:** 49-67.

Bernard-Griffiths, J., Peucat, J.J., Menot, R.P. 1991. Isotopic (Rb-Sr, U-Pb and Sm-Nd) and trace element geochemistry of eclogites from the Pan-African belt: a case study of REE fractionation during high-grade metamorphism. *Lithos,* **27:** 43-57.

Bettencourt, J.S., Tosdal R.M., Leite Jr, W.R., Payolla, B.L. 1999. Mesoproterozoic rapakivi granites of Rondônia Tin Province, southwestern border of Amazonian craton, Brazil-I: Reconnaissance U-Pb geochronology and regional implications. *Precambrian Research,* **95:** 41-67.

Brito Neves, B. B., Cordani, U.G. 1991. Tectonic evolution of South America during the Late Proterozoic. *Precambrian Research,* **53**: 23-40.

Brito Neves, B. B., Schmus, W. R.V., Santos, E. J., Campos Neto, M. C., Kozuch, M. 1995. O Evento Cariris Velhos na Província Borborema: integração de dados, implicações e perspectivas. *Revista Brasileira de Geociências,* **25:** 279-296.

Brito Neves, B.B., Santos, E.J., Van Schmus, W.R. 2000. Tectonic history of the Borborema Province, northeastern Brazil. In: *Tectonic Evolution of South America, 31st International Geological Congress,* Cordani, U., Milani, E.J., Thomaz Filho, A., Campos, D.A. (eds). Rio de Janeiro, Brazil, 151-182.

Brito Neves, B.B., Passareli, C.R, Basei, A.A.S. & Santos E.J. 2003. U-Pb age of some classic granites of the Borborema Province. IV South American Symposium of Isotope Geology, Salvador, Brazil, 158-159.

Caby, R. 2003. Terrane assembly and geodynamic evolution of centralwestern Hoggar: a synthesis. Journal of African Earth Sciences, **37:** 133-159.

Caby, R., Arthaud, M.H. 1986. Major Precambrian nappes of the Brazilian Belt. Ceará, Northeast Brazil. *Geology,* **14:** 871-874.

Castaing, C., Thiéblemont, C., Triboulet, C., Chevremont, P. 1994. Paleogeographical reconstructions of the Pan-Africano/Brasiliano Orogen: closure of an oceanic domain or intracontinental convergence between major blocks? *Precambrian Research,* **69:** 327-344.

Castro, N.A. 2004. *Evolução geológica proterozóica da região entre Madalena e Taperuaba, domínio tectônico Ceará Central (Província Borborema).* Tese de Doutorado, Universidade de São Paulo, Brasil.

Castro, N. A., Basei, M.A.S., Campos Neto, M.C. 2004. Geocronologia e evolução tectônica Proterozóica do Domínio Ceará Central (Região entre Madalena e Taperuaba, Província Borborema, NE do Brasil). *Simpósio de 40 Anos de Geocronologia no Brasil*, USP-São Paulo, 74.

Cavalcante, J.C. 1999. Limites e evolução geodinâmica do Sistema Jaguaribeano, Província Borborema, Nordeste do Brasil. Dissertação de Mestrado, Universidade Federal do rio Grande do Norte.

Cavalcante, J.C., Vasconcelos, A.M., Medeiros, M.F., Paiva, I.P., Gomes, F.E.M., Cavalcante, S.N.,Cavalcante, J.E., Melo, A.C.R., Duarte Neto, V.C. & Benevides, H.C. 2003. *Mapa Geológico do Estado do Ceará – Escala 1:500.000*. Fortaleza, Ministério das Minas e Energia, CPRM.

Corfu, F., Hanchar, J. M., Hoskin, P. W. O., Kinny, P. D. 2003. An atlas of zircon textures. *In Zircon.* (eds. J. M. Hanchar and P. W. O. Hoskin) In: *Reviews of Mineralogy and Geochemistry* **53,** Mineralogical Society of America, Washington, D.C. 469-500.

Costa, F.G., de Araújo, C.E.G, Vasconcelos, A.M., Palheta, E.S.M, Justo, A.P. 2010. O Complexo Tamboril-Santa Quitéria: evidências de s*lab breakoff* durante colisão continental neoproterozóica, norte da Província Borborema. *45° Congresso Brasileiro de Geologia,* Belém-PA (CD-ROM).

Cunha, F.S.S. 2007. Condicionamento Estrutural das zonas de cislhamento da região de Forquilha, Domínio Ceará Central: uma abordagem integrada de sensoriamento remoto e geologia estrutural. Tese de Doutorado, Centro de Ciências exatas e da Terra, UFRN.

Dantas, E.L., Hackspacher, P.C., Van Schmus, W.R., Brito Neves, B.B. 1998. Archean accretion in the São José do Campestre Massif, Borborema Province, Northeast Brazil. *Revista Brasileira de Geociências*, **28:** 221-228.

Dantas, E.L., Van Schmus, W.R., Hackspacher, P.C, Fetter, A.H., Brito Neves, B.B., Cordani, U., Nutman, A.P., Williams, I.S. 2004. The 3.4-3.5 Ga São José do Campestre massif, NE Brazil: remnants of the oldest crust in South America. *Precambrian Research,* **130:** 113-137.

Davies, J.H. & Von Blanckenburg, F. 1995. Slab breakoff: a model of lithosphere detachment and its test in the magmatism and deformation of collisional orogens. *Earth Planetary Science Letters*, **129:** 85 102.

de Araújo, C.E.G, Píneo, T.R.G, Caby, R., Costa, F.G., Cavalcante, J.C., Vasconcelos, A.M., Rodrigues, J.B. 2010a. Provenance of the Novo Oriente Group, southwestern Ceará Central Domain, Borborema Province (NE-Brazil): A dismembered segment of a magma-poor passive margin or a restricted rift-related basin? *Gondwana Research* **6**: 265-273.

de Araújo, C.E.G, Píneo, T.R.G, Costa, F.G., Palheta, E.S.M., Cavalcante, J.C., Vasconcelos, A.M., Moura, C.A.V. 2010b. $^{207}Pb/^{206}Pb$ Zircon ages of pre- and syn-collisional granitoids from the Tamboril-Santa Quitéria granitic-migmatitic complex, Ceará Central Domain, Borborema Province (NE Brazil): geodynamic implications. *VII-SSAGI South American Symposium on Isotope Geology,* Brasília-DF (CD-ROM)

de Wit, M. J., Stankiewicz, J., Reeves, C. 2008. Restoring Pan-African–Brasiliano connections: more Gondwana control, less Trans-Atlantic corruption. In: *West Gondwana: Pre-Cenozoic Correlations Across the South Atlantic Region*, Pankhurst, R.J., Trouw, R.A.J., Brito Neves, B.B., de Wit, M.J. (eds). Geological Society of London, Special Publications, **294:** 399-412.

Duclaux, G., Ménot, R.P., Guillot, S., Agbossoumondé, Y., Hilairet, N. 2006. The mafic layered complex of the Kabyé massif (north Togo and north Benin): Evidence of a Pan-African granulitic continental arc root. *Precambrian Research,* **151:** 101-118.

El-Hadj, T., Affaton, P., Louis, P., Socohou, A. 1997. Gravity characteristics of the Pan-African Orogen in Ghana, Togo and Benin (West Africa). *Journal of African Earth Sciences,* **24:** 241-258.

Ernst R.E., Wingate M.T.D., Buchan K.L., Li Z.X. 2008. Global record of 1600–700 Ma Large Igneous Provinces (LIPs): Implications for the reconstruction of the proposed Nuna (Columbia) and Rodinia supercontinents. *Precambrian Research*, **160**: 159-178.

Fetter, A.H. 1999. U–Pb and Sm–Nd Geochronological constraints on the crustal framework and geological history of Ceará State, NW Borborema Province, NE Brazil: implications for the assembly of Gondwana. Ph.D. Thesis, University of Kansas.

Fetter, A,H,, Van Schmus, W.R., Santos, T.J.S., Arthaud, M.H., Nogueira, Neto J.A. 2000. U–Pb and Sm–Nd geochronological constraints on the crustal evolution and basement architecture of Ceará State, NW Borborema Province, NE Brazil: implications for the existence of the Paleoproterozoic supercontinent "Atlantica". *Revista Brasileira de Geociências,* **30:** 102-106.

Fetter, A.H., Santos, T.J.S., Van Schmus, W.R., Hackspacher, P.C., Brito Neves, B.B., Arthaud, M.H., Nogueira Neto, J.A., Wernick, E. 2003. Evidence for Neoproterozoic continental arc magmatism in the Santa Quitéria batholith of Ceará State, NW Borborema Province, NE Brazil: implications for assembly of West Gondwana. *Gondwana Research,* **6:** 265-273.

Garcia, M.G.M., Arthaud, M.H. 2004. Caracterização de trajetória P–T em *nappes* brasilianas: região de Boa Viagem/Madalena – Ceará Central (NE Brasil). *Revista de Geologia*, *Universidade Federal do Ceará*, **17:** 173-191.

Hackspacher, P.C., Van Schmus, W.R., Dantas, E.L. 1990. Um embasamento Transamazônico na Província Borborema. 36° Congresso Brasileiro de Geologia, Natal RN, 2683-2696.

Lesquer, A., Beltrão, J.F., Abreu, F.A.M. 1984. Proterozoic links between northeastern Brazil and West Africa: a plate tectonic model based on gravity data. *Tectonophysics,* **110:** 9-26.

Martins, G. 2000. Litogeoquímica e controles geocronológicos da Suíte Metamórfica Algodões - Choró. Tese de Doutorado, Instituto de Geociências - UNICAMP, Brasil.

Martins, G., Oliveira, E.P., Lafon, J.M. 2009. The Algodões amphibolite–tonalite gneiss sequence, Borborema Province, NE Brazil: geochemical and geochronological evidence for Palaeoproterozoic accretion of oceanic plateau/back-arc basalts and adakitic plutons. *Gondwana Research,* **15:** 71-85.

Matos, J.B., Schorscher, J.H.D., Geraldes, M.C., Souza, M.Z.A., Ruiz, A.S. 2004. Petrografia, geoquímica e geocronologia das rochas do orógeno Rio Alegre, Mato Grosso: um registro de crosta oceânica Mesoproterozóica no SW do Craton Amazônico. *Geologia USP (Revista do Instituto de Geociências-USP)*. Série Científica. **4:** 75-90.

Monié, P., Caby, R., Arthaud, M.H. 1997. The Neoproterozoic Brasiliano Orogeny in Northeast Brazil: $^{40}Ar/^{39}Ar$ and petrostructural data from Ceará, *Precambrian Research,* **81:** 241-264.

Neves, S.P., Bruguier, O., Silva, J.M.R., Bosch, D., Alcantara, V.C., Lima, C.M. 2009. The age distribuitions of detrital zircons in metassedimentary sequences in eastern Borborema Province (NE Brazil): Evidence for intracontinental sedimentation and orogenesis? *Precambrian Research*, **175:** 187-205.

Nogueira Neto, J.A. 2000. Evolução Geodinâmica das faixas granulíticas de granja e cariré, extremo noroeste da Província Borborema. PhD. Thesis Universidade Estadual Paulista-UNESP 171.

O'Brien, P.J, Rötzler, J. 2003. High-pressure granulites: formation, recovery of peak conditions and implications for tectonics. *Journal of Metamorphic Geology*, **21:** 3-20.

Oliveira, E.P., Toteu, S.F., Araújo, M.N.C., Carvalho, M.J., Nascimento, R.S., Bueno, J.F., McNaughton, N., Basilici, G. 2006. Geologic correlation between the Neoproterozoic Sergipano belt (NE Brazil) and the Yaoundé belt (Cameroon, Africa). *Journal of African Earth Science,* **44**: 470–478.

Paixão, M.A.P., Nilson, A.A., Dantas, E.L. 2008. The Neoproterozoic Quatipuru ophiolite and the Araguaia fold belt, central-northern Brazil, compared with correlatives in NW Africa. In: *West Gondwana: Pre-Cenozoic Correlations Across the South Atlantic Region*, Pankhurst, R.J., Trouw, R.A.J., Brito Neves, B.B., de Wit, M.J. (eds). Geological Society of London, Special Publications, **294:** 297-318.

Pattison, D. R. M., 2003. Petrogenetic significance of orthopyroxene-free garnet +clinopyroxene + plagioclase-bearing metabasites with respect to the amphibolite and granulite facies. *Journal of Metamorphic Geology*, **21:** 21-31.

Pedrosa-Soares, A.C., Noce, C.M., Wiedemann, C.M., Pinto, C.P. 2001. The Araçuaí–West Congo orogen in Brazil: An overview of a confined orogen formed during Gondwanland assembly.*Precambrian Research*, **110**: 307-323.

Pimentel, M.M., Fuck, R.A. 1992. Neoproterozoic crustal accretion in central Brazil. *Geology,* **20**: 375-379.

Rogers, J.J.W., Santosh, M. 2002. Configuration of Columbia, a Mesoproterozoic supercontinent. *Gondwana Research,* **5:** 5-22.

Rogers, J.J.W., Santosh, M. 2009. Tectonics and surface effects of the supercontinent Columbia. *Gondwana Research,* **15:** 373-380.

Ruiz, A.S., Geraldes, M.C., Matos, J.B., Teixeira, W., Van Schumus, W.R., Schmitt, R.S. 2004. 1590-1520 Ma Cachoeirinha magmatic arc and its tectonic implications for the Mesoproterozoic SW Amazonian craton crustal evolution. *Anais da Acadêmia Brasileira de Ciências*, **76:** 807-824.

Sá, J.M.; Bertrand, J.M.; Leterrier, J. 1997. Geocronologia U-Pb e geoquímica de ortognaisses Paleo e Mesoproterozóicos da região de Taquaritinga-PE. In: *SBG, Simpósio de Geologia do Nordeste*, **17**. Fortaleza-CE, resumos expandidos, 108-112.

Santos, E.J., Schmus, W.R.V., Kozuch, M.,Brito Neves, B.B. 2010. The Cariris Velho tectonic event in Northeast Brazil. *Journal of South American Earth Sciences,* **29:** 61-76.

Santos, T.J.S.; Santos, A. A.; Dantas, E.L.; Fuck, R.A.; Parente, C.V. 2003. Nd Isotopes and the provenance of metassediments of the Itataia Group, northwest Borborema Province, NE Brazil. *IV Symposium on South American Isotope Geology,* Salvador, Brazil (CD-ROM).

Santos, T.J.S, Fetter, A.H, Hackspacher, P.C., Schmus, W.R.V., Nogueira Neto, JA. 2004. Structural and geochronological studies of the Médio Coreaú Domain, NE Brazil: Constraints on Brasiliano/Pan-African tectonic evolution in the NW part of the Borborema Province. *Journal of the Virtual Explorer* (Online) **17** xx.

Santos, T.J.S., Fetter, A.H., Nogueira Neto, J.A. 2008b. Correlation of the West margin of the Transbrasiliano – Kandi Lineament in the Borborema Province (NE Brazil) and Pharusian Belt (NW Africa). In: *West Gondwana: Pre-Cenozoic Correlations Across the South Atlantic Region*, Pankhurst, R.J., Trouw, R.A.J., Brito Neves, B.B., de Wit, M.J. (eds). Geological Society of London, Special Publications, **294:** 101-119.

Santos, T.J.S., Garcia, M.G.M., Amaral, W.S., Caby, R., Wernick, E., Arthaud, M.H., Dantas, E.L., Santosh, M. 2009. Relics of eclogite facies assemblages in the Ceará Central Domain, NW Borborema Province, NE Brazil: Implications for the assembly of West Gondwana. *Gondwana Research,* **15:** 454-470.

Silva, L.C, Armstrong, R., Pimentel, M. M., Scandolara, J., Ramgrab, J., Wildner, W., Angelim, L. A., Vasconcelos, A. M., Rizzoto, G., Quadros, M. L. E. S., Sander, A., Rosa, A. L. Z. 2002. Reavaliações da evolução geológica em terrenos Pré-Cambrianos brasileiros com base em novos dados U-Pb SHRIMP, parte 3. Províncias Borborema, Mantiqueira Meridional e Rio Negro Jurena. *Revista Brasileira de Geociências* **32(4)**, 529-544.

Teixeira, M.L.A. 2005. Integração de Dados aerogeofísicos, Geológicos e Isotópicos do Limite Norte do Complexo Tamboril-Santa Quitéria-CE, Província Borborema. Dissertação de Mestrado, Instituto de Geociências, Universidade de Brasília.

Tohver, E., Trindade, R.I.F., Solum, J.G., Hall, C.M., Riccomini, C., Nogueira, A.C. 2010. Closing the Clymene ocean and bending a Brasiliano belt: Evidence for the Cambrian formation of Gondwana, southeast Amazon craton. *Geology*, **38:** 267-270.

Torres, P.F.M., Cavalcante, J.C., Smith, E.P., Vasconcelos, A. M., Oliveira, F.V. 2010. Mapa geológico da Folha Quixadá (B-24-V-C-VI), CPRM-SBG – Serviço Geológico do Brasil, Fortaleza-CE, Escala 1:250.000.

Trompette, R. 1994. *Geology of western Gondwana, Pan-African/Brasiliano aggregation of South America and Africa*. A.A. Balkema: Rotterdam.

Van Schumus, W.R., Brito Neves, B.B., Hackspacher, P., Babinski, M. 1995. U-Pb and Sm-Nd geochronological studies of eastern Borborema Province, northeastern Brazil: initial conclusions. *Journal of South America Earth Science,* **8**: 267-288.

Van Schmus, W.R., Oliveira, E.P., Da Silva Filho, A., Toteu, S.F., Penaye, J., Guimarães, I.P. 2008. Proterozoic links between the Borborema Province, NE Brazil, and the Central African Fold Belt, In: *West Gondwana: Pre-Cenozoic Correlations Across the South Atlantic Region*, Pankhurst, R.J., Trouw, R.A.J., Brito Neves, B.B., de Wit, M.J. (eds). Geological Society of London, Special Publications, **294:** 69-99.

Vauchez, A., Neves, S., Caby, R., Corsini, M., Egydio-Silva, M., Arthaud, M.H., Amaro, V.1995. The Borborema shear zone system, NE Brazil. *Journal of South American Earth Sciences.* **8**: 247-266.

Zhao, G.C., Sun, M., Wilde, S.A., Li, S.Z., 2004. A Paleo-MesoProterozoic supercontinent: assembly, growth and breakup. *Earth-Science Reviews,* **67:** 91-123.

ANEXO 01

"Amaral, W.S., Nogueira Neto, J.A., Santos, T.J.S., Wernick, E., Dantas, E.L., Matteini, M.,. 2010. **High-pressure granulites from Cariré, NW of the Borborema Province-Brazil: tectonic setting, geothermobarometry and U-Pb, Lu-Hf, Sm-Nd geochronology.** *Gondwana Research* **(Submetido)**".

High-pressure granulites from Cariré, Borborema Province, NE Brazil: tectonic setting, geothermobarometry and U-Pb, Lu-Hf and Sm-Nd geochronology

Wagner da Silva Amaral[a]*, José de Araújo Nogueira Neto[b], Eberhard Wernick [c], Ticiano José Saraiva dos Santos[a], Elton Luiz Dantas[d], Massimo Matteini[d]

[a] *Instituto de Geociências, Universidade Estadual de Campinas (UNICAMP), Caixa Postal 6152, CEP: 13081-970, Campinas-SP, Brazil*
[b] *Departamento de Geologia, Universidade Federal do Ceará (UFC),CEP 60455-760, Fortaleza-CE, Brazil*
[c] *Instituto de Geociências e Ciências Exatas, Universidade Estadual Paulista (UNESP), CEP 130503-186, Rio Claro-SP, Brazil*
[d] *Instituto de Geociências, Universidade de Brasília (UnB), CEP 70910-900, Brasília-DF, Brazil*

ABSTRACT

In the northwest region of the Ceará Central Domain, Borborema Province, an elongated area of mylonitic diorites and granodiorites are structurally controlled by NE-SW strike-slip faults. Granitic material, layers, and lenses of felsic and mafic granulites occur along the main shear zones. Petrographic, geothermobarometric, and geochronological (LA-MC-ICPMS U-Pb and Lu-Hf in zircon and Sm-Nd whole-rock) data are presented and discussed for these rocks. Felsic granulites are composed of orthopyroxene + clinopyroxene + plagioclase + quartz ± hornblende ± garnet ± biotite ± feldspar while the mafic granulites comprised clinopyroxene + plagioclase + garnet + hornblende ± rutile ± quartz. The P-T conditions recorded range from 9.4 to 8.3 kbar and from 804 to 870 °C for the felsic granulites, and from 13.6 to 10.2 kbar and from 910 to 750°C for the mafic granulites. U-Pb zircon ages of granodiorites host rocks are 2157 and 2044 Ma. The felsic granulites yielded the U-Pb age of 2110 Ma, while the mafic granulites yielded U-Pb zircon ages of 613 and 589 Ma for the metamorphic recrystallization. Sm-Nd and Lu-Hf T_{DM} ages for the mafic granulites are similar (around 1.6-1.3 Ga), and share positive values of ε_{Nd} and ε_{Hf}, which suggest that these mafic rocks derived from a juvenile Mesoproterozoic crust. In addition, the felsic granulites and the granodiorites have similar $T_{DM\text{-}Nd}$ and U-Pb ages (with positive values of ε_{Nd}), that indicates a Paleoproterozoic mantle source for these rocks.

Keywords: *Granulites, High pressure, Geothermobarometry, Lu-Hf, Borborema Province*

INTRODUCTION

High-pressure granulites and eclogites have been described in a variety of orogenic belts (*e.g*. Del Lama et al*.,* 2000; Zhao et al., 2001; Baldwin et al*.,* 2003; Zhang et al., 2006, Reno et al., 2009; Xiaochun et al., 2009; Sajeev et al., 2010), and considered to be related to subduction and collisional events as well as key rocks for the understanding of crustal exhumation and cooling processes during the tectonic evolution of these belts (Carswell, 1990; O'Brien, 2001; O'Brien and Rötzler, 2003).

The Borborema Province, NE-Brazil, represents part of an orogenic belt resulting from the convergence of the Amazonian, West African-São Luis and Congo-São Francisco cratons during the assembly of West Gondwana (Almeida et al., 1977, 1981, Brito Neves and Cordani, 1991). In a highly simplified model, the main tectonic aspects of the Borborema Province result from a complex interplay of a younger transcurrent belt, which is the most important tectonic feature of the collisional stage of the Pan-African/Brasiliano orogenic belt, developing on an

older thrust belt. The strike-slip phase played an important role in structuring the Borborema Province as a complex mosaic composed of six crustal domains bounded by expressive strike-slip belts. Each domain is characterized by a particular rock association, metamorphism, tectonic structure and geochronological evolution (Van Schmus *et al.,* 1995, 2008, Brito Neves et al, 2000). The northern part of the Borborema Province is limited by the Atlantic Ocean to the north and east, the Parnaíba Basin to the west, and by the Patos Lineament to the south and comprises the Médio Coreaú, Ceará Central and Rio Grande do Norte domains bounded by the Transbrasiliano, Senador Pompeu and Patos lineaments (Brito Neves et al, 2000) (Figure 1).

Mafic and felsic granulites / retrograded eclogites occur as lenses or major continuous areas in supra- and infracrustal host rocks in several domains of the Borborema Province (Beurlen et al., 1992, Fetter, 1999, Nogueira Neto, 2000, Fetter et al., 2003, Castro, 2004, Arthaud, 2008, Santos et al., 2008, 2009). This paper presents geothermobarometric and isotopic ($U\text{-}Pb_{(zircon)}$, $Lu\text{-}Hf_{(zircon)}$ and $Sm\text{-}Nd_{(whole\ rock)}$) data for granulite lenses hosted by tonalitic/granodioritic gneissic rocks from the Cariré region, Ceará Central Domain, aiming at a better understanding their metamorphic and tectonic evolution. The data obtained are compared with those for major granulitic areas in tectonic contact with medium-grade orthogneisses, migmatites, and schists from the Granja region (Médio Coreaú Domain) and the retrograded eclogite lenses hosted by medium- to high-grade metasedimentary rocks from the Forquilha region (Ceará Central Domain) (Figure 2). Also a comparison of the northern Borborema and West African high-grade rocks is presented to enlighten their occurrences in West Gondwana.

GEOLOGICAL SETTING

The Médio Coreaú Domain

The Médio Coreaú Domain (MCD) is an infra-supracrustal complex comprising Paleoproterozoic to Neoproterozoic rocks (Fetter, 1999). Its northwestern and southeastern boundaries are, respectively, the Paleoproterozoic São Luis-West African craton (Boher *et al.,* 1992) and the Paleoproterozoic/Neoproterozoic Ceará Central Domain (Fetter *et al.,* 1997) (Figure 2).

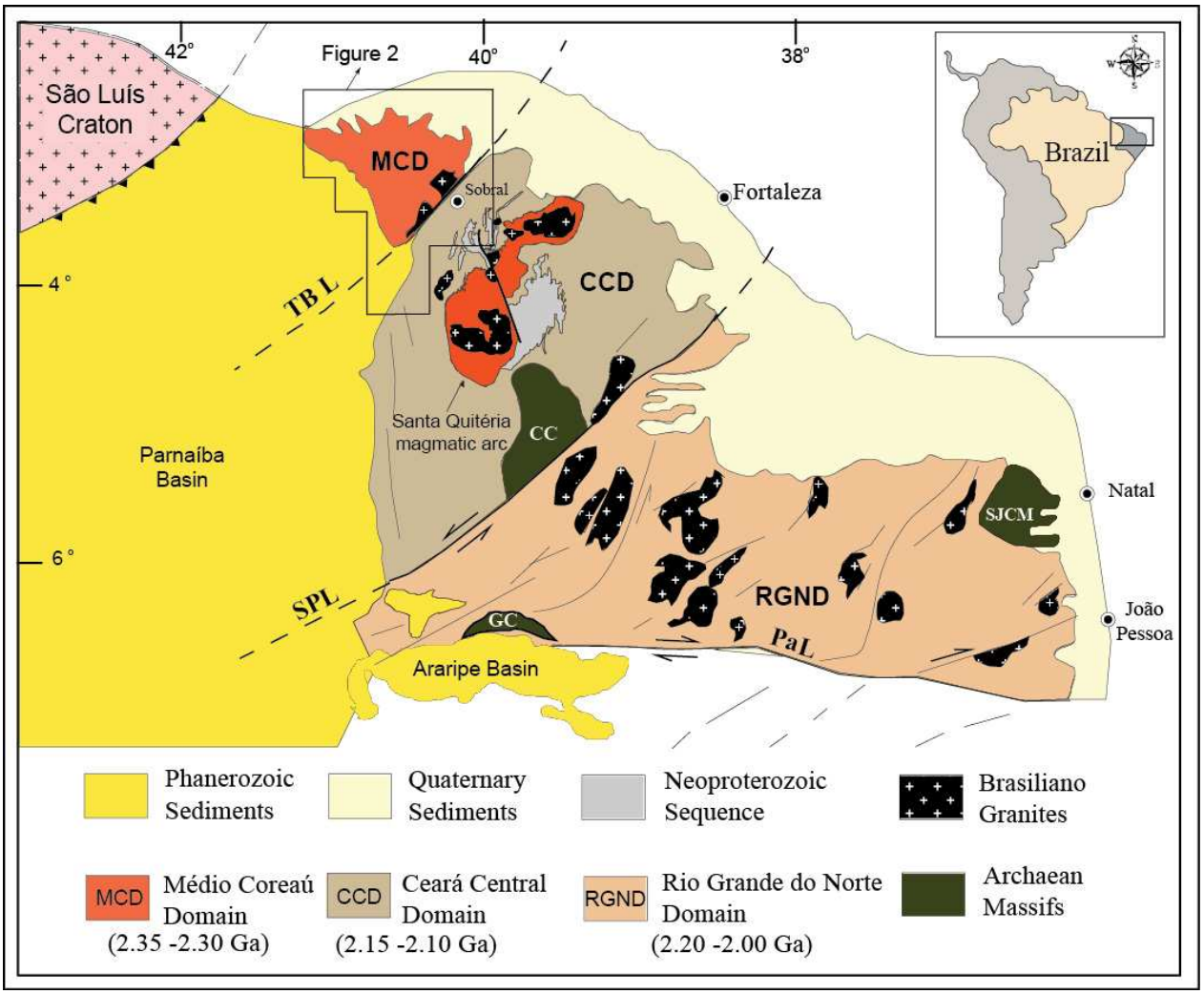

Figure 1: Geological map of the northern block of the Borborema Province, showing the three main domains and Brasiliano granitic plutons situated north of the Patos Lineament (PaL): Cruzeta Complex (CC); São José do Campestre Massif (SJCM); Granjeiro Complex (GC); Transbrasiliano Lineament (TBL); Senador Pompeu Lineament (SPL); Médio Coreaú Domain (MCD); Ceará Central Domain (CCD); Rio Grande do Norte Domain (RGND).

The MCD basement rocks comprise mainly migmatitic orthogneisses with tonalite-trondhjemite-granodiorite (TTG) affinities, as well as hornblende gneisses, amphibolites and subordinate leucogranites. The gneisses are early Paleoproterozoic (2.36-2.29 Ga) with Nd crustal residence ages (T_{DM}) between 2.61 and 2.38 Ga. The mainly positive ε_{Nd} values obtained for the TTG gneisses suggest a mantle-derived origin and evolution in an arc-type setting (Fetter et al., 1995, 2000, Fetter 1999, Nogueira Neto, 2000, Santos et al., 2001, 2008).

The overlying supracrustal volcanosedimentary rocks belong either to the Ubajara Group (U-Pb zircon age = 1785 ± 2 Ma for a meta-rhyolite, Santos et al., 2002) or to the Neoproterozoic Martinópole (U-Pb zircon age = 777 ± 11 Ma for a meta-rhyolite, Fetter et al., 2003) and Jaibaras groups, the latter deposited in a Transbrasiliano Lineament reactivation basin (Oliveira and Mohriak, 2003).

The infra- and supracrustal rocks are intruded by syn- to post-tectonic Brasiliano granite plutons (Figure 2). The late tectonic magmatism in MCD (e.g. Chaval granite) occurred between 590 and 560 Ma. A U-Pb zircon crystallization age of 532 ± 6 Ma has been obtained for the post-tectonic magmatism, represented by the Meruoca and Mucambo monzogranites (Fetter, 1999; Santos et al., 2008).

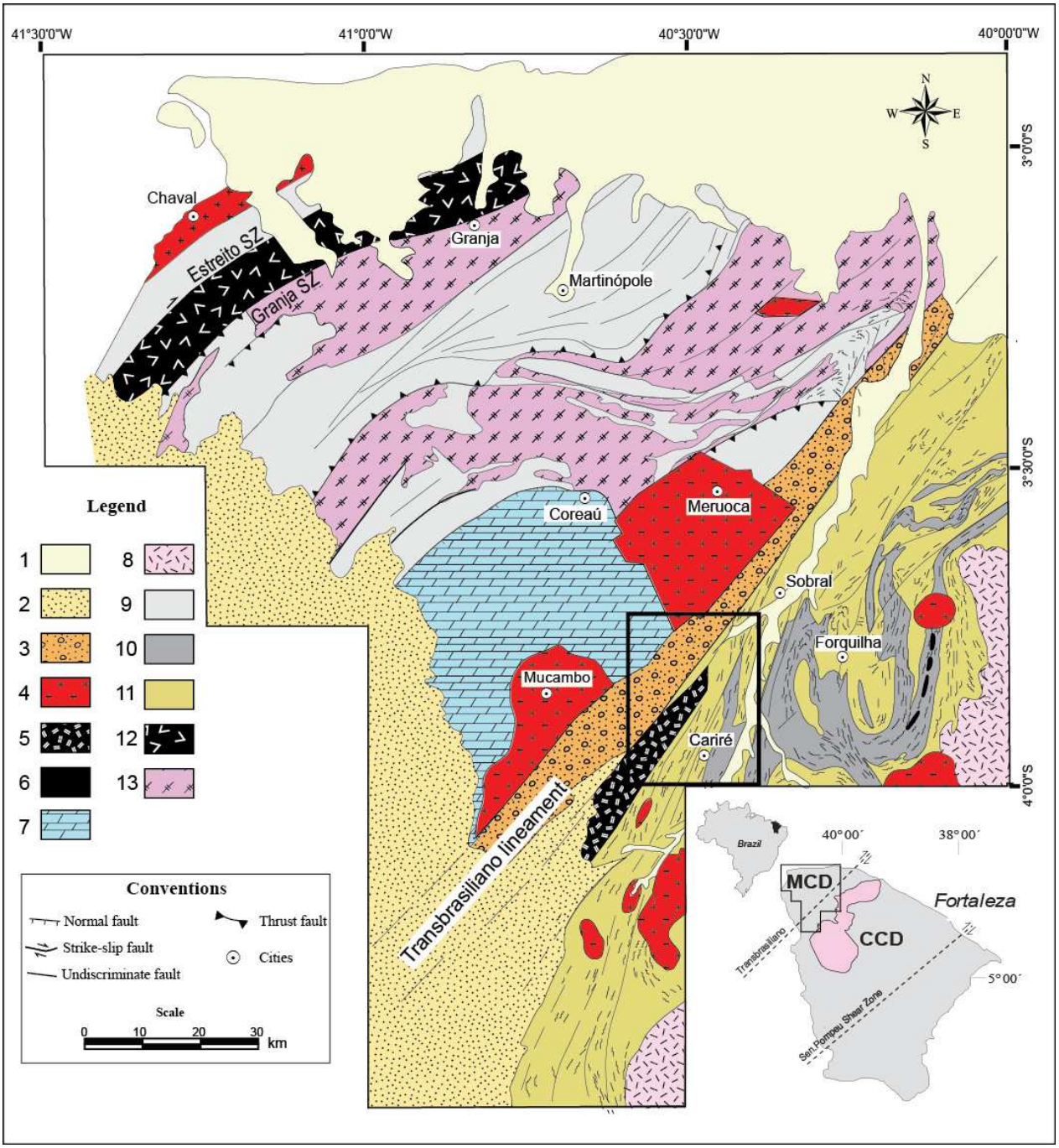

Figure 2: Geological map of the Médio Coreaú (MCD) and Central Ceará Domains (CCD). Legend: 1. Alluvial cover; 2. Parnaíba basin; 3. Jaibaras basin; 4. Brasiliano granites and monzogranites; 5. Cariré granulites; 6. Forquilha retrograded eclogites; 7. Ubajara basin; 8. Santa Quitéria magmatic arc; 9. Martinópole Group; 10. Ceará Group; 11. Canindé Complex; 12. Granja Granulites; 13. Basement migmatites and gneisses. Detail: see Figure 3.

The Granja Granulite Complex

The Granja Granulite Complex (GGC) is about 10 km wide and 50 km long and constitutes a NE-SW trending belt composed mainly of sillimanite-garnet schists and gneisses, felsic and mafic granulites, and subordinated medium-grade orthogneisses and amphibolites. Its boundaries are marked by the Granja and Estreito dextral shear zones, which put the high-grade rocks in contact with basement gneisses and migmatites to the southeast and supracrustal Martinópole rocks to the northwest, respectively.

The P-T conditions for felsic and mafic granulites and the medium-grade gneisses are respectively, between 7-10 kbar and 750-840 °C and 4-6 kbar and 550-700 °C (Nogueira Neto, 2000).

GGC khondalites and enderbites (felsic granulites) yielded three sets of geochronological ages: i) U-Pb zircon ages of 2.2 Ga (Fetter et al., 1995) and of 2176 ± 29 Ma (Gaudette et al., 1998) and Pb-Pb zircon age of 2.088 ± 24 Ma (Gaudette et al., 1998); ii) a ^{40}Ar-^{39}Ar isochron age of 601 ± 4 Ma obtained using two biotite separates, one taken from the foliation of a granulite and the other representing inclusion in garnet (Monié et al., 1997); iii) ^{40}Ar-^{39}Ar age of 557 ± 4.8 and 575 ± 2.5 Ma for pargasitic amphibole and biotite from granulites (Monié et al., 1997) and U-Pb titanite age of 554 Ma and a garnet/whole rock Sm-Nd isochron age of 545 Ma (Fetter, 1999). The first set of data represents the crystallization age of the granulite protoliths (Fetter et al., 1995; Gaudette et al., 1998); the second the granulitic metamorphism of the protoliths (Nogueira Neto 2000), and the third the regional cooling age of the granulites during their tectonic uplift (Fetter, 1999, Monié et al., 1997).

The Ceará Central Domain

The Ceará Central Domain (CCD) encompasses an intricate geological mosaic composed of: (1) the Cruzeta Complex, which is an Archean inlier enveloped by (2) the Paleoproterozoic Canindé Complex comprising juvenile high-grade felsic orthogneisses and migmatites, with ages ranging from 2.14 to 2.10 Ga (Fetter et al., 2000; Martins et al., 2009); (3) Early Proterozoic/Neoproterozoic supracrustal volcanosedimentary metamorphic rocks represented by the Ceará Complex and Novo Oriente Group (Arthaud et al. 2008, de Araújo et al. 2010); (4) the

Neoproterozoic 220 km long, NE–SW trending, high-K, calc-alkaline Santa Quitéria batholith with an area of about 10.000 km^2. The batholith has been considered as a fragment of a larger continental magmatic arc (Fetter et al., 2003; Arthaud et al., 2008). It is considered either as intrusive in Paleoproterozoic basement rocks and supracrustal Ceará Complex rocks (Fetter et al., 2003, Castro 2004) or as a huge allochthonous tectonic slab thrown over the enclosing rocks (Caby and Arthaud, 1986).

The Forquilha Eclogite Zone

In the Forquilha region, east of the Transbrasiliano Lineament in the Ceará Central Domain (CCD), retrograded mafic eclogites occur in a narrow, 30 km long, N-S trending belt (Figure 2). These rocks occur as flat lenses and boudins up to 300 meters long, hosted by variably migmatized garnet-sillimanite ± kyanite-biotite gneisses. The mafic rocks comprise different types of garnet-clinopyroxene amphibolites (Santos et al., 2009, Amaral et al., 2010a).

Metamorphism evolved from amphibolite facies conditions to the north to eclogite facies conditions to the south. Maximal recorded P-T conditions are around 17 kbar and 770 °C (Santos et al., 2009). The protoliths of the metamafic rocks are ocean-island, ocean-floor tholeiites and minor alkali basalts (Amaral et al., 2010a). The U-Pb zircon ages of the protolith crystallization varies between 1.51-1.57 Ga, whereas the age of the high-pressure metamorphism is around 650 Ma (Amaral et al., 2010b). Sm-Nd T_{DM} ages vary between 1.57-1.91 Ga (for N-MORB-like compositions) and between 2.28-2.81 Ga (for alkali-basalt compositions), suggesting a varying enrichment of their mantle sources (Amaral, 2010).

The Cariré Granulite Region

In the Cariré region, near the Transbrasiliano Lineament in the CCD, the high-pressure rocks are represented by mafic (clinopyroxene-garnet amphibolite) and felsic (enderbitic) granulites (Figure 3). Both occur as erratic lenses and boudins in highly sheared granodiorites, diorites, tonalites and derived migmatites. The structural evolution comprises two phases: 1) a compressive thrusting deformation with NW vergence which brought up to shallower crustal levels the deep seated granulitic rocks, and 2) a NE-SW strike-slip deformation in a ductile

regime with a final transtraction stage controlling the development of molassic basins (*e.g.* Jaibaras basin) and magma ascent (*e.g.* Mucambo and Meruoca plutons) (Fetter, 1999; Nogueira Neto, 2000; Amaral et al., 2008) (Figure 3).

The protoliths of the mafic granulites are N-MORB-like tholeiitic basalts, whereas the felsic granulites are rocks of calc-alkaline affinity (Nogueira Neto, 2000). A synthesis of the Cariré geochronological data is presented in Table 1.

Table 1: Geochronological ages for rocks of the Cariré Granulite Region.

Lithology	**Methods**	**Ages (Ga)**		**Reference(s)**
		(U-Pb) or (Pb-Pb)	**Nd-T_{DM}**	
Felsic granulite	$(Sm\text{-}Nd)_{WR}$	-	2.23	Nogueira Neto *et al.,* (1995)
Felsic granulite	$(U\text{-}Pb)_{Zr}$	2.10 ± 11 Ga	-	Fetter (1999)
Felsic granulite	$(U\text{-}Pb)_{Zr}$	573 ± 38 Ma	-	Fetter (1999)
Sheared Granite	$(U\text{-}Pb)_{Zr}$ and $(Sm\text{-}Nd)_{WR}$	564 ± 94 Ma	1.73	Nogueira Neto *et al.,* (1997b)
Granodiorite	$(Sm\text{-}Nd)_{WR}$	-	2.31	Nogueira Neto *et al.,* (1995)
Granodiorite	$(Pb\text{-}Pb)_{Zr}$	2.11 Ga	2.30	Ferreira *et al.,* (1996)
Mafic granulite	$(U\text{-}Pb)_{Ti}$ and $(Sm\text{-}Nd)_{WR}$	563 Ma	1.39	Nogueira Neto *et al.,* (1997a)
Mafic granulite	$(U\text{-}Pb)_{Ti}$ and $(Sm\text{-}Nd)_{WR}$	544 ± 15 Ma	1.37	Fetter (1999)

WR: whole rock; Zr: zircon; Ti: titanite

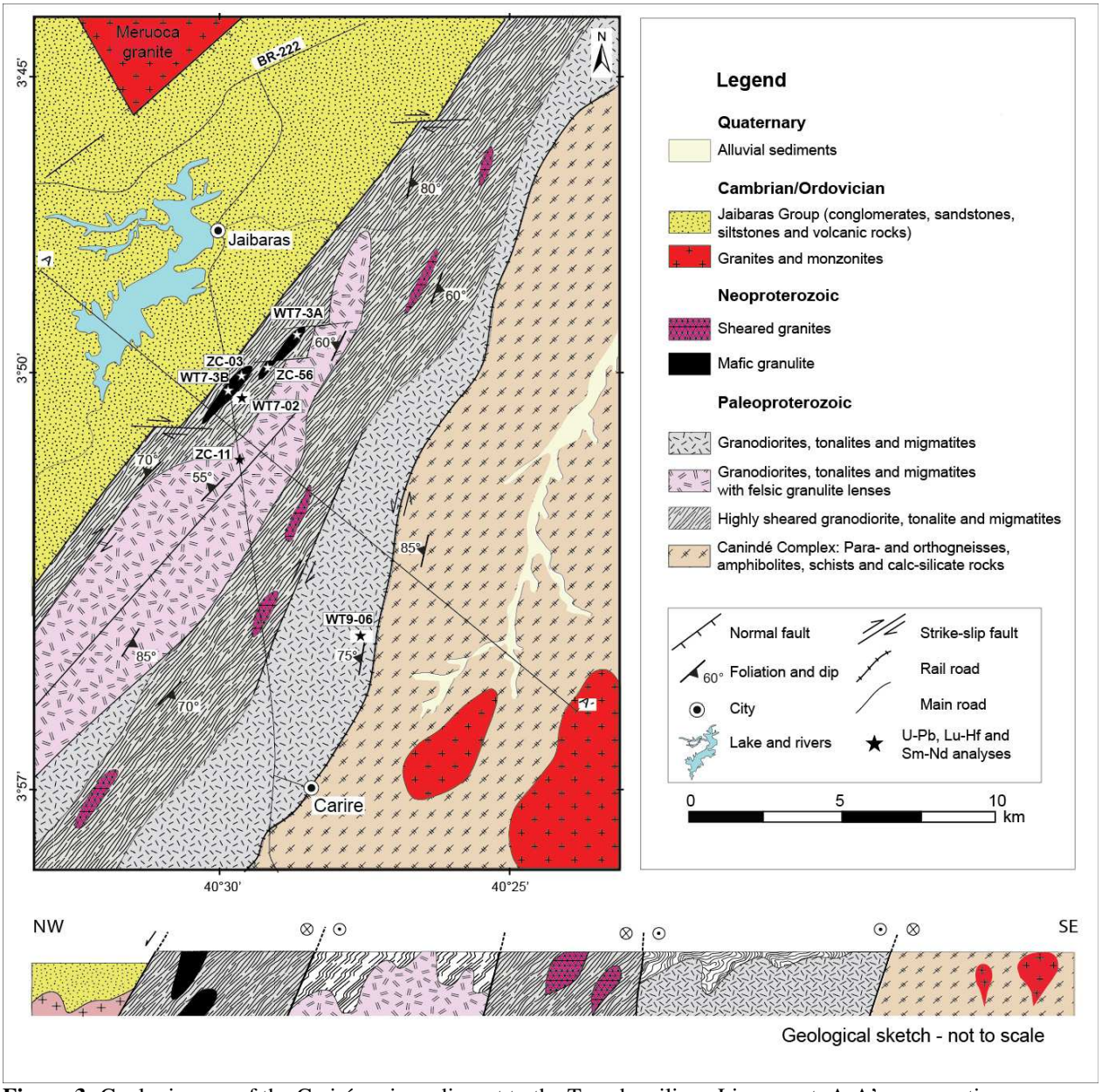

Figure 3: Geologic map of the Cariré region adjacent to the Transbrasiliano Lineament. A-A' cross section.

PETROGRAPHY

The felsic granulites (enderbites) occur as flat lenses in 100-200 meter wide, NE-SW trending belts of intensely sheared granodiorites, tonalites and diorites (Figures 4a-b). The characteristic paragenesis is plagioclase (Pl) + orthopyroxene (Opx) + biotite (Bt) + quartz (Qtz) ± clinopyroxene (Cpx) ± garnet (Grt) ± hornblende (Hbl). In the more undeformed rocks, a

mainly granoblastic mosaic texture composed of plagioclase (30-40 % vol.) and quartz (20-30 % vol.) is typical and relicts of decussate texture may occur. Rare garnet (8-10% vol.) is often rimmed by plagioclase and biotite together with rare small orthopyroxene (10-20% vol.) lamellae, suggesting decompression. Rare clinopyroxene (0-8% vol.) is always granoblastic. Small exsolved clinopyroxene lamellae occur in orthopyroxene prisms. In the more deformed rocks the foliation is defined by biotite flakes (10-20% vol.) and amphibole prisms (0-10% vol.), both in contact with orthopyroxene / clinopyroxene, as well as by small felsic bands with ribbon quartz. A rock banding defined by variable amounts of opx +qtz +pl is common (Figure 4c) and some large deformed garnet grains represent pre-kinematic porphyroblasts.

The mafic (clinopyroxene-garnet) granulites occur as up to fifty-meter long and ten-meter wide foliated (Figures 4d) or massive lenticular bodies in strongly sheared granodiorites. The typical paragenesis is plagioclase + clinopyroxene + hornblende + garnet ± quartz ± ilmenite ± rutile (Figure 4e). The absence of orthopyroxene in this type of granulites is typical (O'Brien and Rötzler, 2003). Xenomorphic poikiloblastic garnet crystals up to 3 cm in diameter are immersed in a granoblastic matrix of clinopyroxene, hornblende and plagioclase (Figure 4f). The poikiloblasts (30% vol.) are frequently rimmed by plagioclase and hornblende (Figure 4f and g). Clinopyroxene, ilmenite, rutile and zircon inclusions are common; some quartz inclusions display typical radial fracturing (Figure 4h). Clinopyroxene (10-20% vol.) occurs either as isolated xenomorphic crystals in the mosaic texture or as inclusion in garnet. Symplectitic intergrowth with plagioclase is frequent. It is often replaced or rimmed by retrograde amphibole (10-25% vol.). Most of plagioclase (15-25% vol.) usually occurs as aureoles around garnet or in symplectites with clinopyroxene.

The mafic granulites were affected by hydrothermal fluids; saussuritization of plagioclase and retrograde chlorite and zoisite growing in garnet fractures are the main evidences of this process.

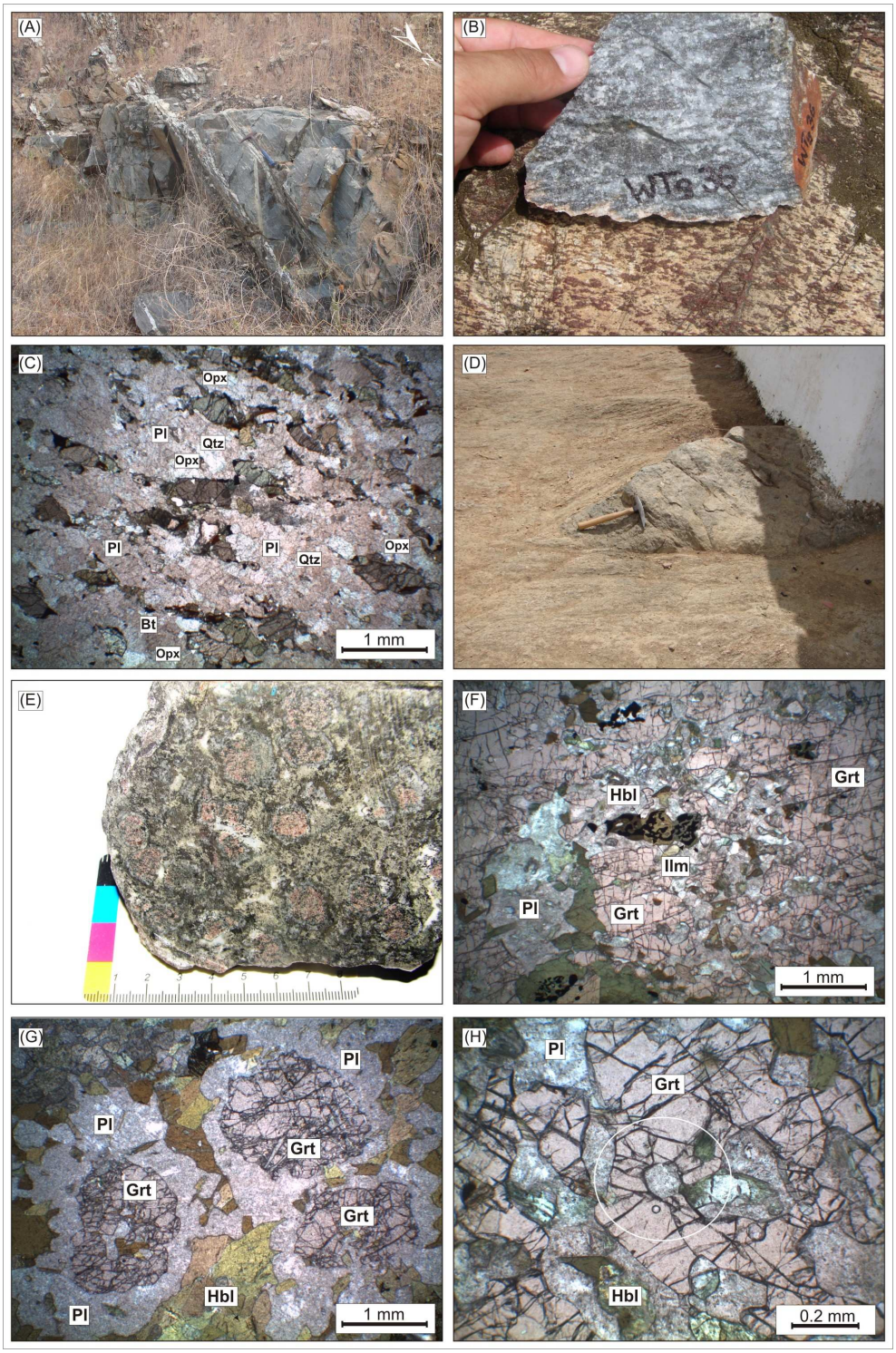

Figure 4: Field and petrographic characteristics of the Cariré granulites: A) An approximately 2m-thick felsic granulite belt sub-concordant with the mylonitic orthogneisses foliation. B) Detail of an enderbite sample showing well-delineated bands of biotite and orthopyroxene. C) Photomicrograph showing well-defined mafic (Opx + Bt) and felsic (Qtz + Pl) bands. D) Mafic granulite lens hosted in sheared granodiorite. E) The detail shows the mineral association common in the mafic granulites: garnets up to 3 cm in diameter, rimmed by plagioclase in a matrix of amphibole and clinopyroxene. F) Photomicrograph of xenoblastic and poikiloblastic garnet with ilmenite and hornblende inclusions. G) Garnet crystals with well-defined Pl and Hbl aureoles. H) Detail of quartz inclusions in garnet with radial fractures.

MINERAL CHEMISTRY

Four mafic and felsic granulites samples from Cariré were selected for mineral chemistry and thermobarometry. Mineral analyses were carried out at the Electron Microprobe Laboratory at the University of São Paulo, using a JEOL/JXA-8600 electron microprobe microanalyser with five spectrometers, operating in EDS and WDS modes. The Tracor Northern/Noran Instrument (1990) analysis system operated under the following routine conditions: a) beam current of 20 nA; b) beam diameter of 5μ and; c) accelerating voltage of 15 kV.

Representative mineral analyses are given in Tables 2, 3, 4, 5 and 6. Fe^{3+} was calculated according to Droop (1987). Mineral abbreviations follow Kretz (1983). The rare garnet in felsic granulites has the following molecular proportions: 53.83-62.42% Alm, 14.73-20.24% Py, 18.50-23.59% Gross, and 2.41-4.70% Spss (Figure 5a). Clinopyroxene is represented by a rather homogeneous diopside, whereas orthopyroxene has a wide compositional variation between $En_{38.8}$ and $En_{49.74}$ (Figure 5b). The chemical composition of biotite is intermediate between phlogopite and annite with Fe/(Fe+Mg) varying from 0.45 to 0.55 (Figure 5c). The amphibole is a Fe-pargasite, with ANa+AK > 0.50, Ti < 0.50 and Fe^{+3} < Al (Figures 5d-e). Plagioclase composition is about constant, always plotting in the andesine (An_{32-50}) field (Figure 5f).

Mafic granulite garnet has higher Ca and lower Fe contents and therefore higher Gross contents ($Alm_{44.54-61.00)}$, $Py_{11.32-19.13}$, $Gross_{21.17-37.04}$, $Spss_{1.92-3.80}$) than the felsic granulite garnet (Figure 5a). When included in garnet, Cpx has lower Ca and Mg contents and higher Fe and Al contents in relation to symplectitic Cpx. Chemically the clinopyroxene is diopside and augite (Figure 4b). Amphibole is richer in Fe and poorer in Mg when in contact with the plagioclase and diopside symplectites. However, amphibole is more aluminous if included in garnet. Despite these differences, all amphiboles are calcic and according to ANa+AK, Ti, Fe^{+3} and Al contents, they are classified as Fe-hornblende / tschermakitic hornblende / Fe-tschermakitic hornblende (Figures 5d-e). Symplectitic plagioclase intergrown with clinopyroxene is more sodic (An_{26-29}) than plagioclase rims (An_{39-52}) surrounding garnet (Figure 5f).

Table 2.
Representative analyses of garnet from felsic and mafic granulites. (FG: Felsic granulite; MG: Mafic granulite)

Sample	ZC-30	ZC-30	ZC-11b	ZC-56b	ZC-56b	ZC-56b	ZC-56b
Rock	FG	FG	FG	MG	MG	MG	MG
Position	Rim	Core	Core	Rim	Core	Rim	Core
SiO_2	38.43	39.12	37.61	37.97	37.88	38.29	37.88
TiO_2	0.20	0.07	0.02	0.05	0.04	0.06	0.00
Al_2O_3	20.89	21.17	21.36	21.35	21.66	21.99	21.60
FeO	26.85	27.24	29.22	24.84	27.64	27.27	25.94
MnO	1.67	1.07	1.66	1.12	1.70	0.84	0.71
MgO	4.85	5.09	3.78	3.75	3.56	4.02	3.74
CaO	6.78	6.50	3.78	9.75	7.48	8.87	10.41
Na_2O	0.00	0.00	0.00	0.03	0.11	0.00	0.03
Total	99.98	100.26	100.32	99.55	100.12	101.34	100.42
Si	3.08	3.06	2.97	3.00	2,98	2.97	2.96
Al^{IV}	0.00	0.00	0.03	0.01	0,01	0.03	0.04
Al^{VI}	1.96	1.95	1.96	1.99	1,99	1.98	1.94
Ti	0.01	0.00	0.00	0.00	0,02	0.00	0.00
Fe^{2+}	1.71	1.78	1.93	1.67	1,82	1.76	1.70
Mg	0.58	0.59	0.45	0.44	0,41	0.47	0.44
Mn	0.09	0.07	0.11	0.08	0,11	0.06	0.05
Ca	0.58	0.55	0.56	0.81	0,63	0.74	0.87
Alm	57.69	58.75	52.84	45.48	61.09	48.26	44.54
Gross	19.75	18.50	23.60	33.27	21.19	30.34	35.66
Py	19.64	20.24	18.86	18.18	14.08	19.13	17.84
Spss	2.92	2.21	4.71	3.08	3.83	2.27	1.93

Total cations calculated for 6 oxygens.

Table 3.
Representative analyses of plagioclase from felsic and mafic granulites.

Sample	ZC-11b	ZC-11b	ZC-11b	ZC-30	ZC-30	ZC-03	ZC-03	ZC-03
Rock	FG	FG	FG	FG	FG	FG	FG	FG
Position	Core	Rim	Core	Rim	Core	Core	Rim	Core
SiO_2	58.29	56.26	57.84	58.41	57.13	58.96	59.00	57.55
Al_2O_3	25.91	26.38	26.12	26.38	27.58	26.46	25.20	26.06
FeO	0.00	0.13	0.08	0.16	0.31	0.13	0.00	0.10
CaO	8.78	9.67	9.03	8.61	9.75	8.22	7.98	9.04
Na_2O	7.36	6.91	7.06	5.84	5.17	6.44	8.07	7.37
K_2O	0.21	0.23	0.15	0.33	0.17	0.40	0.34	0.26
Total	100.62	99.77	100.49	99.73	100.12	100.61	100.67	100.41
Si	10.42	10.20	10.51	10.46	10.22	10.48	10.54	10.33
Al	5.45	5.63	5.46	5.56	5.88	5.54	5.30	5.51
Fe	0.00	0.02	0.02	0.02	0.05	0.02	0.00	0.02
Ca	1.68	1.88	1.44	1.65	1.87	1.57	1.53	1.74
Na	2.55	2.43	2.57	2.03	1.80	2.22	2.80	2.57
K	0.05	0.05	0.10	0.08	0.04	0.09	0.08	0.06
Ab	59.60	55.70	62.60	54.00	48.50	57.30	63.50	58.80
An	39.30	43.10	34.90	44.00	50.50	40.40	34.70	39.80
Or	1.10	1.20	2.40	2.00	1.10	2.30	1.80	1.40

Total cations calculated for 8 oxygens.

Table 4.
Representative analyses of pyroxene from felsic and mafic granulites.

Sample	ZC11b	ZC11b	ZC11z	ZC11z	ZC56b	ZC56b
Rock	FG	FG	FG	FG	MG	MG
Position	Core	Rim	Rim	Core	Core	Rim
SiO_2	48.21	50.85	52.16	51.17	51.71	51.58
TiO_2	0.11	0.16	0.11	0.23	0.25	0.14
Al_2O_3	0.72	0.59	1.09	1.53	1.46	1.48
FeO	35.40	35.12	11.50	12.67	12.90	11.89
Cr_2O_3	0.02	0.05	0.09	0.02	0.00	0.00
MnO	0.67	0.69	0.24	0.26	0.50	0.26
MgO	13.76	13.52	12.23	12.12	11.45	11.41
CaO	0.78	0.81	21.86	20.48	21.99	21.90
Na_2O	0.08	0.00	0.37	0.41	0.40	0.28
K2O	0.00	0.00	0.01	0.03	0.09	0.02
Total	99.75	101.94	99.71	99.05	100.79	99.06
Si	1.91	1.98	1.97	1.95	1.944	1.97
Al	0.03	0.02	0.03	0.05	0.056	0.03
Ti	0.00	0.01	0.26	0.24	0.007	0.00
Fe	0.10	0.20	0.00	0.01	0.275	0.30
Mg	0.81	0.79	0.69	0.69	0.642	0.65
Mn	0.02	0.02	0.01	0.01	0.016	0.01
Ca	0.03	0.03	0.89	0.84	0.886	0.90
Na	0.01	0.00	0.03	0.03	47	0.02
K	0.00	0.00	0.00	0.00	34.077	0.00
WO	1.62	1.70	44.37	41.52	44.055	44.86
EN	39.82	39.54	35.56	35.92	33.762	33.47
FS	58.56	58.76	17.34	18.79	17.874	19.24
JD	0.00	0.00	1.15	1.02	0.472	1.12

Total cations calculated for 6 oxygens.

Table 5.
Representative analyses of amphibole from felsic and mafic granulites.

Sample	ZC-30	ZC-30	ZC-03	ZC-03	ZC-56b	ZC-56b
Rock	FG	FG	MG	MG	MG	MG
Position	Core	Core	Rim	Core	Rim	Core
SiO_2	41.85	41.96	43.15	43.30	42.99	41.34
TiO_2	2.23	2.63	2.02	2.24	1.21	1.64
Al_2O_3	11.33	11.15	11.38	10.92	10.90	12.24
FeO	18.13	18.24	18.73	18.84	19.25	19.04
Cr_2O_3	0.04	0.03	0.00	0.07	0.09	0.08
MnO	0.22	0.21	0.31	0.31	0.20	0.26
MgO	9.13	9.18	9.16	9.18	9.14	8.08
CaO	11.22	11.30	11.70	11.57	11.27	11.47
Na_2O	1.20	1.24	1.50	1.34	1.18	1.22
K_2O	1.57	1.62	1.29	1.23	0.87	1.08
Total	96.93	97.54	99.28	99.06	97.25	96.47
Si	6.38	6.37	6.43	6.46	6.49	6.33
Al^{IV}	1.63	1.63	1.57	1.54	1.51	1.67
Al^{VI}	0.41	0.36	0.43	0.38	0.42	0.54
Cr	0.01	0.00	0.00	0.01	0.01	0.01
Ti	0.26	0.30	0.23	0.25	0.14	0.19
Fe^{3+}	0.25	0.22	0.18	0.22	0.48	0.29
Fe^{2+}	0.07	0.06	2.11	2.08	1.88	2.11
Mn	0.01	0.01	0.02	0.02	0.01	0.02
Mg	0.00	0.00	2.04	2.04	2.06	1.85
Ca	1.83	1.84	1.87	1.85	1.82	1.88
Na	0.09	0.09	0.36	0.31	0.25	0.30
K	0.31	0.31	0.25	0.23	0.17	0.21

Total cations calculated for 23 oxygens.

Table 6.
Representative analyses of biotite from Cariré Granulite Zone, felsic granulites.

Sample	ZC-30	ZC-30	ZC11b	ZC11b	ZC11b	ZC11b
Rock	**FG**	**FG**	**FG**	**FG**	**FG**	**FG**
Position	**Core**	**Rim**	**Rim**	**Rim**	**Core**	**Core**
SiO_2	36.40	36.18	36.94	34.56	35.58	35.61
TiO_2	5.19	5.10	4.50	4.55	5.83	5.79
Al_2O_3	14.42	14.01	14.55	14.56	14.54	14.11
FeO	19.36	20.17	22.24	21.76	20.19	20.04
MnO	0.09	0.09	0.13	0.07	0.04	0.01
MgO	10.76	10.27	10.13	10.30	10.13	10.45
BaO	0.00	0.00	0.52	0.67	0.73	0.61
CaO	0.00	0.00	0.00	0.00	0.00	0.00
Na_2O	0.00	0.04	0.03	0.11	0.02	0.00
K_2O	9.66	9.73	9.48	9.18	9.10	9.55
Total	95.92	95.64	98.84	95.97	96.26	96.24
Si	5.79	5.81	5.79	5.61	5.69	5.70
Al^{IV}	2.21	2.20	2.21	2.39	2.31	2.30
Al^{VI}	0.49	0.45	0.47	0.39	0.43	0.36
Ti	0.62	0.62	0.53	0.56	0.70	0.70
Fe^{2+}	2.58	2.71	2.91	2.95	2.70	2.68
Mn	0.01	0.01	0.02	0.01	0.01	0.00
Mg	2.55	2.46	2.37	2.49	2.41	2.49
Na	0.00	0.01	0.01	0.04	0.01	0.00
K	1.96	1.99	1.89	1.90	1.86	1.95

Total cations calculated for 11 oxygens.

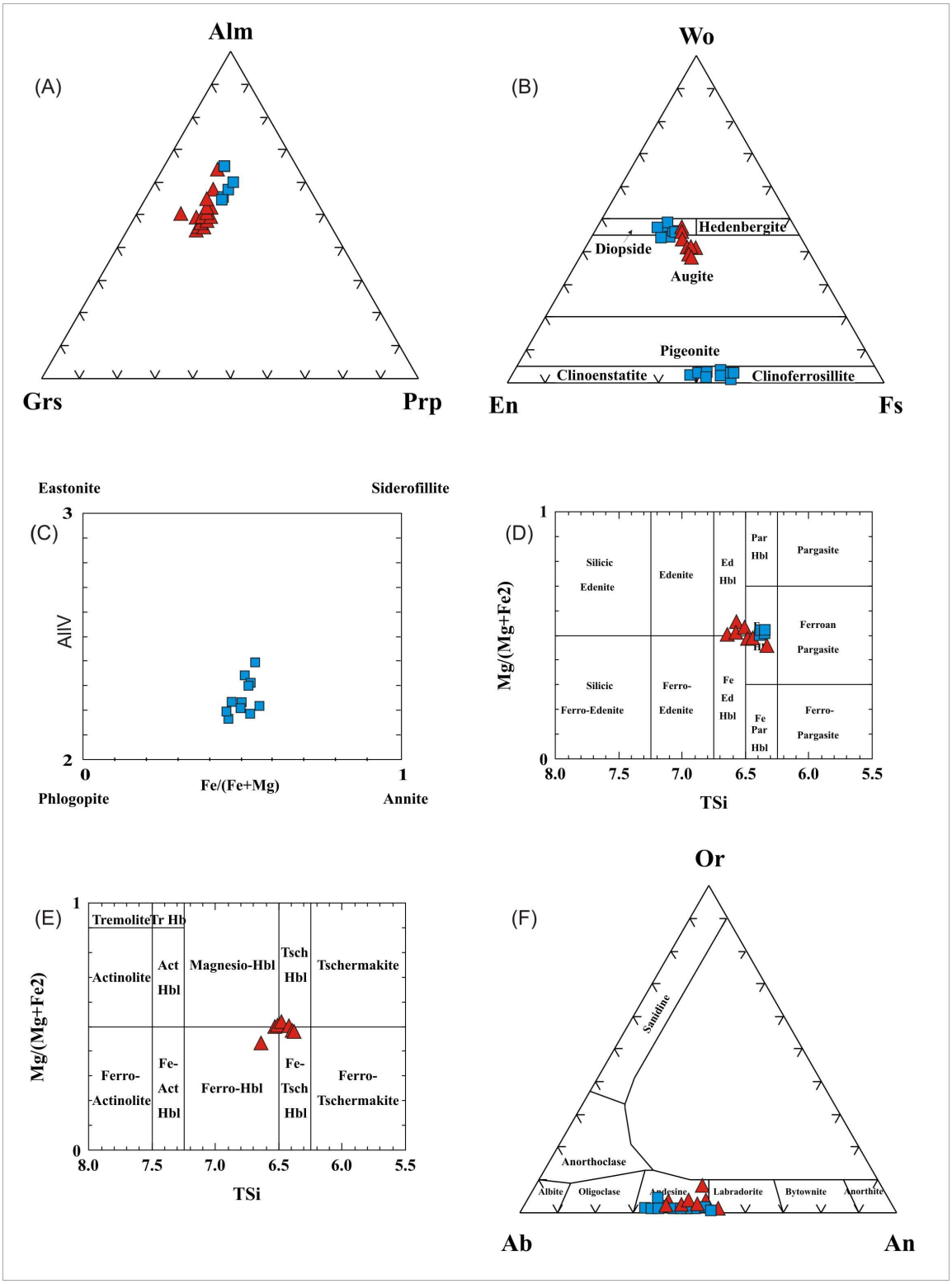

Figure 5: Mineral chemistry diagrams for felsic granulites (blue square) and mafic granulites (red triangles). a) garnet composition in the Almandine-Grossular-Pyrope diagram. b) Chemical classification of pyroxenes (Morimoto *et al.* 1988). c) Chemical classification of biotite in felsic granulites. d) Chemical classification of amphiboles showing variation from edenitic hornblende to Fe-pargasitic hornblende, whereas e) compositions vary from Fe-hornblende to Fe-tschermakite in hornblende from metabasic rocks (Leake *et al.* 1997). f) Chemical classification of plagioclase.

P–T CONDITIONS

The thermobarometric calculations were carried out with the internally-consistent thermodynamic data bank named *Thermobarometry with estimation of equilibration state* – "TWEEQU" (Berman, 1991; Berman, 1998). This method considers the integration of several metamorphic reactions for equilibrium mineral parageneses, which were plotted in P-T diagrams for visual analysis.

For the felsic granulites (samples ZC11-b and ZC30-c), different temperature intervals were obtained with the application of the Grt-Opx and Cpx-Opx geothermometers, the lower interval given by the former (625-779 °C, calibration after Harley, 1982) and the higher given by the latter (820-866 °C). The results obtained (Wood and Banno, 1973, Wells, 1977) are rather concordant. Likewise, the estimated pressures given by the Grt-Opx-Pl-Qtz geobarometer were rather concordant for all proposed calibrations (Newton and Perkins, 1982, Perkins and Chipera, 1985, Eckert et al., 1991). The integration of the P-T data by TWEEQU results in a maximal P-T estimation between 8.3 and 9.4 kbar and 804 and 870 ºC. The mentioned data are presented in Figure 6a and 6b and listed in Table 7 and are considered as very good.

For the mafic granulites (samples ZC56-1 and ZC56-2), the temperature obtained by means of the Grt-Cpx geothermometer were rather homogeneous, between 715 and 839 °C (calibration after Ellis and Green, 1979, Dahl, 1980, Powell, 1985 and Krogh, 1988); only the calibration after Sengupta *et al.* (1989) yielded temperatures between 830 and 880 °C. The estimated pressures obtained by means of the Grt-Cpx-Pl-Qtz geobarometer were rather variable, between 6.6 and 10.4 kbar (calibration after Newton and Perkins, 1982) and 9.3 and 13.3 kbar (calibration after Eckert et al., 1991). The integration of the P-T data by TWEEQU results in maximal P-T conditions between 10.2 and 13.6 kbar and 750 and 911 ºC. The mentioned data are presented in Figure 6c and d and listed in Table 7.

The variation of the estimated pressure for the mafic granulites may also reflect the variable amounts of retrograded hornblende in these rocks. Some authors (*e.g.* Bucher and Frey, 1994, Blatt and Tracy, 1996) consider that the Grt + Cpx + Pl ± Hbl ± Qtz association occur in both amphibolite and granulite facies. However, the estimated pressure by both the Grt-Cpx-Pl-Qtz geobarometer and TWEEQU is clearly somewhat higher for the mafic granulites in relation to the felsic ones. Also petrographic features clearly classify the Cariré metamafic rocks as of the

high-pressure granulite facies. The Grt + Cpx + Pl + Qtz assemblages, free of Opx, are typical of high-pressure granulitic rocks, represented by the orthopyroxene breakdown-reaction Opx+Pl = Grt +Cpx + Qtz (O'Brien and Rötzler, 2003, Pattison 2003). Many other authors (*e.g.*Winkler, 1979, Yardley, 1989, Carswell and O'Brien, 1993) consider the Gr-Cpx-Pl-Qtz association as typical of rocks of high-pressure granulite facies. Therefore, the Cariré region reflects an association of high-temperature felsic and high-pressure mafic granulites, both put together by thrust faults and later on dismembered by strike-slip faults.

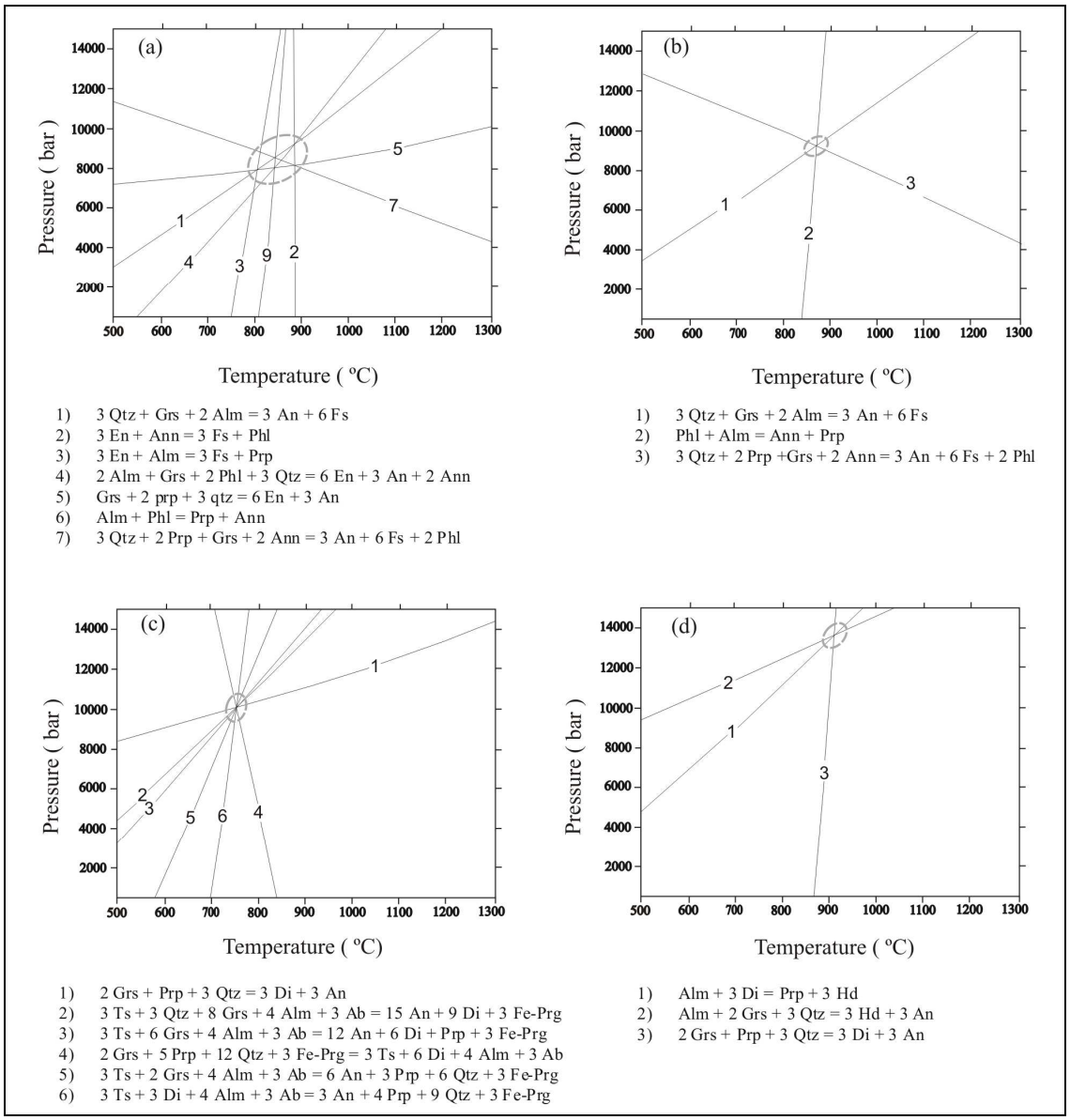

Figure 6: Reactions according to TWEEQU for felsic granulites (a and b) and mafic granulites (c and d). a) P = 8.8 ± 0.55 kbar and T = 826 ºC (sample ZC11-b); b) P ~ 9.36 kbar and T ~ 867 ºC (sample ZC30-2); c) P ~10.23 kbar and T ~ 750 ºC (sample ZC-56b-1); d) P ~ 13.60 kbar and T ~ 911 ºC (sample ZC-56b-2).

Table 7. Comparative P and T values for the Cariré high-grade metamorphic rocks.

Felsic ganulites		Mafic granulites	
Grt-Opx (T ºC)	**Grt-Opx-Pl-Qtz (P kbar)**	**Grt-Cpx (T ºC)**	**Grt-Cpx-Pl-Qtz (P kbar)**
(Hr) 625 -779	(N & P) 7.1-9.7	(E & G) 753-773	(N & P) 6.6-10.4
	(P & C) 7.9-10.7	(D) 781-839	(P & H) 8.6-12.4
Cpx-Opx (TºC)	(E *et al.,*) 7.3-10.0	(P) 735-755	(E *et al.,*) 9.3-13.3
(W & B) 820-829		(K) 715-738	
(We) 881-866		(S *et al.,*) 830-880	
	TWEEQU		**TWEEQU**
	804-870 ºC		750-900 ºC
	8.3-9.4 kbar		10.2-13.6 kbar

(D) = Dahl (1980)
(E *et al.,*) = Eckert *et al.,* (1991)
(E & G) = Ellis & Green (1979)
(Hr) = Harley (1984)
(K) = Krogh (1988)
(N & P) = Newton & Perkins (1982)
(P) = Powell (1985)
(P & C) = Perkins & Chipera (1985)
(P & H) = Powell & Holland (1988)
(S *et al.,*) = Sengupta *et al.,* (1989)
(We) = Wells (1977)
(W & B) = Wood & Banno (1973)

U-Pb, Sm-Nd and Lu-Hf GEOCHRONOLOGY

ANALYTICAL PROCEDURES

For *in situ* U-Pb and Lu-Hf analyses, zircon concentrates were extracted from 1 to 30 kg of rock samples, firstly by crushing with a jaw crusher to 500 µm size, than panning and lastly purification using a Frantz isodynamic separator. Final purification was achieved by hand-picking under a binocular microscope. The selected grains were placed on epoxy mounts, polished and cleaned with 3% nitric acid before analysis. Backscattered electron (BSE) images were used for spot targeting. BSE images were acquired with a LEO 430i and EDS scanning electron microscope at the Institute of Geosciences, State University of Campinas – UNICAMP, Brazil.

The U-Pb and Lu-Hf isotopic analyses were performed on zircon grains from four samples, using a Thermo-Fisher Neptune MC-ICP-MS coupled with a Nd:YAG UP213 New Wave laser ablation system, installed in the Laboratory of Geochronology of the University of Brasilia – UnB.

The U–Pb analyses on zircon grains were carried out following Bühn et al. (2009), using the standard-sample bracketing method (Albarede et al., 2004). During the analytical session, zircon standard Temora-2 was analyzed as an unknown sample.

In all analyses, the common Pb correction was unnecessary due to the low signal of common ^{204}Pb (<30 cps) and high $^{206}Pb/^{204}Pb$. Concordia diagrams (2σ error ellipses), concordia ages and upper intercept ages were calculated using the Isoplot/Ex software (Ludwig, 2001).

Lu-Hf isotopes were analyzed using zircon grains selected from four different samples, which were previously analyzed with U-Pb method. Lu-Hf isotopic analyses were carried out following Matteini *et al*. (2010).

The $\varepsilon_{Hf}(t)$ values were calculated using the decay constant $\lambda = 1.865 * 10^{-11}$, proposed by Scherer *et al.* (2006) and the $^{176}Lu/^{177}Hf$ and $^{176}Hf/^{177}Hf$ CHUR values of 0.0332 and 0.282772 proposed by Blichert-Toft and Albarede (1997). The two stage depleted mantle Hf model ages (T_{DM} Hf) were calculated using $^{176}Lu/^{177}Hf = 0.0384$ and $^{176}Hf/^{177}Hf = 0.28325$ for the depleted mantle and $^{176}Lu/^{177}Hf$ value of 0.0113 for the average crust (Chauvel and Blichert-Toft, 2001).

During the analytical session, replicate analyses of GJ-1 standard zircon were carried out, resulting in a $^{176}Hf/^{177}Hf$ ratio of 0.282006 ± 16 2σ ($n = 25$), which is in agreement with the reference value for GJ standard zircon obtained by Morel et al. (2008).

The bulk rock Sm–Nd isotopic analyses were carried out at the Geochronology Laboratory of the University of Brasília. Sample dissolution was done in Teflon Savillex beakers or in Parr-type Teflon bombs. Sm and Nd extraction from whole-rock powders and garnet concentrates followed the technique of Richard *et al*. (1976), in which the separation of the REE as a group, using cation-exchange columns precedes reversed-phase chromatography for the separation of Sm and Nd, using columns loaded with HDEHP (di-2-ethylhexyl phosphoric acid) supported on Teflon powder. We have also used the REE-Spec and Ln-Spec resins for REE and Sm–Nd separation. A mixed ^{149}Sm–^{150}Nd spike was used. Sm and Nd samples were loaded onto Re filaments of a double filament assembly. Sm and Nd isotopic analyses were carried out, using a Finnigan MAT-262 mass spectrometer. Uncertainties on Sm/Nd and $^{143}Nd/^{144}Nd$ ratios are considered to be better than ± 0.05% (1σ) and ± 0.003% (1σ), respectively, based on repeated analyses of international rock standards BCR-1 and BHVO-1. The $^{143}Nd/^{144}Nd$ ratios were normalized to a $^{146}Nd/^{144}Nd$ ratio of 0.7219. The Nd procedure blanks were smaller than 100 pg.

RESULTS

U-Pb ZIRCON ANALYSES

The U-Pb zircon analyzes were preceded by cathodoluminescence (CL) and backscattered electron (BSE) images (Figures 7 and 8). Results are listed in Tables 8 and 9 and plotted in Concordia diagrams in Figure 9.

Two mafic granulite samples (WT7-3A and WT7-3B) contain two zircon populations. In one, the crystals are slightly yellow/brown, elongated to oval, and sometimes preserve their prismatic faces (Figure 7a, b, c, d). Cathodoluminescence images show low luminescent core and an outer zoned shell either regular or patchy (Figure 7a-b). The second population comprises more iso-dimensional, rounded to ovoid, up to 100 μm-sized, slightly pinkish grains. Absence of inclusions is typical and prismatic faces are sometimes preserved showing a "soccer-ball" habit. The rare internal intergrowth structures are chaotic (Figure 7e, f, g), a typical feature for zircon grown under granulite facies conditions (Vavra et al., 1996, 1999, Schaltegger et al., 1999, Corfu et al., 2003).

Fifteen raster analyses in zircon grains from the first population (sample WT7-3A) yielded a Concordia U-Pb age of 612.9 ± 3.3 Ma (MSWD = 0.0089; Figure 9a, Table 8). However, some grains yielded slightly older punctual ages between 617 and 628 Ma (Figure 7a, b, c, d and Table 9). Eight zircon grains from the second population (sample WT7-3B) yielded a Concordia U-Pb age of 589 ± 8.7 Ma (MSWD = 0.17; Figure 9b, Table 8).

Two granodiorite samples were analyzed, one less deformed (WT9-06) and the other (WT7-02) intensively sheared and hosting mafic granulites (Figure 3). The zircon populations of both samples are rather similar; some grains from the more deformed rock show more intensively fractured rims. The light brown, predominantly prismatic grains display a well-defined nucleus and a thick, less luminescent rim with outer ill-defined overgrowths (Figure 8). Rounded and oval zircon grains are less frequent.

Analyses of zircon cores and rims from the mylonitic granodiorite define in the Discordia diagram an upper intercept U-Pb age of 2.157 ± 26 Ma (MSWD = 2.8; Figure 9c, Table 9), and a lower intercept age of 587 ± 31 Ma (Figure 9e), respectively. Zircon grains from the undeformed granodiorite (sample WT9-06) yielded U-Pb age of 2.044 ± 46 Ma (MSWD = 4.9; Figure 9d, Table 9).

Five zircon fractions from felsic granuite (Sample ZC-11Z), investigated by conventional ID-TIMS, are quite discordant and thus yield a less precise crystallization age of 2.110 ± 66 Ma (Figure 9F) The effects of high temperature and high pressure during granulite-grade metamorphism probaly contributed to a high degree of Pb-loss and possibly to recrystallization of these zircon grains, making them plot along the lower part of the discordia line. In this case, the lower intercept age of 573 ± 35 Ma, considering the error, could reflect the timing of final granulite-grade metamorphism (Fetter, 1999).

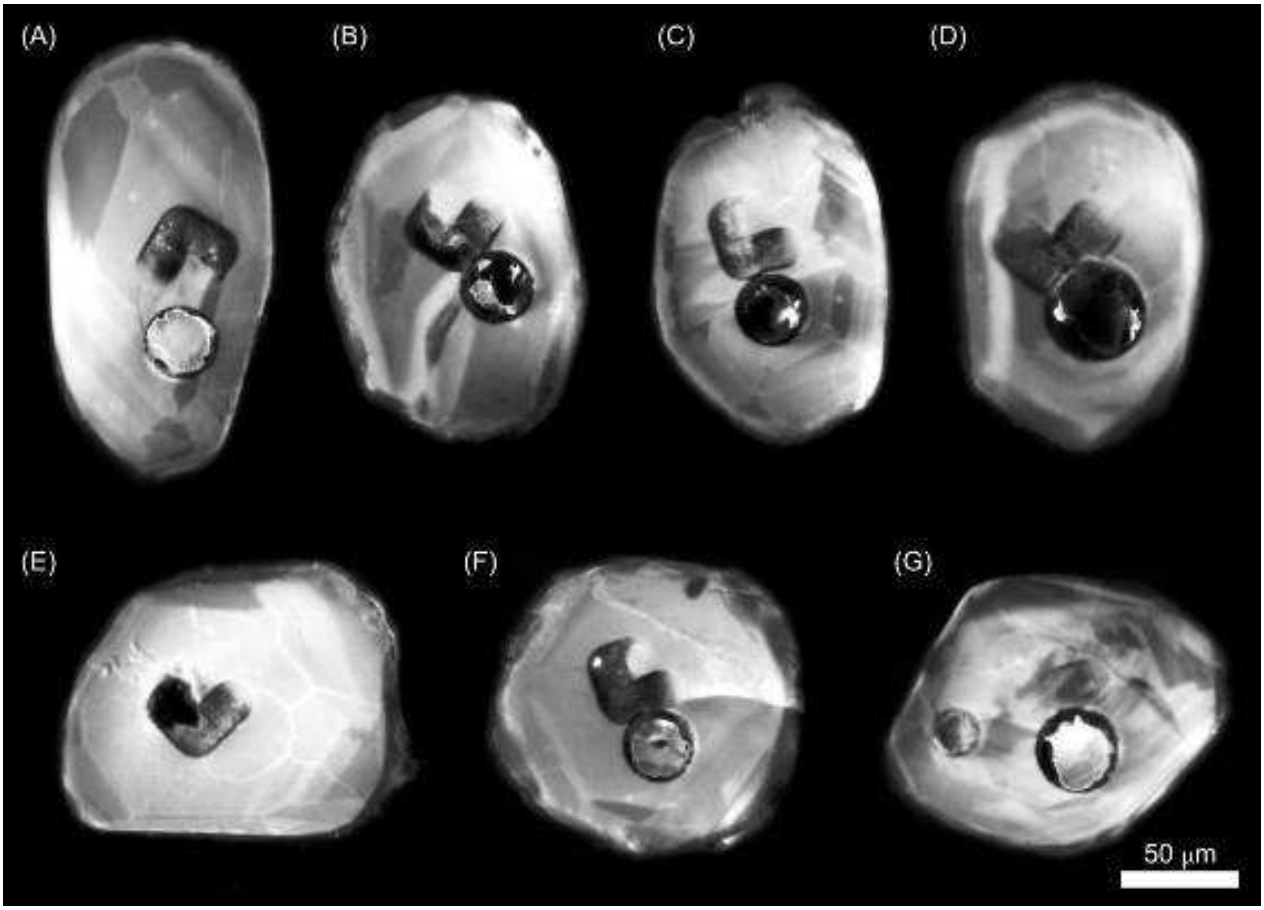

Figure 7: Cathodoluminescence image (CL) of zircon analyzed by LA-MC-ICPMS (mafic granulite sample WT7-3A). A) Larger and more elongated zircon from the first population (Z15: 619± 6.4 Ma). B) Oval zircon from the first population, showing inherited core rimmed by a highly luminescent overgrowth (Z3: 621 ± 6.4 Ma). C) Oval zircon from the first population rimmed by a thin, oscillatory chaotic layer. Its core yielded the oldest age for the mafic granulites (Z14: 628.6±6.6 Ma). D) Slightly elongated zircon, preserving some external euhedral faces (Z4: 617 ± 6.4 Ma). E) A more homogeneous zircon from the second population, lacking well-defined faces and a homogeneous core (Z8: 602± 6.2 Ma). F) "Soccer ball" grain preserving a single homogeneous core rimmed by a discrete overgrowth (Z13: 612.3 ± 6.3 Ma). G) Sub-euhedral, ovoid zircon from the second population with chaotic core (Z1: 613± 6.3 Ma). Zircon grains from the second population show all the characteristics of the metamorphic zircon and recorded the same or similar ages to those obtained by the concordia diagram.

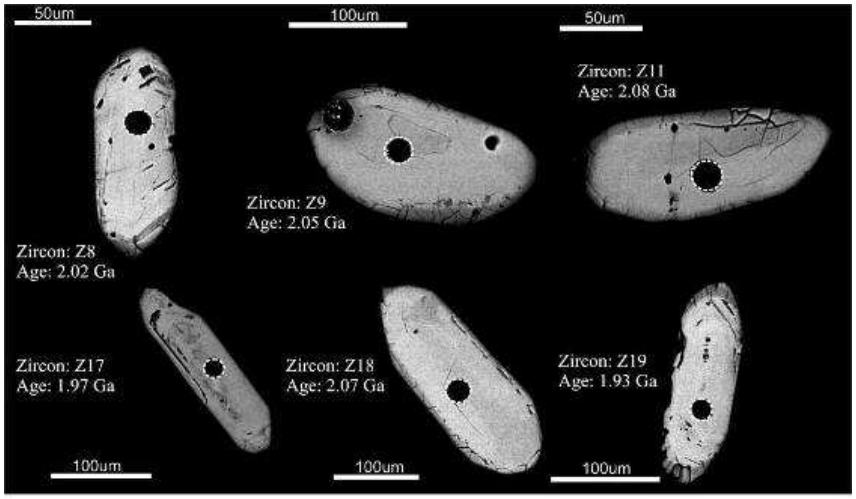

Figure 8: Back-scattered electron image of zircon grains from granodiorite sample WT9-06. Elongated grains show intergrowth evidence and fracturing at the rims. 30 μm-sized spots analyzed by the U-Pb method using LA-ICP-MS.

Table 8.
Results of *in situ* U–Pb LA-MC-ICP-MS zircon analyses.

Sample	**Isotopic ratios**							**Ages (Ma)**						
	Th/U	**$^{207}Pb/^{206}Pb$**	***2σ* (%)**	**$^{206}Pb/^{238}U$**	***2σ* (%)**	**$^{207}Pb/^{235}U$**	***2σ* (%)**	**$^{207}Pb/^{206}Pb$**	***2σ* abs**	**$^{206}Pb/^{238}U$**	***2σ* abs**	**$^{207}Pb/^{235}U$**	***2σ* abs**	**Rho**
Sample WT7-3A: Mafic Granulite														
Z1	0.01	0.060	0.9	0.100	2.6	0.829	2.8	601.9	20.1	616.1	15.5	613.1	6.3	0.92
Z2	0.01	0.061	1.1	0.100	2.6	0.839	2.9	636.5	23.6	613.8	15.4	618.7	6.5	0.86
Z3	0.02	0.061	1.0	0.101	2.6	0.844	2.8	623.5	21.8	621.0	15.5	621.6	6.4	0.89
Z4	0.01	0.060	1.0	0.101	2.6	0.836	2.8	614.3	20.7	617.6	15.6	616.9	6.4	0.92
Z6	0.02	0.060	1.0	0.099	2.6	0.819	2.8	599.1	20.7	609.6	15.3	607.4	6.2	0.91
Z7	0.01	0.061	1.0	0.098	2.6	0.827	2.8	636.7	21.4	605.0	15.1	611.7	6.3	0.89
Z8	0.02	0.061	1.0	0.097	2.6	0.809	2.8	629.3	21.6	594.8	14.9	602.0	6.2	0.89
Z9	0.01	0.060	0.9	0.099	2.6	0.825	2.8	613.2	20.2	610.3	15.4	610.9	6.3	0.92
Z10	0.01	0.060	1.0	0.099	2.6	0.818	2.8	606.2	20.8	606.8	15.3	606.7	6.2	0.91
Z11	0.03	0.060	1.0	0.100	2.6	0.830	2.8	602.9	21.5	616.8	15.6	613.9	6.4	0.90
Z12	0.03	0.060	0.9	0.100	2.6	0.823	2.8	595.1	20.6	613.8	15.4	609.8	6.2	0.91
Z13	0.01	0.060	0.9	0.100	2.6	0.828	2.8	597.5	20.3	616.3	15.4	612.3	6.3	0.92
Z14	0.05	0.061	1.1	0.102	2.7	0.857	2.9	627.5	23.3	629.0	15.9	628.6	6.6	0.87
Z15	0.02	0.061	1.0	0.101	2.6	0.840	2.8	623.8	20.8	617.6	15.4	618.9	6.4	0.91
Sample WT7-3B: Mafic Granulite														
Z2	0.01	0.060	4.5	0.094	4.3	0.778	6.2	600.0	94.6	580.7	23.8	584.6	27.3	0.67
Z3	0.02	0.059	4.9	0.094	4.8	0.768	6.9	578.6	103.8	578.6	26.3	578.6	29.8	0.68
Z5	0.01	0.059	4.2	0.093	3.8	0.762	5.6	576.5	88.4	575.1	20.7	575.4	24.4	0.63
Z6	0.01	0.060	5.1	0.097	4.2	0.805	6.6	605.4	107.0	598.1	24.0	599.6	29.6	0.60
Z8	0.01	0.060	6.8	0.094	5.2	0.781	8.6	613.1	140.9	578.9	28.7	585.9	37.5	0.60
Z9	0.04	0.060	4.9	0.099	5.4	0.818	7.3	593.1	103.1	610.9	31.7	607.1	33.0	0.75
Z10	0.01	0.058	4.6	0.101	4.8	0.807	6.6	526.5	96.7	620.3	28.6	600.5	29.7	0.73
Z11	0.03	0.059	5.7	0.098	5.2	0.803	7.7	578.7	118.6	604.1	29.9	598.8	34.2	0.66

Table 9
Results of *in situ* U–Pb LA-MC-ICP-MS zircon analyses.

Sample	Isotopic ratios						Ages (Ma)						
	$^{207}Pb/^{206}Pb$	2σ (%)	$^{206}Pb/^{238}U$	2σ (%)	$^{207}Pb/^{235}U$	2σ (%)	$^{207}Pb/^{206}Pb$	2σ abs	$^{206}Pb/^{238}U$	2σ abs	$^{207}Pb/^{235}U$	2σ abs	Rho
Sample WT7-02:Granodiorite													
z13	0.133	1.6	0.336	2.4	6.150	2.8	2133.8	27.1	1868.2	38.4	1997.4	24.7	0.78
z17	0.129	1.0	0.296	3.7	5.285	3.8	2088.3	18.4	1673.9	54.4	1866.5	32.8	0.98
z18	0.129	1.0	0.341	2.3	6.080	2.5	2087.0	18.4	1892.9	37.6	1987.3	22.0	0.93
z19	0.128	1.1	0.345	2.9	6.083	3.1	2067.6	18.8	1911.9	47.9	1987.8	26.9	0.97
z23	0.129	1.0	0.332	2.1	5.902	2.3	2081.0	17.8	1850.3	33.3	1961.5	20.0	0.91
z28	0.126	1.1	0.303	2.3	5.266	2.5	2045.8	19.2	1704.2	34.1	1863.3	21.5	0.91
z64	0.132	1.0	0.350	2.3	6.392	2.5	2129.3	17.7	1936.0	37.8	2031.2	21.8	0.94
z14	0.060	1.0	0.102	2.1	0.848	2.3	612.4	22.4	626.3	12.3	623.3	10.7	0.89
z33	0.058	1.1	0.096	2.1	0.775	2.4	545.5	23.5	591.9	11.9	582.4	10.4	0.88
z37	0.057	1.0	0.095	2.1	0.742	2.3	488.0	22.9	582.5	11.5	563.6	10.0	0.89
z39	0.059	1.1	0.090	2.0	0.732	2.3	568.1	22.9	555.4	10.9	557.9	9.9	0.88
z43	0.058	1.0	0.094	2.0	0.755	2.3	538.5	22.7	579.5	11.3	571.2	10.0	0.89
z45	0.058	1.1	0.093	2.1	0.743	2.4	527.9	23.3	573.2	11.6	564.1	10.2	0.89
z58	0.060	1.0	0.097	2.0	0.795	2.3	589.2	22.4	595.2	11.5	594.0	10.2	0.88
z59	0.061	1.1	0.093	2.1	0.781	2.3	636.9	24.1	572.9	11.3	586.0	10.5	0.84
Sample WT9-06: Granodiorite													
Z5	0.126	1.4	0.314	0.9	5.440	1.0	2037.2	23.9	1761.2	13.7	1891.2	8.8	0.87
Z6	0.117	0.8	0.259	2.5	4.172	2.6	1905.7	13.7	1486.5	32.5	1668.5	20.8	0.96
Z8	0.125	3.0	0.340	2.0	5.830	2.3	2022.2	52.7	1884.4	32.8	1950.9	19.4	0.84
Z9	0.127	0.7	0.374	0.9	6.525	1.1	2050.4	12.0	2048.1	15.6	2049.3	9.8	0.71
Z11	0.124	0.8	0.362	1.2	6.167	1.5	2008.0	13.8	1991.7	21.1	1999.7	12.7	0.82
Z12	0.123	5.7	0.324	3.9	5.511	4.2	2004.9	98.4	1809.8	60.9	1902.4	35.6	0.90
Z17	0.121	0.7	0.297	1.3	4.961	1.5	1973.3	13.1	1676.3	18.7	1812.7	12.4	0.86
Z19	0.119	5.9	0.306	4.1	5.009	4.2	1934.1	101.5	1723.5	61.9	1820.8	34.9	0.99

$^{207}Pb/^{235}U$ calculated using $^{207}Pb/^{206}Pb/(^{238}U/^{206}Pb \times 1/137.88)$. Rho is the error correlation defined as $err^{206}Pb/^{238}U/err^{207}Pb/^{235}U$

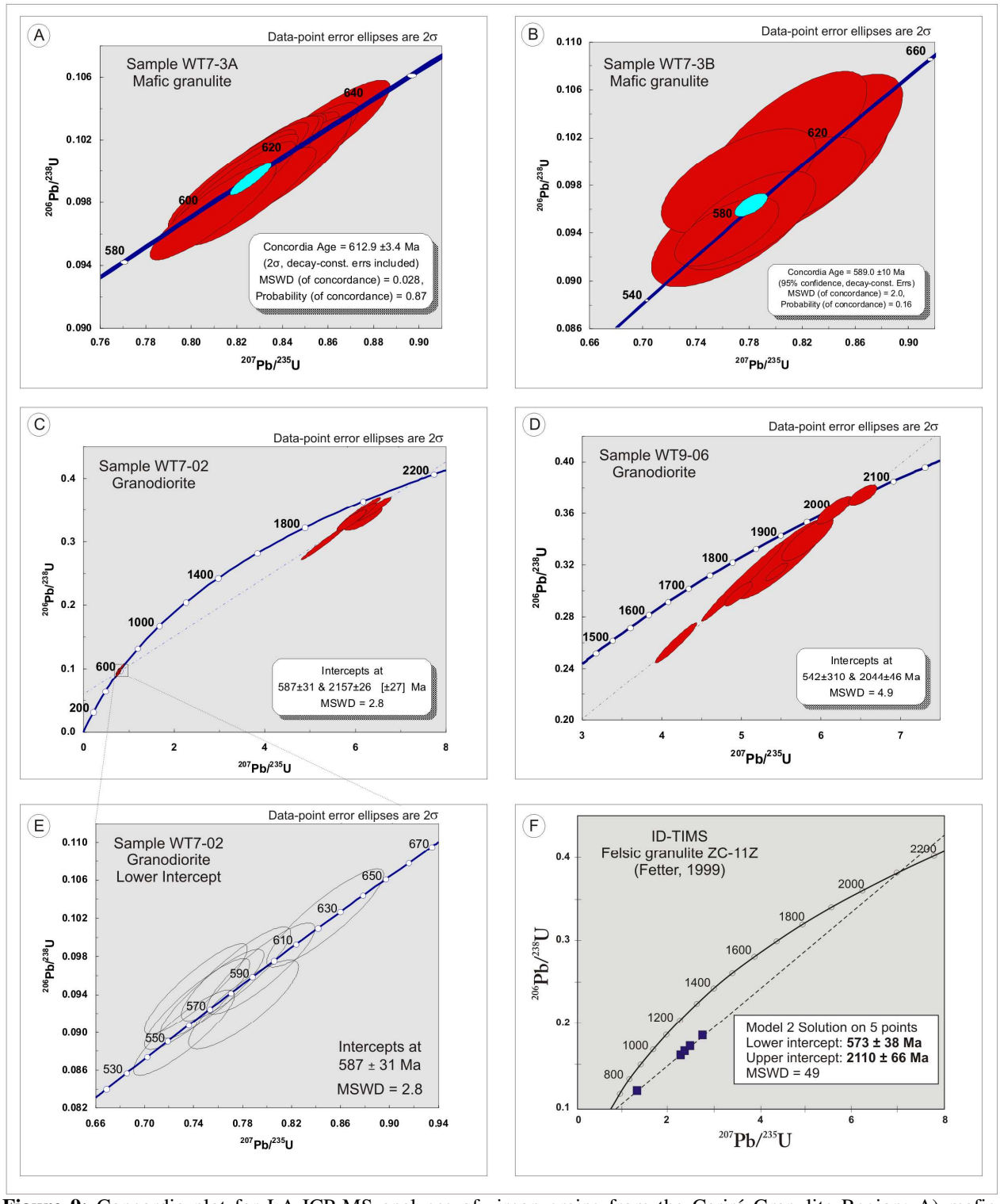

Figure 9: Concordia plot for LA-ICP-MS analyses of zircon grains from the Cariré Granulite Region: A) mafic granulite (sample WT7-3A); B) mafic granulite (sample WT7-3B); C) mylonitic granodiorite (sample WT7-02); D) granodiorite (sample WT9-06); E) Lower intercep of sample WT9-06; F) ID-TIMS analyses of zircon grains from a felsic granulite (sample ZC-11Z) (Fetter, 1999) .

Lu–Hf ANALYSES OF ZIRCON

Ten zircon grains from the mafic granulite (WT7-3A), yielded Lu-Hf T_{DM} ages between 1.28 and 1.35 Ga for an assumed crystallization age of 800 Ma, and εHf $_{(t=800)}$ values between + 0.96 and +2.29 (Table 10).

Table 10: Results of *in situ* Lu–Hf LA-MC-ICP-MS zircons analyses.

Sample	$^{176}Lu/^{177}Hf$	2σ	$^{176}Hf/^{177}Hf$	2σ	*t* (Ma)	$(^{176}Hf/^{177}Hf)t$	2σ	$\varepsilon_{Hf}(t)$	1σ	T_{DM} (Ga)
Sample WT7-3A										
WT7-3A_Z1	1.83504E-05	0.0000003	0.28241853	0.0000261	800	0.28241831	0.0000261	0.96	±0.42	1.35
WT7-3A_Z2	1.83392E-05	0.0000003	0.28242919	0.0000211	800	0.28242897	0.0000230	1.33	±0.30	1.33
WT7-3A_Z3	2.64246E-05	0.0000002	0.28242222	0.0000314	800	0.28242191	0.0000314	1.08	±0.60	1.35
WT7-3A_Z4	1.55805E-05	0.0000002	0.28243576	0.0000281	800	0.28243557	0.0000281	1.57	±0.49	1.32
WT7-3A_Z7	2.05986E-05	0.0000004	0.28243734	0.0000171	800	0.28243709	0.0000171	1.62	±0.09	1.32
WT7-3A_Z9	1.31275E-05	0.0000005	0.28241973	0.0000227	800	0.28241957	0.0000227	1.00	±0.29	1.35
WT7-3A_Z10	1.1072E-05	0.0000002	0.28245619	0.0000267	800	0.28245606	0.0000267	2.29	±0.44	1.28
WT7-3A_Z14	3.23002E-05	0.0000033	0.28243988	0.0000251	800	0.2824395	0.0000251	1.71	±0.38	1.31
WT7-3A_Z13	1.99627E-05	0.0000004	0.28242279	0.0000301	800	0.28242255	0.0000301	1.11	±0.55	1.35
WT7-3A_Z15	2.76092E-05	0.0000003	0.28242387	0.0000147	800	0.28242354	0.0000147	1.14	±0.01	1.34

WHOLE-ROCK Sm-Nd DATA

The Nd isotopic evolution diagram (Figure 10) displays all data listed in Table 11, together with the isotopic compositions of the Central Ceará Domain basement gneisses (Fetter, 1999). The mafic granulite samples WT7-3A and ZC-56b yielded positive $\varepsilon_{Nd\ (800)}$ values between + 3.00 and +3.26, but sample ZC-03 has a slightly negative $\varepsilon_{Nd\ (800)}$ value (-1.76). The data were calculated assuming a crystallization age around 800 Ma for the mafic granulites based on zircon U-Pb concordia data for mainly felsic metavolcanic rocks considered as representing the initial Borborema rifting magmatism (Fetter et al., 2003, Castro, 2004, Arthaud, 2008). The resulting T_{DM} values vary between 1.37 and 1.61 Ga (Table 11), suggesting a juvenile Mesoproterozoic derivation. The results are concordant with the Lu-Hf T_{DM} ages between 1.28 and 1.35 Ga found on euhedral zircon grains. The felsic granulites (ZC-11f and ZC-11z) yielded negative $\varepsilon_{Nd\ (800)}$ values between -11.20 and -12.80 and T_{DM} ages around 2.2 Ga (Table 11). This age plots on the evolutionary trend for the Ceará Central Domain basement presented by Fetter (1999 – Figure 10).

Table 11.
Sm–Nd isotopic data for the Cariré Granulite Region.

Sample	Sm (ppm)	Nd (ppm)	$^{147}Sm/^{144}Nd$	$^{143}Nd/^{144}Nd$	Age (U-Pb) (Ma)	εNd(0)	εNd t=800Ma	T_{DM} (Ma)
Mafic Granulite								
WT7-3A (wr)	3.765	12.587	0.1808	0.512708	800	1.37	2.62	-
ZC-03 (wr)	5.47	24.03	0.1378	0.512239	800	-7.8	-3.3	1.61
ZC-56B (wr)	3.09	10.79	0.1729	0.512675	800	0.7	2.6	1.39
ZC-56B (wr)*	3.45	11.92	0.1747	0.51269	800	1.01	2.7	1.37
Felsic granulite (wr)								
ZC-11F	3.66	18.63	0.11879	0.511657	2200	-19.1	-13.2	2.23
ZC-11Z	2.17	11.98	0.10922	0.511525	2200	-21.7	-15	2.22

* repeated analyses

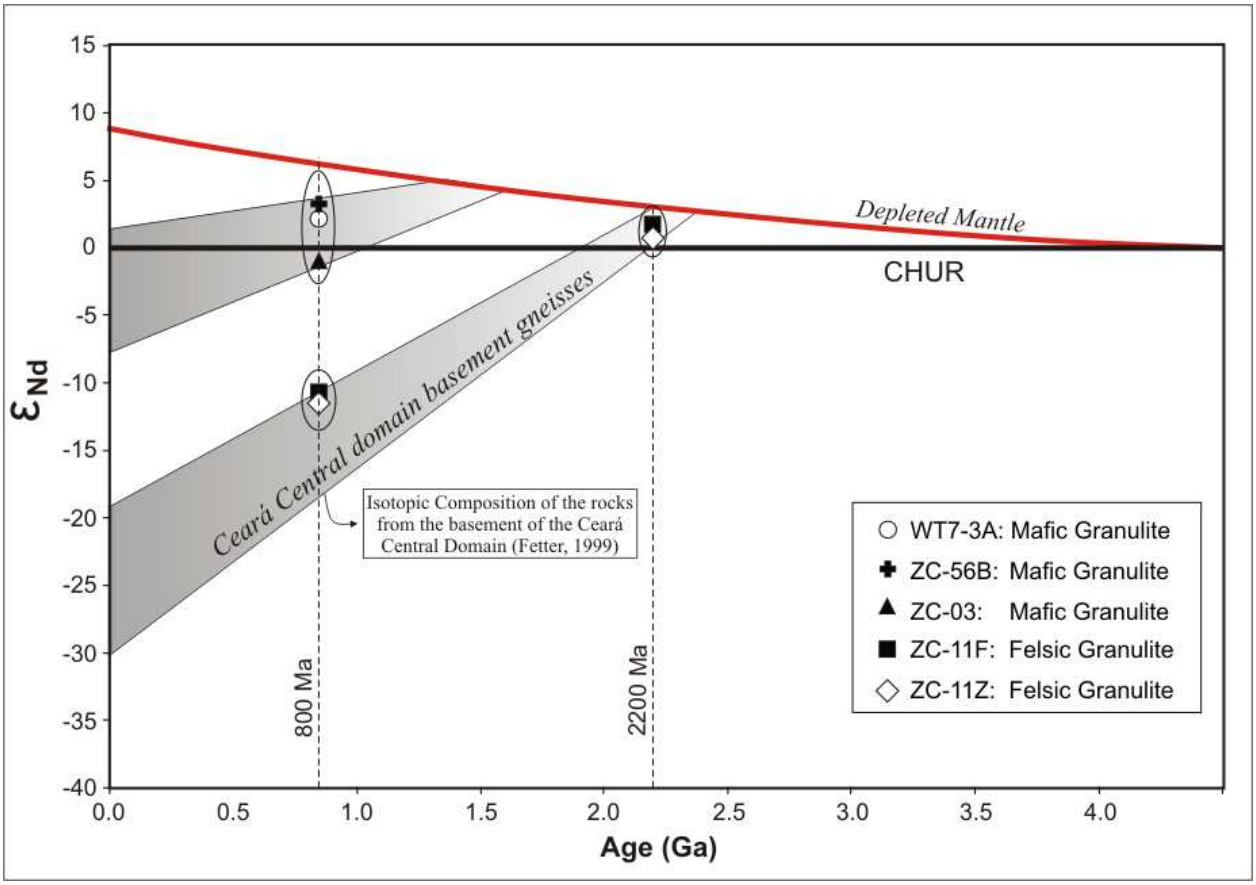

Figure 10: Diagram ε_{Nd} *versus* time showing evolutionary tendency for mafic and felsic granulites from the Cariré Region Ceará Central Domain. Also shown is the isotopic evolution for the basement gneisses from the Ceará Central Domain (Fetter, 1999).

DISCUSSION AND CONCLUSIONS

In the Cariré Granulite Region mafic and felsic granulites occur as more or less deformed and disrupted lenses in strongly sheared granodiorite, diorite, tonalite and correlated migmatites. Both types of granulites are clearly associated with thrust faults and later on disrupted in the frame of a huge regional Transbrasiliano strike-slip belt. During their uplift the granulites underwent decompression as assigned by plagioclase aureoles around garnet and augite-andesine symplectites. The absence of orthopyroxene characterizes the metamafic rocks as high-pressure granulite generated under estimated maximal P-T conditions of 10.2-13.6 kbar and 750-911 ºC (Winkler, 1979, Yardley, 1989, Carswell and O'Brien, 1993). The felsic high-grade rocks crystallized under estimated maximal P-T conditions of 8.3-9.4 kbar and 804-870 ºC. The occurrence of orthopyroxene in these rocks indicate lower metamorphic pressures (O'Brien and Rötzler, 2003, Pattison 2003).

The estimated maximal P-T conditions (Figure 6), the contrasting composition and the divergent geochronological data for the felsic and mafic granulites stress out the differences in their geological evolution. The felsic granulites represent a Paleoproterozoic (Figure 9F), juvenile (Table 11), charnockitic/enderbitic, calc-alkaline, arc-related (Nogueira Neto, 2000) lower crust magmatism with weak signs of a Late Precambrian recrystallization (Figure 9F). The mafic granulites result from high-grade metamorphism (Figure 6, Table 7) of possible Mesoproterozoic mantle-derived (Table 11), mainly N-MORB type basalts (Nogueira Neto, 2000) in a subduction environment. Alternatively the pre-metamorphic rocks represent Neoproterozoic magma extracted by partial melting of 2.0 Ga old mafic protoliths. However, this hypothesis is restricted by the narrow range of the Sm-Nd and Lu-Hf T_{DM} ages respectively between 1.37-1.61 and 1.28 - 1.35 Ga.

The T_{DM} ages calculation assumed a crystallization age of 800 Ma considered as the age of the early Borborema rifting stage. However, this magmatism, even if supported by some geochronological dating (Fetter *et al*., 2003; Castro, 2004; Arthaud, 2008), is still only weakly supported by geological data. The U-Pb zircon age of 749 ± 5 Ma for a garnet amphibolite was achieved in only one crystal (Arthaud, 2008), and some of the correlated felsic metavolcanics are completely deformed by thrust faults. Another possible crystallization age of 630 Ma for the mafic protoliths is quite close to the granulite metamorphism age of 612 ± 3.3 Ma (Figure 9a).

However, the choice of this younger crystallization age does not considerably change the T_{DM} ages and ε_{Nd} and ε_{Hf} (t=0) values. On the other hand, when the Mesoproterozoic crystallization age of 1.57 Ga (calculated on the basis of data obtained for the retrograded eclogites from the Forquilha Eclogite Zone – Amaral *et al*., 2010b) is considered, the T_{DM} age for sample ZC-56B results younger than its U-Pb zircon age (Table 11).

The overall high-pressure metamorphic conditions for the Cariré mafic granulites are supported by the nearby Forquilha Eclogite Zone (about 35 km far from such granulites), whose estimated maximal P-T conditions are 17-22 kbar and 750-770°C (Santos et al. 2009, Amaral, 2010). Also for this zone the main pre-metamorphic protoliths are N-MORB basalts (Amaral *et al*., 2010a). However, the U-Pb zircon age for the Forquilha eclogite metamorphism is somewhat older, between 630-650 Ma (Amaral *et al*., 2010b).

The uplift of the granulitic rocks occurred in a tectonic regime characterized by a strike-slip shear belt overprinting a former thrust belt. The main exhumation is promoted by older thrust and reverse faulting; a final oblique uplift is linked to the younger shear faults. The dip angle of the predominant NE-SW trending transcurrent faults is often around 75° and of the stretching lineation is dominantly 10-15° SW. As the extention of many faults is more than 100 km, the final uplift is in some cases rather considerable. The ^{40}Ar-^{39}Ar mineral ages obtained for the strike-slip phase of the Granja Granulite Complex are around 575 Ma, but the transcurrent movements could have continued up to 540 Ma (Monié *et al.*, 1997). These ages also agree with a U-Pb titanite age of 554 Ma and a garnet/whole rock Sm/Nd isochron age of 545 Ma, for sheared granulites from the Granja Complex, which are considered as expressing the final regional uplift-related cooling episode (Fetter and Van Schmus, 1996). The same range of ages was obtained for the sheared granodiorites and felsic granulites from the Cariré Region, considering the lower U-Pb zircon concordia intercept (Figure 9 C-F). In turn, the strike-slip faults usually define the tectonic boundaries of larger granulitic areas, *e.g.* the Granja Granulite Complex, or dismembered granulite and eclogite bodies in a sequence of lenses or boudins as in the Cariré Region and in the Forquilha Eclogite Zone.

In the transoceanic extension of the Borborema Province in Western Africa, a large number of high-grade bodies (retrograded eclogites, felsic and mafic granulites) occur in extensive intercontinental shear zones (*e.g.* Kandi and 4°50' lineaments) of the Dahomeyide belt. The Derouvaru, Kabyé, Djabatouré, Lato-Agou, Akuse granulites/eclogite massifs are

outstanding examples, all of them with evidence of migmatization and retrograde metamorphism (Affaton et al., 2000, Caby 1989, Trompette, 1994, Attoh et al., 1997, Agbossoumondé et al., 2001, Duclaux et al., 2006).

Petrographic evidences show that eclogite-facies metamorphism preceded the granulite event in the Dahomeyide suture zone (Attoh, 1998). The estimated thermobarometric conditions for the eclogite are between 13 ± 2 kbar and 650 ± 50 °C, and 19 ± 4 kbar and 700 ± 95 °C. For the rocks from the high-pressure granulite/amphibolite facies, the conditions are 5±1 kbar and 560 ± 60 °C, and 8 ± 2 kbar and 720 ± 60 °C (Agbossoumondé *et al*., 2001).

The mafic eclogites and granulite protoliths show a dominant N-MORB geochemical signature (Agbossoumondé *et al*., 2004, Attoh and Morgan, 2004, Duclaux *et al*., 2006).

The maximal age of the Kabyé Massif protoliths is between 1300 and 1400 Ma (Nd mean crustal residence ages). The ages obtained for the granulite metamorphism were 640 ± 50 Ma (U-Pb ages obtained using multigrain zircon fractions) and 612.5 ± 0.8 Ma (Pb-Pb zircon evaporation method) (Bernard-Griffiths *et al*., 1991, Affaton *et al*., 2000). Comparable granulites from the Amalaoulaou Massif yielded a protolith age of 800 ± 50 Ma (U-Pb ages on multigrain zircon fractions) (Caby, 1987). The ages for the protolith of the eclogites from the Lato-Agou Massif (South Togo) fall in the 1150 to 820 ± 130 Ma interval (Nd mean crustal residence ages and U-Pb ages on zircon), and for the eclogite formation between 640 and 600 Ma (whole-rock Rb-Sr and zircon U-Pb ages) (Bernard-Griffiths *et al*., 1991). The age obtained for the formation of the Akuse Massif granulite (SE Ghana) was 610 ± 2 Ma (zircon U-Pb ages), and for nappe stacking and blasto-mylonitization between 590 and 560 Ma (Ar-Ar ages) (Attoh *et al*., 1991, 1997, House and Attoh, 1996). In the same region, U-Pb dating of rutile from a garnet-hornblende gneiss yielded an age of 576 ± 2 Ma, interpreted as the regional cooling age at around 400°C (Hirdes and Davis, 2002).

The Paleoproterozoic Kara orthogneisses, reworked during the Pan-African/Brasiliano orogenies, yield a mineral Rb-Sr isochron and muscovite Ar-Ar ages of 592 ± 17 Ma, interpreted as the cooling age (Bernard-Griffiths *et al*., 1991, Attoh *et al*., 1997). The Ho orthogneisses (SE Ghana), located at the same latitude of the Lato-Agou Massif and comparable to the Kara rocks, yielded a whole-rock Rb-Sr isochron age of 2176 ± 44 Ma. These rocks underwent tectonic reworking and metamorphism at 610 Ma (U-Pb multigrain zircon) and cooled at 579 ± 0.4 Ma (muscovite Ar-Ar age) (Attoh *et al*., 1991, 1997).

The geological setting, mineral assemblages, thermobarometric data, chemical compositions and isotopic data obtained for the African granulites, eclogites and orthogneisses coincide with those for medium- and high-grade rocks from the NW domains of the Borborema Province. The similarity between the Brazilian and Western African rocks suggest, once more, a clear geological correlation between the transoceanic Brasiliano/Pan-African orogenic areas, which once belonged to Western Gondwana.

ACKNOWLEDGMENTS

The authors are grateful to CNPq (*Conselho Nacional de Desenvolvimento Científico e Tecnológico*) for the Ph.D. Scholarship granted to the first author, to FAPESP (*Fundação de Amparo a Pesquisa do Estado de São Paulo*, grants 03/07663-3 and 07/58535-6) for laboratory work support, and CNPq/MCT (Millenium Project 42.0222/2005-7) and INCTET for field work support.

REFERENCES

Affaton, P., Kröner, A., Seddoh, K.F. 2000. Pan-African granulite formation in the Kabye Massif of northern Togo (West Africa): Pb–Pb zircon ages. *International Journal of Earth Sciences,* **88:** 778-790.

Agboumoussonde Y, Menot RP, Guillot S. 2001. Metamorphic evolution of Neoproterozoic eclogites from south Togo (West Africa). *Journal of African Earth Sciences,* **33**: 227-244.

Agbossoumondé Y. Guillot S, Menot, RP. 2004. Pan-African subduction–collision event evidenced by high-P coronas in metanorites from the Agou massif (southern Togo). *Precambrian Research,* **135**: 1-21.

Albarede, F., Telouk, S., Blichert-Toft, J., Boyet, M., Agranier A., Nelson, B.2004. Precise and accurate isotopic measurements using multiple-collector ICPMS, *Geochimica and Cosmochimica Acta,* **68:** 2725-2744.

Almeida, F.F.M. 1977 *O Cráton do São Francisco*. *Revista Brasileira de Geociências,* **7:** 349-364.

Almeida, F.F.M., Hasui, Y., Brito-Neves B.B., Fuck, R.A. 1981. *Brazilian structural provinces: an introduction. Earth Science Reviews*, **17:** 1-29.

Amaral, W. S., Nogueira Neto, J. A., Santos, T.J.S., Fetter, A.H., Arthaud, M.H. 2008. Faixa Granulítica de Cariré, Domínio Ceará Central: Idades Modelo Sm-Nd e Lu-Hf, U-Pb (zircões) e Contexto Geológico. In: 44° Congresso Brasileiro de Geologia, Curitiba. Anais do 44° Congresso Brasileiro de Geologia. p. 17

Amaral, W.S., Santos, T. J. S., Wernick, E. 2010a. Occurrence and geochemistry of metamafic rocks from the Forquilha Eclogite Zone, central Ceará NE Brazil: Geodynamic implications. *Geological Journal* (DOI: 10.1002/gj.1224).

Amaral, W. S. ; Santos, T. J. S. ; Wernick, E. ; Matteini, M. ; Dantas, E. L. ; Moreto, C. P. N. 2010b. U-Pb, Lu-Hf and Sm-Nd geochronology of rocks from the Forquilha Eclogite Zone, Ceará Central Domain, Borborema Province, NE-Brazil. *VII-SSAGI South American Symposium on Isotope Geology,* Brasília-DF (CD-ROM)

Amaral, W.S. 2010. Análise geoquímica, geocronológica e geotermobarométrica das rochas de alto grau metamórfico, adjacentes ao arco magmático de Santa Quitéria, NW da Província Borborema. Ph.D Thesis, Universidade de Campinas-UNICAMP.

Arthaud, M.H., Caby, R., Fuck, R.A. Dantas, E.L., Parente, C.V., 2008. Geology of the northern Borborema Province, NE Brazil and its correlation with Nigeria, NW Africa. In: Pankhurst, R.J., Trouw, R.A.J., Brito Neves, B.B. & de Wit, M.J. (eds) West Gondwana: Pre-Cenozoic Correlations Across the South Atlantic Region. *Geological Society, London, Special Publications,* **294:** 49-67.

Attoh, K. 1998. High-pressure granulite facies metamorphism in the Pan-African Dahomeyide orogen, West Africa. *The Journal of Geology,* **106 :** 236-246

Attoh, K., Hawkins, D., Bowring, S.A., Allen, B., 1991. U–Pb zircon ages of gneisses from Pan-African Dahomeyide orogen, West Africa. *EOS Transactions American Geophysical Union,* **72:** 299.

Attoh, K., Dallmeyer, R.D, Affaton, P. 1997. Chronology of nappe assembly in the Pan-African Dahomeyide orogen, West Africa: evidence from $^{40}Ar/^{39}Ar$ mineral ages. *Precambrian Research*, **82**: 153-171.

Attoh, K., Morgan, J., 2004. Geochemistry of high-pressure granulites from the Pan-African Dahomeyide orogen, West Africa: constraints on the origin and composition of the lower crust. *Journal of African Earth Sciences,* **39:** 201-208.

Baldwin, J.A., Bowring, S.A., Williams, M.L. 2003. Petrological and geochronological constraints on high pressure, high temperature metamorphism in the Snowbird tectonic zone, Canada, *Journal of Metamorphic Geology*, **21**: 81-98.

Berman, R. G. 1991. Thermobarometry using multi-equilibrium calculations: a new technique, with petrological application. *Canadian Mineralogist,* **29**: 833-855.

Berman, R. G. 1998. Thermobarometry With Estimation of Equilibration State (TWEEQU) - Versão 2.02. G SC.

Bernard-Griffiths, J., Peucat, J.J., Ménot, R.P. 1991. Isotopic (Rb-Sr, U/Pb and Sm/Nd) and trace element geochemistry of eclogites from the Pan-African belt: a case study of REE fractionation during high-grade metamorphism. *Lithos,* **27**: 43-57.

Beurlen H, Da Silva Filho AF, Guimarães IP, Brito SB. 1992. Proterozoic C-Type eclogites hosting unusual Ti-Fe±Cr±Cu mineralization in northeastern Brazil. *Precambrian Research* **58:** 195-214.

Blatt,H., Tracy,R. J. 1996. *Petrology: Igneous, Sedimentary, and Metamorphic*. New York: W.H. Freeman.

Boher, M., Abouchami, W., Michard, A., Albarede, F., Arndt, N. Y. 1992. Crustal growth in West Africa at 2.1Ga. *Journal of Geophysical Research*, **97:** 345-369.

Bucher,K., Frey,M. 1994. *Petrogenesis of Metamorphic Rocks*. Berlin: Springer-Verlag.

Brito-Neves, B.B., Santos, E.J., Van Schmus, W.R., 2000. Tectonic history of the Borborema Province, northeastern Brazil. In: Cordani, U., Milani, E.J., Thomaz Filho, A., Campos, D.A. (eds) Tectonic Evolution of South America, 31st International Geological Congress, Rio de Janeiro, Brazil, 151-182.

Bühn, B., Pimentel, M.M., Matteini, M, Dantas, E. 2009. High spatial resolution analysis of Pb and U isotopes for geochronology by *laser ablation* multi-collector inductively coupled plasma mass spectrometry (LA-MC-ICP-MS), *Anais da Acadêmia Brasileira de Ciências,* **81:** 99-114.

Caby R.,1987. The Pan-African belt of West Africa from the Sahara desert to the Gulf of Benin. In : Schaer, J.P., Rodgers, J. (eds) *The anatomy of mountain ranges*. Princeton University Press, Princeton, New Jersey, 129-170.

Caby, R. 1989. Precambrian terrenes of Benin-Nigeria and northeast Brazil and the Late Proterozoic South Atlantic fit. *Geological Society of America Special Paper,* **230**: 145-158.

Caby, R., Arthaud, M.H. 1986. Major Precambrian nappes of the Brazilian Belt, Northeast Brazil. *Geology*, **14:** 871-874.

Carswell, D.A. 1990. Eclogite Facies Rocks, Blackie, Glasgow.

Carswell, D. A., O'Brien, P. J. 1993. Thermobarometry and geotectonic significance of high-pressure granulites: examples from the Moldanubian Zone of the Bohemian Massif in Lower Austria. *Journal of Petrology*, **34:** 427-459.

Castro, N.A. 2004. *Evolução geológica proterozóica da região entre Madalena e Taperuaba, domínio tectônico Ceará Central (Província Borborema).* Ph.D Thesis, Universidade de São Paulo-USP.

Chauvel, C., Blichert-Toft, J.E. 2001. A hafnium isotope and trace element perspective on melting of the depleted mantle, *Earth and Planetary Science Letters,* **190**: 137-151.

Dahl, P. S. 1980. The termal-composicional dependence of Fe^{+2}-Mg distributions between coexisting garnet and pyroxene: applications to geothermometry. *American Mineralogist,* **65**: 854-866.

de Araújo, C.E.G, Píneo, T.R.G, Caby, R., Costa, F.G., Cavalcante, J.C., Vasconcelos, A.M., Rodrigues, J.B. 2010a. Provenance of the Novo Oriente Group, southwestern Ceará Central Domain, Borborema Province (NE-Brazil): A dismembered segment of a magma-poor passive margin or a restricted rift-related basin? *Gondwana Research* **6**: 265-273.

Del Lama, E.A., Zanardo, A., Oliveira, M.A.F, Morales, N. 2000. Exhumation of high-pressure granulites of the Guaxupe Complex, southeastern Brazil, *Geological Journal,* **35:** 231-249.

Droop, G.T.R., 1987. A general equation for estimating Fe^{3+} concentrations in ferromagnesian silicates and oxides from microprobe analyses, using stoichiometric criteria, *Mineralogical Magazine,* **51**: 431-437.

Duclaux, G., Ménot, R.P., Guillot, S., Agbossoumondé, Y., Hilairet, N., 2006. The mafic layered complex of the Kaby´ e massif (north Togo and north Benin): Evidence of a Pan-African granulitic continental arc root. *Precambrian Research,* **151:** 101-118.

Eckert, J. O. Jr., Newton, R. C., Kleppa, O. J. 1991. The þH of reaction and recalibration of garnet-pyroxene-plagioclase-quartz geobarometers in the CMAS system by solution calorimetry. *American Mineralogist,* **76**: 148-160.

Ellis, D. J, Green, D. H. 1979. An study of the effect of Ca upon garnet-clinopyroxene Fe-Mg exchange equilibria. *Contribution to Mineralogy and Petrology,* **71**: 13-22.

Ferreira, M. A. A., Abreu, F. A. M., Moura, C. A. V., Gorayeb, P. S. S. 1996. Resultados Isotópicos Pb-Pb em Zircão na Faixa de Alto Grau de Cariré. In: SBG, Congresso Brasileiro Geologia, 39, Salvador, Anais, **6**: 542-544.

Fetter, A. H. 1999. U/Pb and Sm/Nd Geochronological Constraints on the Crustal Framework and Geologic History of Ceará State, NW Borborema Province, NE Brazil: Implications for the Assembly of Gondwana. Ph.D Thesis, Kansas University, Lawrence.

Fetter, A. H., Santos, T. J. S., Nogueira Neto, J. A., Van Schmus, W. R. 1995. Geocronologia U/Pb em zircão e Sm/Nd em rocha total do Estado do Ceará - resultados iniciais. In: SBG, Simpósio de Geologia do Nordeste, 16, Recife, Boletim Resumos, **14**: 418-422.

Fetter A.H., Van Schmus W.R., Santos T.S., Arthaud M., Nogueira Neto J. 1997. Geologic history and framework of Ceará State: Northwest Borborema Province, NE Brazil. *South American Symposium on Isotope Geology*, Brazil, 112-114.

Fetter, A.H., Van Schmus, W.R., Santos, T.J.S. Nogueira Neto, J.A., Arthaud, M.H. 2000. U-Pb and Sm/Nd geochronological constraints on the crustal evolution and basement architecture of Ceará State, NW Borborema Province, NE Brazil: Implications for the existence of the Paleoproterozoic supercontinent "Atlantica". *Revista Brasileira de Geociências,* **30:** 102-106.

Fetter, A.H., Santos, T.J.S., Van Schmus, W.R., Hackspacher, P.C., Brito Neves, B.B., Arthaud, M.H., Nogueira Neto, J.A., Wernick, E. 2003. Evidence for Neoproterozoic continental arc magmatism in the Santa Quitéria batholith of Ceará State, NW Borborema Province, NE Brazil: implications for assembly of West Gondwana. *Gondwana Research* **6:** 265-273.

Gaudette H.E., Lafon J.M., Macambira M.J.B., Moura C.A.V., Scheller T. 1998. Comparison of single filament Pb evaporation/ionization zircon ages with conventional U-Pb results: examples from Precambrian of Brazil. *Journal of South America Earth Science,* **11:** 351-363.

Gorayeb, P. S. S., Abreu, F. A. M. 1989. A faixa de alto grau da Região de Cariré-CE. In: SBG, Simpósio Nacional de Estudos Tectônicos, 2, Fortaleza, Boletim Resumos, **11**: 260-263.

Hansen, B. 1981. The transition from pyroxene granulite facies to garnet clinopyroxene granulite facies: experiments in the system CaO–MgO–Al2O3–SiO2. *Contributions to Mineralogy and Petrology*, **76:** 234-242.

Harley, S. L. 1984. An experimental study of the partitioning of Fe and Mg between garnet and orthopyroxene. *Contributions to Mineralogy and Petrology*, **86:** 359-373.

Harley, S.L. 1989. The origins of granulites: a metamorphic perspective. *Geology Magazine,* **126:** 215-247.

Hirdes, W., Davis, D.W. 2002. U-Pb zircon and rutile metamorphic ages of Dahomeyan garnet-hornblende gneisses in southeastern Ghana, West Africa. *Journal of African Earth Sciences,* **35:** 445-449.

House, M., Attoh,K. 1996. Ar/Ar laser mapping of hornblende porphyroclasts from the Panafrican Dahomeyide orogen, West Africa, *EOS Transactions American Geophysical Union* **77** .

Kretz, R., 1983. Symbols of rock-forming minerals, *American Mineralogist,* **68**: 277–279.

Krogh, E. J. 1988. The garnet-clinopyroxene Fe-Mg geothermometer – a reinterpretation of existing experimental data. Contributions of Mineralogy and Petrology, **99**: 44-48.

Leake, B. E., Schumacher, J. C., Smith, D. C.;Ungaretti, L., Whittaker, E. J. W., Youzhi, G. 1997. Nomenclature of amphiboles. *European Journal of Mineralogy*, **9:** 623-651.

Ludwig, K. 2001. Isoplot/Ex, rev. 2.49, *A Geochronological Toolkit for Microsoft Excel. Berkeley Geochronology Center, Special Publications 1a*.

Matteini, M., Dantas, E. L., Pimentel, M. M., Buhn, B. 2010. Combined U-Pb and Lu-Hf isotope analyses by laser ablation MC-ICP-MS: methodology and applications. *Anais da Academia Brasileira de Ciências,* **82 (2):** 479-491.

Martins, G., Oliveira, E.P., Lafon, J.M. 2009. The Algodões amphibolite–tonalite gneiss sequence, Borborema Province, NE Brazil: geochemical and geochronological evidence for Palaeoproterozoic accretion of oceanic plateau/back-arc basalts and adakitic plutons. *Gondwana Research,* **15:** 71-85.

Monié, P., Caby, R., Arthaud, M.H. 1997. The Neoproterozoic Brasiliano Orogeny in Northeast Brazil: $^{40}Ar/^{39}Ar$ and petrostructural data from Ceará, *Precambrian Research,* **81:** 241-264.

Morel, M.L.A., Nebel, O., Nebel-Jacobsen, Y.L., Miller J.S., Vroon, P.Z. 2008. Hafnium isotope characterization of the GJ-1 zircon reference material by solution and laser-ablation MC-ICPMS, *Chemical Geology* **255**: 231-235.

Morimoto, N., Ferguson, A.K., Ginzburg, LV., Ross M., Seifert, F.A., Seifert, J. Seifert, Z., Aoki K., Gottardi, G. 1988. Nomenclature of pyroxenes, *American Mineralogist,* **73:** 1123-1133.

Newton, R. C., Perkins, D. 1982. Thermodynamic calibration of geobarometers based on the assemblages garnet-plagioclase-orthopyroxene (clinopyroxene)-quartz. American Mineralogist, **67**: 203-222.

Nogueira Neto, J.A. 2000. Evolução Geodinâmica das faixas granulíticas de granja e cariré, extremo noroeste da Província Borborema. PhD. Thesis Universidade Estadual Paulista-UNESP 171.

Nogueira Neto, J. A., Santos, T. J. S., Fetter, A. H., Veríssimo, C. U. V., Nogueira, J. F. 1995. Tectônica transpressiva - transtrativa e posicionamento de corpos graníticos na região de Cariré - NW do Ceará. In: SBG, Simpósio Nacional de Estudos Tectônicos, 5, Gramado, Resumos Expandidos, 202-204.

Nogueira Neto, J. A., Fetter, A. H., Legrand, J. M., Santos, T. J. S., Hackspacher, P. C. 1997a. Idade Neoproterozóica em Granulitos de Cariré (NW do Ceará): U/Pb em Titanita e Idade Modelo (TDM) - Resultados Iniciais. In: SBG, Simpósio Nacional de Estudos Tectônicos, **6,** Pirenópoles, Resumos Expandidos, 101-103.

Nogueira Neto, J. A., Fetter, A. H., Santos, T. J. S., Nogueira, J. F., Hackspacher, P. C.1997b. Datação U/Pb em Zircão e Idade Modelo (TDM) de Corpo Granítico Sin-Cinemático da Região de Cariré - NW do Ceará. In: SBG, Simpósio de Geologia do Nordeste, 17, Fortaleza, Boletim Resumos, **15**: 95-97.

O'Brien, P.J. 1989. The petrology of retrograded eclogites of the Oberpfalz Forest, northeastern Bavaria, West Germany, *Tectonophysics,* **157**:195-213.

O'Brien, P.J. 2001. Subduction followed by collision: Alpine and Himalayan examples, *Physics of the Earth and Planetary Interiors,* **127**: 277-291.

O'Brien, P.J, Rötzler, J. 2003. High-pressure granulites: formation, recovery of peak conditions and implications for tectonics. *Journal of Metamorphic Geology*, **21:** 3-20.

Oliveira, D.C. and Mohriak, W.U. 2003. Jaibaras trough: an important element in the early tectonic evolution of the Parnaíba interior sag basin, Northern Brazil. *Marine and Petroleum Geology* **20**: 351-383.

Pattison, D. R. M., 2003. Petrogenetic significance of orthopyroxene-free garnet +clinopyroxene + plagioclase-bearing metabasites with respect to the amphibolite and granulite facies. *Journal of Metamorphic Geology*, **21:** 21-31.

Perkins, D. Iii And Chipera, S. J. 1985. Garnet-orthopyroxene-plagioclase-quartz geobarometry: refinements and application to the English Riversubprovince and the Minnesota River Valley. *Contrib. Mineral. Petrol.,* **89**: 69-80.

Powell, R. 1985. Regression diagnostics and robust regression in geothermometer/geoberometer calibration: garnet-clinopyroxene geothermometer revisited. *Journal of Metamorphic Geology*, **3**: 231-243.

Powell, R., Holland, T. J. B. 1988. An internally consistent dataset with uncertainties and correlations: 3. Applications to geobarometry, worked examples and a computer program. *Journal of metamorphic Geology,* **6**:173-204.

Richard, P., Shimizu, N., Allegre, C.J. 1976. $^{143}Nd/^{144}Nd$, a natural tracer: an application to oceanic basalts, *Earth Planetary Science Letters,* **31:** 269-278.

Reno, B.L, Brown, M., Kobayashi, K., Nakamura, E., Piccoli, P.M, Trouw, R.A.J. 2009. Eclogite–high-pressure granulite metamorphism records early collision in West Gondwana: new data from the Southern Brasília Belt, Brazil. **Journal of the Geological Society*, 166:*** 1013-1032.

Santos, T. J. S., Nogueira Neto, J. A., Fetter, A. H., Hackspacher, P. C. 2001. Petrografia e Litogeoquímica das Rochas do Embasamento Cristalino da Região de Granja - CE. *Revista de Geologia (UFC),* **14:** 33-48.

Santos, T. J. S., Souza, G. M., Queiroz, H. B., Nogueira Neto, J. A., Parente, C. V. 2002. Tafrogênese estateriana no embasamento paleoproterozóico do NW da Província Borborema: Uma aboradagem petrográfica, geoquímica e geocronológica. In: XLI Congresso Brasileiro de Geologia, João Pessoa. *Anais do XLI Congresso Brasileiro de Geologia.* p.337.

Santos, T. J. S., Garcia, M.G. M., Amaral, W. S., Caby, R., Wernick, E., Arthaud, M. H., Dantas, E. L., Santosh, M., 2009. Relics of eclogite facies assemblages in the Ceará Central Domain, NW Borborema Province, NE Brazil: Implications for the assembly of West Gondwana. *Gondwana Research*, **15:** 454-470.

Santos, T.J.S., Fetter, A.H., Nogueira Neto, J.A., 2008. Correlation of the West margin of the Transbrasiliano – Kandi Lineament in the Borborema Province (NE Brazil) and Pharusian Belt (NW Africa). In: Pankhurst, R.J., Trouw, R.A.J., Brito Neves, B.B. & de Wit, M.J. (eds) West Gondwana: Pre-Cenozoic Correlations Across the South Atlantic Region. Geological Society, London, Special Publications, **294:** 101-119.

Schaltegger, U., Fanning, C.M., Günther, D., Maurin, J.C., Schulmann, K., Gebauer, D. 1999. Growth, annealing and recrystallization of zircon and preservation of monazite in high-grade metamorphism: conventional and in-situ U-Pb isotope, cathodoluminescence and microchemical evidence.*Contributions to Mineralogy and Petrology,* **134:** 186-201.

Scherer, E., Münker, C., Mezger, K. 2006. Calibration of the lutetium–hafnium clock, *Science,* **293:** 683-687.

Sajeev, K., Jaehoon, J., Sanghoon, K., Weon-Seo K., Sung, W. K., Komiya, T., Itaya, T., Hyung-Sup, J., Park, Y. 2010. High *P–T* granulite relicts from the Imjingang belt, South Korea: Tectonic significance. *Gondwana Research,* **17:** 75-86.

Sengupta, P., Dasgupta, S., Bhattacharya, P. K., Hariya, Y. 1989. Mixing behavior in quaternary garnet solid solution and extended Ellis and Green garnet-clinopyroxene geothermometer. Contributions to Mineralogy and Petrology, **103**: 223-227.

Trompette, R. 1994. Geology of Western Gondwana (2000-500 Ma.). Pan-African / Brasiliano Aggregation of South America and Africa.Balkema. 350p.

Vauchez, A., Neves, S., Caby, R., Corsini, M., Egydio-Silva, M., Arthaud, M.H., Amaro, V.1995. The Borborema shear zone system, NE Brazil. *Journal of South American Earth Sciences.*8:247-266.

Vavra, G., Gebauer, D. Schmid R., Compston, W. 1996. Multiple zircon growth and recrystallization during polyphase Late Carboniferous to Triassic metamorphism in granulites of the Ivrea Zone (Southern Alps): an ion microprobe (SHRIMP) study, *Contributions to Mineralogy and Petrology,* **122**: 337-358.

Vavra, G., Schmid, R., Gebauer, D. 1999. Internal morphology, habit and U-Th-Pb microanalysis of amphibolite-to-granulite facies zircons: geochronology of the Ivrea Zone (Southern Alps). *Contributions to Mineralogy and Petrology,* **134:** 380-404.

Weiss, C.S. 1803. Über die Gebirgsart des sächsischen Erzgebirges, welche unter dem Namen Weiss-Stein neuerlich bekannt gemacht worden ist. *Neue Schriften Gesellschaft Naturforschender Freunde*, **4:** 342-366

Wells, P. R. A. 1977. Pyroxene thermometry in simple and complex systems. *Contributions to Mineralogy and Petrology,* **62**: 129-139.

Winkler, H. G. F. 1979. *Petrogenesis of Metamorphic Rocks*, 5th edn. Springer-Verlag, New York Inc. 348.

Wood, B. J., Banno, S. 1973. Garnet-orthopyroxene and orthopyroxene-clinopyroxene relationships in simple and complex systems. *Contributions to Mineralogy and Petrology,* **42**: 109-124.

Xiaochun, L., Jianmin, H.Y. Z., Yuxing, L., Chunjing, W., Xiaohan L. 2009. Late Neoproterozoic/Cambrian high-pressure mafic granulites from the Grove Mountains, East Antarctica: *P–T–t* path, collisional orogeny and implications for assembly of East Gondwana. *Precambrian Research,* **174:** 181-199

Yardley, B. W. D. 1989. *An Introduction to Metamorphic Petrology.* Longman Scientific,Harlow.

Zhang, J., Zhao, G., Sun, M., Wilde, S., Li,S., Liu, S. **2006.** High pressure mafic granulites in the Trans-North China Orogen: tectonic significance and age *Gondwana Research*: **9,** 349-362.

Zhao, G.C., Cawood, P.A, Wilde G.C., Lu, L.Z. 2001. High-pressure granulites (retrograded eclogites) from the Hengshan Complex, North China Craton: petrology and Tectonic implications, *Journal of Petrology,* **42**: 1141-1

ANEXO 02

"Amaral, W.S., Santos, T.J.S., Wernick, E. 2010. **Occurrence and geochemistry of metamafic rocks from the Forquilha Eclogite Zone, central Ceará (NE Brazil): Geodynamic implications.** *(Special Issue) Geological Journal* (DOI: 10.1002/gj.1224) **(Publicado)**".

Disponível para download em:

http://onlinelibrary.wiley.com/doi/10.1002/gj.1224/abstract

Occurrence and geochemistry of metamafic rocks from the Forquilha Eclogite Zone, central Ceará (NE Brazil): Geodynamic implications

By

WAGNER DA SILVA AMARAL[1], TICIANO JOSÉ SARAIVA SANTOS[1] and EBERHARD WERNICK[2]*

[1] IG - Instituto de Geociências, Universidade Estadual de Campinas -UNICAMP, PO. Box 6152, CEP 13081-970, Campinas, SP – Brazil.

[2] IGCE- Universidade Estadual Paulista (UNESP), Av. 24 A, CEP 13506-900, Rio Claro, SP – Brazil.

*Corresponding author E-mail: wsa.geo@gmail.com

ABSTRACT

In the northern region of the Borborema Province, a 30 km-long mafic/ultramafic belt of HP rocks, called Forquilha Eclogite Zone (FEZ), has been recently discovered in the Central Domain of Ceará State. The belt comprises three groups of rocks: (1) garnet amphibolites, (2) retrograded eclogites and (3) clinopyroxene-garnet amphibolites, all of them being hosted in garnet ± kyanite + sillimanite schists and orthogneisses which are often migmatized. The geochemical analyses of 30 representative samples confirm differences among the three groups that were initially classified by petrography. The garnet amphibolites are the most depleted rocks, with relatively flat $(REE)_{PM}$ pattern and $(SPIDER)_{PM}$ pattern with negative Rb, Th, Nb, Sr and Zr anomalies. It is the most fractionated group, ranging from picrobasalts to andesites. Fractional crystallization and mineral accumulation are indicated by Eu and Sr anomalies. The data show geochemical affinities with island-arc basalts The retrograded eclogites display flat $(REE)_{PM}$, but without Eu anomalies. Nb/La ratios are low and variable, as for slightly enriched MORB from ocean floor or intra-oceanic back-arc environments. However, a genetic link with the Group 1 rocks cannot be completely discarded. The clinopyroxene-garnet amphibolites are the most enriched group. $(REE)_{PM}$ and $(SPIDER)_{PM}$ patterns show many features of alkaline basalts. In the Nb/Yb vs. Th/Yb diagram the data cluster near the E-MORB standard. Several geochemical aspects of these rocks fit well those from the HP/UHP Pan-African/Brasiliano Suture Zone in the Dahomeyides/Hoggar regions of West Africa. However differences in their extent and lack of alignment preclude a direct correlation among these zones.

KEY WORDS Borborema Province; HP/UHP; retrograded eclogites; Pan-African Belt; geochemistry

1. INTRODUCTION

Eclogites are important rocks for reconstructing the tectonic evolution of orogenic belts, as they represent, in many cases, the exhumed remnants of deep seated sutures. In the Pharusian Belt NW Africa, high-pressure (HP) mafic/ultramafic rocks define a suture zone about three thousand kilometers long, from Algeria to the Gulf of Guinea (Black *et al.,* 1994; Trompette, 1994; Attoh, 1998; Caby, 2003). The continuation of this oceanic suture zone in northeast Brazil, beneath the Phanerozoic Parnaíba Basin (Figure 1), is speculated based on the high density gravity anomalies identified over this area (Lesquer *et al.,* 1984; Trompette, 1994; El-Hadj *et al.,* 1997; Fetter *et al.,* 2003).

The Central Hoggar in Algeria, NW Africa (Figure 1) is made of four distinct crustal blocks termed as LATEA (Liégeois *et al.,* 2003). These terranes were accreted during the Pan-African Orogeny (650-525 Ma) and are part of a single passive margin upon which mafic eclogites, garnet amphibolites and clinopyroxene-garnet amphibolites metamorphosed at 15 kbar-790°C were tectonically emplaced and thrusted around 686 Ma (Boughrara, 1999; Liégeois *et al.,* 2003). These metamafic rocks are interlayered with metasedimentary rocks and orthogneiss in the Tin Begane region, in the northern part of Laouni terrane (Derridj *et al.,* 2003; Caby, 2003).

In the Ceará Central Domain of the Borborema Province (BP), NE Brazil, high grade migmatitic garnet ± sillimanite ± kyanite metasediments (often khondalites/kinzigites) from the Ceará Group comprise more or less frequently small to large lenses/horizons of quartzites, marbles and calc-silicate rocks. In northwest part of this domain a four kilometre-thick and thirty kilometre- long mafic/ultramafic belt of high/ultrahigh pressure (HP/UHP) metamorphic rocks, called the Forquilha Eclogite Zone, has been recently discovered (Santos *et al.,* 2008a). The highest metamorphic conditions recorded in the retrograded eclogites are T~770°C and P~ 17.3 kbar (Santos *et al.,* 2009). In addition to the retrograde eclogites, the Forquilha Eclogite Zone, several varieties of clinopyroxene-garnet amphibolites and garnet amphibolites are also present. These rocks occur as small dismembered boudins, erratic blocks and sheets within the host aluminous metasediments and often in strongly sheared granodioritic gneisses. Both varieties of host rocks are frequently migmatized.

Concordant lenses of high pressure metaultramafic and metamafic rocks in migmatites and orthogneisses also occur in the Pajeú-Paraíba Belt in the Transversal Domain of the BP. The

geochemical signature of these eclogite facies rocks points to a tholeiitic basaltic composition related to an island-arc evolution. They are probably associated with an enriched mantle source underlying a subduction zone. Positive and negative gravimetric anomalies in these metaultramafic and metamafic rocks suggest the presence of a possible NE-SW to E-W continental collision zone (Beurlen *et al*., 1992, Almeida *et al.,* 2009). However, the absence of detailed chemical data hinder the comparison of these rocks with those from the FEZ.

In Africa the pre-metamorphic nature of the mafic/ultramafic rocks, which are mainly retrograded eclogites and granulites, is disputable. They dominantly display a magmatic geochemical characteristic often comparable with N-MORB and IAT (John *et al.,* 2003; Attoh and Morgan, 2004). This geotectonic link is supported by coexisting amphibolites facies rocks (Wang *et al.,* 2008). The coexisting eclogites show considerable geochemical variation reflecting an intra-continental rift environment (Rao and Rai, 2006). In contrast to the magmatic heritage, some HP/UHP rocks seem to have been derived from metasedimentary, mainly calc-silicate rocks (Jahn *et al.,* 2001). Still in other cases, the chemical classification of the eclogites is quite uncertain, due to mainly three factors: i) metamorphic differentiation leading to the separation of the former homogeneous mafic igneous protoliths and associated near-monomineralic rocks (hornblendites, pyroxenites and garnet felses) (Rumble *et al.,* 2005); ii) contamination by crustal materials (Duclaux *et al.,* 2006) and iii) selective extraction and/or addition of some mobile trace elements during the different stages of prograde and retrograde metamorphism associated with dehydration and re-hydration (Bernard-Griffiths *et al.,* 1991).

In the Dahomeyide Belt in Togo, west Niger and also in the central Hoggar (Tin Begane area), geochemical signatures of the HP/UHP mafic rocks from the suture zone are mainly interpreted as more or less similar to those from island-arc tholeiites (IAT) with some N-MORB contribution. However, all the studied areas also comprise highly anomalous samples of dubious classification (Castaing *et al.,* 1994; Attoh, 1998; Liégeois *et al.,* 2003; Attoh and Morgan, 2004; Duclaux *et al.,* 2006).

In this paper, we present geochemical data for 30 samples belonging to garnet amphibolites, clinopyroxene-garnet amphibolites and retrograded eclogites suite from the Forquilha Eclogite Zone (FEZ) to evaluate their pre-metamorphic nature, geotectonic setting and their comparison with the Pharusian/Dahomeyide suture complex rocks.

2. GEOLOGICAL SETTING

The Borborema Province has been in focus related to the discussions on the tectonics and assembly of West Gondwana (e.g. Fetter *et al*., 2003; Bueno *et al*., 2009; Guimarães *et al*., 2009; Cordani *et al.,* 2009). The northwestern part of the Borborema Province comprises two crustal blocks: the Ceará Central Domain (CCD) and Médio Coreaú Domain (MCD), bounded by the Transbrasiliano Lineament, considered as an extension in South America of the African Kandi/4° 50' Lineament (Figure 1) (Caby, 1989; Trompette, 1994; Brito Neves *et al.,* 2000). The MCD basement mainly comprises tonalite-trondhjemite-granodiorite (TTG) orthogneisses, as well as minor areas of amphibolite facies gneisses and migmatites, amphibolites, leucogranites, mafic granulites, enderbites, leptynites, and kinzigites of Brasiliano age metamorphism (Santos *et al.,* 2004). U-Pb and Sm-Nd ages are mainly Paleoproterozoic (2.36-2.30 Ga) and yield Nd crustal residence ages (T_{DM}) between 2.61 and 2.38 Ga (Fetter *et al.,* 2000; Santos *et al.,* 2009). Most the $\varepsilon_{Nd\ (t\ =\ crystallization\ age)}$ values of these gneisses are positive (0.4 to 1.9); so they are considered as the products of a juvenile crustal growth in an arc-type setting (Fetter *et al.,* 2000; Santos *et al.,* 2009). The CCD basement also comprises juvenile middle Paleoproterozoic Canindé Complex including migmatites, orthogneisses, kinzigites and amphibolites. U-Pb zircon ages of 2.1 Ga and T_{DM} between 2.45 to 2.3 Ga with slightly negative to positive $\varepsilon_{Nd\ (t\ =\ crystallization\ age)}$ suggest a predominantly depleted mantle contribution with incipient crustal contamination (Fetter, 1999; Martins *et al.,* 2009; Castro, 2004).

In both domains, the supracrustal sequences rest on the basement rocks. In the MCD they are represented by the Ubajara and Martinópole Groups; in the CCD by the Ceará Group. These rocks belong to the greenschist and amphibolite facies and represent proximal, platformal volcano-sedimentary sequence comprising slates, quartzites, marbles, metagreywackes, metapelitic gneisses as well as felsic to mafic metavolcanics.

The Martinópole deposition age, established by U-Pb zircon data from a metarhyolite, is 777 ± 11 Ma (Fetter *et al.,* 2003). The Nd model ages for the basal schists of this group varies between 1.24 and 1.32 Ga, and the data suggest a significant genetic contribution of Neoproterozoic juvenile volcanic material (Santos *et al*., 2008b). The upper unit displays Nd model ages between 1.61 and 2.69 Ga, which are interpreted as a mixture between

Neoproterozoic juvenile material and older Paleoproterozoic basement gneisses (Fetter *et al.,* 2003; Santos *et al.,* 2008a).

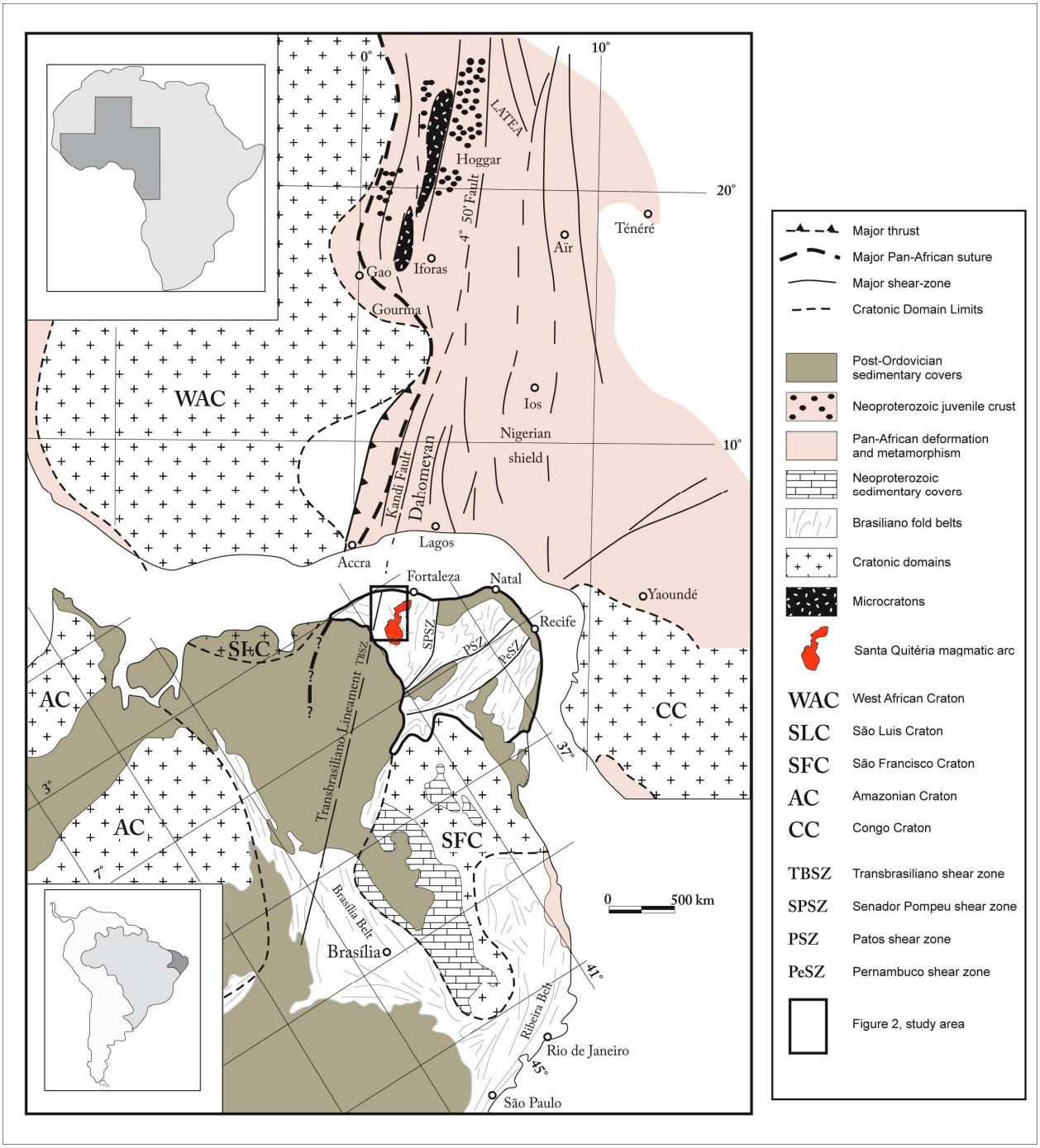

Figure 1: The Borborema Province in the context of the Western Gondwana supercontinent (modified after Caby, 1989 and Arthaud *et al.* ,2008).

In the Ceará Group, metarhyolites yield U-Pb zircon ages between 800 to 750 Ma, which are considered as representing an initial continental Neoproterozoic rifting stage (Fetter, 1999;

Arthaud *et al.,* 2008). However, the real age of the Ceará group is still uncertain. Rare HP/UHP metamorphic rocks from the Ceará Group, including garnet-amphibolites, clinopyroxene-garnet amphibolites and retrograded eclogites in the Forquilha Eclogite Zone and the Itatira areas crop out respectively on the western and eastern sides of the Santa Quitéria magmatic arc (Figure 2; Castro, 2004; Garcia and Arthaud, 2004; Amaral and Santos, 2008).

The Santa Quitéria batholith (Figure 2) is a continental magmatic arc covering an area of about 40,000 km^2, and comprising a large variety of lithologies including gabbro, tonalite, monzogranite, granodiorite, and granitic rocks emplaced in at least two major magmatic cycles. U-Pb zircon and Sm-Nd whole rock data indicate an emplacement age between *ca*. 665 and 591 Ma (Fetter *et al.,* 2003). Nd isotopic signatures of plutonic rocks suggest a mixture between juvenile Neoproterozoic magmas and the enclosing Paleoproterozoic gneisses from the Canindé Complex. The late magmatic stage comprises numerous post-tectonic granitic isotropic intrusions such as the Serra da Barriga, Pajé, and Taperuaba plutons (Figure 2). The final magmatic activity is a widespread episode of aplitic and pegmatitic dyke emplacement, the latter frequently tourmaline-bearing.

The main tectonic regional trend in the MCD and CCD is NE-SW resulting from numerous older thrusts and younger strike-slip shear zones, the former with a dominantly W-NW vergence (Santos *et al.,* 2008a).

3. FIELD OCCURRENCE AND SAMPLES DESCRIPTION

The Forquilha garnet-bearing mafic rocks crop out as lenses and boudins of 15 to 300 m in length and 10 to 70 m in width within garnetiferous metapelites (Figures 3a and b). Locally, the association of the lenses with calc-silicate rocks is common. The mafic rocks comprise layers enriched either in diopside (diopsidites), amphiboles (hornblendites) and garnet. All the studied samples were collected from the centre of homogeneous bodies since their margins are more schistose as well as biotite and amphibole-rich, a result of penetrative deformation and copious hydration. The surrounding host metasediments are represented by aluminous metatexites and diatexites (garnet-sillimanite ± kyanite-biotite graphitic gneisses = kinzigites). The metabasites comprise varying abundance of garnet, pyroxenes, amphiboles and quartz, which are the main constituents of these rocks. Along the Forquilha Eclogite Zone, the metamorphic conditions

increase from north (amphibolite facies) to south (eclogite facies). The mineralogical variation allowed a preliminary field classification into three rock groups which is also confirmed by petrographic studies: garnet amphibolites, retrograde eclogites now exposed mainly as clinopyroxene-garnet amphibolites with typical decompression textures, and clinopyroxene-garnet amphibolites.

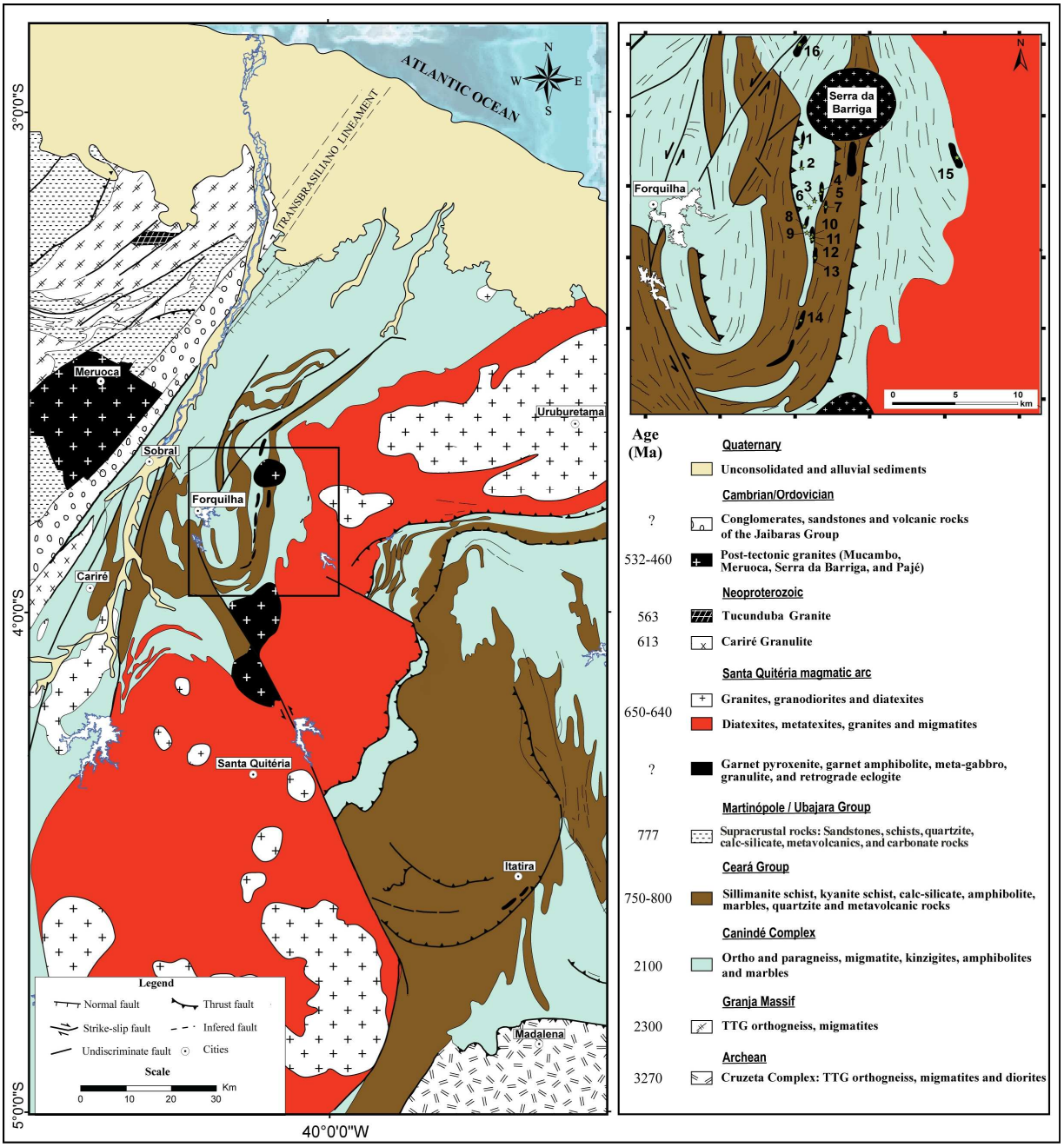

Figure 2: Simplified geologic map of the Médio Coreaú Domain and the Ceará Central Domain in the NW part of the Borborema Province. The locations of the samples collected for this study are: 1) TJF6-296; 2) RM-220, 3) WT8-53E, 4) W8-10 (A-F), 5) WT7-53D, 6) VC-57 (E-G-g), 7) RM-120A, 8) RM-107 (C-D), 9) RM-182, 10)VC-60, 11) RM-179, 12) TJF5-181, 13) TJF6-302, 14) TJF6-335 (A-D), 15) VC-4 (A-B), 16) WT7-25.

The garnet amphibolites are composed of garnet (20-25% vol.), diopside (5-10%), amphibole (30-40 %), plagioclase (An_{10-20})(20-25%), quartz (10-15%), rutile (< 1%), ilmenite (<3%) titanite (<3%), apatite (<3%), and epidote (<1%). Symplectitic hornblende + quartz intergrowth textures are rare. Coronal plagioclase surrounding garnets is more common (Figures 3c and d).

The retrograde eclogites are composed of amphiboles (25-30% vol.), diopsidic clinopyroxene (15-17%), garnet (35%), albitic plagioclase (10-15%), quartz (~5%); rutile, apatite, ilmenite, titanite, carbonate and opaque minerals as recurrent accessories. Sample TJF6-302 contains a larger amount of apatite than the other samples of this group. The proportion between plagioclase and pyroxene is variable, with either the former or the latter mineral dominating. The most complex symplectites are formed by clinopyroxene + plagioclase + quartz ± amphibole, but two other types have also been observed: ilmenite + clinopyroxene and ilmenite + plagioclase. The major part of the symplectites are pseudomorphs of omphacite (Figures 3e and f).

The peak metamorphic conditions are around 770 °C temperature and 17.3 kbar pressure as determined using the mineral assemblage: Na-rich clinopyroxene (jadeite) + pyrope-rich garnet + quartz + rutile. The P-T path of the retrograded eclogites indicates that the rock passed through eclogite facies → granulite facies → amphibolite facies → greenschist facies. Rocks from this group occur locally associated with scapolite-, biotite- and phlogopite-rich calc-silicate rocks. Detailed description of the petrographic characteristics as well as mineral chemistry data and metamorphic conditions were previously presented and discussed (Santos *et al.* 2009).

The clinopyroxene-garnet amphibolites comprise mainly garnet (27-35% vol.), clinopyroxene, dominantly diopside (15-20 %), amphibole (25-30 %), plagioclase (An_{10-20}) (20%), quartz (10%), rutile (< 1%), ilmenite (<2%), sphene (2%) and apatite (2%). The most common symplectites are represented by clinopyroxene + plagioclase ± amphibole intergrowths (Figures 3g and h) which originated during the exhumation path of the former eclogite facies rocks. The garnets are poikiloblastic with inclusions of drop-shaped quartz, rutile, titanite and zircon or xenoblastic with irregular rims. Plagioclase frequently occurs as recrystallized grains in coronas around garnets.

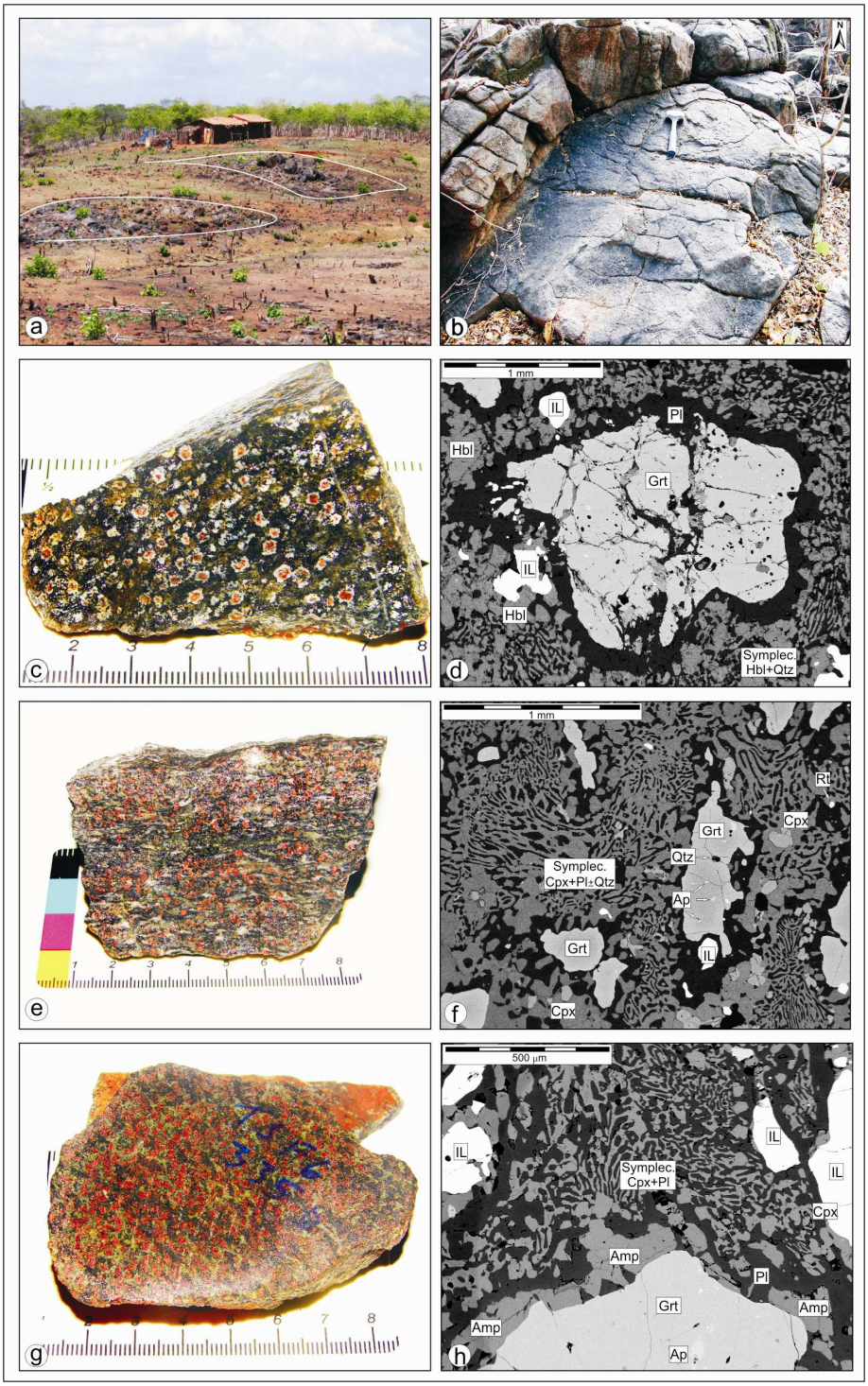

Figure 3: a) Most common lenticular form of occurrence of metamafic rocks; b) detail of the lenticular form of an retrograde eclogite; c) detail of a representative sample of garnet amphibolites, where garnets form coronas and hornblende is the main mineral; d) garnets with inclusions of drop-shaped quartz and plagioclase aureoles in hornblende (Hbl); e) mesoscopic sample of a retrograded eclogite with oriented amphiboles and pyroxenes; f) microphotograph of a sample representative of retrograde eclogites: garnet (Grt), clinopyroxene (Cpx), apatite (Ap), ilmenite (IL), rutile (Rt) and clinopyroxene + plagioclase (Pl) ± quartz (Qtz) symplectites; g) diopside-rich sample representative of clinopyroxene garnet amphibolites; h) microphotograph of a cpx-garnet amphibolite, where symplectites of Cpx+ Pl and narrow amphibole (Amp) rim surrounding the garnets.

4. GEOCHEMISTRY

Major, minor and trace elements for 30 metabasic rocks from the Forquilha Eclogite Zone are listed in Table 1. The samples include 5 garnet amphibolites, 6 clinopyroxene-garnet amphibolites and 19 retrograde eclogites.

Major and minor elements for the 10 samples with a (*), were obtained by ICP-ES; trace elements (including REE) by ICP-MS; reference standard was 50 – 18/CBS. Analytical uncertainty for major elements is 1%; 15% for minor and trace elements. Analyses were performed by ACME Analytical Laboratories, LTD, British Columbia, Canada.

Major, minor and trace elements for the other 20 samples were performed at the Institute of Geosciences, State University of Campinas – UNICAMP. Major and minor elements were determined by XRF according to the method described by Vendemiatto and Enzweiler (2001), with minor modifications. Glass disks were prepared by fusing of 1g of pre-ignited sample with 6g of lithium $LiBO_2/Li_2B_4O_7$ Claisse 50:50 flux, for 15 min in a Pt-Au crucibles and molds fluxer. Analyses were performed with a sequential WD-XRF spectrometer (PanAnalytical - PW 2404). Loss on ignition (LOI) was measured by heating 4g of dry sample at 1000 ºC in pre-ignited porcelain crucibles for 1.5 hours. The accuracy of results was checked by simultaneous analysis of the standards BHVO-2 (USGS) and WS-E (SARM).

Trace elements were determined by inductively coupled plasma mass spectrometry (ICP-MS), after total digestion with HF/HNO3 (Paar bombs, 4 days, 180°C), similar to the procedure described by Navarro *et al.* (2008). Quality control was performed by simultaneous analysis of the basalt standards BRP-1 and BHVO-2. The equivalent quality of the two data sets was assured by some samples analyzed in both laboratories; in mean the analytical differences were lower than 10%.

SiO_2 ranges between 43.35 and 53.23 wt %; mean SiO_2, Na_2O and K_2O values are 48.82%, 2.3% and 0.21% respectively, and the Mg# varies between 65.92 and 27.14. Mg# was calculated assuming an initial pre-metamorphic Fe_2O_3 / FeO oxidation ratio of 0.20 (Le Maitre *et al.,* 1989). All samples are of basaltic composition, except samples VC-54A and VC-57E, respectively with an ultramafic and intermediate composition.

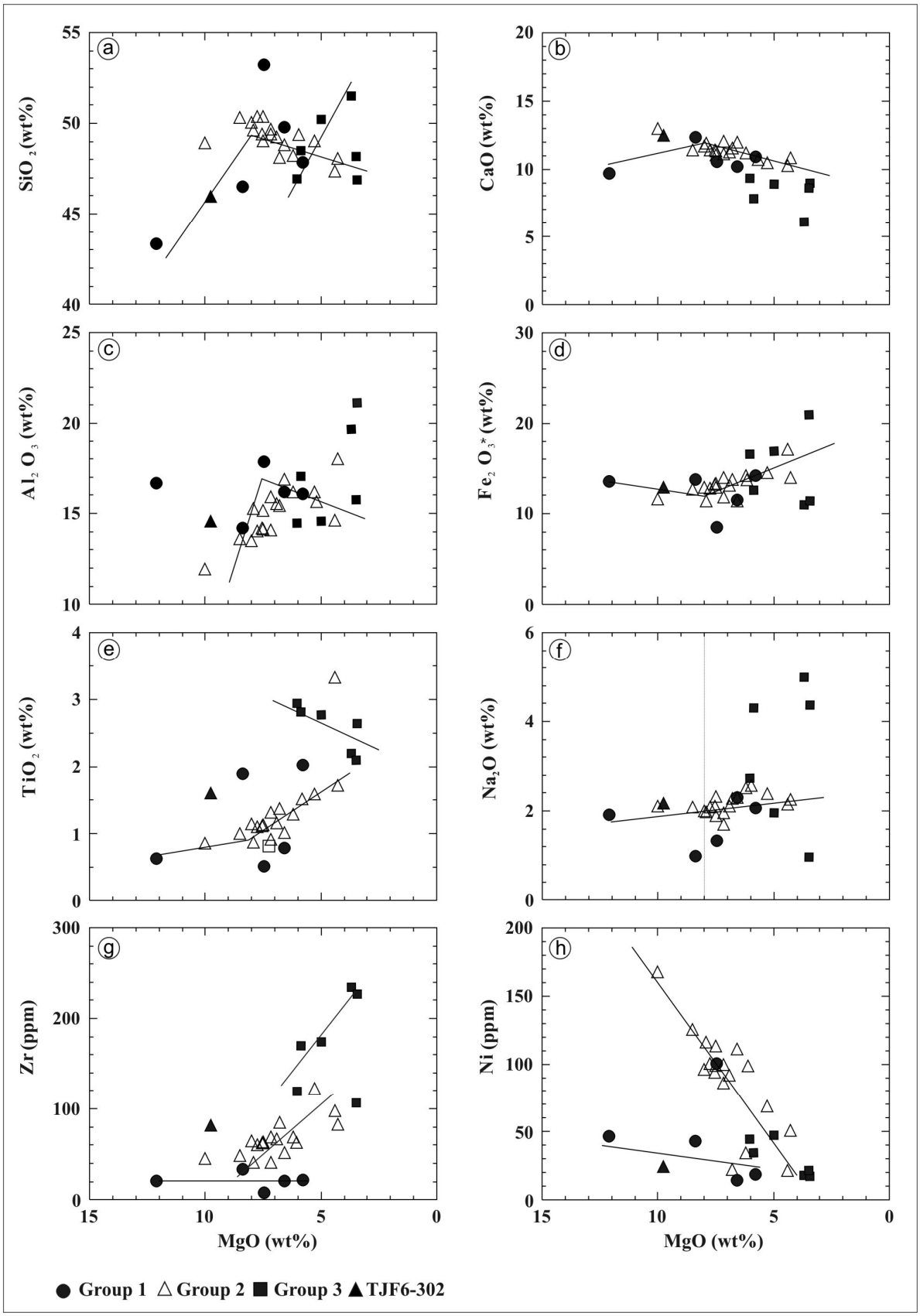

Figure 4: Fenner diagram for a) SiO_2; b) CaO; c) Al_2O_3; d) Fe_2O_3*; e) TiO_2; f) Na_2O; g) Zr; h) Ni.

The MgO *vs.* SiO_2, CaO, Al_2O_3, Fe_2O_3* TiO_2, Na_2O, Zr and Ni diagrams (Figures 4a-h) of garnet amphibolites (filled circles), retrograde eclogites (filled and empty triangles) and clinopyroxene-garnet amphibolites (filled squares), show a mainly segmented evolution, which is a typical feature of the basaltic rocks that have undergone initial olivine fractionation followed by the separation of olivine + clinopyroxene + plagioclase. The Mg-rich segment comprises part of the Group 1 samples; the other part is located on the MgO-poor segments which include the majority of the Group 2 samples. CaO contents in all samples are around 10%, which is the N-MORB standard value. In the MgO *vs*. Al_2O_3 diagram almost all the rocks present Al_2O_3 contents around 15%, with the exception of the clinopyroxene-garnet amphibolites, TJF6-335A and TJF6-335C, respectively with 19.67 % and 21.14 % Al_2O_3, which represent possible plagioclase enriched cumulate rocks (Figure 4c). The MgO *vs*. P_2O_5 diagram (not shown) indicates high P contents for the sample TJF6-302, reflecting its high apatite content. In general, the samples are depleted in alkalis (diagram not shown). The retrograde eclogite group presents $Na_{8.0}$ = ~2 (Figure 4f). This value suggests crustal thickness between 4 and 6 km, compatible with a MORB oceanic crust and high protolith melting rates (Klein and Langmuir, 1987; Castillo *et al.,* 2000; Klein, 2005). However this result is questionable as Na is a typical mobile element which subjected to large variations during initial ocean floor hydration, followed by progressive metamorphism, dehydration, retrograde metamorphism and re-hydration. Also, some anomalous values of mobile elements (mainly Sr, K, Rb, Ba, LREE) indicate a possible geochemical fractionation during the high-grade metamorphism and/or retrograde metamorphism (Bernard-Griffith *et al.,* 1991; Peacock, 1993).

Zr, Nb, Ti, Y and La suggest a good fit between geochemical and petrographic data for the three defined groups. The most depleted Group 1, has the highest Y/Nb and lowest Zr/Y ratios; the Group 2, has intermediate Y/Nb and Zr/Y ratios, whereas Group 3, the most enriched one, has the lowest Y/Nb and highest Zr/Y ratios (Figures 5a and b). Considering a pre-metamorphic basaltic nature for the studied rocks, the Y_{PM} *vs* Zr_{PM}, Nb_{PM} *vs.* La_{PM}, Y_{PM} *vs.* Ti_{PM}, La_{PM} *vs.* La/Lu, Zr/Nb *vs.* Y/Nb and Zr/Nb *vs.* Zr/Y data define two evolution trends, for groups 1 and 2, whereas Group 3 shows a rather outstanding position in the majority of the diagrams. Considering the N-MORB pattern (Sun and McDonough, 1989), Group 3 is distinctive from the other two by high Zr_{PM}, La_{PM}, Nb_{PM} and Ti_{PM} normalized values. The relationship between Groups 1 and 2 in the above mentioned diagrams are of three types: i) the data plot on converging

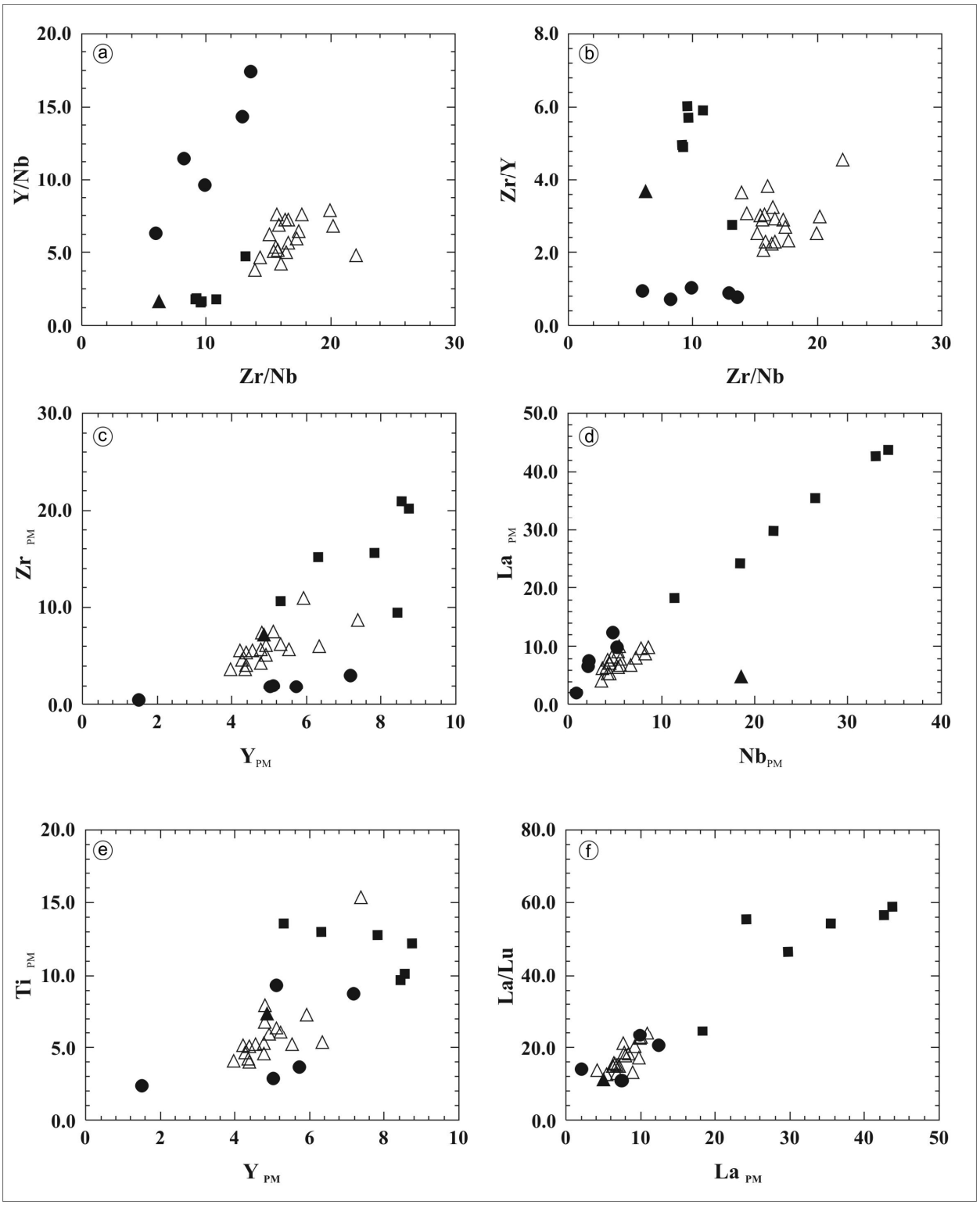

Figure 5: Plots for the Forquilha Eclogite Zone samples in the: a) Zr/Nb *vs*. Y/Nb, b) Zr/Nb *vs.* Zr/Y, c) Y_{PM} *vs.* Zr_{PM}, d) Nb_{PM} *vs.* La_{PM} , e) Y_{PM} *vs.* Ti_{PM} and f) La_{PM} *vs.* La/Lu diagrams.

evolutionary trends (e.g. Figure 5a, c and d); ii) the data plot on parallel evolutionary trends (e.g. Figure 5b); iii) the data for both groups plot on a same evolutionary trend (e.g. Figures 5e and f).

These relationships suggest that groups 1 and 2 may represent either different types of tholeiitic magmas or that both groups are linked by an ACF process.

All samples together define a Ce/La linear correlation of approximately 2:1 (diagram not shown), similar to the MORB standard and for tholeiitic plume tracks (Schilling *et al.* 1983; Humphris and Thompson, 1983). This ratio is also valid for sample TJF6-302, which is clearly La_{PM}-depleted (Figure 5d). Ce contents vary between 3.1 and 68.8 ppm (average of 7.5 ppm in N-MORB) and La contents between 1.4 and 30.0 ppm (average of 2.5 in N-MORB) (Sun and McDonough, 1989).

Groups 1 and 2 present low La/Lu ratios. Except sample WT8-10B, La_{PM} values for Group 3 are higher than 20 and La/Lu values are high. La/Lu and La_{PM} values for the eclogite TJF6-302 are distinctive, supporting a possible chemical mobilization of some mobile elements during the successive metamorphic events (Figure 5f).

In the TAS diagram (not shown) the Group 1 sample VC-54A is classified as picrobasalt and VC-57e as andesitic basalt. All other samples are basalts. Group 3 is on average more alkali enriched, with some samples plotting close to the sub-alkaline/alkaline boundary. In the Nb/Y *vs.* Zr/TiO* 0.0001 diagram (Figure 6a) the samples of Group 1 plot in the sub-alkaline basalt field, Group 2 at the andesite/basalt fields boundary and Group 3 at the sub-alkaline/alkaline basalt fields boundary. In the SiO_2 *vs.* FeO_T/MgO (not shown) and the AFM diagrams (Figures 6b) groups 1 and 2 are classified as tholeiitic rocks. Also, the majority of Group 3 samples plot in the tholeiitic rocks field with the exception of samples TJF6-335A, C and D which plot at the tholeiitic/calc-alkaline boundary, a position also occupied by the mean mafic lower crust composition (Rudnick and Fountain, 1995). All samples plot in the oceanic tholeiitic basalt field in the Zr/10000 P_2O_5 *vs.* Nb/Y diagram with exception of sample TJF6-302 (Figure 6c).

Groups 1 and 2 are classified as ’low MgO and Zr-tholeiites‘ (MgO < 10% Zr < 100 ppm) whereas the Group 3 samples are ’low MgO and high Zr tholeiites‘ (Figure 4g). All groups are ’low Zr/Nb tholeiites‘ (MgO < 10 % and Zr/Nb < 30), common in several oceanic plateaus (Kerr and Mahoney, 2007).

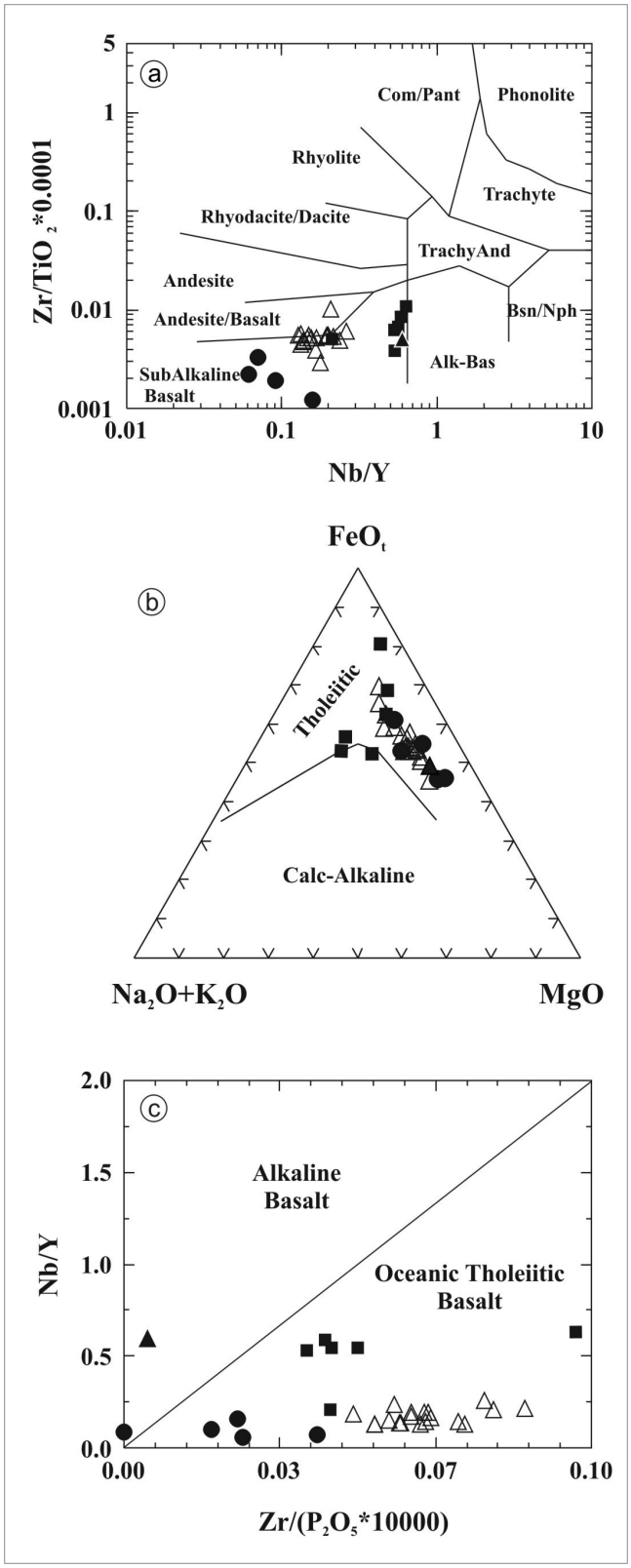

Figure 6: a) Nb/Y *vs.* (Zr/TiO_2 * 0.0001) diagram, fields from Winchester and Floyd (1977); b) FeO_T:(Na_2O+K_2O):MgO diagram, fields from Irvine and Barragar (1971); c) Zr/(10000 P_2O_5) *vs.* Nb/Y diagram, fields from Floyd and Winchester (1975).

Several other discrimination diagrams (Figures 7a, b, c) also suggest an oceanic environment (N-MORB to T-MORB) for the groups 1 and 2 rocks, which data overlap partially, and again assign the outstanding position of the Group 3 samples. The La/Ta *vs.* Tb/Ta diagram shows a continuous enrichment from Group 1 to Group 2 along a line through the central part (primitive mantle) of the diagram (Figure 7d).

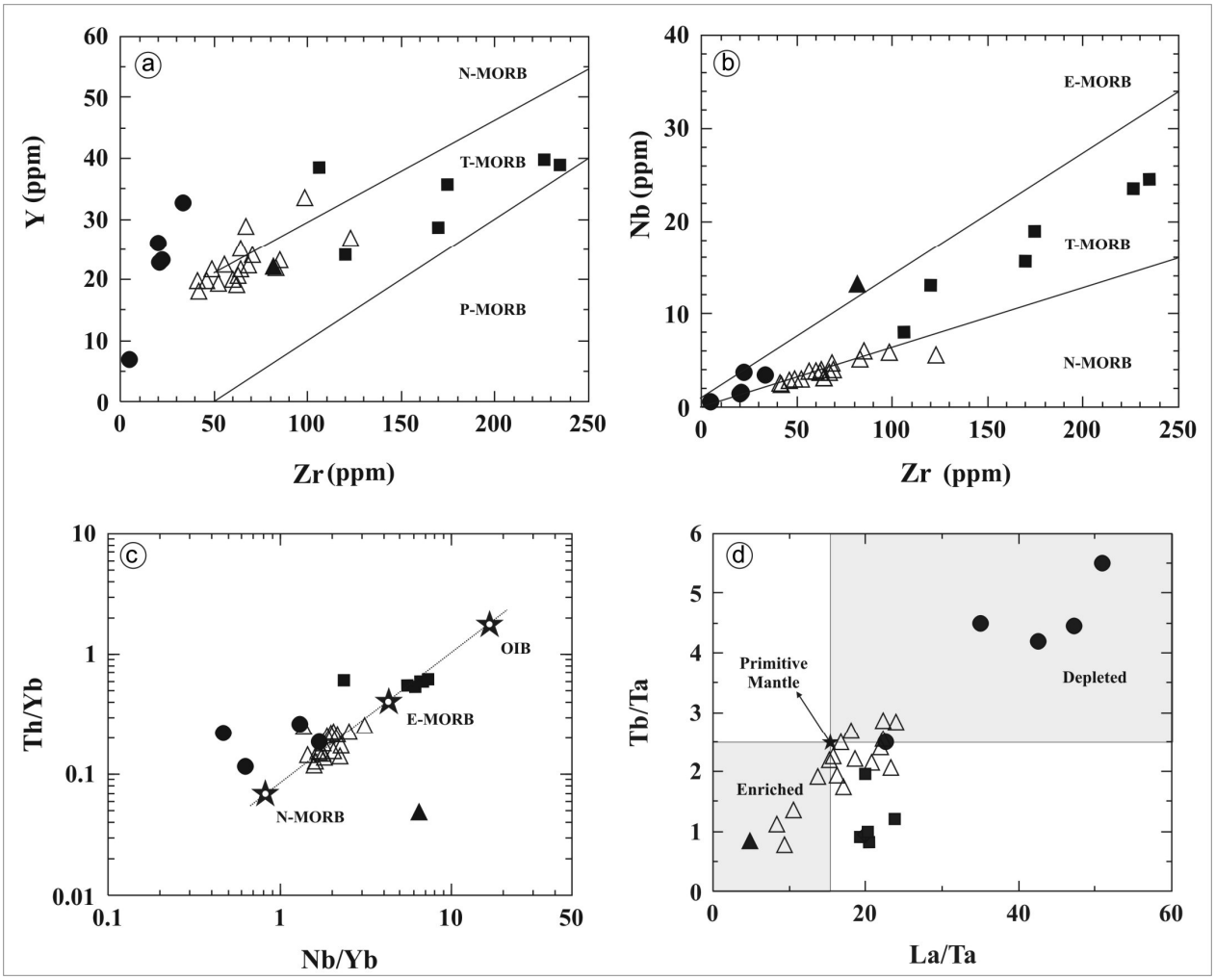

Figure 7: a) Zr *vs.* Y diagram, fields after Le Roex (1987); b) Zr *vs.* Nb diagram, fields after Le Roex (1987); c) Nb/Yb *vs.* Th/Yb diagram, composition of N-MORB, E-MORB, OIB, Upper Continental Crust (UCC), Lower Continental Crust (LCC) are from Sun and McDonough (1989) and Taylor and McLennan (1985); d) La/Ta *vs.* Tb/Ta diagram, modified from Cabanis and Lècolle (1989); primordial mantle from Wood *et al.* (1979).

The chemical variation of the three groups is clarified in the tectonic Ti/1000 vs. V, Sr/Ce vs. Sm/Ce, La/Yb vs. Th/Ta and in the ternary Y-La-Nb diagrams (Figures 8a, b, c, d). In the Ti/1000 vs. V diagram, groups 1 and 2 plot respectively in the island-arc tholeiites and ocean floor basalts fields, whereas Group 3 occupies the alkali basalts field (Figure 8a). This

characterization is confirmed by the Sr/Ce vs. Sm/Ce diagram (Figure 8b). The classification of Group 2 as mainly ocean floor basalts is supported by the La/Yb *vs*. Th/Ta diagram (Figure 8c). In the ternary diagram (Figure 8d) the Group 1 rocks plot dominantly in the orogenic field, whereas Group 2 rocks exhibit mainly slightly enriched ocean floor or back-arc basalts characteristics. Group 3 samples consistently cluster in the alkaline basalts field. Once again, sample TJF6-302 occupies an exceptional position.

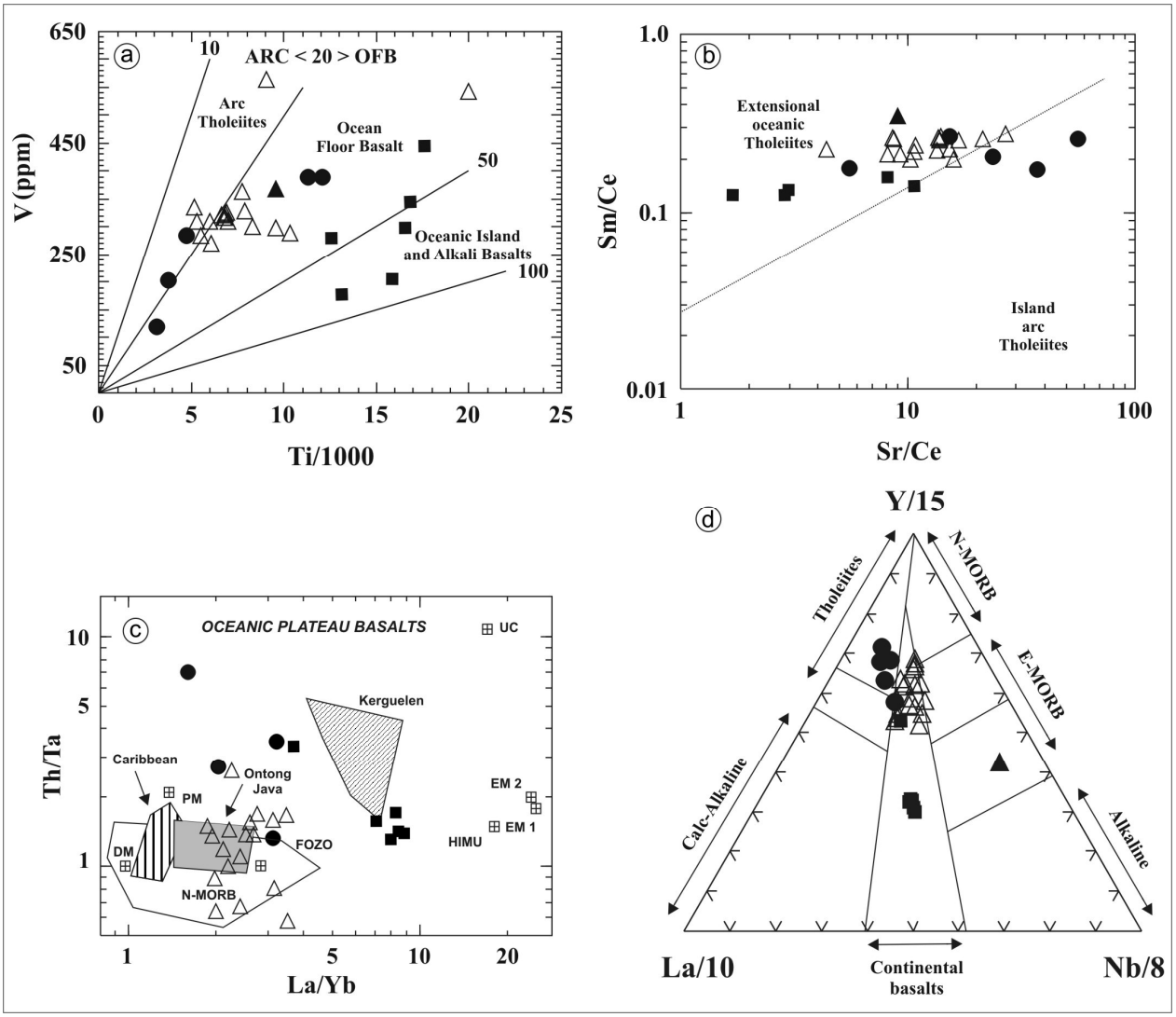

Figure 8: a) Ti/1000 *vs.* V diagram; fields after Shervais (1982); b) Sr/Ce *vs*. Sm/Ce diagram, fields after Kampunzu and Mohr (1991); c) La/Yb *vs.* Th/Ta diagram; internal geotectonic units after Condie (2001); d)Y-La-Nb diagram; fields after Cabanis and Lècolle (1989).

REE_{PM} and $(SPIDER)_{PM}$ pattern for groups 1, 2 and 3, the sample TJF6-302, the N-MORB (Sun and McDonough, 1989) and Mafic Lower Crust (MLC) (Rudnick and Fountain,

1995) are presented in Figures 9 and 10. The vertical line separates the more mobile LREE from the MREE and HREE.

The REE pattern envelope for Group 1 is relatively flat and very narrow (Figure 9a). HREE values are lower that those for the N-MORB, but always higher than those for MLC. The La-Sm segment is slightly more tilted then the nearly horizontal Sm-Lu segment. The most evolved rock has a $La_{(Rock/PM)}$ value of 11. $(La/Yb)_{PM}$ ratios vary between 1.14 and 2.32. The decreasing La-Sm segment is similar to that of lower crust pattern reflecting a low LREE enrichment, whereas the more immobile Sm-Lu segment is quite similar to that of MORB pattern. The samples present small positive or negative Eu anomalies (Figure 9d).

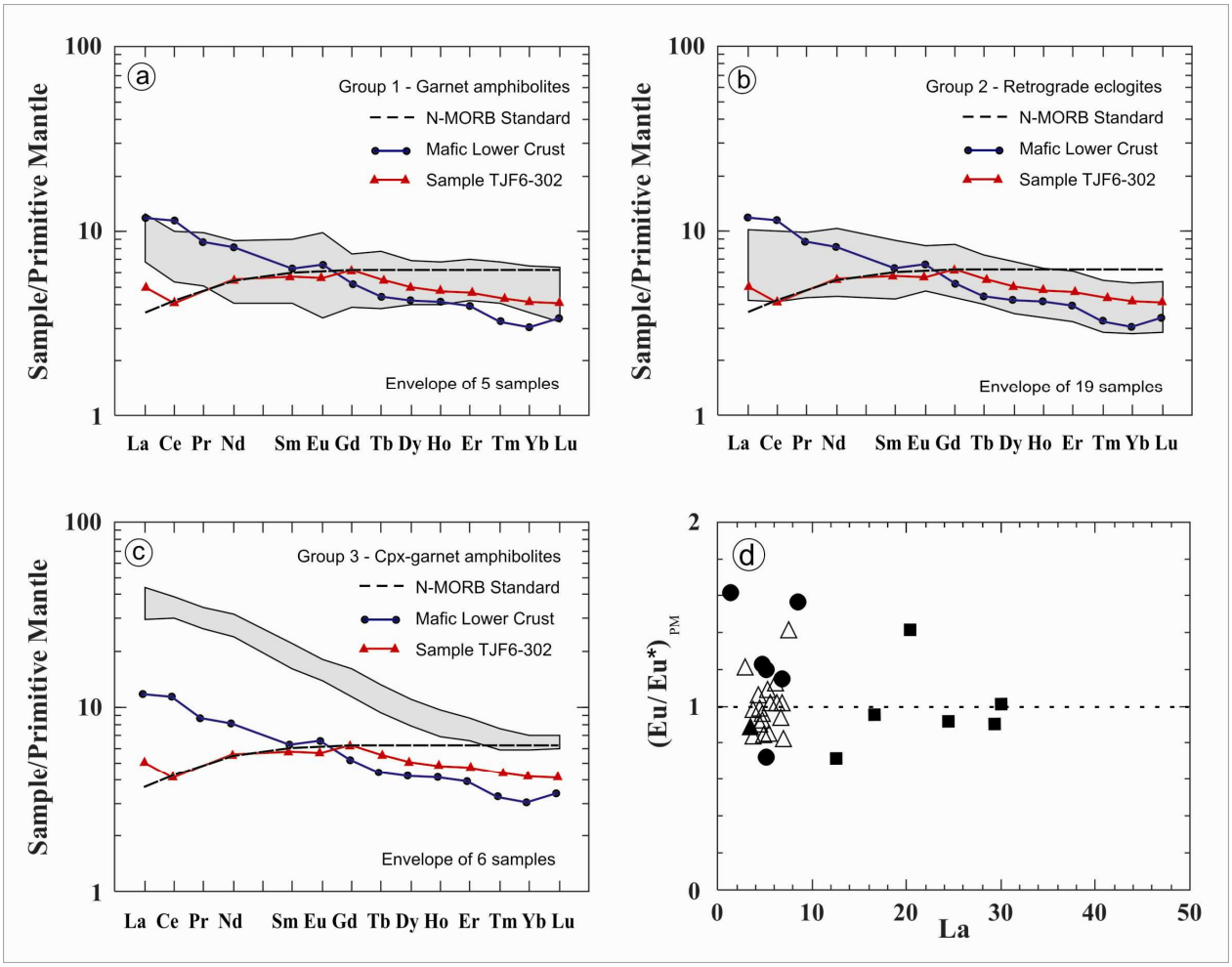

Figure 9: a) REE_{PM} pattern for a) Group 1; b) Group 2; c) Group 3; d) La_{PM} *vs.* $(Eu/Eu^*)_{PM}$ plot, Primitive Mantle and N-MORB Standard from Sun and McDonough (1989); Mafic Lower Crust from Rudnick and Fountain (1995).

Group 1 $(SPIDER)_{PM}$ pattern (Figure 10a) is characterized by positive Ba, U, and La anomalies and negative Rb, Th, Nb and Zr anomalies. Sr anomalies follow the Eu anomalies in the REE pattern (Figure 10a). Group 1 has the lowest Nb/La ratios. As for the LREE, the normalized values for elements more mobile than Sr differ significantly from those in N-MORB pattern, but approximately follow the MLC pattern, mainly for Nd, Sr, Ce, La, Nb, Th, Ba and Rb.

The Group 2 $(REE)_{PM}$ pattern envelope (Figure 9b) is quite similar to that for Group 1 considering the MREE and HREE. However, significant positive or negative Eu anomalies are lacking, a feature which fits the data in the La *vs.* $(Eu/Eu^*)_{PM}$ diagram (Figure 9d). The La-Sm segment is almost horizontal and the Sm-Lu segment somewhat tilted. The normalized HREE

values follow approximately those for MLC. Tm, Yb and Lu values for the more evolved samples are still lower then those for N-MORB. The most evolved rock has a $La_{(Rock/PM)}$ value of 10. $(La/Yb)_{PM}$ ratios vary between 1.33 and 2.53. The highest $(La/Yb)_{PM}$ ratio for groups 1 and 2 is similar. LREE for sample TJF6-302, with exception of La, are quite similar to those of MORB pattern.

The $(SPIDER)_{PM}$ pattern envelope has an irregular shape, with strong positive Ba and Ta anomalies and a minor Sr anomaly. The pattern shows positive and negative Zr anomalies, but a negative Nb anomaly is missing (Figure 10b). Group 2 presents low but variable Nb/La ratios (Figure 10d).

The Group 3 $(REE)_{PM}$ envelope is clearly more tilted with significantly higher LREE. The lowest normalized HREE values are about the same as those of N-MORB and much higher than those of MLC. $La_{(Rock/PM)}$ varies between 30 and 45. Enrichment is indicated by higher $(La/Yb)_{PM}$ ratios, between 2.63 and 7.32. The lack of positive and negative Eu anomalies is supported by Figure 9d. The MLC pattern and the Group 3 envelope are almost parallel.

The Group 3 $(SPIDER)_{PM}$ envelope is very narrow with exception of the strong Sr and Ba anomalies (Figure 10c). In general, all the samples show high Nb contents (8.10 – 24.50 ppm) and low Nb/La ratios, which are only slightly higher than those for Group 1 and overlap partially the Group 2 values (Figure 10d). The notable feature is that the Group 3 pattern differs from those for groups 1 and 2 considering either all the employed elements or only the immobile elements.

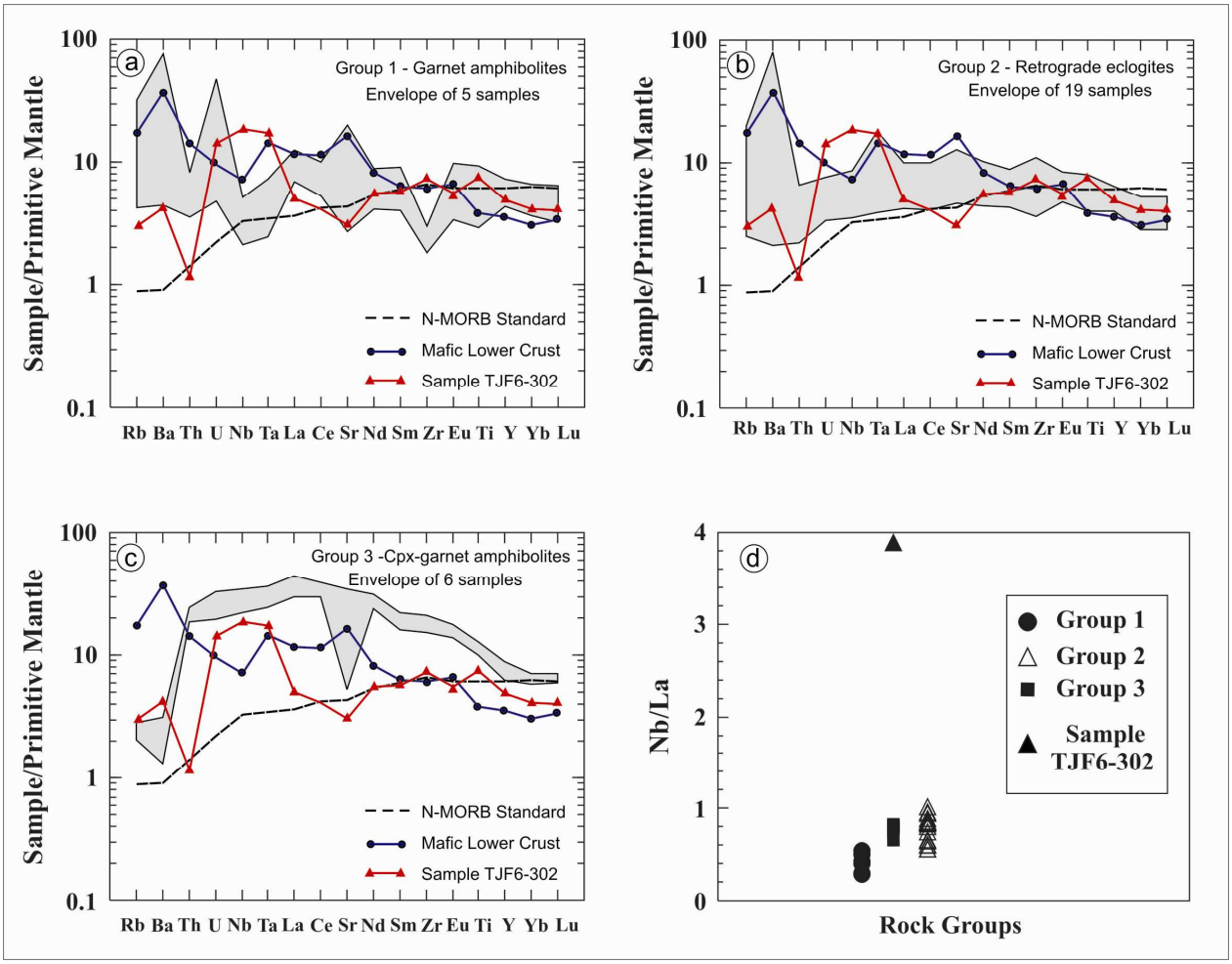

Figure 10: $(SPIDER)_{PM}$ pattern for Group 1 (a); Group 2 (b); Group 3 (c); d) Nb/La plot, Primitive Mantle and N-MORB (dashed line) from Sun and McDonough (1989); Mafic Lower Crust from Rudnick and Fountain (1995).

5. DISCUSSION

The petrographic and geochemical characteristics of the investigated rocks allow their classification into three groups. Group 1, composed essentially of garnet amphibolites, shows a relatively flat $(REE)_{PM}$ pattern, but the $(La\text{-}Sm)_{PM}$ segment shows a slight decreasing trend, as opposed to the N-MORB pattern. Basaltic andesites, the most evolved rocks, occur only in this group. The $(REE)_{PM}$ envelope is quite narrow indicating the homogeneity of the data. The positive and negative Eu anomalies indicate a low degree of plagioclase ± pyroxene fractionation and accumulation. The $(SPIDER)_{PM}$ patterns are characterized by negative Rb, Th, Nb, Sr and Zr anomalies and the Nb anomalies are more negative than those for the N-MORB and MLC standards. Variations in Eu and Sr contents suggest discrete processes of plagioclase and/or

pyroxene accumulation or fractionation. Group 1 shows the lowest Nb/La ratio and the Zr/Nb ratios varying between 6 and 14. The sum of these data suggests an affiliation with island-arc tholeiites for Group 1. This hypothesis is supported by the Ti/1000 *vs.* V, Sr/Ce *vs.* Sm/Ce and Y-La-Nb diagrams, among other characteristics (Figures 8a, b, c).

The Group 2 $(REE)_{PM}$ pattern envelope is also flat and quite narrow. Positive or negative Eu anomalies are lacking, indicating low fractionation and/or contamination, an aspect supported by the La *vs.* $(Eu/Eu^*)_{PM}$ diagram (Figure 9d). Comparing groups 2 and 1 the HREE suggest a slightly more primitive nature for the former. Group 2 is characterized by low and variable Nb/La ratios which are only slightly higher than those for Group 1, but some data overlap is seen. Also, the La and Lu ranges of both groups are quite similar, but the Sm-Lu segment of Group 2 is somewhat more tilted. This aspect may be related to the more enriched nature of this group. In the La/Ta *vs.* Tb/Ta diagram (Figure 7d) groups 1 and 2 plot on a same trend and the majority of the more enriched Group 2 samples plot close to the primitive mantle composition (Wood *et al.,* 1979). Group 2 also display higher Zr/Nb ratios (15-22). In several tectonic environments discrimination diagrams like the Ti/1000 *vs.* V (Figure 8a), Sr/Ce vs. Sm/Ce (Figure 8b) and Y-La-Nb (Figure 8c), the geochemical characteristics of Group 2 are dominantly comparable with rocks formed in an extensional (meso-oceanic ridge or intra-oceanic back-arc) environments. The partial overlap of Group 1 and Group 2 data is attributed to their same tholeiitic nature. In many papers (e.g. Castaing *et al.,* 1994; Attoh and Morgan, 2004; Rao and Rai, 2006) dealing with the reconstruction of the geotectonic environment for mafic eclogitic/granulitic rocks based on geochemical data, the data plots transgressing the classification boundaries as observed in the present case are common. Some geochemical characteristics of Group 2 samples can be correlated to the melting of a partly depleted (or more primitive) mantle source as indicated by the La/Ta *vs.* Tb/Ta diagram (Figure 7d).

In geotectonic models, the protolith of eclogites and granulites in subduction zones are basically either ocean floor rocks (e.g. Duclaux *et al.,* 2006) or roots of island arcs (e.g. Yamamoto, 1993; Agbossoumondé *et al.,* 2004; Duclaux *et al.,* 2006). In the latter case, the derived UHP/HP rocks show a clear orogenic geochemical signature, a feature that is clearly displayed in Group 1 but not so well expressed by the Group 2 samples, with the exception of the HREE. Therefore, a pre-metamorphic MORB-type origin for this group is considered. This interpretation agrees with the clockwise P-T path of the Forquilha retrograde eclogites (Santos *et*

al., 2009). However, a genetic link between groups 1 and 2 cannot be completely discarded, even if the eclogitization of arc-related rocks results in an anti-clockwise P-T path (e.g. Agbossoumondé *et al.,* 2004).

The Group 3 rocks comprise mainly clinopyroxene-garnet amphibolites with distinctly different geochemical features. The narrow $(REE)_{PM}$ pattern envelope is the steepest among the three groups with a $(La/Yb)_{PM}$ ratio between 2.64 and 6.35. The overall geochemical signature of this group is comparable to that of typical alkaline basalts (Figures 6a; 7d; 8a,c,d). The samples plot close to the E-MORB composition in the Nb/Yb *vs.* Th/Yb diagram (Figure 7c), a feature supported by their high Nb contents (8.10-24.50 ppm) (Figure 7b). In all the diagrams, Group 3 samples always define an outstanding trend or field (e.g. Figures 5d,e). The $(SPIDER)_{PM}$ pattern envelope shows strong negative Ba and Sr anomalies suggesting plagioclase fractionation, a feature which is also supported by the large La variation in this group (Figure 9d). Typical fractionation features are also indicated by the low Zr/Nb, K/Ba and Y/Nb ratios (Wilson, 1989). Several geochemical features are compatible with E-MORB (Figure 7c), ocean island basalts (Figure 8a,c) or enriched back-arc basalts (Figure 8b).

The $(REE)_{PM}$ pattern for sample TJF6-302 is approximately sub-horizontal with a slowly increasing Ce-Sm segment (Figure 9). The LREE pattern, with the exception of La, shows good fit with N-MORB, whereas the HREE pattern is close to MLC and the lower values of groups 1 and 2. The $(SPIDER)_{PM}$ pattern is characterized by positive Ba, U, Nb, Ta, Zr and Ti anomalies and negative Th, Sr and Eu anomalies. Considering only the more immobile elements, the best fit for TJF6-302 is Group 2. The discordant plotting of this sample in the Nb_{PM} *vs*. La_{PM} (Figure 5d), $Zr/(10000\ P_2O_5)$ *vs.* Nb/Y (Figure 6c), Nb/Yb *vs*. Th/Yb (Figure 7c), Y-Nb-La diagrams (Figure 8d), besides its outstanding Nb/La ratio (Figure 10d) can be due to its high apatite content and the selective REE/trace elements of this mineral. The geochemical discrepancies are insufficient to infer a possible metasedimentary origin for sample TJF6-302, but some selective changes in the concentration of the compatible elements in the protolith due to prograde and retrograde metamorphic episodes cannot be discarded.

In the Dahomeyides two geochemical/geotectonic groups of mafic/ultramafic eclogites/granulites were defined (Affaton *et al.,* 1980; Bernard-Griffiths *et al.,* 1991; Castaing *et al.,* 1994; Agbossoumodé *et al.,* 2001, 2004; Caby, 2003; Attoh and Morgan, 2004; Duclaux *et al.,* 2006). The first and rarer category comprises mainly eclogites with a clockwise metamorphic

P-T evolution and geochemical signature of MORB. The second group includes mainly granulites with a more complex P-T evolution path with magmatic arc imprints. Examples of bodies with MORB-like signature are the Lato and Toutouto Hills where eclogites grade to granulites followed by retrogression to the amphibolite and greenschist facies (Agbossoumondé *et al.,* 2004). The Agou and Kabié complexes are examples of bodies with calc-alkaline affinities (Duclaux *et al.,* 2006). The association of the two groups of rocks led to two conflicting interpretations. In the first model, the MORB-related rocks represent the subduction of a former oceanic domain surrounding the continental passive margin of the West African Craton (WAC) and the arc-related rocks are considered the roots of a magmatic arc, emplaced and cooled in a supra-subduction zone at the base of the western active continental margin of the Saharian Metacraton (SMC) (Agbossoumodé *et al.,* 2004; Duclaux *et al.,* 2006). This suggests that the closure of the oceanic domain between the WAC and the SMC from 640 to 610 Ma was mainly accommodated by oceanic subduction beneath the SMC before the Pan-African/Brasiliano collision and Gondwana supercontinent amalgamation (Duclaux *et al.,* 2006). In the second model, the association of both rock groups represents the subduction products of an island arc system with genetically linked back-arc or intra-arc basin basalts with an overall relict ophiolitic imprint (Attoh and Morgan, 2004).

The emplacement of basic magmas at the base of the SMC active margin crust (or in the western part of the Benin-Nigerian Shield) leads to two petrogenetic problems: 1) the possibility of a change in the composition of the mafic magmas due to contamination of continental crustal rocks (contamination of basic magmas up to 10% by sediments was proposed for the Kabyé Massif; Duclaux *et al.,* 2006); and 2) the necessity of a geochemical distinction between the arc root rocks and the mafic lower crust rocks. A geochemical comparison of IAT and N-MORB related eclogites/granulites from the Dahomeyiedes with the mafic lower crust (Rudnik and Fountain, 1995) is presented by Attoh and Morgan (2004). However, no distinct geochemical differences among the three groups were noted. Consequently the geochemical modeling of mixing between MLC and IAT or N-MORB is difficult, including the consideration of the variable and selective mobilization of elements during the successive metamorphic events which include dehydration and rehydration of the rocks.

One of the main geological differences between the Dahomeyides subduction zone and the Forquilha Eclogite Zone (FEZ) is its position in relation to the Pan-African 4°50'-Kandi-

Transbrasiliano shear zone. In the Dahomeyides the mafic HP rocks are located to the west of this lineament, whereas the FEZ is distributed in the eastern domain. However, more to the north, in the Hoggar region, similar HP/UHP rocks also occur with an eastern position in the Tin Begane area of the LATEA terranes (Caby, 2003; Derridj *et al.,* 2003). Here, several P-T-t paths with a Franciscan-type loop were defined with P-T conditions ranging from *ca.* 15 kbar-790°C (eclogite stage) to 4 kbar-500°C (greenschist retrogression) (Liégeois *et al.,* 2003). Whole-rock chemistry of two garnet amphibolites and one clinopyroxene-garnet amphibolite show enrichment in LILE and depletion in HFSE suggesting as island-arc environment for the garnet amphibolites similar to the Group 1 from the Forquilha region. The clinopyroxene-garnet amphibolite has a composition closer to the N-MORB (Liégeois *et al.,* 2003) like the Group 2 rocks in the FEZ.

6. CONCLUSIONS

The Forquilha Eclogite Zone includes an association of three groups: Group 1 comprises garnet amphibolites with island-arc imprint; Group 2 has an assemblage of retrograde eclogites with mainly MORB-like geochemical features, and Group 3 comprises clinopyroxene-garnet amphibolites with enriched basalt characteristics. Some of the defined geochemical characteristics may not be of primary origin as occasional selective extraction/addition of some trace elements during the successive metamorphic episodes cannot be discarded. However, the narrow $(REE)_{PM}$ and $(SPIDER)_{PM}$ pattern envelopes as well as the occurrence of anomalies, which allow meaningful petrologic interpretations, and some constant element ratios in all three groups indicate that this process was not of major importance.

All the groups of rocks described here mainly occur as boudins and mega-boudins up to fifty metres long enclosed in aluminous HP metasedimentary gneisses and migmatites represented mainly by kinzigites and khondalites locally associated with calc-silicate rocks, marbles and quartzites.

The retrograde eclogites with a clockwise P-T path show peak metamorphic conditions around 17 kbar and 770°C. They are interpreted to represent a slab of oceanic rocks that underwent high-grade metamorphism at deep levels of an intraoceanic subduction zone. Their exhumation occurred during the Pan-African/Brasiliano Orogeny by an intensive thrust tectonic

episode which affected the northwestern part of the Ceará Central Domain in the Borborema Province during the plate collision stage.

The FEZ shows geochemical characteristics similar to those observed in rocks from the HP/UHP Pan-African Suture Zone which surrounds the WAC in the Lato and Toutouto Hills region (south of Togo) and also, more northwards, in the Mali and Hoggar regions. In this region the high pressure mafic rocks, like in the FEZ, are located to the east of the 4°50'-Kandi-Transbrasiliano lineament. Therefore the petrographic, metamorphic, geochemical and geotectonic similarities in the two considered regions suggest a possible intercontinental correlation between the Forquilha Eclogite Zone and the Pharusian suture complex through the Dahomeyides.

ACKNOWLEDGEMENTS

The authors are grateful to the CNPq (Conselho Nacional de Desenvolvimento Científico e Tecnológico) for the PhD Scolarship, FAPESP (Fundação de Amparo a Pesquisa do Estado de São Paulo, grant 03/07663-3 and 07/58535) for financial support of laboratory work and CNPq/MCT (millenium project proc. 42.0222/2005-7) for financial support of field works. The authors also thank to Prof. Elson Paiva de Oliveira and for stimulating discussions, Prof. Renaud Caby for his review and comments and Allen Fetter for help with English correction. We also thank the two anonymous reviewers for the improvement of this paper and Guest Editor M.Santosh for editorial help, suggestions and corrections.

REFERENCES

Affaton, P., Sougy, J., Trompette, R. 1980. The tectono-stratigraphic relationships between the Upper Precambrian and Lower Paleozoic Volta basin and the Pan African Dahomeyide orogenic belt (West Africa). *American Journal of Science* **280**, 224-248.

Agboumoussonde, Y., Menot, R.P., Guillot, S. 2001. Metamorphic evolution of Neoproterozoic eclogites from south Togo (West Africa). *Journal of African Earth Sciences* **33**, 227-244.

Agbossoumondé, Y., Guillot, S., Menot, R.P. 2004. Pan-African subduction–collision event evidenced by high-P coronas in metanorites from the Agou massif (southern Togo). *Precambrian Research* **135**, 1-21.

Almeida, C.N., Guimarães, I.P., Beurlen, H., Topitsch, W. 2009. Caracterização geoquímica de rochas metamáficas e metaultramáficas da Faixa Pajeú-Paraíba, Província Borborema – NE Brasil. *Anuário do Instituto de Geociências – UFRJ* **32**, 46-61.

Amaral, W.S., Santos, T.J.S. 2008. Airborne geophysical and tectonics of the Ceará Central Domain, eastern region of the Santa Quitéria magmatic arc, Borborema Province, NE Brazil. *Brazilian Journal of Geophysics* **26**, 527-542.

Arthaud, M.H., Caby, R., Fuck, R.A., Dantas, E.L., Parente, C.V. 2008. Geology of the northern Borborema Province, NE Brazil and its correlation with Nigeria, NW Africa. In: *West Gondwana: Pre-Cenozoic Correlations Across the South Atlantic Region*, Pankhurst, R.J., Trouw, R.A.J., Brito Neves, B.B., de Wit, M.J. (eds). Geological Society of London, Special Publications **294,** 49-67.

Attoh, K. 1998. High-pressure granulite facies metamorphism in the Pan-African Dahomeyide Orogen, West Africa, *Journal of Geology* **106,** 236-246.

Attoh, K., Morgan, J. 2004. Geochemistry of high-pressure granulites from the Pan-African Dahomeyide orogen, West Africa: constraints on the origin and composition of the lower crust. *Journal of African Earth Sciences* **39**, 201-208.

Bernard-Griffiths, J., Peucat, J.J., Menot, R.P. 1991. Isotopic (Rb-Sr, U-Pb and Sm-Nd) and trace element geochemistry of eclogites from the Pan-African belt: a case study of REE fractionation during high-grade metamorphism. *Lithos* **27,** 43-57.

Beurlen, H., Da Silva Filho, A.F., Guimarães, I.P., Brito, S.B. 1992. Proterozoic C-Type eclogites hosting unusual Ti-Fe±Cr±Cu mineralization in northeastern Brazil. *Precambrian Research* **58,** 195-214.

Black, R, Latouche, L., Liegeóis, J.P., Caby, R., Bertrand, J.M. 1994. Pan African displaced terranes in the Tuareg shield (Central Sahara). *Geology* **22,** 641-644.

Boughrara, M. 1999. Analyse pétrologique et géochronologique de la région de Tin Begane (Hoggar, Algérie): un exemple de datation d'une série métamorphique en contexte polycyclique. Thése Museum National d'Histoire Naturelle, Paris, France, 361 pp.

Brito Neves, B.B., Santos, E.J., Van Schmus, W.R. 2000. Tectonic history of the Borborema Province, northeastern Brazil. In: *Tectonic Evolution of South America, 31st International Geological Congress,* Cordani, U., Milani, E.J., Thomaz Filho, A., Campos, D.A. (eds). Rio de Janeiro, Brazil, 151-182.

Bueno, J.F., Oliveira, E.P., McNaughton, N.J., Laux, J.H. 2009. U-Pb dating of granites in the Neoproterozoic Sergipano Belt, NE Brazil : Implications for the timing and duration of continental collision and extrusion tectonics in the Borborema Province. *Gondwana Research* **15,** 86-97.

Cabanis, B., Lecolle, M. 1989. Le diagramme La/10-Y/15-Nb/8: un outil pour la discrimination des series volcaniques et la mise en evidence des processus de mélange et/ou de contamination crustale, *Comptes Rendus Academie des Sciences, Paris* Ser. II **309**, 2023-2029.

Caby, R. 1989. Precambrian terranes of Benin Nigeria and Northeast Brazil and the Late Proterozoic South Atlantic. *Geological Society of America*, Special Papers **230**, 145-158.

Caby, R. 2003. Terrane assembly and geodynamic evolution of central–western Hoggar: a synthesis. *Journal of African Earth Sciences* **37**, 133-159.

Castaing, C., Thiéblemont, C., Triboulet, C., Chevremont, P. 1994. Paleogeographical reconstructions of the Pan-Africano/Brasiliano Orogen: closure of an oceanic domain or intracontinental convergence between major blocks? *Precambrian Research* **69**, 327-344.

Castillo, P.R., Klein, E., Bender, J., Langmuir, C., Shirey, S., Batiza, R., White, W. 2000. Petrology and Sr, Nd, and Pb isotope geochemistry of mid-ocean ridge basalt glasses from the 11°45′N to 15°00′N segment of the East Pacific Rise, *Geochemistry Geophysics Geosystems* **1,** 1011, doi:10.1029/1999GC000024.

Castro, N.A. 2004. *Evolução geológica proterozóica da região entre Madalena e Taperuaba, domínio tectônico Ceará Central (Província Borborema).* PhD. Thesis, Universidade de São Paulo, Brazil.

Condie, K.C. 2001. *Mantle plumes and their record in earth history*. Cambridge University. Press, Oxford: United Kingdom.

Cordani, U.G., Teixeira, W.T., D'Agrella-Filho, M.S., Trindale, R.I. 2009. The position of the Amazonian Craton in supercontinents. *Gondwana Research* **15**, 396-407.

Derridj A, Ouzegane K, Kienast JR, Belhai D. 2003. *P–T–X* evolution in clinopyroxene-garnet amphibolites from Tin Begane (Central Hoggar, Algeria). *Journal of African Earth Sciences* **37,** 257-268.

Duclaux, G., Ménot, R.P., Guillot, S., Agbossoumondé, Y., Hilairet, N. 2006. The mafic layered complex of the Kabyé massif (north Togo and north Benin): Evidence of a Pan-African granulitic continental arc root. *Precambrian Research* **151,** 101-118.

El-Hadj, T., Affaton, P., Louis, P., Socohou, A. 1997. Gravity characteristics of the Pan-African Orogen in Ghana, Togo and Benin (West Africa). *Journal of African Earth Sciences* **24**, 241-258.

Fetter, A.H. 1999. *U–Pb and Sm–Nd Geochronological constraints on the crustal framework and geological history of Ceará State, NW Borborema Province, NE Brazil: implications for the assembly of Gondwana.* Ph.D. Thesis, University of Kansas.

Fetter, A.H., Santos, T.J.S., Van Schmus, W.R., Hackspacher, P.C., Brito Neves, B.B., Arthaud, M.H., Nogueira Neto, J.A., Wernick, E. 2003. Evidence for Neoproterozoic continental arc magmatism in the Santa Quitéria batholith of Ceará State, NW Borborema Province, NE Brazil: implications for assembly of West Gondwana. *Gondwana Research* **6,** 265-273.

Fetter, A,H,, Van Schmus, W.R., Santos, T.J.S., Arthaud, M.H., Nogueira, Neto J.A. 2000. U–Pb and Sm–Nd geochronological constraints on the crustal evolution and basement architecture of Ceará State, NW Borborema Province, NE Brazil: implications for the existence of the Paleoproterozoic supercontinent "Atlantica". *Revista Brasileira de Geociências* **30,** 102-106.

Floyd, P.A., Winchester, J.A. 1975. Magma type and tectonic setting discrimination using immobile elements. *Earth and Planetary Science Letters* **27**, 211-218.

Garcia, M.G.M., Arthaud, M.H. 2004. Caracterização de trajetória P–T em *nappes* brasilianas: região de Boa Viagem/Madalena – Ceará Central (NE Brasil). *Revista de Geologia*, Universidade Federal do Ceará **17,** 173-191.

Guimarães I.P., da Silva Filho, A.F., Araújo, D.B., de Almeida, C.N., Dantas, E. 2009. Trans-alkaline magmatism in the Serrinha-Pedro Velho Complex, Borborema Province, NE Brazil and its correlations with the magmatism in eastern Nigeria. *Gondwana Research* **15**, 98-110.

Humphris, S.E., Thompson, G. 1983. Geochemistry of rare earth elements in basalts from the Walvis ridge: implications for its origin and evolution. *Earth Planet Science Letters* **66**, 223-242.

Humphris, S.E., Thompson, G., Schilling, J.G., Kingsley, R.H. 1985. Petrological and geochemical variations along the Mid-Atlantic Ridge between 46°S and 32°S: influence of the Tristan da Cunha mantle plume. *Geochimica et Cosmochimica Acta* **49,** 1445-1464.

Irvine, T.N., Barragar, W.R.A. 1971. A guide to the chemical classification of the common volcanic rocks. *Canadian Journal Earth Science* **8,** 523-548.

Jahn, B., Caby, R., Monié, P. 2001. The oldest UHP eclogites of the world: age of UHP metamorphism, nature of protoliths and tectonic implications. *Chemical Geology* **178**, 143-158.

John T., Schenk, V., Haase, K., Scherer, Tembo, F. 2003. Evidence for a Neoproterozoic ocean in south-central Africa from mid-ocean-ridge-type geochemical signatures and pressure-temperature estimates of Zambian eclogites. *Geology* **31**, 243-246.

Kampunzu, A,B,, Mohr, P. 1991. Magmatic evolution and petrogenesis in the East African rift system. In: Magmatism in Extensional Structure Settings–The Phanerozoic African Plate, Kampunzu, A.B., Labala, R.T. (eds). Springer: Verlag Heidelberg **85**,136.

Kerr, A.C., **Mahoney JJ. 2007**. Oceanic plateaus, problematic plumes, potential paradigms. *Chemical Geology* **241**, 332-353.

Klein, E.M. 2005. Geochemistry of the Igneous Oceanic Crust. *Treatise on Geochemistry* **3**: 433-463.

Klein, E.M., Langmuir, C.H.1987. Global correlations of ocean ridge basalt chemistry with axial depth and crustal thickness. *Journal of Geophysics Research,* **92,** 8089-8115.

Liégeois, J.P., Latouche, L., Boughrara, M., Navez, J., Guiraud, M. 2003. The LATEA metacraton (Central Hoggar, Tuareg Shield, Algeria): behavior of an old passive margin during the Pan-African orogeny. *Journal of African Earth Sciences* **37**, 161-190.

Le Maitre, R., Bateman, P., Dudek, A., Keller, J., Lameyre, J., Le Bas, M., Sabine, P., Schmid, R., Sorensen, H., Streckeisen, A., Woolley, A., Zanettin, B. 1989. A classification of igneous rocks and glossary of terms: Recommendations of the International Union of Geological Sciences Subcommission on the Systematics of ingeous rocks, Le Maitre, R.W. (ed.). Oxford, *Blackwell,* 193 pp.

Le Roex, A,P. 1987. Source regions of mid-ocean ridge basalts: Evidence for enrichment processes. In: *Mantle metasomatism*, Menzies, M., Hawkesworth, C. (eds). Academic Press: London; 389-421.

Lesquer, A., Beltrão, J.F., Abreu, F.A.M. 1984. Proterozoic links between northeastern Brazil and West Africa: a plate tectonic model based on gravity data. *Tectonophysics* **110**, 9-26.

Martins, G., Oliveira, E.P., Lafon, J.M. 2009. The Algodões amphibolite–tonalite gneiss sequence, Borborema Province, NE Brazil: geochemical and geochronological evidence for Palaeoproterozoic accretion of oceanic plateau/back-arc basalts and adakitic plutons. *Gondwana Research* **15,** 71-85.

Navarro, M.S., Andrade, S., Ulbrich, H., Gomes, C.B., Girardi, V.A.V. 2008. The direct determination of rare earth elements in basaltic and related rocks using ICP-MS: Testing the efficiency of microwave oven sample decomposition procedures. *Geostandards and Geoanalytical Research* **32,** 167-180.

Peacock, S.M. 1993. The importance of blueschist eclogite dehydration reactions in subduction oceanic crust. *Geological Society of America Bulletin* **105**, 684-694.

Rao, D.R., Rai, H. 2006. Signatures of rift environment in the production of garnet-amphibolites and eclogites from Tso-Morari region, Ladakh, India: A geochemical study. *Gondwana Research* **9,** 512-523.

Rudnik, R.L., Fountain, D.M. 1995. Nature and composition of the continental crust: a lower crustal perspective. *Reviews of Geophysics* **33**, 267-309.

Rumble, D., Liou, J.G., Jahn, B. 2005. Continental crust subduction and ultrahigh pressure metamorphism. *Treatise on Geochemistry* **3**, 293-319.

Santos, T.J.S, Fetter, A.H, Hackspacher, P.C., Schmus, W.R.V., Nogueira Neto, JA. 2004. Structural and geochronological studies of the Médio Coreaú Domain, NE Brazil: Constraints on Brasiliano/Pan-African tectonic evolution in the NW part of the Borborema Province. *Journal of the Virtual Explorer* (Online) **17** xx.

Santos, T.J.S., Fetter, A.H., Hackspacher, P.C., Schmus, W.R.V., Nogueira Neto, J.A. 2008a. Neoproterozoic tectonic and magmatic episodes in the NW sector of the Borborema Province, NE Brazil, during assembly of western Gondwana. *Journal of South American Earth Sciences* **25**, 271-284.

Santos, T.J.S., Fetter, A.H., Nogueira Neto, J.A. 2008b. Correlation of the West margin of the Transbrasiliano – Kandi Lineament in the Borborema Province (NE Brazil) and Pharusian Belt (NW Africa). In: *West Gondwana: Pre-Cenozoic Correlations Across the South Atlantic Region*, Pankhurst, R.J., Trouw, R.A.J., Brito Neves, B.B., de Wit, M.J. (eds). Geological Society of London, Special Publications **294**, 101-119.

Santos, T.J.S., Garcia, M.G.M., Amaral, W.S., Caby, R., Wernick, E., Arthaud, M.H., Dantas, E.L., Santosh, M. 2009. Relics of eclogite facies assemblages in the Ceará Central Domain, NW Borborema Province, NE Brazil: Implications for the assembly of West Gondwana. *Gondwana Research* **15**, 454-470.

Schilling, J.G., Zajac, M., Evans, R., Johnston, T., White, W., Devine, J.D., Kingsley, R. 1983. Petrologic and geochemical variations along the Mid-Atlantic ridge from 29°N to 73°N. *American Journal Science* **283,** 510-586.

Shervais, J.M. 1982. Ti-V plots and the petrogenesis of modern and ophiolitic lavas. *Earth and Planetary Science Letters* **59**, 101-118.

Sun, S.S., McDonough, W.F. 1989. Chemical and isotopic systematics of ocean basalts: implications for mantle composition and processes. In: *Magmatism in the Ocean Basins,* Saunders, A.D., Norry, M.J. (eds). Geological Society of London, Special Publication **42**, 313-345.

Taylor, S.R., McLennan, S.M. 1985. The *Continental Crust: Its Composition and Evolution.* Blackwell, Oxford.

Trompette, R. 1994. *Geology of western Gondwana, Pan-African/Brasiliano aggregation of South America and Africa*. A.A. Balkema: Rotterdam.

Vendemiatto, M.A., Enzweiler, J. 2001. Routine control of accuracy in silicate rock analysis by X-ray fluorescence spectrometry, *Geostandards Newsletter* **25**, 283-291.

Wang, W.L., Aitchison, J.C., Ching, H.L., Zeng, Q.G. 2008. Geochemistry and geochronology of the amphibolite blocks in ophiolitic mélanges along Bangong-Nujiang suture, central Tibet. *Journal of Asian Earth Sciences* **33**, 122-138.

Wilson, M. 1989. *Igneous Petrogenesis.* Unwin Hyman: London.

Winchester, J.A., Floyd, P.A. 1977. Geochemical discrimination of different magma series and their differentiation products using immobile elements. *Chemical Geology* **20**, 325-343.

Wood, D.A., Tarney, J., Saunders, A.D., Bougault, H., Jorton, J.L., Treuil, M., Cann, J.R. 1979. Geochemistry of basalts drilled in the north Atlantic by IPOD Leg 49: implications for mantle heterogeneity. *Earth and Planet Science Letters* **42**, 1925-1930.

Yamamoto, H. 1993. Contrasting metamorphic P-T-time paths of the Kohistan granulites and tectonics of the western Himalayas. *Journal of Geological Society (London)* **150**, 843-856.

Table 1. Major and trace element data for the metabasic rocks of the NW Borborema Province, NE Brazil

Sample	VC-54A*	VC-57F*	TJF5-181*	VC-54B*	VC-57E*	VC-57G*	WT8-10E	TJF6-296*	VC-60*	WT8-10A	WT8-10D	WT8-10C	RM-107C	RM-220	RM-120A
Rock	GA	GA	GA	GA	GA	RE	RE	RE	RE	RE	RE	RE.	RE.	RE.	RE.
Major elements (wt.%)															
SiO_2	43.35	46.50	47.87	49.77	53.23	47.38	48.08	48.14	48.25	48.80	48.95	49.04	49.05	49.25	49.40
TiO_2	0.63	1.89	2.02	0.79	0.52	3.33	1.72	1.38	1.29	1.02	0.87	1.59	1.14	1.16	0.92
Al_2O_3	16.67	14.22	16.06	16.17	17.83	14.63	18.03	15.43	16.18	16.88	11.97	16.21	14.16	15.53	15.91
Fe_2O_{3t}	13.58	13.72	14.25	11.54	8.47	17.15	14.01	13.76	14.25	11.38	11.67	14.49	13.32	13.16	11.86
MnO	0.23	0.18	0.19	0.20	0.11	0.18	0.18	0.19	0.20	0.17	0.20	0.20	0.25	0.20	0.17
MgO	12.11	8.40	5.79	6.56	7.46	4.41	4.29	6.80	6.21	6.58	10.01	5.26	7.51	6.93	7.17
CaO	9.71	12.33	10.91	10.20	10.56	10.26	10.82	11.51	11.17	11.99	12.99	10.46	11.02	11.23	12.08
Na_2O	1.92	0.99	2.06	2.31	1.34	2.16	2.26	2.28	2.51	2.31	2.11	2.38	2.32	2.12	1.70
K_2O	0.18	0.79	0.29	0.33	0.18	0.13	0.17	0.21	0.16	0.21	0.42	0.19	0.36	0.13	0.23
P_2O_5	0.05	0.18	0.09	0.08	0.00	0.16	0.14	0.11	0.08	0.09	0.06	0.16	0.10	0.09	0.08
LOI	1.40	0.80	0.30	1.80	0.10	0.10	0.10	0.10	0.00	0.40	0.37	0.09	0.06	0.16	0.24
Total	98.71	99.01	99.31	99.02	99.64	98.65	99.80	99.91	100.30	99.80	99.60	100.00	99.30	100.00	99.80
Mg#	41.10	37.59	33.03	36.82	41.00	27.32	40.84	35.30	33.86	56.59	65.92	45.01	55.97	54.28	57.68
Trace elements (ppm)															
V	202.00	389.00	389.00	284.00	118.00	124.20	288.00	270.40	200.20	271.00	335.00	299.00	325.00	310.00	285.00
Ni	46.70	42.90	18.70	14.60	100.20	5.90	51.00	6.10	4.80	111.40	167.70	69.10	99.30	91.60	85.80
Rb	4.00	20.50	2.70	7.90	3.10	0.10	4.20	1.00	0.50	9.00	7.30	5.60	9.10	4.90	6.00
Sr	56.20	416.70	229.40	382.00	173.50	2.70	200.10	5.90	3.80	251.80	114.90	187.80	100.00	143.60	154.90
Y	22.90	32.70	23.30	26.10	6.90	0.10	21.90	0.10	0.10	19.40	19.90	27.00	20.70	28.90	19.80
Zr	20.70	33.60	21.90	20.40	4.90	7.00	83.30	11.00	11.00	52.20	45.80	123.20	63.00	67.10	40.80
Nb	1.60	3.40	3.70	1.50	0.60	23.30	5.20	19.60	19.90	3.00	2.90	5.60	4.00	3.80	2.60
Ba	43.50	532.90	30.80	247.90	13.70	222.20	36.50	129.40	98.10	112.10	274.70	292.50	188.80	21.90	560.10
Ta	0.11	0.20	0.30	0.10	0.04	0.40	0.34	0.30	0.30	0.31	0.20	0.36	0.26	0.43	0.18
Th	0.30	0.70	0.40	0.70		0.88	0.47	0.75	0.68	0.25	0.22	0.56	0.44	0.29	0.47
U	0.10	0.60	0.10	0.10		0.53	0.12	0.34	0.34	0.08	0.07	0.16	0.12	0.09	0.14
La	5.20	8.50	6.80	5.10	1.40	1.24	5.50	0.78	0.77	5.30	4.40	6.70	5.40	4.50	4.30
Ce	10.20	17.70	15.00	10.30	3.10	98.10	14.80	84.90	68.60	9.40	8.20	17.70	12.30	10.40	10.20
Pr	1.49	2.70	2.37	1.39	0.48	9.80	2.20	13.80	11.90	1.80	1.50	2.70	1.80	1.70	1.50
Nd	6.50	11.00	12.00	5.50	2.40	0.46	11.00	0.30	0.31	8.80	7.50	13.30	8.90	8.70	7.40
Sm	1.80	3.60	4.00	1.80	0.80	2.32	3.30	2.57	2.06	2.60	2.20	3.90	2.60	2.70	2.30
Eu	0.57	1.64	1.48	0.73	0.36	3.56	1.20	2.28	2.26	1.00	0.80	1.40	0.90	1.00	0.90
Gd	2.34	4.48	4.45	2.31	0.94	1.43	4.00	1.23	1.07	3.30	3.00	5.00	3.40	3.50	3.10
Tb	0.49	0.84	0.75	0.55	0.18	3.80	0.66	3.37	3.06	0.54	0.48	0.80	0.56	0.58	0.51
Dy	3.11	5.11	4.14	3.99	0.94	14.50	4.09	17.10	12.00	3.36	3.22	5.02	3.62	3.63	3.25
Ho	0.82	1.11	0.82	0.86	0.25	4.47	0.85	4.13	3.64	0.70	0.71	1.03	0.77	0.77	0.71
Er	2.88	3.35	2.40	3.16	0.65	5.60	2.32	3.97	3.65	1.92	2.02	2.90	2.14	2.13	2.04
Tm	0.44	0.46	0.32	0.50	0.12	0.60	0.32	0.50	0.30	0.26	0.28	0.40	0.30	0.28	0.29
Yb	2.55	2.63	2.17	3.20	0.70	33.60	2.05	23.30	22.30	1.68	1.83	2.58	1.96	1.86	1.90
Lu	0.47	0.41	0.29	0.47	0.10	6.10	0.31	6.80	4.70	0.25	0.28	0.39	0.29	0.29	0.29
$(La/Yb)_{PM}$	1.46	2.32	2.25	1.14	1.44	1.33	1.93	2.49	1.58	2.26	1.73	1.86	1.98	1.74	1.62

Sample	RM-107E	WT7-25	WT8-10F	WT8-53E	RM-182	WT7-53D	RM-107D	RM-179	TJF6-302*	TJF6-335C	VC-57g*	WT8-10B	TJF6-335D	TJF6-335B	TJF6-335A
Rock	RE.	RE.	RE.	RE.	RE.	RE.	RE.	RE.	Eclogite	CGA	CGA	CGA	CGA	CGA	CGA
Major elements (wt.%)															
SiO_2	49.43	49.47	49.63	49.69	50.04	50.30	50.36	50.40	45.99	46.86	46.94	48.19	48.52	50.19	51.48
TiO_2	1.12	1.455	0.88	1.32	1.15	1.00	1.10	1.14	1.60	2.64	2.94	2.09	2.81	2.76	2.19
Al_2O_3	14.20	15.38	15.27	14.08	13.50	13.61	14.02	15.14	14.59	21.14	14.48	15.76	17.05	14.60	19.67
Fe_2O_{3t}	13.25	13.88	11.41	13.96	12.93	12.66	12.78	12.89	12.88	11.41	16.58	20.94	12.57	16.88	10.93
MnO	0.22	0.198	0.18	0.20	0.21	0.20	0.16	0.20	0.19	0.13	0.21	0.27	0.12	0.24	0.12
MgO	7.56	5.96	7.92	7.17	8.01	8.51	7.76	7.49	9.75	3.42	6.02	3.46	5.85	5.00	3.70
CaO	11.37	10.67	11.91	11.09	11.68	11.39	11.37	11.35	12.50	8.99	9.30	8.64	7.80	8.86	6.10
Na_2O	2.11	2.63	1.99	1.95	2.00	2.09	2.08	1.90	2.17	4.37	2.73	0.98	4.31	1.95	4.99
K_2O	0.46	0.32	0.16	0.11	0.15	0.13	0.37	0.08	0.05	0.04	0.18	0.06	0.11	0.05	0.06
P_2O_5	0.10	0.114	0.07	0.11	0.10	0.08	0.10	0.10	1.60	0.53	0.27	0.24	0.34	0.45	0.24
LOI	0.18	0.11	0.17	0.17	0.22	0.03	0.02	0.20	0.10	0.10	0.10	0.86	0.09	0.66	0.05
Total	100.00	100.0	99.60	99.50	100.00	100.00	100.10	100.50	101.42	99.40	99.75	99.80	99.40	100.30	99.40
Mg#	56.26	49.19	61.01	53.66	58.28	60.25	57.79	56.71	39.66	40.33	31.67	27.14	51.20	40.04	43.29
Trace elements (ppm)															
V	317.00	582.00	310.00	329.00	327.00	311.00	322.00	318.00	369.00	205.00	445.00	279.00	346.00	299.00	178.00
Ni	93.90	97.00	116.40	99.40	96.10	125.60	100.50	113.60	24.70	17.50	44.70	21.50	34.20	47.20	18.40
Rb	10.50	2.10	4.00	2.80	4.60	1.60	12.60	2.60	1.90	1.30	2.90	1.70	1.40	1.60	1.80
Sr	117.10	49.00	154.90	126.80	97.70	117.80	140.20	131.20	64.80	731.30	290.50	32.50	158.50	167.50	109.80
Y	19.20	22.00	18.10	23.80	21.70	21.70	20.00	25.20	22.10	39.80	24.10	38.40	28.70	35.60	38.90
Zr	62.40	55.20	41.50	69.00	64.50	48.90	60.10	63.90	81.40	226.60	119.80	106.20	169.40	174.60	234.60
Nb	3.80	3.70	2.50	4.00	3.20	3.00	3.90	3.20	13.20	23.50	13.10	8.10	15.70	18.90	24.50
Ba	93.30	17.80	321.70	103.70	148.00	205.40	85.50	14.80	29.70	22.00	521.50	54.40	21.20	20.60	9.30
Ta	0.27	0.24	0.16	0.56	0.22	0.27	0.74	0.22	0.70	1.47	0.70	0.63	1.01	1.27	1.47
Th	0.43	0.32	0.19	0.36	0.32	0.24	0.43	0.30	0.10	2.06	1.20	2.11	1.59	1.66	2.04
U	0.12	0.09	0.09	0.09	0.09	0.07	0.12	0.08	0.30	0.68	0.20	0.34	0.44	0.41	0.51
La	6.30	5.50	2.90	4.70	4.90	3.70	6.90	3.70	3.40	29.30	16.60	12.60	20.40	24.40	30.00
Ce	12.70	13.40	7.30	11.80	11.20	8.70	13.70	9.50	7.20	68.80	35.80	35.80	53.00	58.70	64.80
Pr	2.00	2.00	1.20	1.80	1.80	1.40	2.00	1.50	1.31	9.50	5.72	4.90	7.30	7.80	9.20
Nd	9.40	9.70	6.00	9.10	9.00	7.20	9.30	7.50	7.40	42.60	27.80	23.10	32.00	34.30	38.40
Sm	2.70	2.90	1.90	2.80	2.90	2.30	2.70	2.40	2.50	9.70	5.61	6.10	7.10	7.30	8.10
Eu	1.00	1.10	0.80	1.00	1.00	0.80	0.90	0.90	0.93	3.00	1.74	1.90	2.70	2.30	2.60
Gd	3.40	3.70	2.60	3.60	3.80	3.10	3.40	3.20	3.64	9.60	5.30	7.70	6.80	7.40	7.70
Tb	0.56	0.63	0.43	0.63	0.63	0.52	0.57	0.55	0.59	1.41	0.84	1.23	1.00	1.16	1.20
Dy	3.66	4.01	2.65	4.11	4.11	3.37	3.71	3.64	3.68	8.11	4.31	7.39	5.77	7.07	7.22
Ho	0.77	0.85	0.56	0.89	0.86	0.72	0.78	0.77	0.77	1.58	0.83	1.48	1.14	1.39	1.43
Er	2.20	2.40	1.56	2.59	2.45	2.08	2.22	2.16	2.23	4.16	2.27	4.02	3.13	3.65	3.91
Tm	0.31	0.33	0.21	0.36	0.34	0.29	0.30	0.29	0.32	0.56	0.35	0.54	0.43	0.49	0.53
Yb	2.02	2.15	1.38	2.35	2.21	1.87	1.96	1.92	2.04	3.48	2.00	3.43	2.87	3.07	3.39
Lu	0.31	0.33	0.21	0.36	0.33	0.29	0.30	0.29	0.30	0.52	0.30	0.51	0.44	0.45	0.51
$(La/Yb)_{PM}$	2.24	1.84	1.51	1.44	1.59	1.42	2.53	1.38	1.20	6.04	5.96	2.64	5.10	5.70	6.35

GA: garnet amphibolites; RE: retrograde eclogites; CGA: clinopyroxene-garnet amphibolites. Where subscript $_{PM}$ for each element means normalized by primitive mantle from Sun and McDonough (1989).

ANEXO 03

"Amaral, W.S., Santos, T.J.S., Dantas, E.L. *(In prep.)* **Sm-Nd and LA-MC-ICP-MS U-Pb, Lu-Hf zircon geochronology of high pressure rocks from the Forquilha Eclogite Zone, Borborema Province, NE-Brazil: an evidence for the break-up of Columbia supercontinent (*Em preparação)*"

Sm-Nd and LA-MC-ICP-MS U-Pb, Lu-Hf zircon geochronology of high pressure rocks from the Forquilha Eclogite Zone, Borborema Province, NE-Brazil: an evidence for the break-up of Columbia supercontinent

Wagner da Silva Amaral[a]*, Ticiano José Saraiva dos Santos[a], Elton Luiz Dantas[b]

[a] *Instituto de Geociências, Universidade Estadual de Campinas (UNICAMP), Caixa Postal 6152, CEP: 13081-970, Campinas-SP, Brazil*
[b] *Instituto de Geociências, Universidade de Brasília (UnB), CEP 70910-900, Brasília-DF, Brazil*

ABSTRACT

This study presents U-Pb, Lu-Hf and Sm-Nd isotopic data of metamafic rocks and their country rocks from the Forquilha Eclogite Zone (FEZ) Borborema Province, aiming the understanding of their geochronological and tectonic evolution. Six metamafic and four metasedimentary high-pressure rocks were selected for in situ zircon and monazite U-Pb and Lu-Hf analyses by LA-MC-ICP-MS. Zircon grains from metamafic rocks are in general colorless to brownish and vary from equant to elongate prisms, with well-defined faces and rounded terminations. The results obtained in the upper intercepts for all metamafic samples vary between 1566 ± 8.8 and 1455 ± 120 Ma. In the lower intercepts, all the discordia curves, suggest ages around 650 Ma. Metamorphic zircon of a clinopyroxene-garnet amphibolite from the south portion of FEZ yielded a concordia age of 614 ± 3.9 Ma. Hf model-ages (zircon grains) from 1.57 to 1.80 Ga, with positive values of $\varepsilon_{Hf\ (t=1.568)}$ varying from +7.46 to + 9.63 and Nd model ages are 1.60 and 1.79 Ga, with positive $\varepsilon_{Nd\ (t=1.500)}$ value +4.11. These values are consistent with ages obtained on zircon crystallization and suggest a mantle source for metamafic high-pressure rocks. For metasedimentary samples, the age distribution shows a source between 2.0 and 2.2 Ga. Two samples showed populations of zircon with rounded nuclei and well defined edges. Concordant ages were obtained at the edges of the crystals at 639 ± 10 Ma and 650.3 ± 2.5 Ma. These values correspond to the oldest metamorphic event in Ceará Central Domain, at eclogite / granulite facies.

1. INTRODUCTION

During the Earth evolution, several phases of break-up and assembly of continental lithosphere are registered forming supercontinents (Condie, 2002; Cordani *et al.,* 2003; Rogers & Santosh, 2002; Zhao *et al.,* 2004, Ernst *et al.,* 2008, Rogers & Santosh, 2009). In the South American platform two breakup events occur before the Gondwanaland assembly and result of break-up of possible Columbia supercontinent (~1.85-1.25 Ga) and Rodinia (1.05-0.75 Ga), around, respectively 1.8-1.6 Ga and 1.0-0.9 Ga which are well documented by geological and geochronological data (Sá *et al.,* 1995; Brito Neves, 1998; Brito Neves *et al.,* 2000; Pimentel *et al.,* 2000), while the geophysical information is incipient (Thover *et al.,* 2006; Bispo-Santos *et al.,* 2008). A supercontinent characterization assembled during the Paleoproterozoic has been termed "Columbia" or "Nuna" (Rogers, 1996; Condie, 2000, 2002; Zhao *et al.,* 2002; Rogers & Santosh, 2002, 2009; Zhao *et al.,* 2004), but reconstructions models are widely controversial. On the other hand, the Rodinia break-up and Gondwana assembly are supported by several

* *e-mail to: wsa.geo@gmail.com*

geological data in the South American (Cordani *et al.,* 2003; Fuck *et al.,* 2008 and references there in).

In the northern region of the Borborema Province, NE Brazil, a 30 km long mafic/ultramafic belt of high-pressure rocks, called Forquilha Eclogite Zone (FEZ), was recently discovered in the Ceará Central Domain (Santos *et al.,* 2008, 2009, Amaral *et al.,* 2010). These rocks occur mainly as boudins and megaboudins up to five hundred meters long enclosed in aluminous metasedimentary gneisses and migmatites represented mainly by kinzigites and khondalites locally associated with calc-silicate rocks, marbles and quartzites.

In this paper we present whole rock Sm-Nd analyses and combined *in situ* U-Pb and Lu-Hf analyse on zircon and monazite obtained by laser ablation multi-collector inductively coupled plasma mass spectrometry (LA-MC-ICP-MS) for metamafic and metasedimentary rocks from the Forquilha Eclogite Zone. These data are used to constrain the timing of formation and metamorphism of the high pressure rocks. Backscattered images (BSE) are used to aid in our interpretation of the U-Pb zircon ages. We also provide some insights of the tectonic evolution model of this portion to West Gondwana.

2. GEOLOGICAL SETTING

The Borborema Province (BP) of northeastern Brazil (Almeida *et al.,* 1981) represents the western part of a major Brasiliano/Pan-African orogenic belt that can be traced into Central Africa, based on pre-drift reconstructions of Gondwana (Figure 1) (e.g., Caby, 1989; Trompette, 1994). This orogenic belt is characterized by large tracts of Palaeoproterozoic gneisses and migmatites surrounding several smaller nuclei of Archaean crust. These basement gneisses are overlain by remnants of Palaeoproterozoic to Neoproterozoic supracrustal rocks, all of which are intruded by ubiquitous Neoproterozoic granitoids and dissected by a network of anastomosing shear zones.

The northern portion of BP, comprises three crustal blocks bounded by major tectonic lineaments: the Rio Grande do Norte, located between the Patos and Senador Pompeu shear zones, composed mainly of reworked Paleoproterozoic gneisses (2.15-2.0 Ga) with minor Archean nuclei and Neoproterozoic rocks (Van Schmus *et al.,* 1995, 2008; Dantas *et al.*, 2004); the Ceará Central, between the Senador Pompeu and Transbrasiliano lineaments, dominated by

juvenile middle Paleoproterozoic gneisses (2.14–2.10 Ga) but also containing inliers of Archean–Neoproterozoic rocks (Fetter *et al.,* 2000, 2003; Santos *et al.,* 2003); and the Médio Coreaú, northwest of the Transbrasiliano lineament, composed of early Paleoproterozoic (2.36–2.30 Ga) juvenile basement and younger late Paleoproterozoic–Neoproterozoic rocks (Fetter *et al.,* 2000).

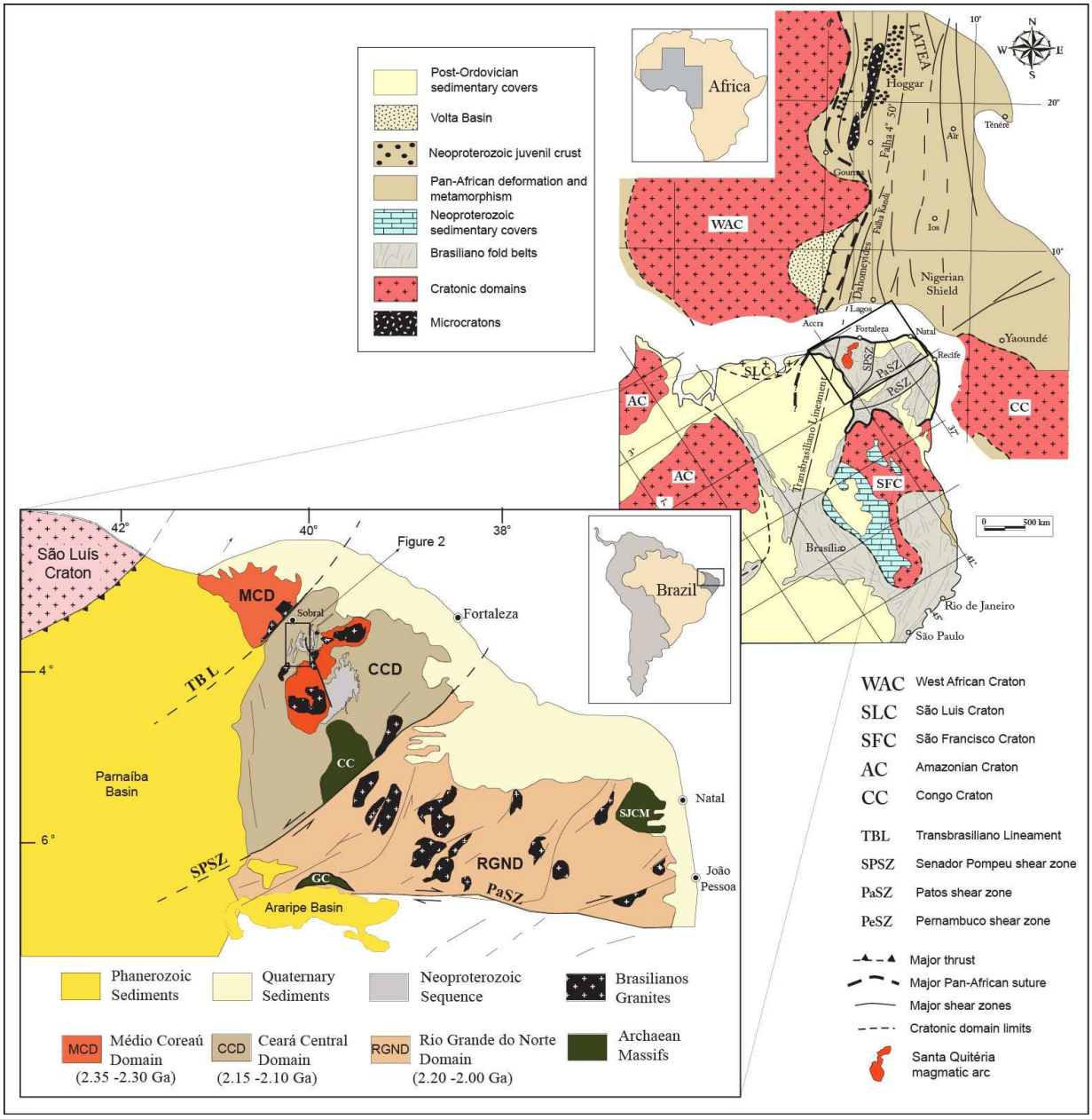

Figure 1: North block of the Borborema Province, showing the main tectonic features and Brasiliano granitic plutons situated north of the Patos shear zone (PaSZ): Cruzeta Complex (CC); SJCM (São José do Campestre Massif; Granjeiro Complex (GC); Transbrasiliano Lineament (TBL); Senador Pompeu shear zone (SPSZ); Médio Coreaú Domain (MCD); Ceará Central Domain (CCD); Rio Grande do Norte Domain (RGND) (After Santos *et al.,* 2009). Rectangle is the study area in the CCD context.

According to Fetter *et al.* (2003), the northwest part of the Ceará Central Domain constitutes an active continental margin developed prior to the amalgamation of West Gondwana. The subduction of Neoproterozoic oceanic crust results in the growth of the Santa Quitéria magmatic arc (SQMA) during the Neoproterozoic. Between the SQMA and the Transbrasiliano lineament occurs a sequence of high metamorphic grade rocks, denominated the Forquilha Eclogite Zone (Santos *et al.,* 2008, 2009; Amaral *et al.,*2010), that comprises an association of biotite gneiss, sillimanite-garnet gneiss, kyanite-garnet gneiss, muscovite-sillimanite quartzite, quartz-muscovite schist, amphibole gneiss, augen granitic gneiss, garnet-bearing leucogranite and metamafic rocks (Figure 2). The metamafic rocks display a predominant N-S low-angle E-dipping foliation and low- medium (up to 30^{o}) E or SE-plunging stretching lineation defined by sillimanite, quartz, biotite, kyanite, and muscovite. The orientation of foliations and lineations and kinematic features (S-C structures, asymmetric feldspar, and mica-fish) indicate an evolutionary history with west-northwestward thrusting progressively changing to an overall dextral strike-slip moviment along NE-SW-trending shear zones (Santos *et al.,* 2009).

The metamafic rocks occur as lenses and/or boudins, ranging from 0.5 to 100 meters in width and 0.2 to 6 km in length, interlayered in banded, partially migmatized gneisses, augen granitic gneiss, and calc-silicate rocks. The metamafic rocks, normally outcrop adjacent to shear zones, are represented by garnet clinopyroxenites and garnet amphibolites, lenses of kinzigite/khondalite association, metagabro-norite rocks, and fine-grained layers and lenses of eclogite and retroeclogite enclosed in metapelitic granulites and orthogneiss migmatite (Santos et al., 2008). These rocks were submitted to amphibolite- to granulite- facies. The metamafic rocks reached eclogite metamorphic condition with P-T around 17 kbar and 770 °C (Santos *et al.,* 2009).

The protoliths of the metamafic rocks include three geochemical affinity groups: garnet amphibolites with island-arc imprint; an assemblage of retrograded eclogites with mainly MORB-like geochemical features and clinopyroxene-garnet amphibolites with enriched basalt characteristics (Amaral *et al.*, 2010).

3. U-Pb, Lu-Hf and Sm-Nd GEOCHRONOLOGY

Ten samples were selected for LA-MC-ICP-MS determinations, including six metamafic rocks and four metasedimentary country rocks. All samples were collected along the Forquilha Eclogite Zone (Figure 2). Zircon grains of two samples were selected for Lu-Hf investigation and eighteen samples were analyzed by the Sm-Nd method.

4. ANALYTICAL PROCEDURES

For U-Pb and Lu-Hf analyses, zircon concentrates were extracted from 1 to 30kg of rock samples by a jaw crusher to a 500µm size, panning and purified using Frantz isodynamic separator technique. Final purification was achieved by hand-picking under a binocular microscope. The selected grains were placed on epoxy mounts, polished and cleaned with 3% nitric acid before analysis. Backscattering electron (BSE) images were used for spot targeting. BSE images were acquired with a LEO 430i and EDS scanning electron microscope at the Institute of Geosciences, State University of Campinas – UNICAMP, Brazil.

The U-Pb and Lu-Hf isotopic analyses were performed on zircon grains from all samples using a Thermo-Fisher Neptune MC-ICP-MS coupled with a Nd:YAG UP213 New Wave laser ablation system, installed in the Laboratory of Geochronology of the University of Brasilia – UnB .

The U-Pb analyses on zircon grains were carried out following Buhn *et al.,* (2009), using the standard-sample bracketing method (Albarede *et al.,* 2004). During analytical session zircon standard Temora-2 was analyzed as an unknown sample. In all analyzed zircon grains the common Pb correction was not necessary due to the low signal of common ^{204}Pb (<30 cps) and high ^{206}Pb/^{204}Pb. Concordia diagrams (2σ error ellipses), concordia ages and upper intercept ages were calculated using the Isoplot/Ex software (Ludwig, 2003).

Lu-Hf isotopes were analyzed on selected zircon grains from two different samples, previously analyzed with U-Pb systematic. Lu-Hf isotopic analyses were carried out following Matteini *et al,* (2010). The $\varepsilon_{Hf}(t)$ values were calculated using the decay constant $\lambda = 1.865 * 10^{-11}$, proposed by Scherer *et al.,* (2006) and the ^{176}Lu/^{177}Hf and ^{176}Hf/^{177}Hf CHUR values of 0.0332 and 0.282772 proposed by Blichert-Toft &Albarede (1997). The two stages depleted

mantle Hf model ages (T_{DM} Hf) were calculated using $^{176}Lu/^{177}Hf = 0.0384$ and $^{176}Hf/^{177}Hf = 0.28325$ for the depleted mantle and $^{176}Lu/^{177}Hf$ value of 0.0113 for the average crust (Chauvel & Blichert-Toft, 2001)

During analytical session replicate analyses of GJ-1 standard zircon were done obtaining a $^{176}Hf/^{177}Hf$ ratio of 0.282006 ± 16 2σ (*n = 25*), in agreement with the reference value obtained by Morel *et al.,* (2008).

The bulk rock Sm–Nd isotopic analyses were carried out at the Geochronology Laboratory of the University of Brasília. Sample dissolution was done in Teflon Savillex beakers or in Parr-type Teflon bombs. Sm and Nd extraction from whole-rock powders and garnet concentrates followed the technique of Richard *et al.,* (1976), in which the separation of the REE as a group using cation-exchange columns precedes reversed-phase chromatography for the separation of Sm and Nd using columns loaded with HDEHP (di-2-ethylhexyl phosphoric acid) supported on Teflon powder. We have also used the RE-Spec and Ln-Spec resins for REE and Sm–Nd separation. A mixed ^{149}Sm–^{150}Nd spike was used. Sm and Nd samples were loaded onto Re filaments of a double filament assembly. Sm and Nd isotopic analyses were carried out using a Finnigan MAT-262 mass spectrometer. Uncertainties on Sm/Nd and $^{143}Nd/^{144}Nd$ ratios are considered to be better than ± 0.05% (1σ) and ± 0.003% (1σ), respectively, based on repeated analyses of international rock standards BCR-1 and BHVO-1. The $^{143}Nd/^{144}Nd$ ratios were normalized to a $^{146}Nd/^{144}Nd$ ratio of 0.7219. The Nd procedure blanks were smaller than 100 pg.

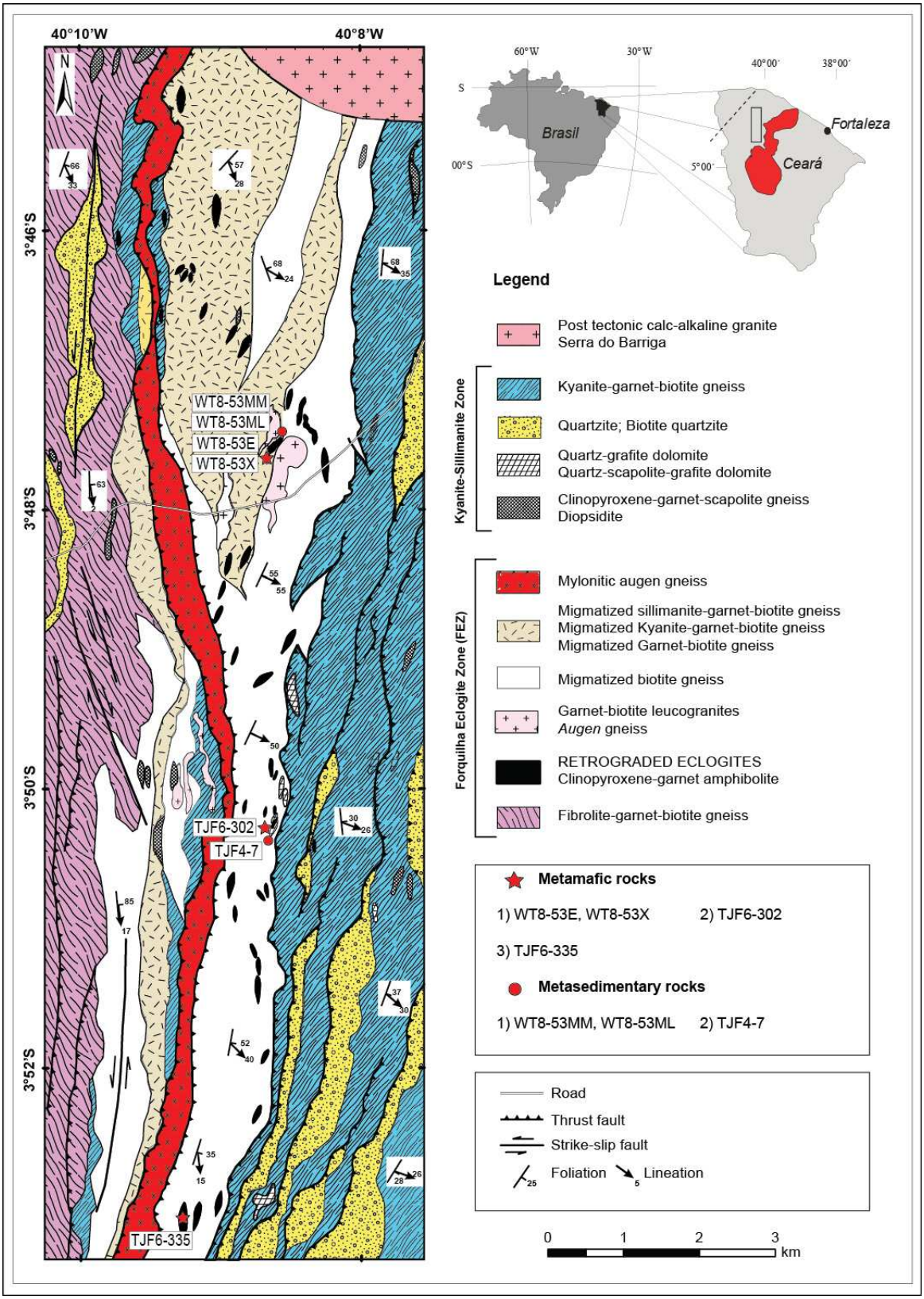

Figure 2: Geological map of the northwestern part of the Forquilha Eclogite Zone, after Ancelmi (2008); samples WT7-25, WT8-12F and WT7-21B are not shown here.

5. U-Pb and Lu-Hf ZIRCON ANALYSES RESULTS
METAMAFIC ROCKS

In the northern portion, the metamafic rocks located in Fazenda Ipueirinha (**374642/9595890**) crop out in an e area of approximately 500,000 m². These rocks are associated with a N-S trend in the vicinity of Serra da Barriga, northeast of Forquilha. Two samples from this region (WT7-25 and WT8-12F) were dated.

WT7-25 is a diopside-bearing garnet amphibolite sample composed of garnet + amphibole + clinopyroxene + quartz + plagioclase and accessory titanite, rutile, apatite and zircon. Several structures are recognized in this amphibolite, among which strongly deformed oval features, outlined by discrete quartz and garnet trails. These features are interpreted as possible metamorphosed pillow lavas. Centimeter-sized cavities filled with quartz that look like drops stretched along the N-S direction were interpreted as having been amygdales. Fine pyroxene-rich layers define a penetrative E-W orientation, which is perpendicular to the main low- to medium-angle orientation.

Sample WT7-25 zircon crystals are yellow to brownish yellow, elongated (3x1 to 4x1), and have sub-rounded terminations; more rarely prismatic faces are still preserved. Less frequently they present fractured rims and well-preserved cores. In general, the grains contain a few inclusions and do not show any evidence of metamictization. Internal structures, such as magmatic oscillatory zoning or metamorphic overgrowth, are not recognized in the back-scattered electron images (Figure 3).

The data are represented in concordia diagrams in which the projection of the discordia curve, drawn using 14 spot analyses, defines an upper intercept of 1566 ± 9 Ma (MSDW=0.52) and lower intercept of 618 ± 32 Ma. The former is interpreted as the crystallization age; the latter may correspond to the age of metamorphism, but the lack of a zircon population around the lower intercept makes this assumption speculative (Figure 4). Nonetheless, high-grade metamorphism must have caused significant Pb loss.

Lu-Hf model ages obtained for the same zircon grains yielded T_{DM} between 1570 and 1810 Ma, with positive ε_{Hf} (t=1566 Ma) values varying between +7.46 and +9.63, which indicates derivation from a juvenile mantle magma (Figure 5).

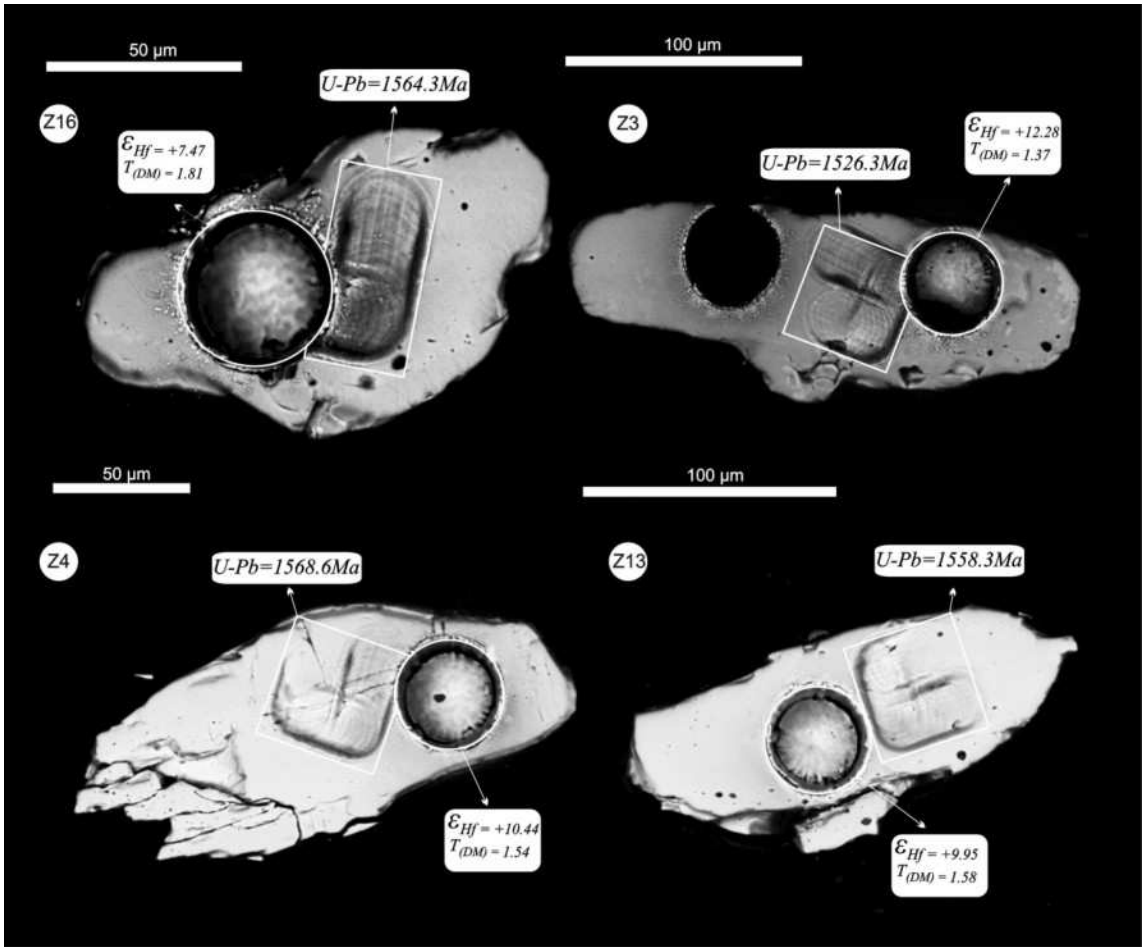

Figure 3: Back-scattered electron image of representative zircon grains from the pyroxene-bearing garnet amphibolite WT7-25. The elongated grains do not show evidence of intergrowth and contain a few oxide inclusions. Note spot analyzed by the U/Pb (raster) and Lu/Hf (spot size = 30 µm) methods with the respective $^{235}U/^{207}Pb$ ages, T_{DM} and ε_{Hf}.

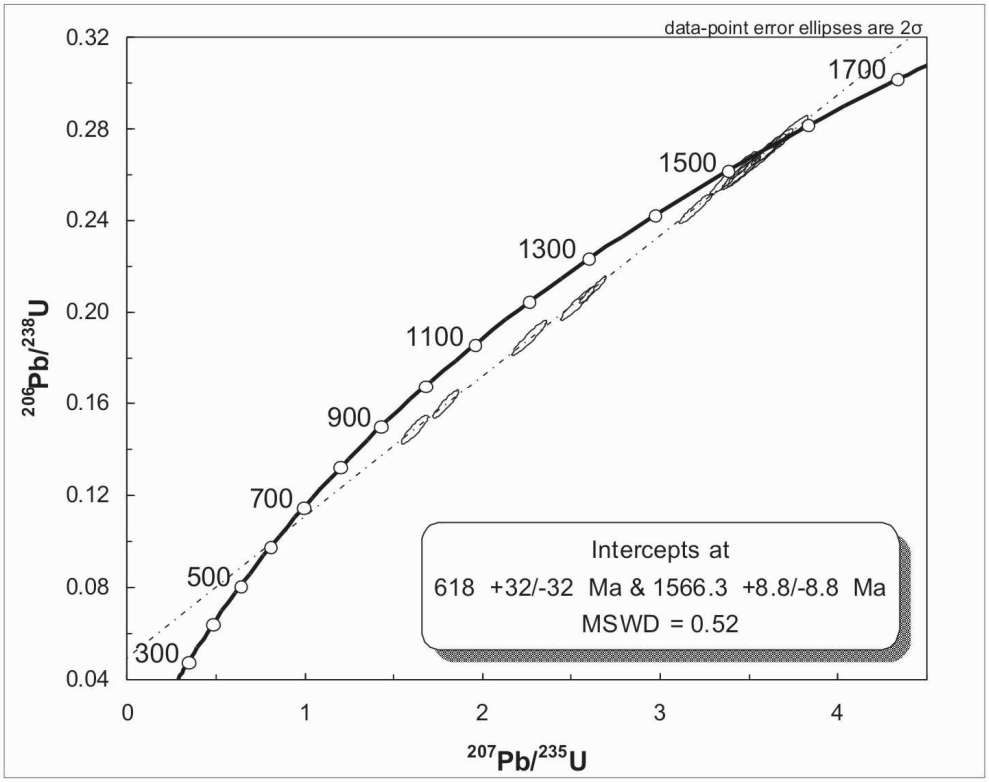

Figure 4: U/Pb concordia diagram (LA-ICPMS) for sample WT7-25 zircon grains, depicting a concordant population around 1.5Ga and a population showing Pb loss.

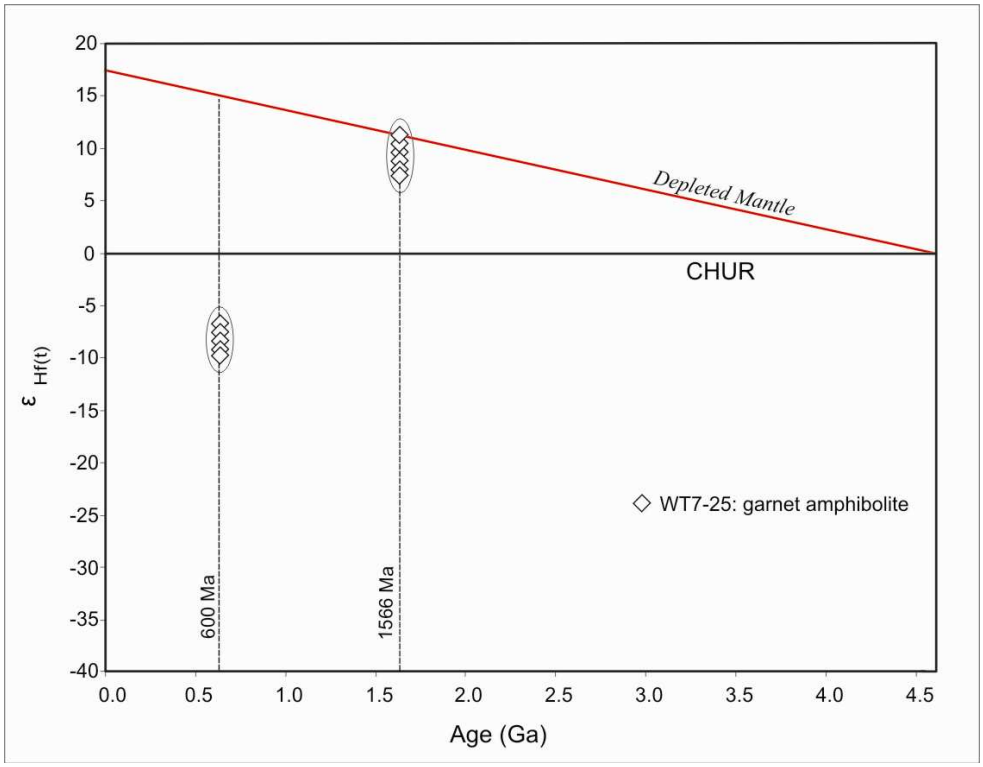

Figure 5: Evolution diagram showing ε_{Hf} values calculated for a crystallization age of 1566 Ma. Strongly positive ε_{Hf} values stand out.

A second sample from the same trend (Figure 6a), richer in pyroxene and classified as clinopyroxene-garnet amphibolite (WT8-12F), shows a higher diopside modal proportion in relation to that of hornblende (Figure 6b). Decompression textures represented by symplectitic clinopyroxene and plagioclase intergrowths are also frequent (Figure 6c).

The majority of the zircon crystals in this amphibolite are inclusions in garnet (Figure 6d). These light-colored crystals are sub-rounded to sub-elongated and may show prismatic rims. As a result of result of metamictization, they contain a large number of fractures filled with oxides. As internal structures were not recognized, the spots were preferably aimed at the cores and at the more homogeneous regions of the crystals (Figure 7).

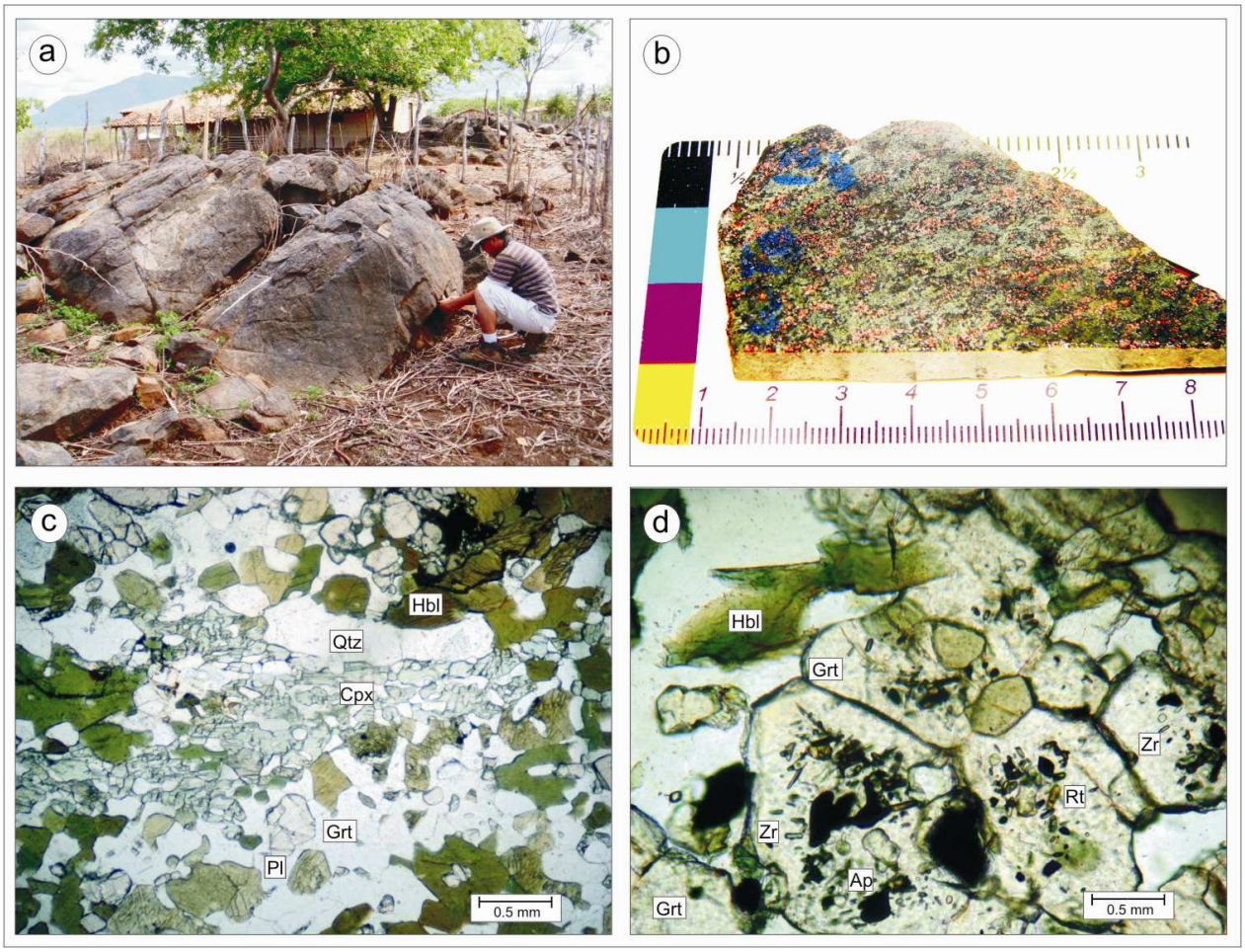

Figure 6: Sample WT8-12F: a) Outcrop where the sample was collected, showing low-angle dip (~35°) towards E-SE; b) arrangement of slightly oriented minerals, such as pyroxenes (green), garnet (pink) and amphiboles (black); c) detail of a polished thin section (10x) showing the main mineral phases: clinopyroxene (Cpx), garnet (Grt), hornblende (Hbl), plagioclase (Pl) and quartz (Qtz). Note the destabilization of Cpx in Hbl + Pl ± Qtz; d) Garnet containing a large number of inclusions, such as zircon (Zr), rutile (Rt) and apatite (Ap).

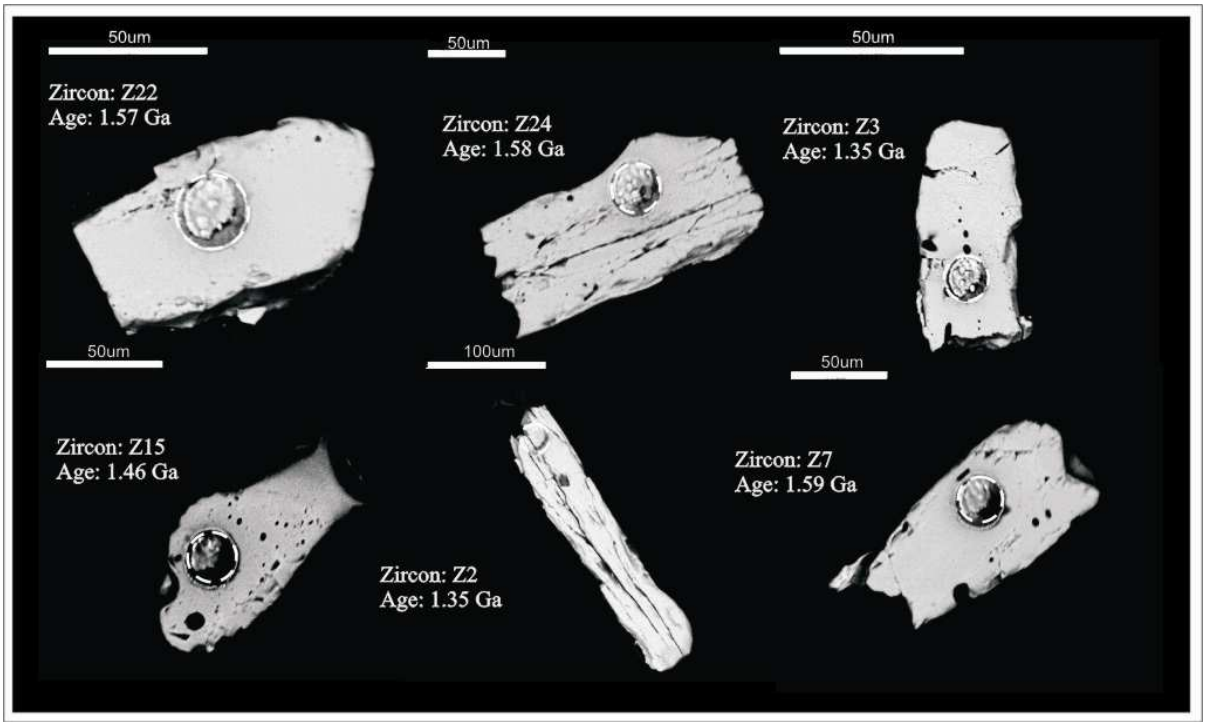

Figure 7: Back-scattered electron image of representative zircon grains from the clinopyroxene-garnet amphibolite WT8-12F. The grains are in part elongated (4x1) and sub-rounded (3x2) and show no intergrowths; Circles spots analyzed by the U/Pb method (30 and 25 µm-sized spots) and corresponding $^{235}U/^{207}Pb$ ages.

In the concordia diagram the data define upper and lower intercept ages of 1546 ± 37 Ma (2σ) and 725 ± 37 Ma (2σ), respectively (Figure 8). The age obtained at the upper intercept was interpreted as the crystallization age of the rock, which agrees with the age of 1566 ± 9 Ma obtained for the garnet amphibolite (WT7-25). In general, Pb loss is evident in most zircon grains.

A mesocratic clinopyroxene-garnet amphibolite (WT8-53E) (Figures 9a-b) from the central portion of the Forquilha high-pressure belt that crops out in the vicinity of Fazenda Cachoeira dos Loretos (**373378/9580594**) was analyzed.

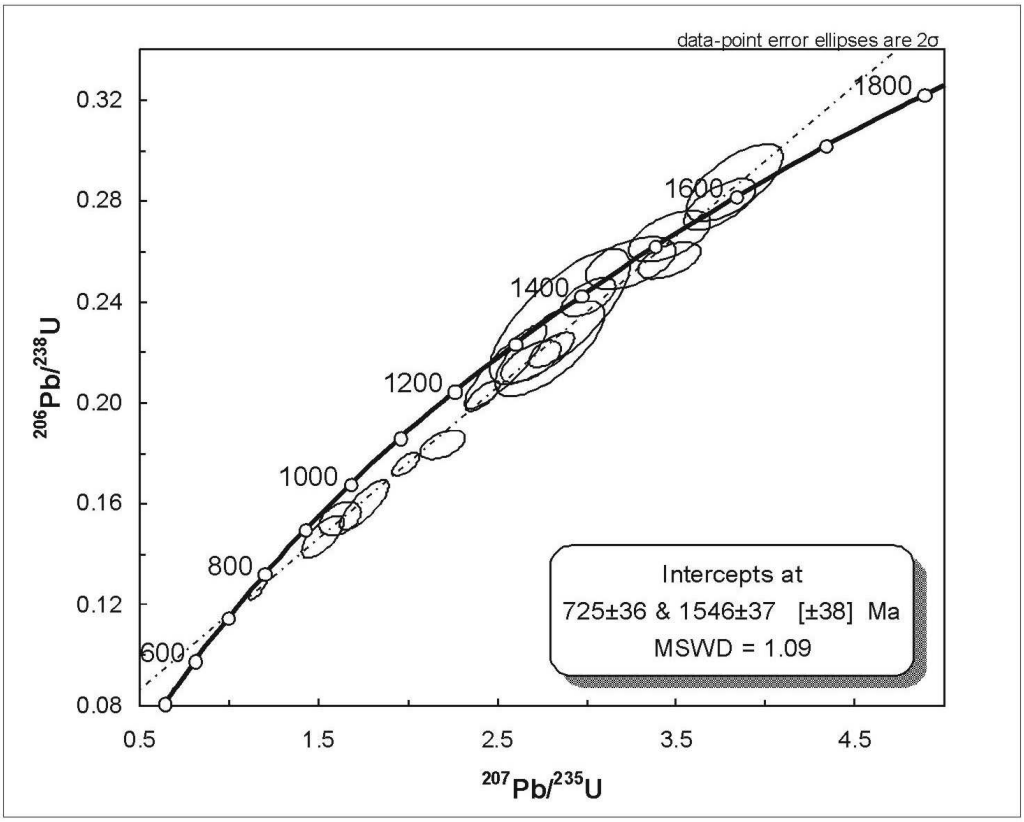

Figure 8: U/Pb Concordia diagram (LA-ICPMS) for sample WT8-12F zircon grains.

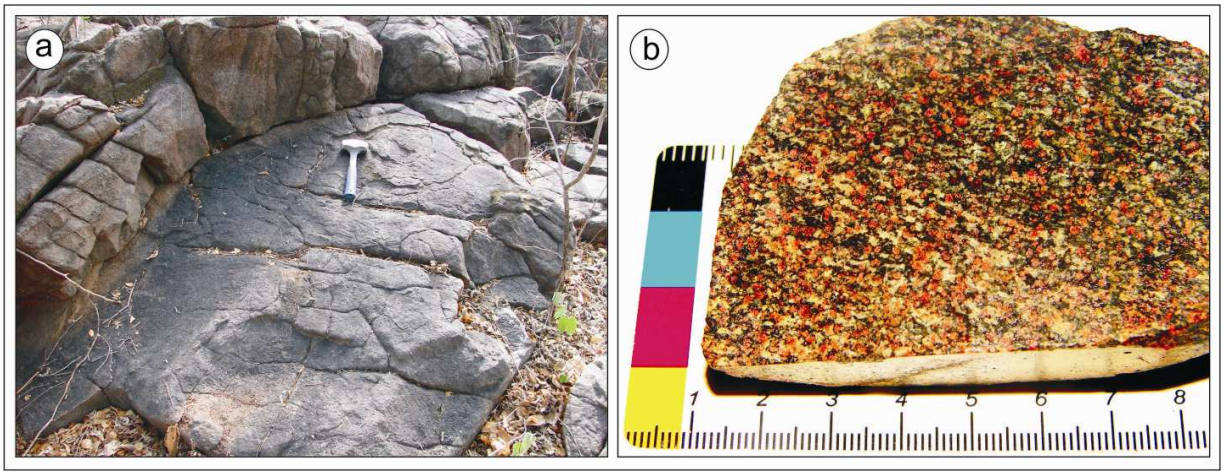

Figure 9: Sample WT8-53E: a) Outcrop in the shape of a meter-sized "lens" intercalated with para-derived migmatites, where sample WT8-53E was collected; b) hand specimen, abundant garnet, pyroxene and amphibole.

Out of 15 grains analyzed, only nine yielded satisfactory results. The concordant zircon grains are light-colored, yellowish or not, euhedral to sub-euhedral, prismatic, and 100 to 200 µm long. Some grains show internal fractures and pyroxene and oxide inclusions. Back-scattered

electron images show that a few crystals have more luminescent sectors. Overgrowth features or internal zoning are lacking (Figure 10).

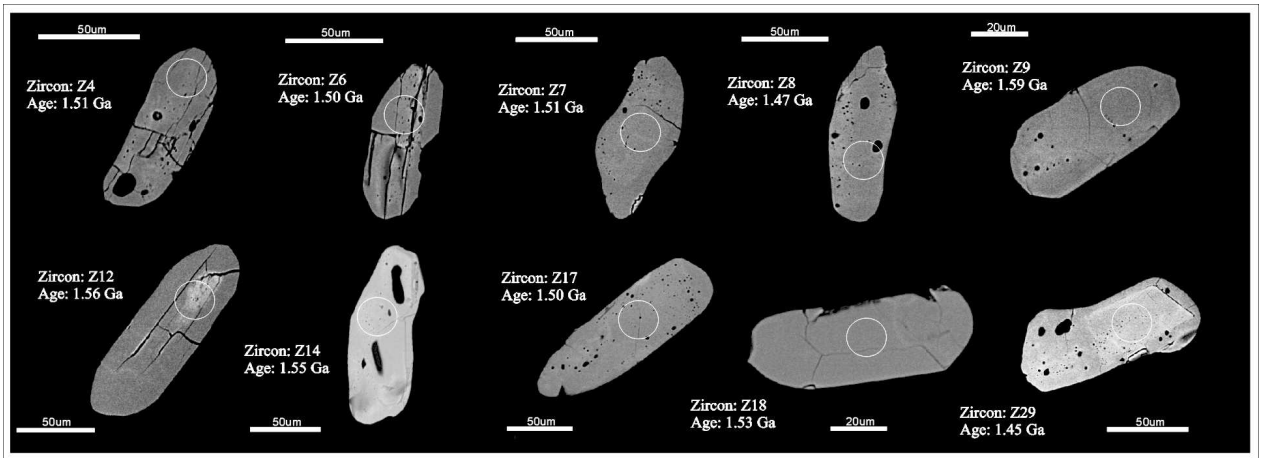

Figure 10: Back-scattered electron images of representative zircon grains from the mesocratic clinopyroxene-garnet amphibolite WT8-53E. The grains are elongated, subhedral, some showing luminescent cores and internal fracturing. Circles indicate spots by the U/Pb method (30 and 25 µm-sized spots) and corresponding $^{235}U/^{207}Pb$ ages.

The data obtained were plotted in the concordia diagram, in which the projection of the discordia curve, drawn using 10 spot analyses, defines an upper intercept of 1559 ± 70 Ma (MSDW=15), interpreted as the crystallization age. Despite the lower intercept indicates a Neoproterozoic thermal event, it cannot be considered representative, as concordant zircon crystals are absent in this intercept (Figure 11).

A leucosome layer (WT8-53X) associated with the metamafic rock was also analyzed, aiming at the characterization of the metamorphic event in both zircon and monazite (Figure 12). The zircon from this rock is light and more elongated (4:1) than that of the clinopyroxene-garnet amphibolite WT8-53E. Most grains present well-delineate external faces, punctual inclusions, fractures in the rims, and well-preserved cores (Figure 13). Due to the excess of Th and U, monazite did not yield satisfactory results.

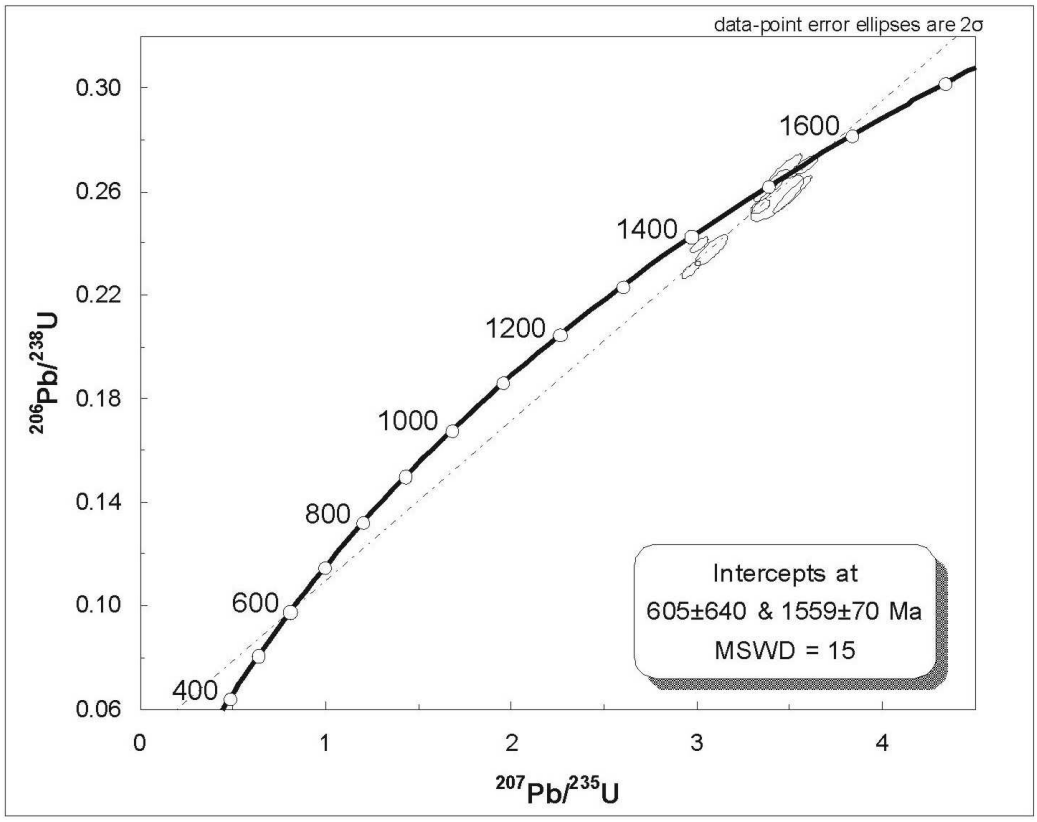

Figure 11: Concordia diagram for U/Pb analyses (LA-ICPMS) of the mesocratic clinopyroxene-garnet amphibolite WT8-53E, showing a concordant age of 1559 ± 70 Ma.

Figure 12: Detail of leucosome from where zircon grains were extracted for analysis. These melts are mainly composed of plagioclase, quartz, garnet and amphibole. Accessory minerals are zircon, apatite and rutile.

In the concordia diagram the results from the zircon analyses define upper and lower intercept ages of 1615 ± 40 Ma (2σ) and 613 ± 130 Ma (2σ), respectively (Figure 14). The age obtained for the upper intercept is interpreted with caution, because there is no zircon older than 1590 Ma. In this case, the zircon of 97.74 % concordance (Z7) yielded $^{207}Pb/^{235}U$ age of 1548 Ma and $^{206}Pb/^{238}U$ = 1524 Ma, similar to the ages obtained for the metamafic rock zircon grains. The age obtained for the lower intercept, although imprecise, aligns with the discordia curve, around 600 Ma.

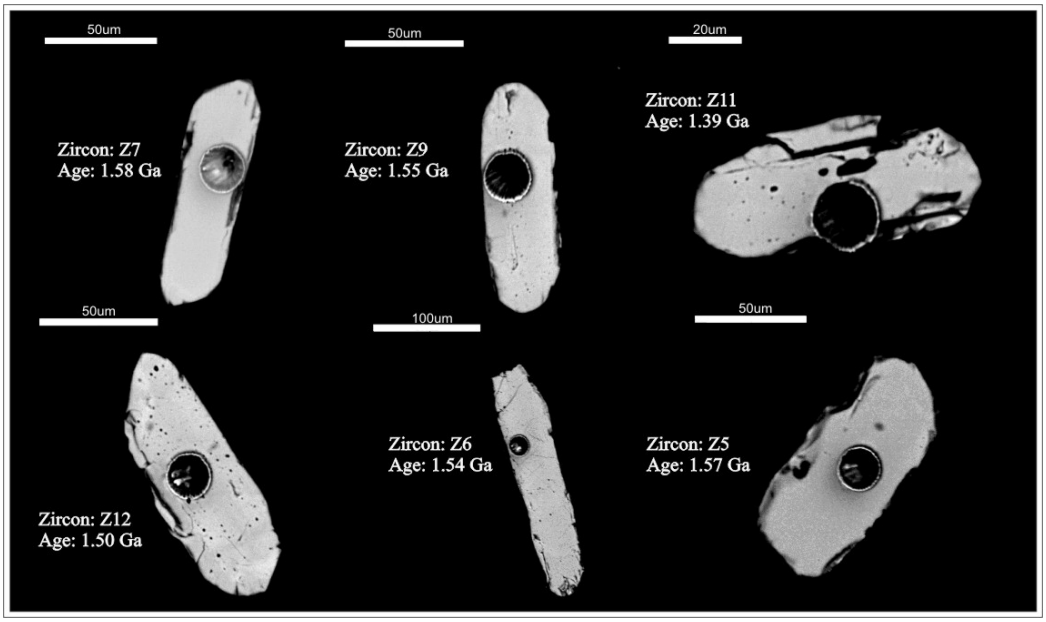

Figure 13: Back-scattered electron images of representative zircon crystals from sample WT8-53X. The grains are elongated, subhedral, and contain punctual inclusions and a few fractures. Circles indicate spots by the U/Pb method (30 and 25 µm-sized spots) and corresponding $^{235}U/^{207}Pb$ ages.

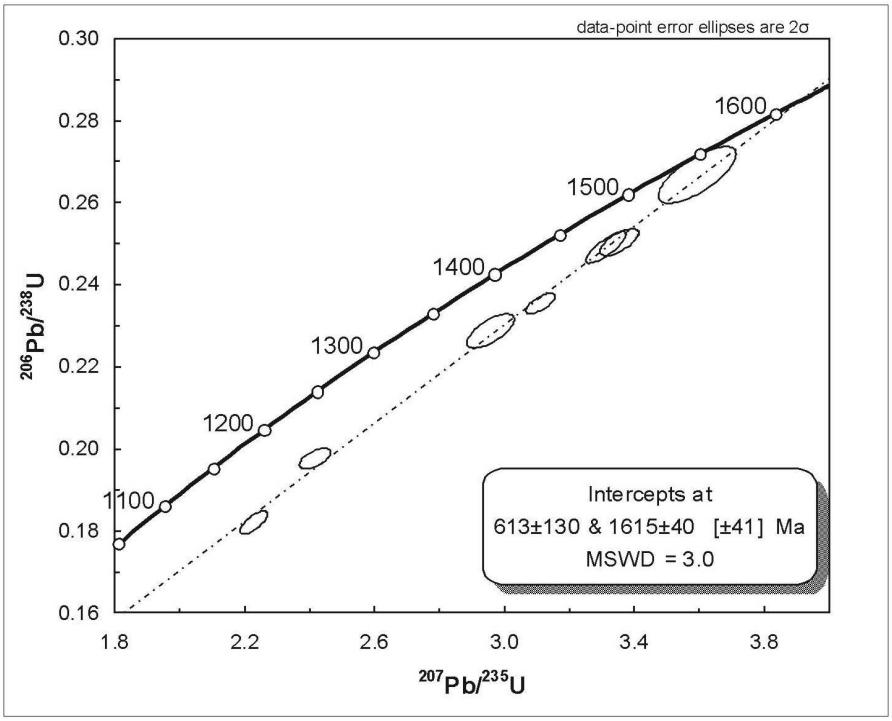

Figure 14: Concordia diagram for the U/Pb analyses (LA-ICPMS) of the leucocratic portion of sample WT8-53X, showing an age of the upper intercept of 1615 ± 40 Ma. The loss of radiogenic Pb is conspicuous.

Rocks cropping out in the southern sector of the Forquilha Eclogitic Zone correspond to the highest pressure conditions, above 17 kbar (Santos *et al.* 2009). One sample from these rocks (TJF6-302) was collected in the Fazenda Cabeça de Touro (**373002/9575854**). It is a retrograded eclogite that occurs associated with calc-silicate rocks and marbles (Figure 15).

The zircon crystals from this retrograded eclogite are of varied colors. Some are transparent, whereas others are slightly yellow. The grains are of 30 to 100 µm in size and oval with rounded (2:1 and 1:1) terminations, or elongated with sub-rounded (3:1) terminations, or even anhedral (Figure 16).

Subtle sector zoning was identified in the back-scattered electron images, but in general internal structures are lacking. Most grains are fractured and contain inclusions, evidencing strong metamictization. It can have caused considerable radiogenic Pb loss, resulting in imprecise ages. No concordant zircon is depicted in the concordia diagram; however, the alignment of grains defines a discordant curve with an upper intercept of 1455 ± 120 Ma (MSWD= 4) (Figure 17). Despite the large error, this age is somewhat close to that obtained for the other metamafic rocks. It is important to stress out that this rock underwent the highest pressure (> 17 kbar) and

temperature (~770 °C) conditions recorded in the Forquilha Eclogite Zone. These conditions may have caused disequilibrium of the zircon isotopic system (Rubatto *et al.*, 1999; 2003).

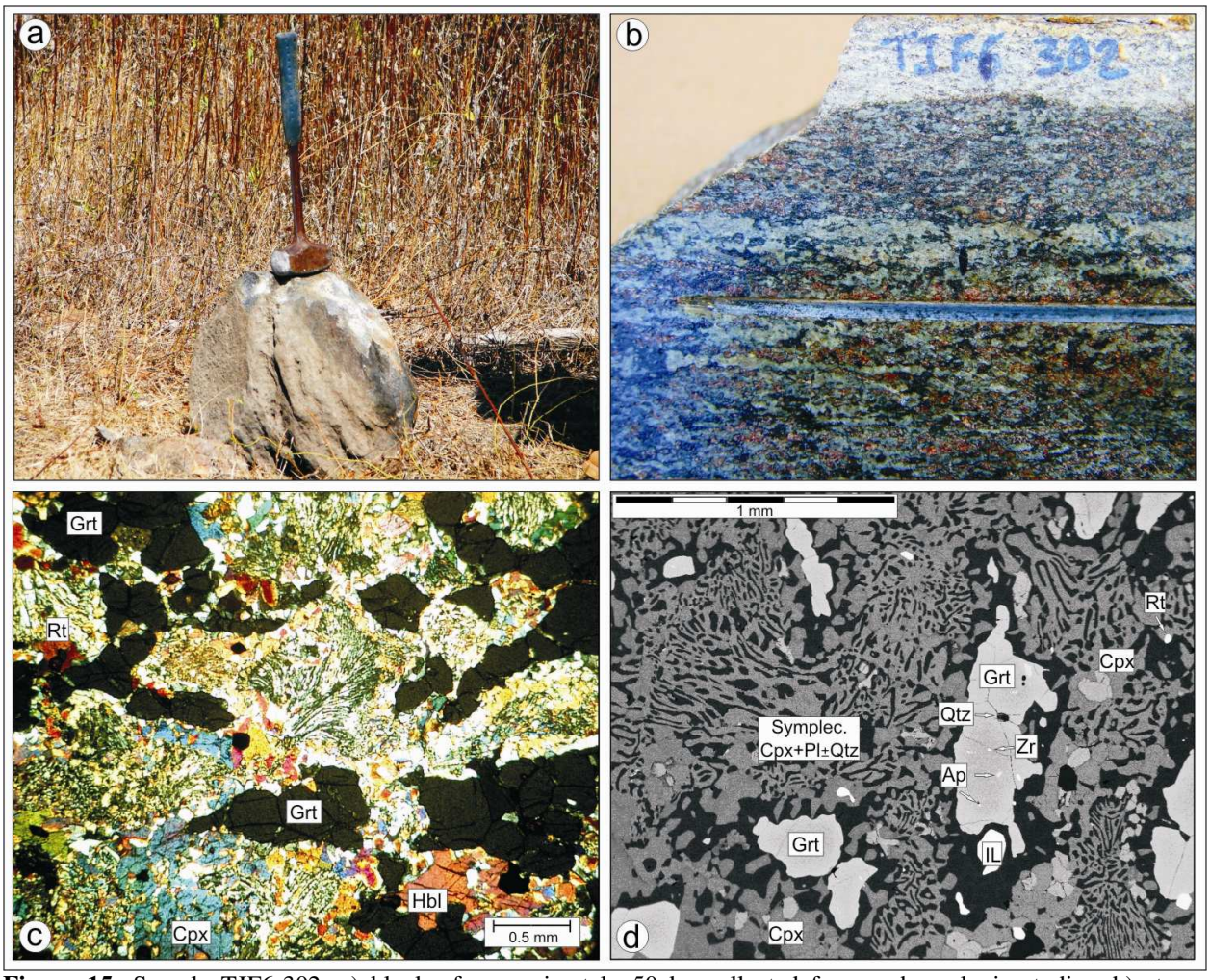

Figure 15: Sample TJF6-302: a) block of approximately 50 kg collected for geochronologic studies; b) strong mineral orientation outlined in hand specimen; c) photomicrograph of thin section showing stretched garnet (grt) and pseudomorphs filled by vermiform intergrowths of clinopyroxene (cpx) + plagioclase (pl) ± quartz (qtz); d) back-scattered electron image showing a large quantity of symplectites and accessory minerals such as zircon (zr) inclusions in garnet, rutile (rt), apatite (ap) and ilmenite (il).

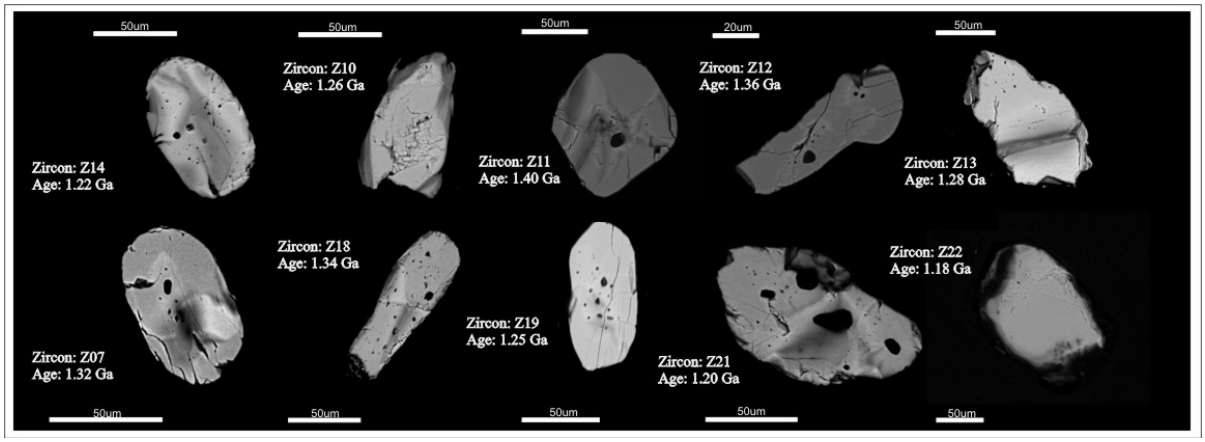

Figure 16: Back-scattered electron images of representative zircon crystals from retrogressed eclogite (sample TJF6-302).

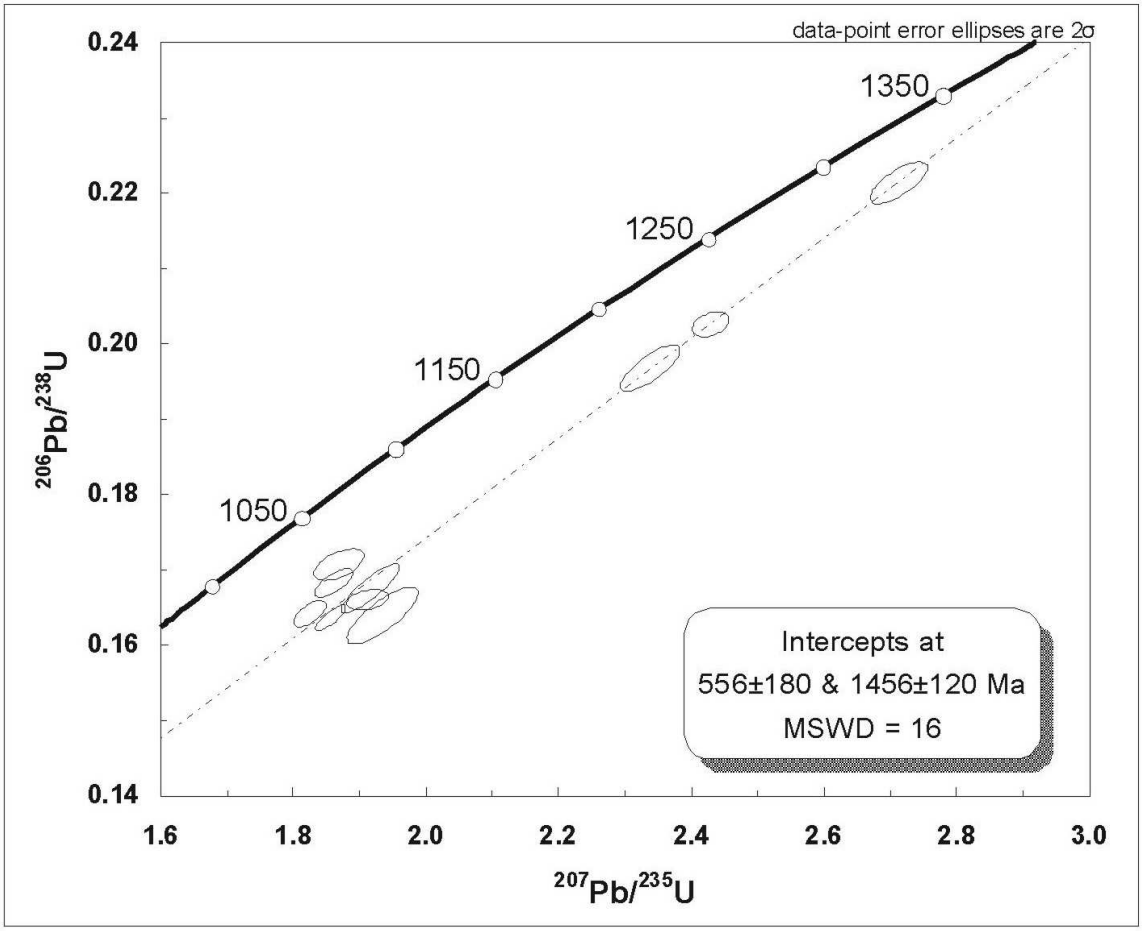

Figure 17: Concordia diagram for U/Pb analyses (LA-ICPMS) of retrogressed eclogite zircon (sample TJF6-302).

A sample from a garnet-clinopyroxene amphibolite of the southern sector (TJF6-335) was collected in the Fazenda Juazeiro (**371970/9570622**). This amphibolite occurs associated with

marble, quartzite and calc-silicate rock. The size of the outcrop is 500 m x 100 m in area (Figure 18a). The predominant granoblastic texture is characterized by garnet dispersed in a slightly foliated, greenish-gray matrix composed of plagioclase, clinopyroxene and amphibole (Figure 18b). The deformation is more intense at the borders of the amphibolite bodies and is marked by a well-developed foliation. The central portion of these bodies is essentially isotropic.

The data obtained from the analysis of 19 zircon crystals define a concordia curve from which an average age cannot be estimated, due to discordant values and probable inheritance around 700-800 Ma (Figure 19). Only eight crystals yielded values close to 100% concordance, which define a concordia age of 614 ± 3.9 Ma (2σ) (Figure 20).

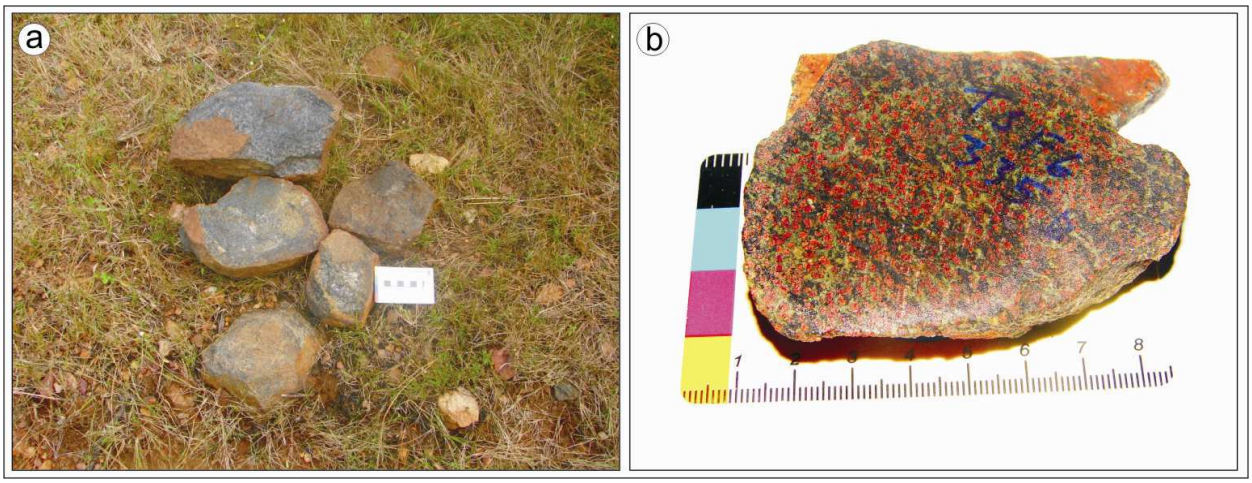

Figure 18: Sample TJF6-335: a) blocks of approximately 30 kg collected for geochronologic studies; b) the predominance of garnet and clinopyroxene is observed in hand specimen.

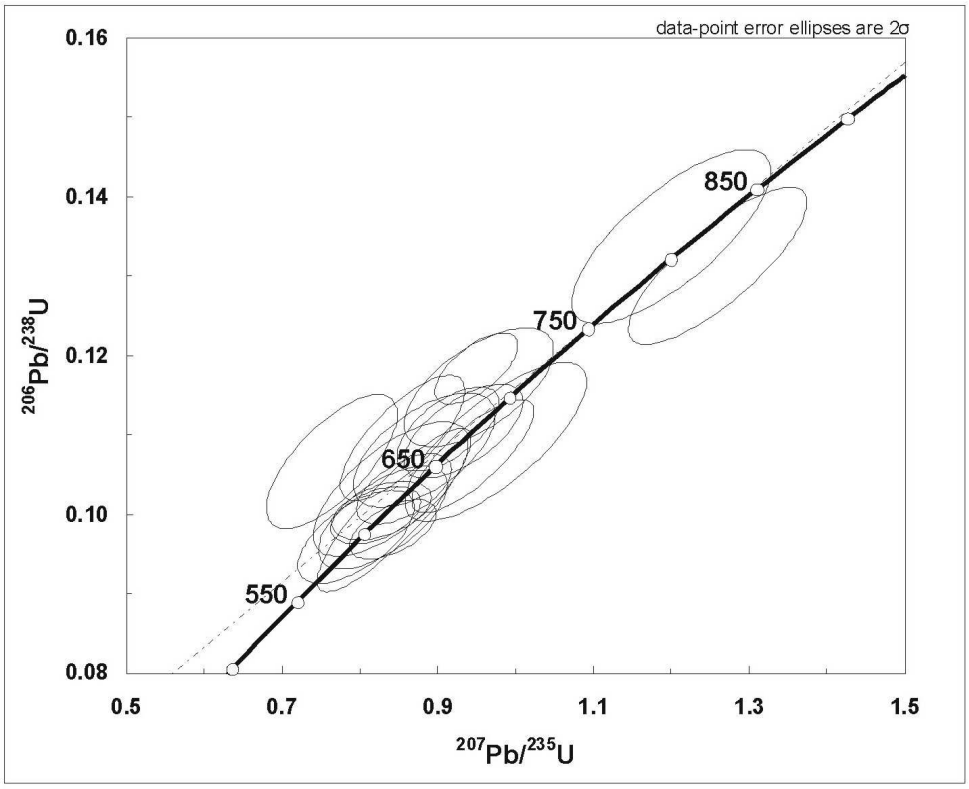

Figure 19: Concordia diagram for U/Pb analyses (LA-ICPMS) of sample TJF6-335.

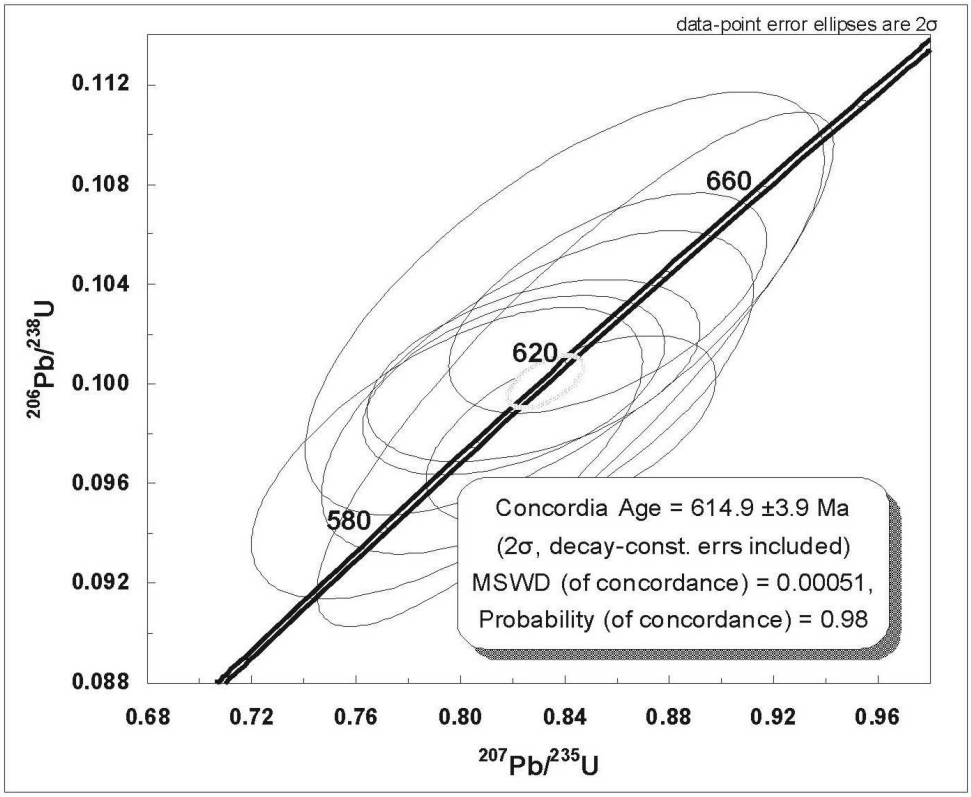

Figure 20: Concordia diagram using U-Pb concordant ages (LA-ICPMS) obtained for zircon crystals from sample TJF6-335.

6. PARA-DERIVED HOST ROCKS

6.1. Migmatitic Kinzigite

The rocks hosting the metamafic rocks from the eclogite belt central portion are kyanite- and sillimanite-bearing, kinzigite migmatitic gneisses. They crop out in an approximately 2 km-long area in Cachoeira dos Loretos (**373378/9580594**) (Figure 2). The rocks are imbricated according to the regional tectonic framework, dipping at low angles eastwards (Figure 21a).

In general, the migmatitic gneisses are aluminous. The melanosome is constituted of centimeter-sized garnet, biotite and plagioclase. The leucosome is constituted of millimeter-sized garnet, plagioclase, quartz, potassic feldspar, kyanite and sillimanite mantled by garnet (Figure 21b-c).

Aiming at a better definition of both zircon provenance and metamorphic event, which are more or less depicted in all lower intercepts of the metamafic rock diagrams, both zircon and monazite from the melanosome (sample WT8-53MM) and leucosome (sample WT8-53ML) were analyzed (Figure 21d).

The melanosome zircon grains were grouped into two families. The crystals of one family are oval in shape and *ca*. 100 μm in size, usually transparent, and contain a few inclusions and fractures (Z5, Z9, and Z10 in Figure 22). Well-defined oscillatory zoning is characteristic of the cores. The grains are enveloped by a later overgrowth. The other family is composed of yellowish, elongated grains, in the average 200-μm long, and usually showing well-defined prismatic faces. Back-scattered electron images illustrate both metamictization occurring along internal structures and a well-defined oscillatory zoning (Figure 22, Z21, Z13, Z14). Fractures are absent in most crystals.

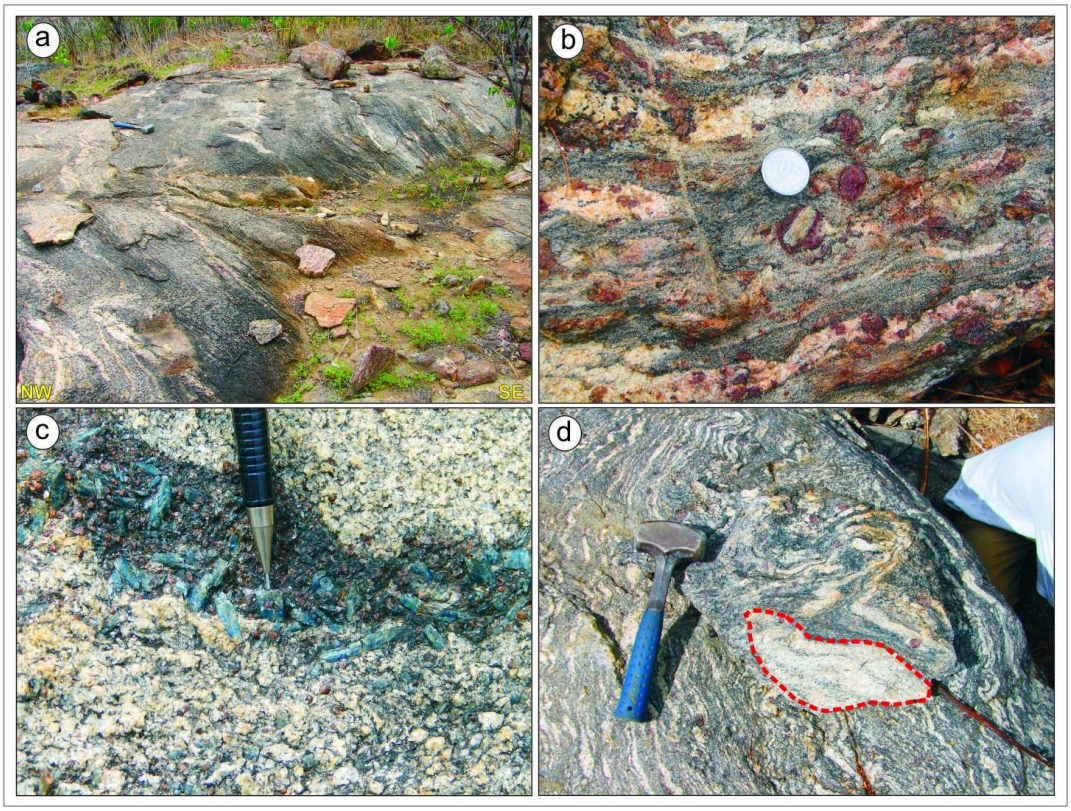

Figure 21 : Samples WT8-53MM and WT8-53ML: a) low-angle (~30°SE) dipping slab-shaped outcrop; b) banding defined by alternating biotite- and garnet-rich melanocratic layers and garnet-, sillimanite-, feldspar- and quartz-rich leucocratic layers; c) centimeter-sized kyanite clustered in biotite and garnet aggregates; d) leucosome sample used for zircon and monazite separation.

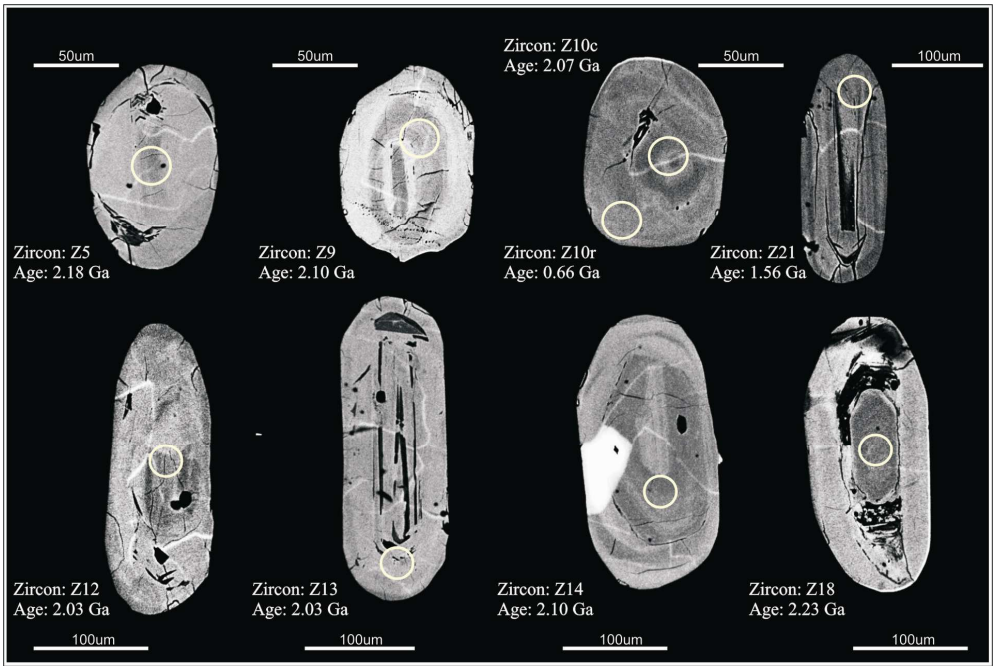

Figure 22: Back-scattered electron images of representative zircon crystals from sample WT8-53MM melanosome. Circles indicate analyzed spot by the U-Pb method (spot size = 30 µm) and corresponding $^{235}U/^{207}Pb$ ages.

Leucosome WT8-53ML also have two zircon families. One family encompasses light brownish, slightly elongated, oval-shaped grains, which may preserve some intact crystal faces (Z10 and Z12 in Figure 23). Zircon cores are enveloped by a thin, intergrown oscillatory layer and show some metamictization. The other population is composed of grains of *ca.* 100 to 150 µm in size. These grains are pink to transparent and ovoid; some contain partially rounded faces. Internal structures are marked by concentric oscillatory zoning. Metamorphic overgrowth, site for punctual analyses, envelopes the zircon crystals (Figure 23, Z11 and Z14).

Monazite grains are relatively uniform, sub-rounded, yellowish to orange, and devoid of inclusions or fractures (Figure 24).

The frequency histogram of Figure 25 represents the data obtained for zircon crystals extracted from the melanosome of migmatite sample WT8-53MM. The age distribution clearly indicates a source between 2.0 and 2.2 Ga. A Neoproterozoic event can also be depicted, even if the analyses were directed to some zircon cores. Archean ages around 3.0 Ga are interpreted as resulting from metamictization that affected some grains with a higher intensity. Only one crystal recorded age close to 1.57 Ga. The others yielded ages distributed in the 1.9 and 2.5 Ga interval (Figure 25).

The data obtained for zircon grains from the leucosome of migmatite sample WT8-53ML define an age of 639 ± 10 Ma (2σ) in the concordia diagram, interpreted as the probable highest-grade metamorphic record (eclogite?/granulite facies) (Figure 26). As for monazite, weighted mean $^{235}U/^{207}Pb$ ratios yielded a mean age of 563 ± 96 Ma (2σ) (Figure 27). Considering the physical-chemical conditions for monazite crystallization at temperatures lower than those for zircon, the age obtained can be interpreted as the record of low-grade metamorphic conditions or even retrograde metamorphism (lower amphibolite facies). Several studies carried out in the Central Ceará Domain involving monazite and titanite dating point to ages around 570-560 Ma, interpreted as the record of a late metamorphism (Nogueira-Neto *et al.,* 1997; Fetter, 1999; Fetter *et al.* 2003).

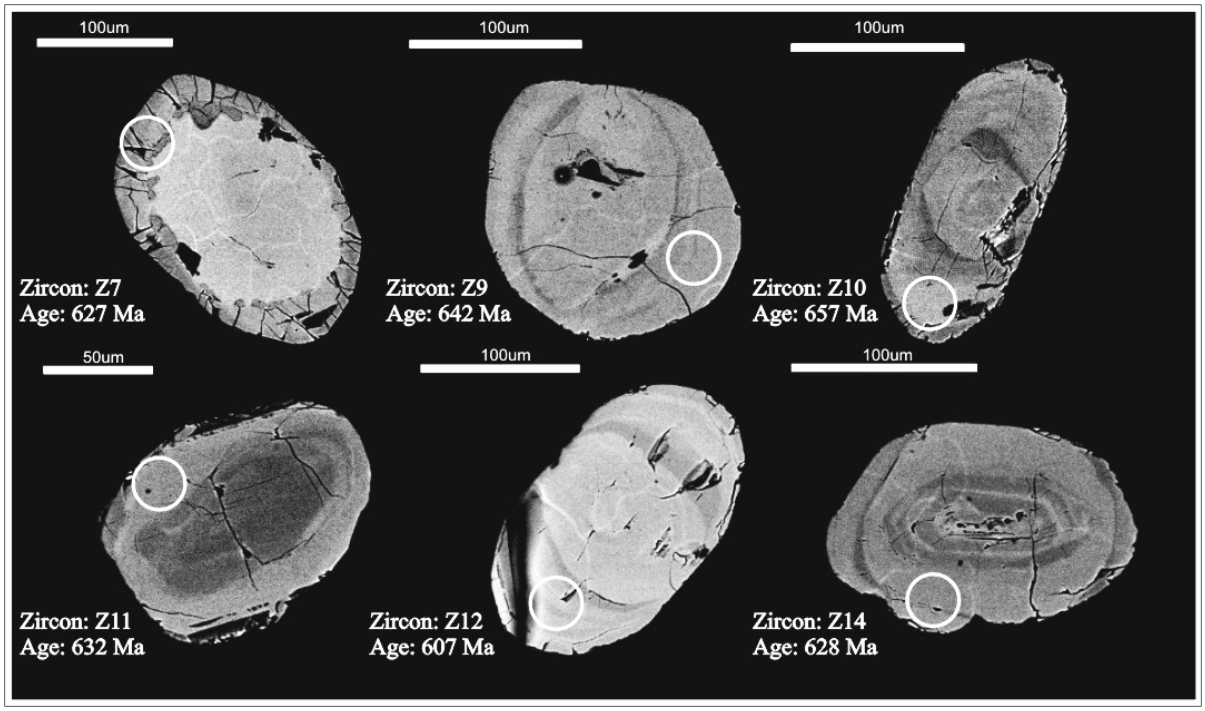

Figure 23: Back-scattered electron images of representative zircon crystals from sample WT8-53ML leucosome. Two populations were identified: one containing elongated grains (Z10 and Z12) and another with ovoid and rounded grains (Z7, Z9, Z11 and Z14). Circles regions analyzed by the U/Pb method (spot size = 25 µm), mostly grain rims, with corresponding $^{235}U/^{207}Pb$ ages.

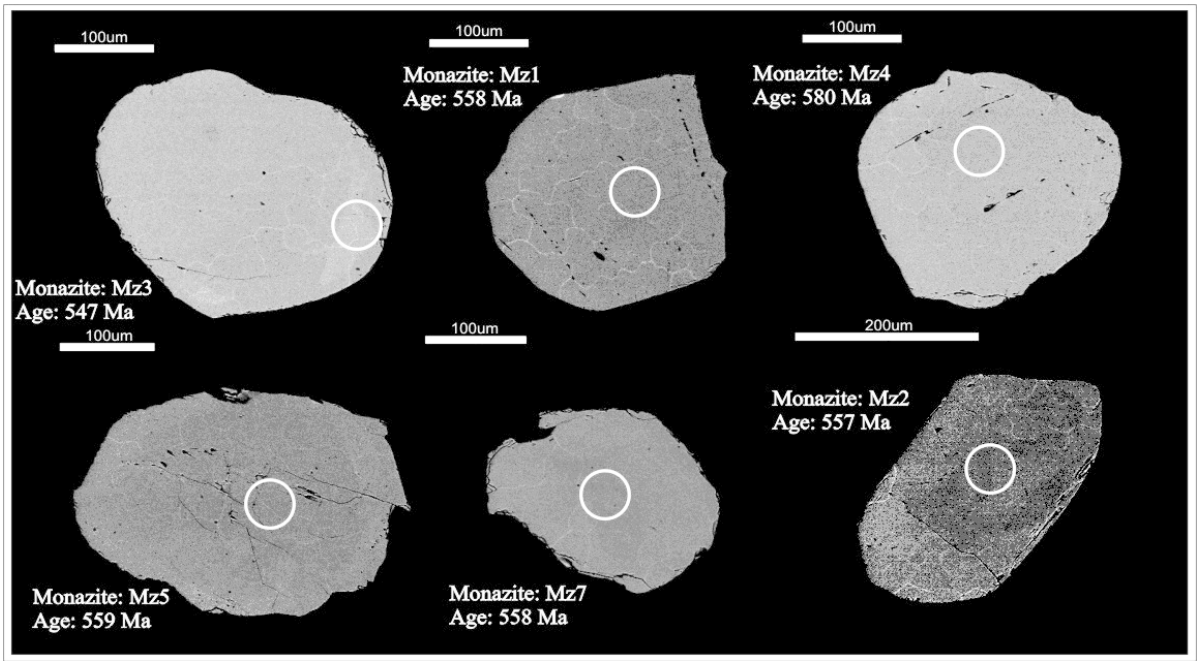

Figure 24: Back-scattered electron images of representative monazite crystals from sample WT8-53ML leucosome. Circles regions analyzed by the U/Pb method (spot size = 30 µm) with corresponding $^{235}U/^{207}Pb$ ages.

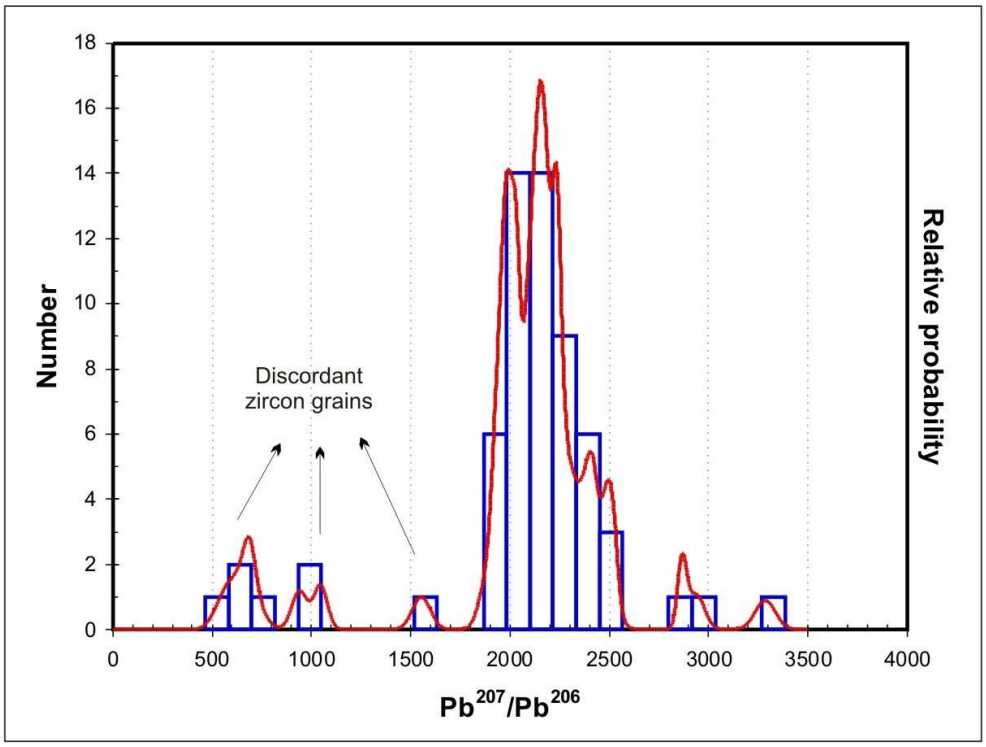

Figure 25: Frequency histogram for the U/Pb analyses of melanosome zircon (sample WT8-53MM).

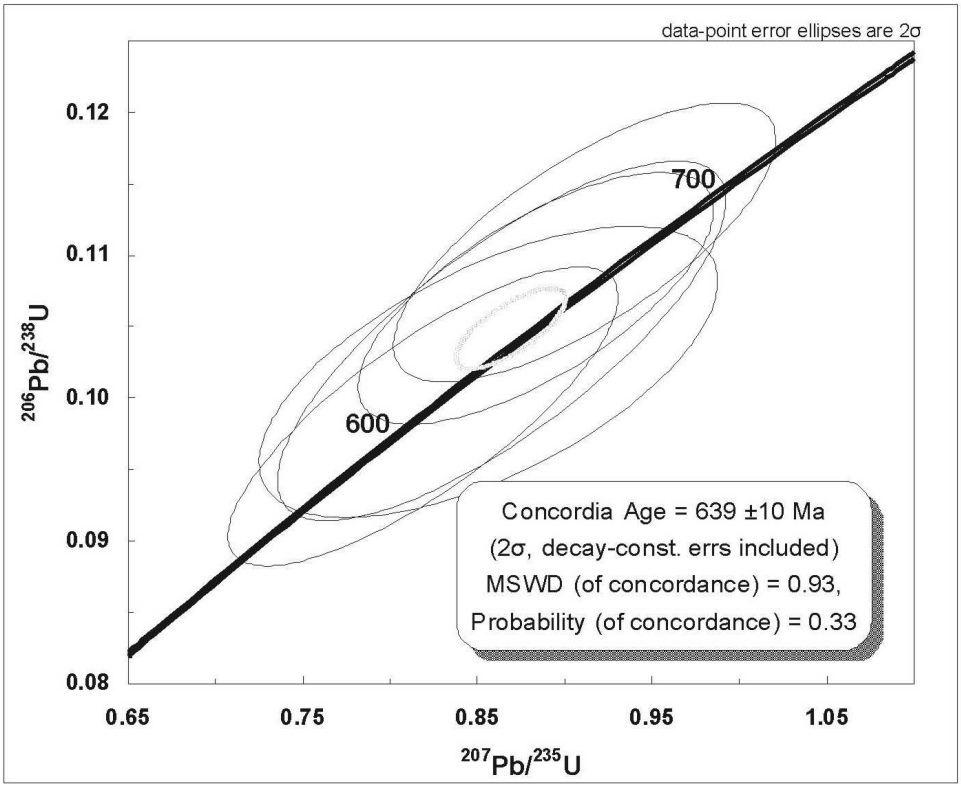

Figure 26: Concordia diagram for U/Pb analyses (LA-ICPMS) of leucosome zircon from host migmatite (sample WT8-53ML).

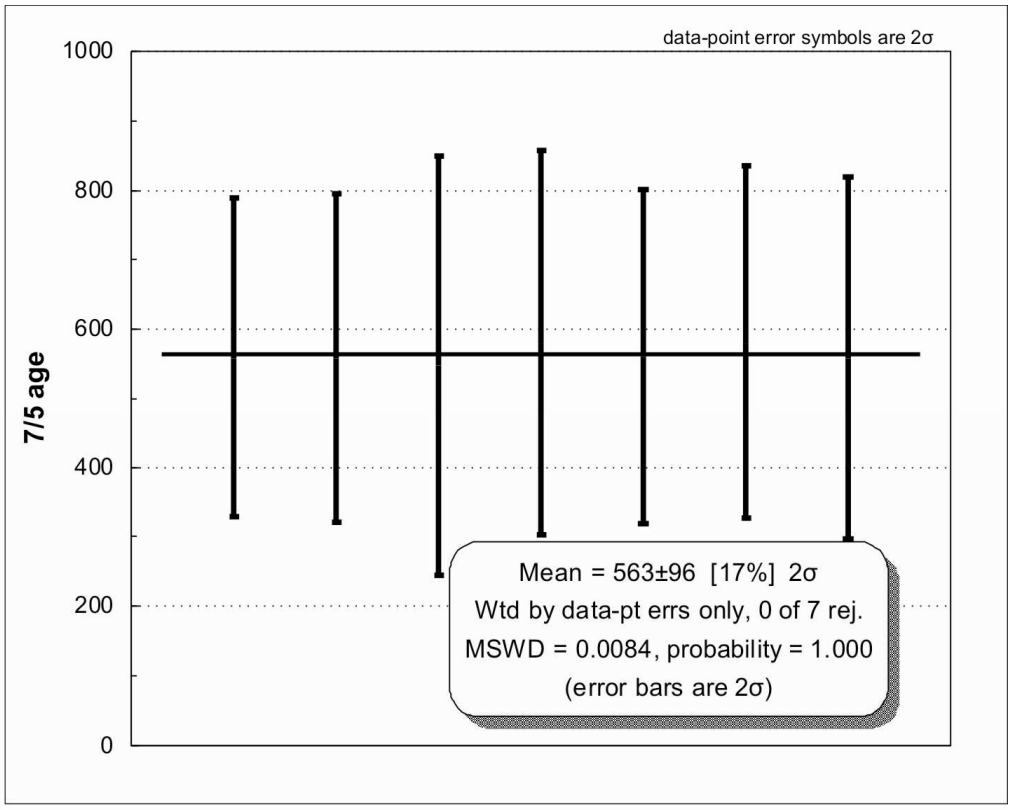

Figure 27: Diagram of weighted mean U/Pb values for leucosome monazite from host migmatite (sample WT8-53ML).

6.2. Sillimanite-garnet-biotite gneiss

Along highway BR-222 (**364731/9580606**), close to Forquilha, an association of aluminous metasedimentary rocks characterized by high-grade paragenesis occur. In these rocks, either sillimanite or kyanite predominates. These rocks trend N-S and dip at low angles (30-40°) to E-SE. They are composed of biotite, muscovite, plagioclase, garnet, quartz, and accessory zircon, titanite, apatite and rutile. Sillimanite (fibrolite) and biotite define downdip to oblique mineral stretching lineation. Small intrafolial folds and garnet and feldspar porphyroblasts indicate tectonic vergence to W-NW. More deformed areas are marked by mylonites and leucogranite injections (Figure 28 a-b), usually constituting thrust fronts.

Zircon and monazite were analyzed aiming at the definition of provenance and metamorphic conditions in a more remobilized portion of this para-derived gneiss (sample WT7-21A). Unfortunately, monazite did not yield satisfactory analytical results, probably due to inheritance or U-Th excess (Figure 29).

Zircon crystals extracted from the para-derived gneiss sample WT7-21B are yellowish, prismatic and elongated (3:1; Z35, Z49 and Z50 in Figure 30) or prismatic and short (2:1 or 1.5:1; Z4, Z9 and Z21 in Figure 30). Concentric oscillatory zoning was probably acquired during magmatic crystallization.

The analyses were carried out preferably at the cores of 56 zircon grains and are represented in the frequency histogram of Figure 31. The Pb^{206}/Pb^{207} ratios point to Paleoproterozoic ages typical of the 2.15 Ga-old Central Ceará Domain basement.

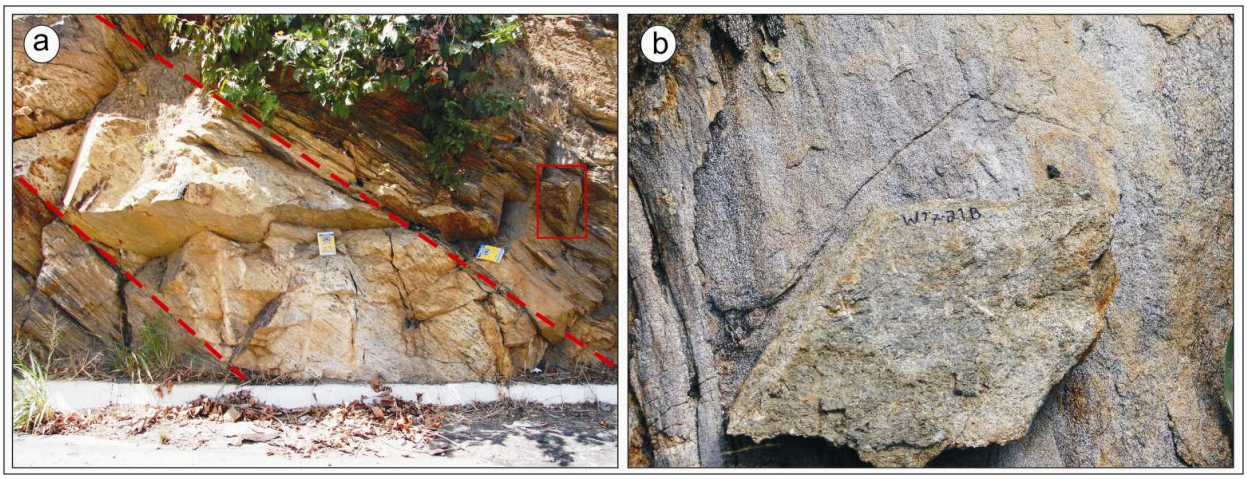

Figure 28: Outcrop along Highway BR-222, where samples WT7-21A (leucogranite) and WT7-21B (sillimanite-garnet-biotite gneiss) were collected. a) Outcrop dipping SE at low-angles (~35°), showing a leucogranite injection (garnet, quartz, feldspar), sampled for monazite dating; b) sillimanite-garnet-biotite gneiss sampled for zircon dating.

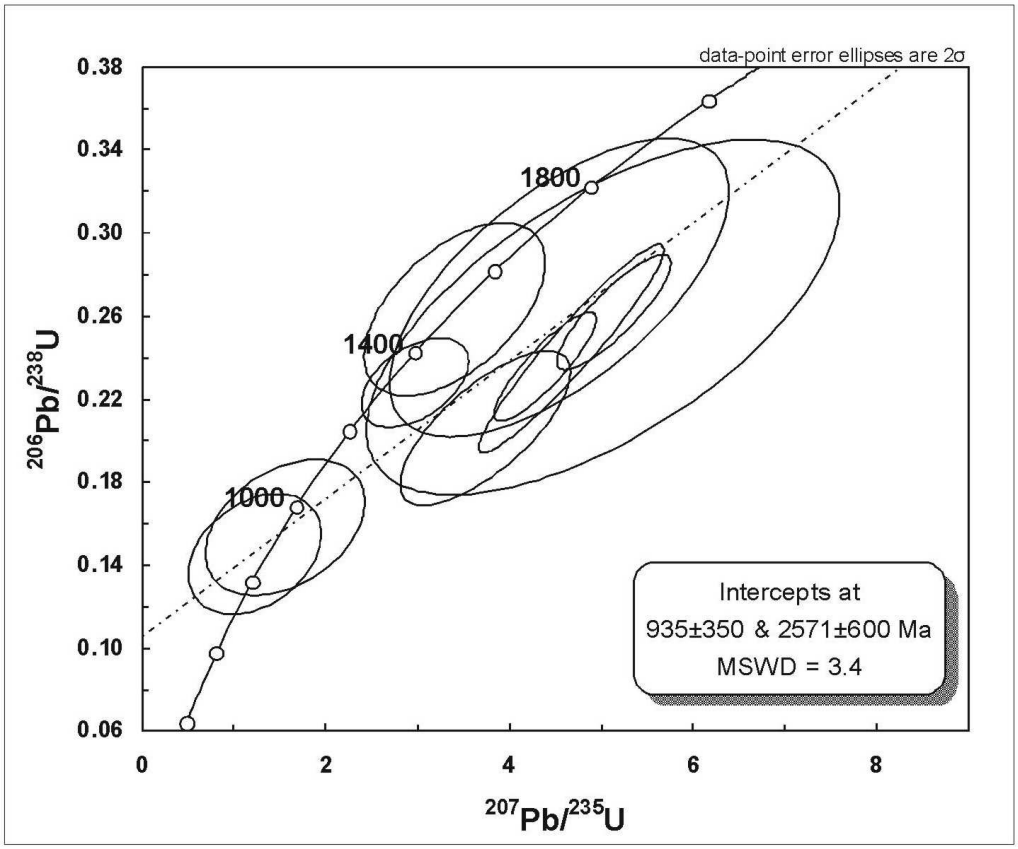

Figure 29: Concordia diagram for U/Pb analyses of monazite from leucogranite sample WT7-21A.

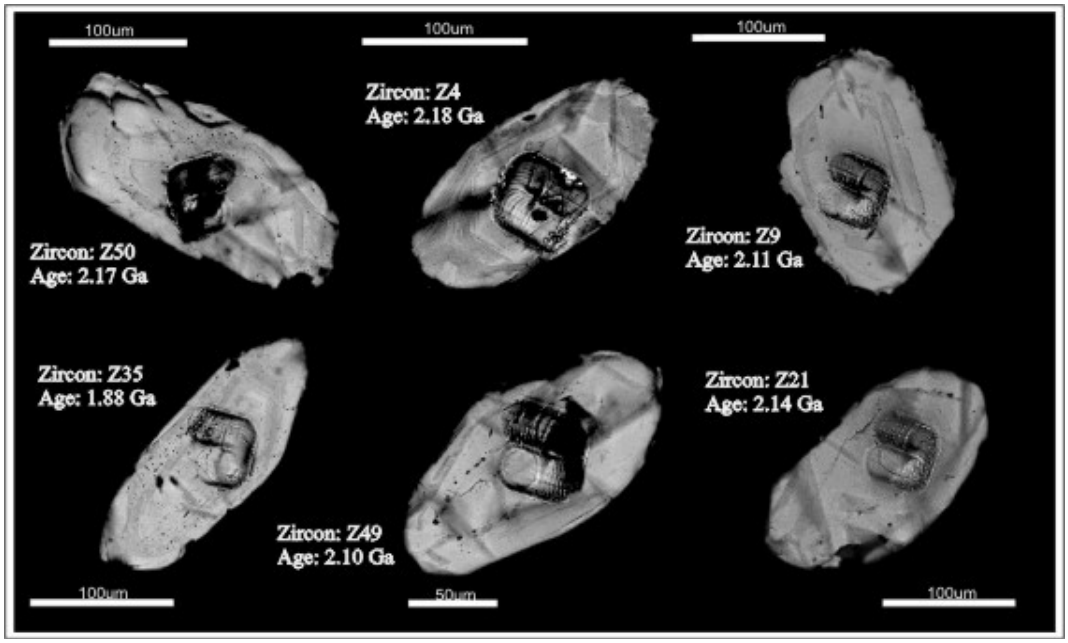

Figure 30: Back-scattered electron images of representative zircon crystals from the sillimanite-garnet-biotite gneiss (sample WT7-21B). Inset: regions analyzed by the U-Pb method (raster) with the corresponding $^{235}U/^{207}Pb$ ages.

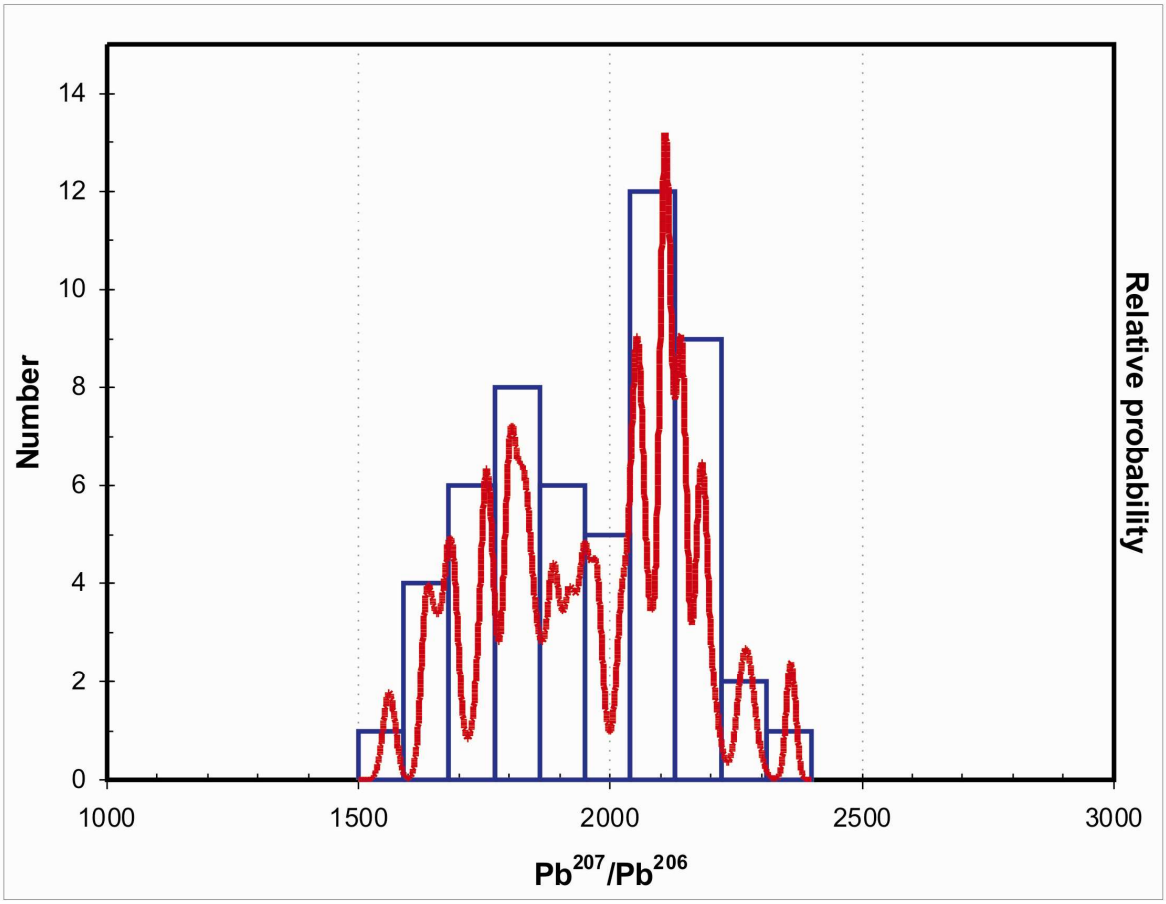

Figure 31: Frequency histogram for the U/Pb analyses of zircon from the sillimanite-garnet-biotite-gneiss sample WT7-21B.

6.3. Calc-silicate rock

Lenses of calc-silicate rocks occur associated with retrogressed eclogites from the Forquilha Belt southern sector (Figure 2). The outcrops are varied in size, exceeding 50 m x 30 m. The calc-silicate rocks are olive green and medium- to coarse-grained (Figure 32). In hand specimen it is possible to individualize biotite (30%), amphibole (15%), pyroxene (25%), plagioclase (15%), quartz (10%) and garnet (5%). These rocks are imbricated with aluminous paragneisses dipping 30° E-SE and characterized by a downdip biotite lineation.

Fifty-one grains that compose two zircon families extracted from a calc-silicate rock sample (TJF4-7) collected in the Fazenda Cabeça de Touro (**373072/9576482**) were analyzed. In one family the grains are yellowish, sub-rounded to rounded (2:1) (Z24, Z47 and Z56 in Figure 33) or prismatic (3:1) (Z41 and Z53 in Figure 33), and show oscillatory zoning. Metamictization is

evidenced by the presence of fractures at crystal rims (Z43, Z 53 and Z56). The explanation for this is given by Corfu *et al*. (2003): provided that the zircon core is richer in U than the rim, the expansion of the core during metamictization will cause fracturing of the more rigid rim. The crystals of the other family are transparent and either rounded (1:1) (Z2 and Z3 in Figure 33) or elongated, with sub-rounded to rounded terminations (Z15 and Z33 Figure 33) (3:1). Neither internal structures nor metamictization are recognized in the back-scattered electron images.

Figure 32: Outcrop of calc-silicate rock, easily recognized by its typical greenish color and karst-like alteration surface. Inset: block sampled for geochronologic studies.

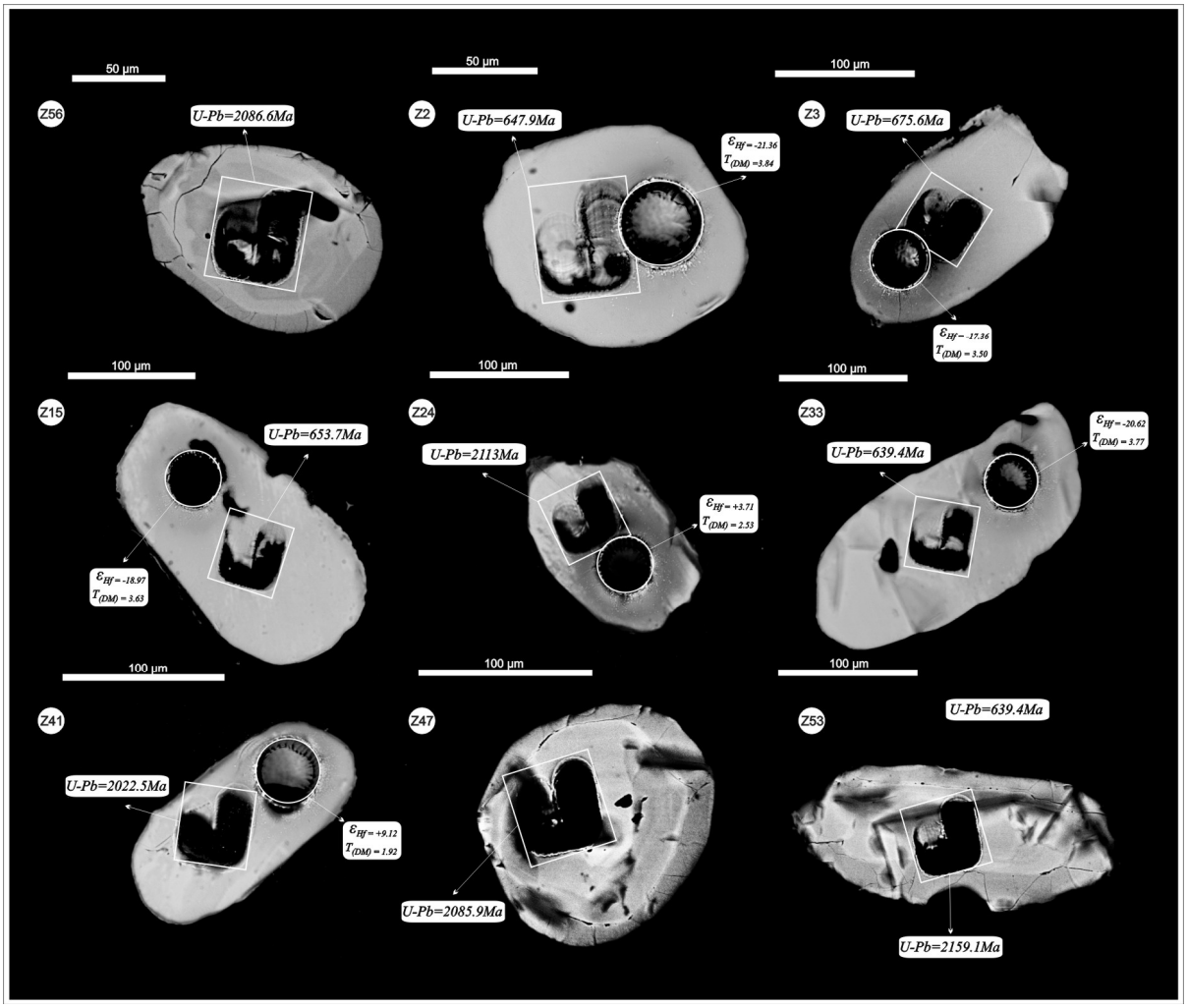

Figure 33: Back-scattered electron images of representative zircon crystals from sample TJF4-7. Circles and rectangles analyzed spot by the U/Pb (raster) and Lu/Hf (spot size = 30 µm) methods with corresponding $^{235}U/^{207}Pb$, T_{DMHf} and ε_{Hf} values.

The data obtained at the cores of the 51 zircon grains are represented in a frequency histogram, which confirms the presence of at least two populations: one in the 640 and 700 Ma interval and the other in the 2000 and 2250 Ma interval (Figure 34). The crystals showing ~100% concordance yielded an age of 650.3 ± 2.5 Ma (Figure 35).

Model ages obtained by the Lu-Hf method applied to the same grains analyzed by the U-Pb method are ~ 650 Ma for concordant zircon grains and ~ 2100 Ma for the Paleoproterozoic grains. The former yielded T_{DM} values between 2.44 and 2.62 with negative ε_{Hf} values (t=650 Ma) varying between –1.91 and –21.36, whereas the latter yielded T_{DM} between 1.92 and 2.45 Ga with positive ε_{Hf} values (t=2100 Ma) varying between +1.39 and +10.88 (Figure 36).

The age of 650.3 ± 2.5 Ma was obtained for sub-euhedral zircon grains that preserved a magmatic inheritance characterized by the prismatic shape. However, back-scattered electron images revealed neither oscillatory zoning nor internal structures. The grains are homogeneous, with no evidence of metamictization. The Lu-Hf data obtained for these Neoproterozoic zircon crystals indicate a Paleoproterozoic mantle derivation (~2.44 Ga) and highly negative epsilon Hf values when calculated to 650 Ma. Therefore it is evident that the zircon crystals that yielded these ages were re-equilibrated during a still not well defined Neoproterozoic metamorphic event. Anyway, this age is the oldest obtained for the Central Ceará Domain metamorphism.

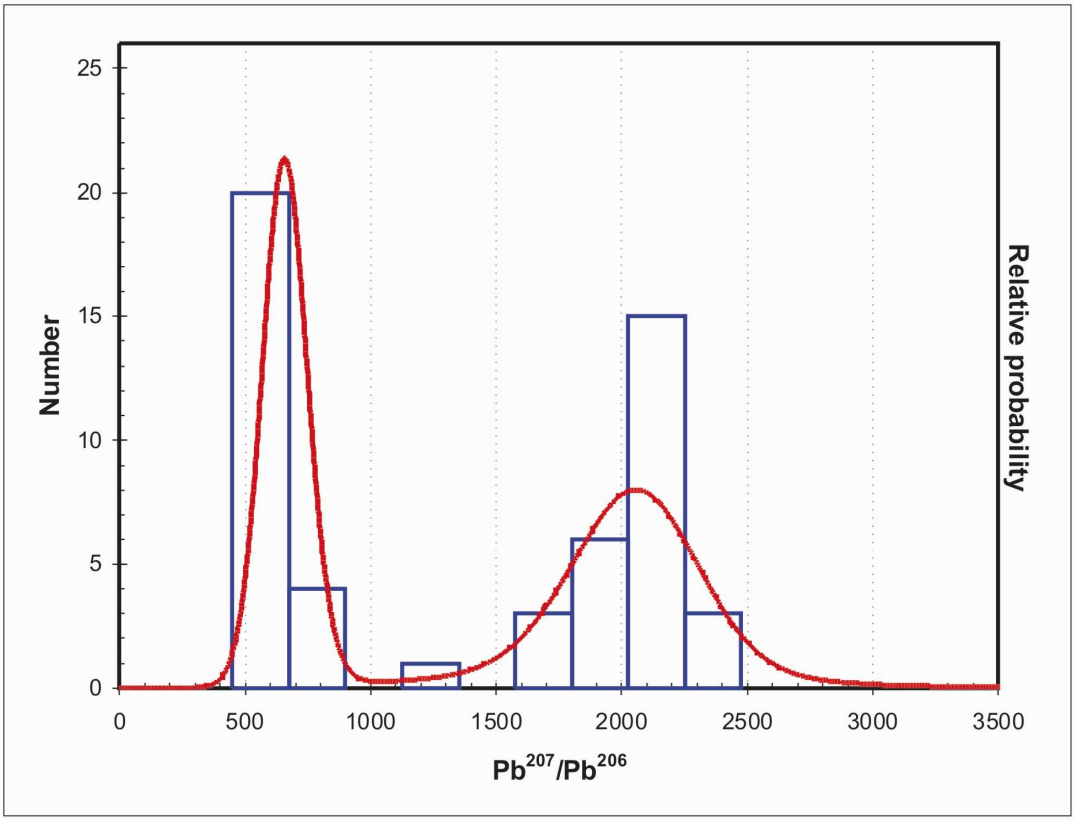

Figure 34: Frequency histogram for U/Pb analyses of sample TJF4-7 zircon.

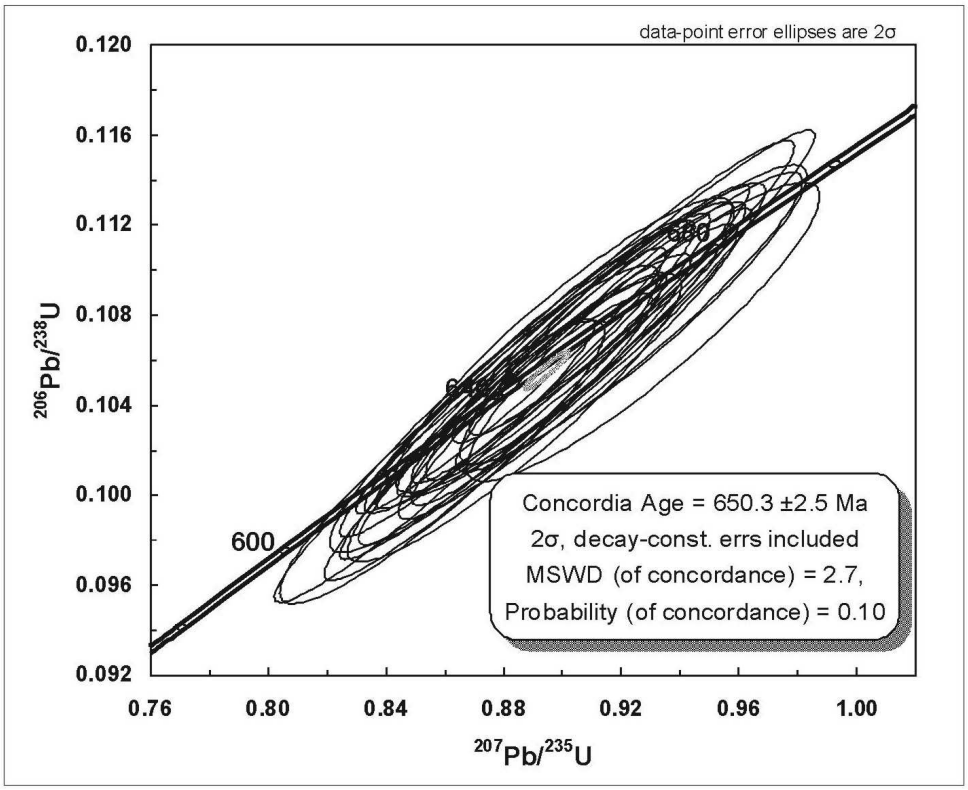

Figure 35: Concordia diagram age for U/Pb analyses (LA-ICPMS) of sample TJF4-7.

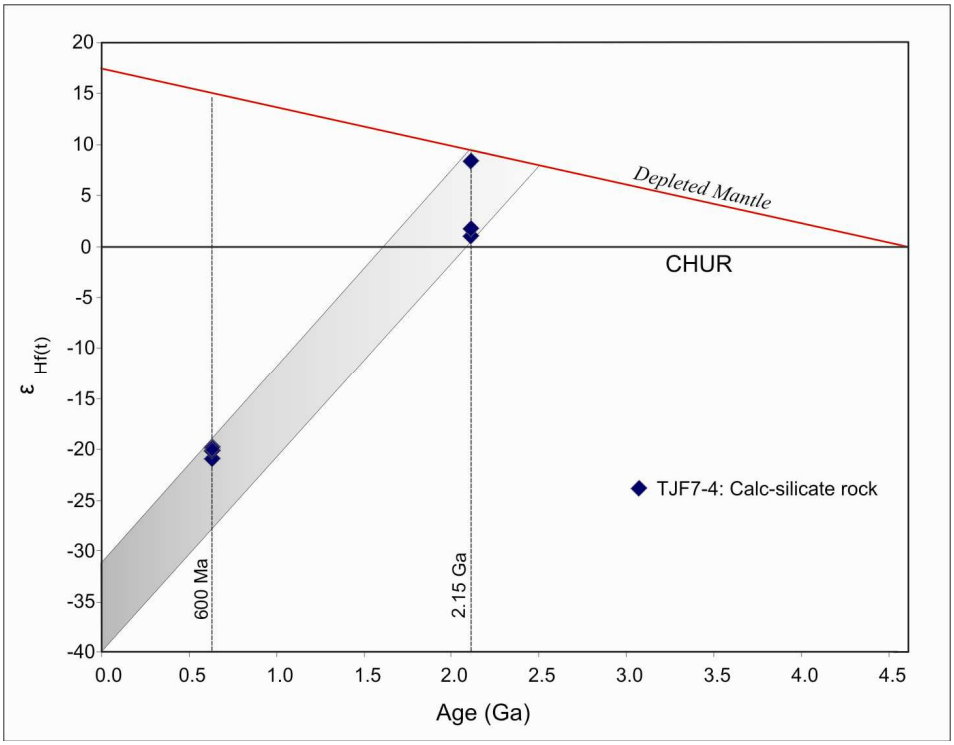

Figure 36: Evolution diagram showing ε_{Hf} values calculated to 2150 and 600 Ma.

7. WHOLE-ROCK Sm-Nd RESULTS

Eighteen samples were analyzed by the whole-rock Sm-Nd method. Four represent garnet amphibolites, 13 clinopyroxene-garnet amphibolites and one, a calc-silicate rock. All samples were collected along the Forquilha Eclogite Zone. The results are summarized in Table 1, and Figure 37.

Table 1: Sm-Nd data obtained for the Forquilha Eclogite Zone rocks.

Samples	Rock	Sm (ppm)	Nd (ppm)	$^{147}Sm/^{144}Nd$	$^{143}Nd/^{144}Nd$ ($\pm 1\sigma$)	$\varepsilon_{Nd}(o)$	T_{DM} (Ga)
VC-54 A	Garnet amphibolite	1.58	6.28	0.1858	0.512634+/-18	-0.07	-
VC-57 E	Garnet amphibolite	0.751	2.383	0.1759	0.512565+/-6	-1.42	1.9
VC-57 F	Garnet amphibolite	3.44	11.17	0.1904	0.512707+/-14	1.34	-
TJF5-181	Garnet amphibolite	3.68	11.97	0.1864	0.512259+/-9	-7.40	-
WT8-53E	Cpx-garnet amphibolite	2.975	9.710	0.1852	0.512141+/-20	-9.69	-
WT7-53D	Cpx-garnet amphibolite	2.480	7.513	0.1995	0.512761+/-15	2.40	-
WT7-25	Cpx-garnet amphibolite	3.150	10.443	0.1823	0.512621+/-19	-0.33	-
WT8-10F	Cpx-garnet amphibolite	1.877	5.948	0.1908	0.512080+/-60	-10.88	-
WT8-10C	Cpx-garnet amphibolite	4.307	14.789	0.1760	0.512647+/-23	0.17	1.57
WT8-10E	Cpx-garnet amphibolite	3.747	12.805	0.1769	0.512575+/-23	-1.24	1.91
WT8 12A	Cpx-garnet amphibolite	8.390	30.610	0.1657	0.512530+/-12	-2.10	1.60
WT8 12C	Cpx-garnet amphibolite	3.266	10.853	0.1819	0.512685+/-8	0.91	-
WT8 12E	Cpx-garnet amphibolite	3.009	9.574	0.1900	0.512743+/-14	2.04	-
TJF6 335C	Cpx-garnet amphibolite	10.144	46.330	0.1324	0.511547+/-44	-21.29	2.81
TJF6 335A	Cpx-garnet amphibolite	8.420	41.770	0.1219	0.511957+/-11	-13.28	1.79
TJF6 335D	Cpx-garnet amphibolite	7.560	33.719	0.1355	0.511870+/-16	-14.99	2.28
WT8 10B	Cpx-garnet amphibolite	6.416	23.913	0.1622	0.512388+/-18	-4.89	1.92
TJF4-7	Calc-silicate rock	6.522	37.553	0.1050	0.511439+/-14	-23.39	2.24

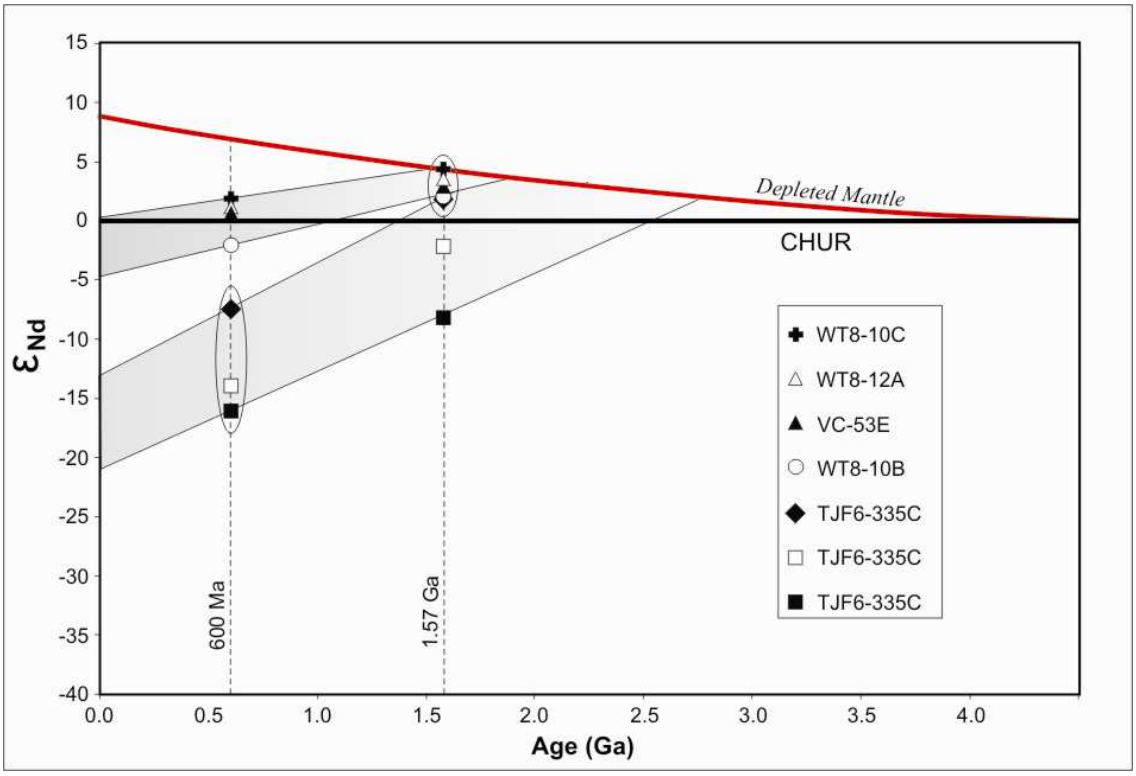

Figure 37: T_{DM} *versus* ε_{Nd} diagram representing the isotopic evolution fields for the Forquilha Eclogite Zone metamafic rocks.

8. DISCUSSION AND CONCLUSION

The U-Pb, Lu-Hf and Sm-Nd isotopic data obtained for the Forquilha Eclogite Zone help to individualize at least two important events that are still scarcely studied in the Central Ceará Domain: a Mesoproterozoic event, constituting the crystallization of the metamafic rocks, and a Neoproterozoic event, which correlates with the high-grade metamorphism recorded in zircon from metasedimentary sequences. The U-Pb and Lu-Hf results are summarized in Table 2.

Considering the group of ages obtained, five intervals are individualized:

2200 – 2000 Ma: Represents the main zircon source for the para-derived sequences that occur along the Forquilha Eclogite Belt (WT8-53 MM, WT8-53 ML, WT7-21B, TJF4-7). This Rhyacian/Orosirian interval is well-known throughout the Central Ceará Domain and represents the formation of the Paleoproterozoic basement in this domain, which is mostly juvenile but records the presence of reworked Archean rocks (Fetter *et al.,* 2000; Castro, 2004; Arthaud, 2008; Martins *et al.,* 2009). The zircon crystals of this time interval are very similar: light yellow with partially prismatic faces and sub-rounded terminations, and show oscillatory zoning probably acquired during magmatic crystallization. Tonalitic orthogneisses that occur between the Santa Quitéria Magmatic Arc (SQMA) and the Transbrasiliano Lineament yield U-Pb crystallization ages of 2.11 Ga (Fetter *et al.,* 2000). These rocks can represent basement slices, a continental lithosphere in which SQMA was installed and later incorporated during collision.

1620 – 1510 Ma: Geochronologic and paleomagnetic data support the hypothesis of the existence of the supercontinent Columbia in the Paleo-Mesoproterozoic (1.9-1.6 Ga) (Rogers and Santosh, 2002). Its fragmentation started *ca.* 1.6 Ga ago, with rifting followed by dike swarms in northern China, Zimbabwe, South Africa, Australia and North America (Rogers and Santosh, 2002; Zhao *et al.,* 2004, Ernst *et al.,* 2008; Rogers and Santosh, 2009). In Brazil, in the southern Amazonian Craton, several anorogenic pulses and supracrustal mafic rock sequences with ages around 1.5 Ga are found in the Rio Negro-Juruena and Rondoniana-San Ignácio belts (Bettencourt *et al.* 1999; Matos *et al.,* 2004; Ruiz *et al.* 2004, Santos *et al.* 2008). In the Central Ceará Domain, the late Paleoproterozoic rocks of ages around 1.8 Ga are related to the Orós Belt bimodal volcanism (Sá *et al.*, 1995) and to metarhyolites of the Bixopá and Itaiçaba region (Cavalcante, 1999). Zircon from the Ceará Group metasedimentary sequences outcropping in the Itatira region were dated by Arthaud (2008), who obtained ages around 1.56 Ga. This author

indicates the Paraíba Transversal Zone as the source area, composed of the Rio Carpina Terrane gabbro-anorthositic and granitic suite with ages between 1.7 and 1.6 Ga, and the Serra de Taquaritinga anorogenic granites of 1.52 Ga of age (Sá *et al.* 1997; Santos *et al.* 2009). Recently, Silva Filho *et al.* (2009) dated zircon populations from the Águas Belas Batholith and Canindé syenogranites of the Pernambuco-Alagoas Domain using SHRIMP. The ages obtained for one population fall in the 1.57-1.67 Ga interval, interpreted as probable enheritance.

Neves (2009) and Neves *et al*. (2009) believe that Mesoproterozoic zircon from the Borborema Province metasedimentary rocks require distal sources, once derivation from relatively proximal sources include zircon populations of ages between 2.2 and 2.0 Ga and 1.2 and 0.9 Ga. These authors suggest a geographic continuity between the Amazonian Craton and the Borborema Province during the formation of the basins where the precursor sediments of the metasedimentary sequences were deposited. Thus the provenance of the Mesoproterozoic zircon grains in the Borborema Province should be related to the Sunsás, Maroni-Itacaiúnas, Tapajós and Rio Negro-Juruena provinces.

In the African counterpart, detrital zircon of ages around 1.5 Ga occur in the Volta River basin, in Ghana (Kalsbeek *et al.* 2008). The source for these crystals is also related to the Amazonian Craton rocks. Deposition took place during the assembly of Rodinia, when the Amazonian and the Western African cratons were put together.

Regarding the Forquilha high-pressure belt, five metamafic rocks yielded zircon populations of ages between 1.5 and 1.6 Ga. The zircon crystals of samples WT7-25 and WT8-12F, collected in the northern sector of the study area, are more irregular than those from the central portion of the belt, which are elongated and contain preserved prismatic faces. These crystals do not record intense metamictization, once the isotopic ratios show good concordance (~98-99%), indicating that the ages obtained for these crystals correspond to crystallization ages. Additionally, model ages obtained by the Lu-Hf method for zircon from clinopyroxene-garnet amphibolite sample WT7-25 yielded $T_{DM(Hf)}$ between 1570 and 1810 Ma, with positive ε_{Hf} values (t=1566 Ma) varying between +7.46 and +9.63. This suggests a juvenile mantle derivation for the zircon crystals of this sample. The other metamafic rocks of the eclogite belt yielded crystallization ages around 1.5 Ga, except for the retrogressed eclogite (TJF6-302) of the southern sector, which yielded an imprecise Mesoproterozoic age. The clinopyroxene-garnet

amphibolite (TJF6-335) of the same sector yielded a concordant age around 615 Ma, which is related to a metamorphic event.

Whole-rock Sm-Nd analyses were carried out in order to attest to the timing of mantle extraction. Even if several samples did not yield satisfactory results due to partial fractionation, $T_{DM(Nd)}$ values between 1.57 and 1.60 Ga and positive ε_{Nd} values (t=1566 Ma) varying between +4.08 and +4.11 were obtained. These values are coherent with the results obtained by the U-Pb and Lu-Hf methods, confirming the existence of metamafic rocks with Mesoproterozoic crystallization ages and juvenile mantle derivation in the Central Ceará Domain.

Geochemical data (Amaral et al., 2010) summarized in Table 2 show that these rocks record an oceanic crust signature and were generated in N- and T-MORB-type extensional settings, which is in accord with the Hf and Nd isotopic signatures.

The data presented here, integrated with those obtained with the application of other analytical methods, attest to the existence of extensional settings in the Borborema Province, with the generation of magmatic rocks in the beginning of the Mesoproterozoic (*ca.* 1.6 Ga).

650 – 630 Ma: U-Pb determinations using zircon extracted from two para-derived rocks – a sillimanite gneiss (WT8-53ML) and a calc-silicate rock (TJF4-7) – resulted in concordant ages, respectively 639 ± 10 Ma and 650 ± 2.5 Ma. The crystals that yielded these ages underwent metamorphism. Zircon grains from the sillimanite gneiss present an igneous core and a well-defined overgrown rim. Two well-defined zircon populations were extracted from the calc-silicate rock, one yielding ages of *ca.* 2.1 Ga and the other of *ca.* 0.65 Ga. Model ages obtained by the Lu-Hf method and carried out in the same crystals analyzed by the U-Pb method were calculated for the Neoproterozoic (*ca.* 650 Ma) and Paleoproterozoic concordant zircons. For the former T_{DM} between 2.44 and 2.62 Ga and negative ε_{Hf} values (t=650 Ma) varying between –17.91 and –21.36 were obtained. The Paleoproterozoic zircon grains define T_{DM} values between 1.92 and 2.45 Ga and positive ε_{Hf} values (t=2100 Ma), varying between +1.39 and +10.88. Hf isotopic compositions are approximately the same of the parental magma from which zircon crystallized, as indicated by high Hf concentrations in this mineral (Blichert-Toft *et al.,* 1997; Andersen *et al.,* 2002; Griffin *et al.,* 2002). Secondary magmatic processes or high-grade metamorphism are unable to reset Hf isotopic compositions. Therefore, the mantle extraction values (T_{DM}) are close or coincide with the timing of zircon crystallization. Thus, positive ε_{Hf}

values calculated for time (t) indicate mantle derivation, whereas negative values suggest crustal derivation for zircon (Amelin *et al.,* 1999).

From the U-Pb analyses of the Santa Quitéria magmatic arc granitoids, Fetter *et al.* (2003) defined the interval between 640 and 620 Ma as the beginning of subduction with polarity to SE. On the other hand, based on conventional U-Pb and U-Th-Pb determinations using monazite and zircon extracted from retrogressed para-derived eclogites of Madalena and Itataia (Ceará), Castro (2004), defined the interval between *ca.* 640-630 Ma as the period of subduction and metamorphism up to the eclogite facies, recorded both in the para-derived sequences and in the oldest granitoids of the Santa Quitéria magmatic arc.

The ages that fall in the 650-630 Ma interval constitute the oldest metamorphic record in the Central Ceará Domain. In the African counterpart, in the Hoggar Province, zircon U-Pb ages obtained for calc-alkaline batholiths of the Iskel magmatic arc suggest that subduction should have started *ca.* 680 Ma ago (Caby, 2003). In the Dahomeyides belt, the Lato Hills eclogites were metamorphosed between 650 and 595 Ma (Bernard-Griffiths *et al.,* 1991).

~620 – 600 Ma: Age interval recorded in slightly rounded, clean zircon grains less than 100 μm in size. Zircon crystals extracted from samples WT7-3A and TJF6-335 are typical of high-temperature granulitic rocks (Corfu *et al.,* 2003). The ages of 612.9 ± 3.3 Ma and 614 ± 3.9 Ma, obtained respectively for concordant zircons from retrogressed eclogites of the Forquilha high-pressure belt southern sector and from mafic granulites of the Cariré region, are interpreted as the medium/high grade metamorphic record (upper amphibolite/granulite facies), mainly characterized in the metamafic rocks.

Several U-Pb analyses of zircon and monazite from deformed igneous rocks of the northwestern portion of the Central Ceará Domain indicate that tangential collision took place after 620 Ma, and the transition to transcurrent tectonics occurred between 614 and 591 Ma. During the transcurrent tectonic regime, several granite plutons were emplaced in transtractive belts (Fetter, 1999). Mica and amphibole cooling ages ($^{40}Ar/^{39}Ar$) obtained by Monié *et al.* (1997) suggest that the transcurrent movements should have continued up to 540 Ma.

~600 – 560 Ma: A still imprecise interval defined by zircon and monazite dating and lower intercepts in concordia diagrams. However, several authors attribute this period to the activity of major shear zones in the Central Ceará and Médio Coreaú domains (Monié *et al.* 1997; Fetter, 1999; Fetter *et al.,* 2003).

Monazite crystals extracted from sample WT8-53ML leucosome yielded an age of 563 ± 96 Ma. Despite the relatively high analytical error, this age was the youngest obtained for the rocks of the Forquilha high-pressure belt.

In the Cariré region, rounded concordant zircon extracted from high-pressure mafic granulites and the rims of zircon grains from a host granodiorite from the same region yielded ages of 589 ± 8.9 Ma and 587 ± 31 Ma respectively. These data are interpreted as the record of the high-grade metamorphism in this region. Nogueira Neto *et al.* (1997) obtained for titanites from the Cariré mafic granulites an age of 563 Ma, which is interpreted as that of the amphibolite-facies metamorphic event associated with the development of a fault system that composes the Transbrasiliano Lineament.

ACKNOWLEDGMENTS

The authors are grateful to CNPq (*Conselho Nacional de Desenvolvimento Científico e Tecnológico*) for the Ph.D. Scholarship granted to the first author, to FAPESP (*Fundação de Amparo a Pesquisa do Estado de São Paulo*, grants 03/07663-3 and 07/58535-6) for laboratory work support, and CNPq/MCT (Millenium Project 42.0222/2005-7) and INCTET for field work support.

Table 2: Summary of U-Pb and Lu-Hf ages for the Forquilha high-pressure belt.

Amostra	*Método*	*Mineral*	*Interceptos*		*Idades*	*Idades*	*Idades de*	*Idades Lu-Hf*		
			Superior	*Inferior*	*Concordantes*	*Monazitas*	*Proveniência*	T_{DM}	$\varepsilon_{Hf}(t_1)$	$\varepsilon_{Hf}(t_2)$
Rochas Metamáficas										
WT7-25	U-Pb / Lu-Hf	Zr	1566 ± 8,8	618 ± 32	-	-	-	~1,57 Ga	+7,46 /+9,63	-
WT8-12F	U-Pb	Zr	1546 ± 37	725 ± 36	-	-	-	-	-	-
WT8-53E	U-Pb	Zr	1559 ± 70	605 ± 640	-	-	-	-	-	-
WT8-53X	U-Pb	Zr	1618 ± 40	604 ± 110	1510 ± 77	-	-	-	-	-
TJF6-302	U-Pb	Zr	1455 ± 120	552 ± 190	-	-	-	-	-	-
TJF6-335	U-Pb	Zr	-	-	614,9 ± 3,9	-	-	-	-	-
Rochas Metassedimentares										
WT8-53MM	U-Pb	Zr	-	-	-	-	~2,1 Ga	-	-	-
WT8-53ML	U-Pb	Zr e Mz	-	-	639 ± 10	563 ± 96	~2,1 Ga	-	-	-
WT7-21B	U-Pb	Zr	-	-	-	-	~2,1 Ga	-	-	-
TJF4-7	U-Pb / Lu-Hf	Zr	-	-	650 ± 2,5	-	~2,1 e 0,65 Ga	~2,44 Ga	- 17,91/ - 21,36	+1,39/+10,88

Zr: Zircon; Mz: Monazite

9. REFERENCES

Affaton, P., Kröner, A., Seddoh, K.F. 2000. Pan-African granulite formation in the Kabye Massif of northern Togo (West Africa): Pb–Pb zircon ages. *International Journal of Earth Sciences,* **88:** 778-790.

Albarede, F., Telouk, S., Blichert-Toft, J., Boyet, M., Agranier A., Nelson, B.2004. Precise and accurate isotopic measurements using multiple-collector ICPMS, *Geochimica and Cosmochimica Acta,* **68:** 2725-2744.

Almeida, F.F.M., Hasui, Y., Brito Neves, B.B., Fuck, R.A. 1981. Brazilian Structural Provinces: an introduction. *Earth Sciences Reviews,* 17**:** 1-29.

Amaral, W.S., Santos, T. J. S., Wernick, E. 2010. Occurrence and geochemistry of metamafic rocks from the Forquilha Eclogite Zone, central Ceará NE Brazil: Geodynamic implications. *Geological Journal* (DOI: 10.1002/gj.1224).

Amelin, Y., Lee, D.C., Halliday, A.N., Pidgeon, R.T. 1999. Nature of the Earth's earliest crust from hafnium isotopes in single detrital zircons. *Nature,* **399:** 252-255.

Andersen, T., Griffin, W.L., Pearson, N.J. 2002. Crustal evolution in the SW part of the Baltic Shield: the Hf isotope evidence. *Journal of Petrology,* **43:** 1725-1747.

Arthaud, M.H. 2008. Evolução neoproterozóica do Grupo Ceará (Domínio Ceará Central, NE Brasil): da sedimentação à colisão continental brasiliana. Ph.D Thesis, Instituto de Geociências, Universidade de Brasília, Brasil.

Attoh, K., Hawkins, D., Bowring, S.A., Allen, B., 1991. U–Pb zircon ages of gneisses from Pan-African Dahomeyide orogen, West Africa. *EOS Transactions American Geophysical Union,* **72:** 299.

Bernard-Griffiths, J., Peucat, J.J., Ménot, R.P. 1991. Isotopic (Rb-Sr, U/Pb and Sm/Nd) and trace element geochemistry of eclogites from the Pan-African belt: a case study of REE fractionation during high-grade metamorphism. *Lithos,* **27**: 43-57.

Bettencourt, J.S., Tosdal R.M., Leite Jr, W.R., Payolla, B.L. 1999. Mesoproterozoic rapakivi granites of Rondônia Tin Province, southwestern border of Amazonian craton, Brazil-I: Reconnaissance U-Pb geochronology and regional implications. *Precambrian Research,* **95:** 41-67.

Bispo-Santos, F., D'Agrella-Filho, M.S., Pacca, I.I.G., Janikian, L., Trindade, R.I.F., Elming, S., Silva, J.A., Barros, M.A.S., Pinho, F.E.C. 2008. Columbia revisited: Paleomagnetic results from the 1790 Ma colider volcanics (SW Amazonian Craton, Brazil). *Precambrian Research* **164**: 40-49.

Black, R., Lameyre, J., Bonin, B. 1985. The structural setting of alkaline complexes. *Journal of African Earth Science,* **3:** 5-16.

Blichert-Toft, J., Frey, F.A., Albarede, F., 1999. Hf isotope evidence for pelagic sediments in the source of Hawaiian basalts. *Science,* **285:** 879-882.

Brito Neves, B.B., Santos, E.J., Van Schmus, W.R. 2000. Tectonic history of the Borborema Province, northeastern Brazil. In: *Tectonic Evolution of South America, 31st International Geological Congress,* Cordani, U., Milani, E.J., Thomaz Filho, A., Campos, D.A. (eds). Rio de Janeiro, Brazil, 151-182.

Buhn, B., Pimentel, M.M., Matteini, M, Dantas, E. 2009. High spatial resolution analysis of Pb and U isotopes for geochronology by *laser ablation* multi-collector inductively coupled plasma mass spectrometry (LA-MC-ICP-MS), *Annals of the Brazilian Academy of Sciences,* **81:** 99-114.

Caby, R. 1989. Precambrian terranes of Benin Nigeria and Northeast Brazil and the Late Proterozoic South Atlantic. *Geological Society of America*, Special Papers, **230:** 145-158.

Caby, R. 2003. Terrane assembly and geodynamic evolution of centralwestern Hoggar: a synthesis. Journal of African Earth Sciences, **37:** 133-159.

Castro, N.A. 2004. *Evolução geológica proterozóica da região entre Madalena e Taperuaba, domínio tectônico Ceará Central (Província Borborema).* Ph.D Thesis, Universidade de São Paulo-USP.

Cavalcante, J.C. 1999. Limites e evolução geodinâmica do Sistema Jaguaribeano, Província Borborema, Nordeste do Brasil. Dissertação de Mestrado, Universidade Federal do rio Grande do Norte.

Chauvel, C., Blichert-Toft, J.E. 2001. A hafnium isotope and trace element perspective on melting of the depleted mantle, *Earth and Planetary Science Letters,* **190**: 137-151.

Condie, K. C., 2000. Episodic continental growth models: afterthoughts and extensions. *Tectonophysics,* **322:** 153-162.

Condie, K. C., 2002. Breakup of a Paleoproterozoic supercontinent. *Gondwana Research*, **5:** 41-43.

Cordani, U.G., Brito-Neves, B.B., D, Agrella-Filho, M.S., 2003. From Rodinia to Gondwana: a review of the available evidence from South America. *Gondwana Research*, **6:** 275–284.

Corfu, F., Hanchar, J. M., Hoskin, P. W. O., Kinny, P. D. 2003. An atlas of zircon textures. *In Zircon.* (eds. J. M. Hanchar and P. W. O. Hoskin) In: *Reviews of Mineralogy and Geochemistry* **53,** Mineralogical Society of America, Washington, D.C. 469-500.

Dantas, E.L., Van Schmus, W.R., Hackspacher, P.C, Fetter, A.H., Brito Neves, B.B., Cordani, U., Nutman, A.P., Williams, I.S. 2004. The 3.4-3.5 Ga São José do Campestre massif, NE Brazil: remnants of the oldest crust in South America. *Precambrian Research,* **130:** 113-137.

DePaolo, D.J. 1988. *Neodymium Isotope Geochemistry*. Springer-Verlag, Berlin, 181p.

Ernst R.E., Wingate M.T.D., Buchan K.L., Li Z.X. 2008. Global record of 1600–700 Ma Large Igneous Provinces (LIPs): Implications for the reconstruction of the proposed Nuna (Columbia) and Rodinia supercontinents. *Precambrian Research*, **160**: 159-178.

Fetter, A.H. 1999. U–Pb and Sm–Nd Geochronological constraints on the crustal framework and geological history of Ceará State, NW Borborema Province, NE Brazil: implications for the assembly of Gondwana*. PhD. Thesis*, Kansas University.

Fetter, A,H,, Van Schmus, W.R., Santos, T.J.S., Arthaud, M.H., Nogueira, Neto J.A. 2000. U–Pb and Sm–Nd geochronological constraints on the crustal evolution and basement architecture of Ceará State, NW Borborema Province, NE Brazil: implications for the existence of the Paleoproterozoic supercontinent "Atlantica". *Revista Brasileira de Geociências,* **30:** 102-106.

Fetter, A.H., Santos, T.J.S., Van Schmus, W.R., Hackspacher, P.C., Brito Neves, B.B., Arthaud, M.H., Nogueira Neto, J.A., Wernick, E. 2003. Evidence for Neoproterozoic continental arc magmatism in the Santa Quitéria batholith of Ceará State, NW Borborema Province, NE Brazil: implications for assembly of West Gondwana. *Gondwana Research,* **6:** 265-273.

Fuck, R.A., Brito Neves, B.B., Schobbenhaus, C. 2008. Rodinia descendants in South America. *Precambrian Research*, **160:** 108-126.

Griffin, W.L., Wang, X., Jackson, S.E., Pearson, N.J., O'Reilly, S.Y., Zhou, X. 2002. Zircon chemistry and magma genesis, SE China: in situ analysis of Hf isotopes, Pingtan and Tonglu igneous complexes. *Lithos,* **61:** 237-269.

Jackson, S.E., Pearson, N.J., Griffin, W.L., Belousova, E.A. 2004. The application of laser ablation-inductively coupled plasma-mass spectrometry to *in situ* U–Pb zircon geochronology. *Chemical Geology*, **211:** 47-69.

Kalsbeek, F., Frei, D., Affaton, P. 2008. Constraints on provenance, stratigraphic correlation and structural context of the Volta basin, Ghana, from detrital zircon geochronology: An Amazonian connection? *Sedimentary Geology*, **212:** 86-95.

Ludwig, K.R. 2003. User's Manual for Isoplot/Ex v. 3.00. A Geochronological Toolkit for Microsoft Excel. BGC Special Publication 4, Berkeley, 71 p.

Martins, G., Oliveira, E.P., Lafon, J.M. 2009. The Algodões amphibolite–tonalite gneiss sequence, Borborema Province, NE Brazil: geochemical and geochronological evidence for Palaeoproterozoic accretion of oceanic plateau/back-arc basalts and adakitic plutons. *Gondwana Research,* **15:** 71-85.

Matos, J.B., Schorscher, J.H.D., Geraldes, M.C., Souza, M.Z.A., Ruiz, A.S. 2004. Petrografia, geoquímica e geocronologia das rochas do orógeno Rio Alegre, Mato Grosso: um registro de crosta oceânica Mesoproterozóica no SW do Craton Amazônico. *Geologia USP (Revista do Instituto de Geociências-USP).* Série Científica. **4:** 75-90.

Matteini, M., Dantas, E. L., Pimentel, M. M., Buhn, B. 2010. Combined U-Pb and Lu-Hf isotope analyses by laser ablation MC-ICP-MS: methodology and applications. *Anais da Academia Brasileira de Ciências,* **82 (2):** 479-491.

Monié, P., Caby, R., Arthaud, M.H. 1997. The Neoproterozoic Brasiliano Orogeny in Northeast Brazil: $^{40}Ar/^{39}Ar$ and petrostructural data from Ceará, *Precambrian Research,* **81:** 241-264.

Morel, M.L.A., Nebel, O., Nebel-Jacobsen, Y.L., Miller J.S., Vroon, P.Z. 2008. Hafnium isotope characterization of the GJ-1 zircon reference material by solution and laser-ablation MC-ICPMS, *Chemical Geology* **255**: 231-235.

Neves, S.P. 2009. Zircões detríticos em rochas metassedimentares proterozóicas na Província Borborema: uma conexão amazônica? In: XXIII Simpósio de Geologia do Nordeste, 2009, Fortaleza. Anais do XXIII Simpósio de Geologia do Nordeste (CD-ROM).

Neves, S.P., Bruguier, O., Silva, J.M.R., Bosch, D., Alcantara, V.C., Lima, C.M. 2009. The age distribuitions of detrital zircons in metassedimentary sequences in eastern Borborema Province (NE Brazil): Evidence for intracontinental sedimentation and orogenesis? *Precambrian Research*, **175:** 187-205.

Nogueira Neto, J. A., Fetter, A. H., Legrand, J. M., Santos, T. J. S., Hackspacher, P. C. 1997. Idade Neoproterozóica em Granulitos de Cariré (NW do Ceará): U/Pb em titânita e idade modelo (T_{DM}) - resultados iniciais. In: SBG, Simpósio Nacional de Estudos Tectônicos, **6:** Pirenópoles, Resumos Expandidos, 101-103.

Pimentel, M.M., Whitehouse, M.J., Viana, M.G., Fuck, R.A., Machado, N. 1997. The Mara Rosa arc in the Tocantins Province: Further evidence for Neoproterozoic crustal accretion in central Brazil. *Precambrian Research,* **81:** 299-310.

Richard, P., Shimizu, N., Allegre, C.J. 1976. $^{143}Nd/^{144}Nd$, a natural tracer: an application to oceanic basalts, *Earth Planetary Science Letters,* **31:** 269-278.

Rogers, J. J. W. 1996. A history of continents in the past three billion years. *Journal of Geology*, **104:** 91-107.

Rogers, J.J.W., Santosh, M. 2002. Configuration of Columbia, a Mesoproterozoic supercontinent. *Gondwana Research,* **5:** 5-22.

Rogers, J.J.W., Santosh, M. 2009. Tectonics and surface effects of the supercontinent Columbia. *Gondwana Research,* **15:** 373-380.

Ruiz, A.S., Geraldes, M.C., Matos, J.B., Teixeira, W., Van Schumus, W.R., Schmitt, R.S. 2004. 1590-1520 Ma Cachoeirinha magmatic arc and its tectonic implications for the Mesoproterozoic SW Amazonian craton crustal evolution. *An. Acad. Bras. Ciênc.* 2004, **76:** 807-824.

Rubatto, D., Gebauer, D., Compagnoni, R. 1999. Dating of eclogite-facies zircons: the age of Alpine metamorphism in the Sesia-Lanzo Zone (Western Alps). *Earth Planetary Science. Letters,* **167:** 141-158.

Rubatto, D., Liati, A., Gebauer, D. 2003. Dating UHP metamorphism. In: Compagnoni R, Carswell DA (eds) Ultra-high pressure metamorphism, vol 5. European Mineralogical Union, Budapest, 341-363.

Sá, J.M., Bertrand, J.M., Leterrier, J. 1997. Geocronologia U-Pb e geoquímica de ortognaisses Paleo e Mesoproterozóicos da região de Taquaritinga-PE. In: *SBG, Simpósio de Geologia do Nordeste*, **17**. Fortaleza-CE, resumos expandidos, 108-112.

Santos, E.J., Lima, H.M., Arruda, S.D.A., Santos, L.C.M.L. 2009. Os diques metamáficos do bloco de Carpina (PE) e seu significado para a evolução do terreno Rio Capibaribe. In: XXIII Simpósio de Geologia do Nordeste, 2009, Fortaleza. Anais do XXIII Simpósio de Geologia do Nordeste (CD-ROM).

Santos, J.O.S., Rizzotto, G.J., Potter, P.E., McNaughton, N., Matos, R.S., Hartmann, L.A., Chemale Jr., F., Quadros, M.E.S. 2008. Age and autochthonous evolution of the Sunsás Orogen in West Amazon Craton based on mapping and U–Pb geochronology. *Precambrian Research,* **165:** 120-152.

Santos, T.J.S., Garcia, M.G.M., Amaral, W.S., Caby, R., Wernick, E., Arthaud, M.H., Dantas, E.L., Santosh, M. 2009. Relics of eclogite facies assemblages in the Ceará Central Domain, NW Borborema Province, NE Brazil: Implications for the assembly of West Gondwana. *Gondwana Research,* **15:** 454-470.

Scherer, E., Münker, C., Mezger, K. 2006. Calibration of the lutetium–hafnium clock, *Science,* **293:** 683-687.

Silva Filho, A.F., Guimarães, I.P., Ferreira, V. P., Sial, A., Cocentino, L., Lima, D. 2009. Geocronologia U-Pb por SHRIMP e geoquímica isotópica do plutão ediacarano Águas Belas, Domínio Pernambuco-Alagoas. In: XXIII Simpósio de Geologia do Nordeste, 2009, Fortaleza. Anais do XXIII Simpósio de Geologia do Nordeste (CD-ROM).

Simonetti, A., Heaman, L.M., Hartlaub, R.P., Creaser, R.A., MacHattie, T.G., Böhm, C. 2005. U-Pb zircon dating by laser ablations-MC-ICP-MS using a new ultiple ion counting Faraday collector array. *Journal of Analytical Atomic Spectrometry,* **20:** 677-686.

Stacey, J.S., Kramers, J.D. 1975. Approximation of terrestrial lead isotope evolution by a two-stage model. *Earth Planetary Science Letters,* **26:** 207-221.

Tohver, E., D, Agrella-Filho, M.S., Trindade, R.I.F., 2006. Paleomagnetic record of Africa and South America for the 1200–500 Ma interval, and evaluation of Rodinia and Gondwana assemblies. *Precambrian Research*, **147**: 193-222.

Trompette, R. 1994. *Geology of western Gondwana, Pan-African/Brasiliano aggregation of South America and Africa*. A.A. Balkema: Rotterdam.

Van Schumus, W.R., Brito Neves, B.B., Hackspacher, P., Babinski, M. 1995. U-Pb and Sm-Nd geochronological studies of eastern Borborema Province, northeastern Brazil: initial conclusions. *Journal of South America Earth Science,* **8**: 267-288.

Van Schmus, W.R., Oliveira, E.P., Da Silva Filho, A., Toteu, S.F., Penaye, J., Guimarães, I.P. 2008. Proterozoic links between the Borborema Province, NE Brazil, and the Central African Fold Belt, In: *West Gondwana: Pre-Cenozoic Correlations Across the South Atlantic Region*, Pankhurst, R.J., Trouw, R.A.J., Brito Neves, B.B., de Wit, M.J. (eds). Geological Society of London, Special Publications, **294:** 69-99.

Zhao, G.C., Cawood, P.A., Wilde, S.A., Sun, M. 2002. Review of global 2.1-1.8 Ga orogens: implications for a pre-Rodinia supercontinent, *Earth-Science Reviews,* **59:** 125-162.

Zhao, G.C., Sun, M., Wilde, S.A., Li, S.Z., 2004. A Paleo-MesoProterozoic supercontinent: assembly, growth and breakup. *Earth-Science Reviews,* **67:** 91-123.

ANEXO 04

“Química mineral e Geotermobarometria das rochas metamáficas e metassedimentares da Faixa Eclogítica de Forquilha”

QUÍMICA MINERAL E GEOTERMOBAROMETRIA

1. APRESENTAÇÃO

A caracterização petrográfica das associações minerais e respectivas relações texturais, adicionadas aos dados de química mineral, permitiram estimar as condições de metamorfismo a que foram submetidas às sequências metamórficas da Faixa Eclogítica de Forquilha (FEF).

Nove amostras representativas de rochas metamáficas e três rochas metassedimentares encaixantes foram selecionadas ao longo do *trend* estrutural N-S da região de Forquilha (Figura 1). A estruturação da FEF é balizada por um sistema de rampas de empurrão, que se iniciam na borda oeste do arco magmático de Santa Quitéria, e são marcadas por planos de foliação com intensidades de mergulho de baixo ângulo (25-35°) e uma lineação de estiramento mineral (L_x) de principalmente sillimanita, cianita com caimento para E-ESE. À medida que se avança para oeste, a intensidade do mergulho dos planos de empurrão aumenta, exibindo ângulos de médio (45º) a alto ângulo (65º) de mergulho e lineações de estiramento mineral com caimento para S-SE.

A coleta das amostras teve como controle de campo a lineação (L_x) responsável pela exposição de rochas mais anfibolíticas no setor norte da FEF, enquanto no setor sul as amostras coletadas são mais enriquecidas em clinopiroxênio e granada e consequentemente, menos retrometamorfisadas.

Para cada amostra segue uma breve descrição petrográfica, os diagramas de classificação química para granada, piroxênio, anfibólio, plagioclásio e mica, bem como os cálculos geotermobarométricos decorrentes das paragêneses minerais em equilíbrio nos distintos estágios metamórficos.

2. MATERIAIS E MÉTODOS

Da região de Forquilha foram feitos estudos petrográficos detalhados, resultando na confecção de 12 lâminas delgadas polidas, metalizadas com película de carbono.

As análises de química mineral quantitativa foram realizadas no Laboratório de Microssonda e Microscopia Eletrônica de Varredura do DMG - Instituto de Geociências - USP, nas fases granada, piroxênio, anfibólio, plagioclásio, feldspatos, biotita e encontram-se disponíveis na seção Tabelas, no final desta Tese. O equipamento utilizado foi uma microssonda eletrônica JEOL, modelo JXA-8600, equipada com cinco espectrômetros, com cristais STE/TAP, TAP/PET, PET/LIF, PET/LIF e PET/LIF.

Nas análises quantitativas (*WDS – Wavelenght Dispersive System*) utilizou-se o sistema de análises automatizado Voyager da NORAN Instruments, nas seguintes condições de rotina: voltagem de aceleração 15 KV; corrente do feixe eletrônico 20nA; diâmetro de feixe incidente de 10 a 5 µm para granada e anfibólio, 5 µm para piroxênio, plagioclásio e mica. Os erros analíticos relativos máximos estimados para os resultados são de ± 1% para os elementos maiores e ± 5% para os elementos menores analisados.

A fórmula estrutural dos minerais foi calculada com auxílio do programa Minpet 2.02, de Richard (1995) que adota os critérios da IMA (*International Mineralogical Association*). O programa utiliza os métodos de Yoder & Tilley (1962) e Cawthorn & Collerson (1974) para o recálculo do piroxênio e o método de Richard e Clarke (1990) para o recálculo do anfibólio. No caso específico do anfibólio, o programa Minpet oferece 5 métodos diferentes de recálculos (*e.g.* Robinson *et al.,* 1982). Neste trabalho optou-se pelo método da média 15-NK e 13-CNK, mais apropriado para o recálculo dos anfibólios segundo a autora (Richard, 1995).

A partir dos dados de química mineral foram realizados estudos geotermobarométricos com o objetivo de quantificar as condições de mais alto grau metamórfico, nas quais as fases granada + clinopiroxênio ± quartzo estavam estáveis (Fácies eclogito). Foram priorizados os pseudomorfos preenchidos por simplectitos de clinopiroxênio e plagioclásio, e as inclusões em granada. As análises de associações, texturalmente em equilíbrio, foram separadas das assembléias cristalizadas em condições retrometamórficas. Os pontos analisados foram, sempre que possível, localizados nos núcleos e nas bordas dos grãos. Para facilitar as análises foram feitos os estudos petrográficos detalhados, imagens de elétrons retro-espalhados e perfis composicionais em granada.

Com exceção de um clinopiroxênio-granada anfibolito (WT7-25K), todas as demais foram plotadas no mapa geológico confeccionado na escala 1:10.000 (Figura 1), onde é possível observar as relações litológicas e estruturais das mesmas.

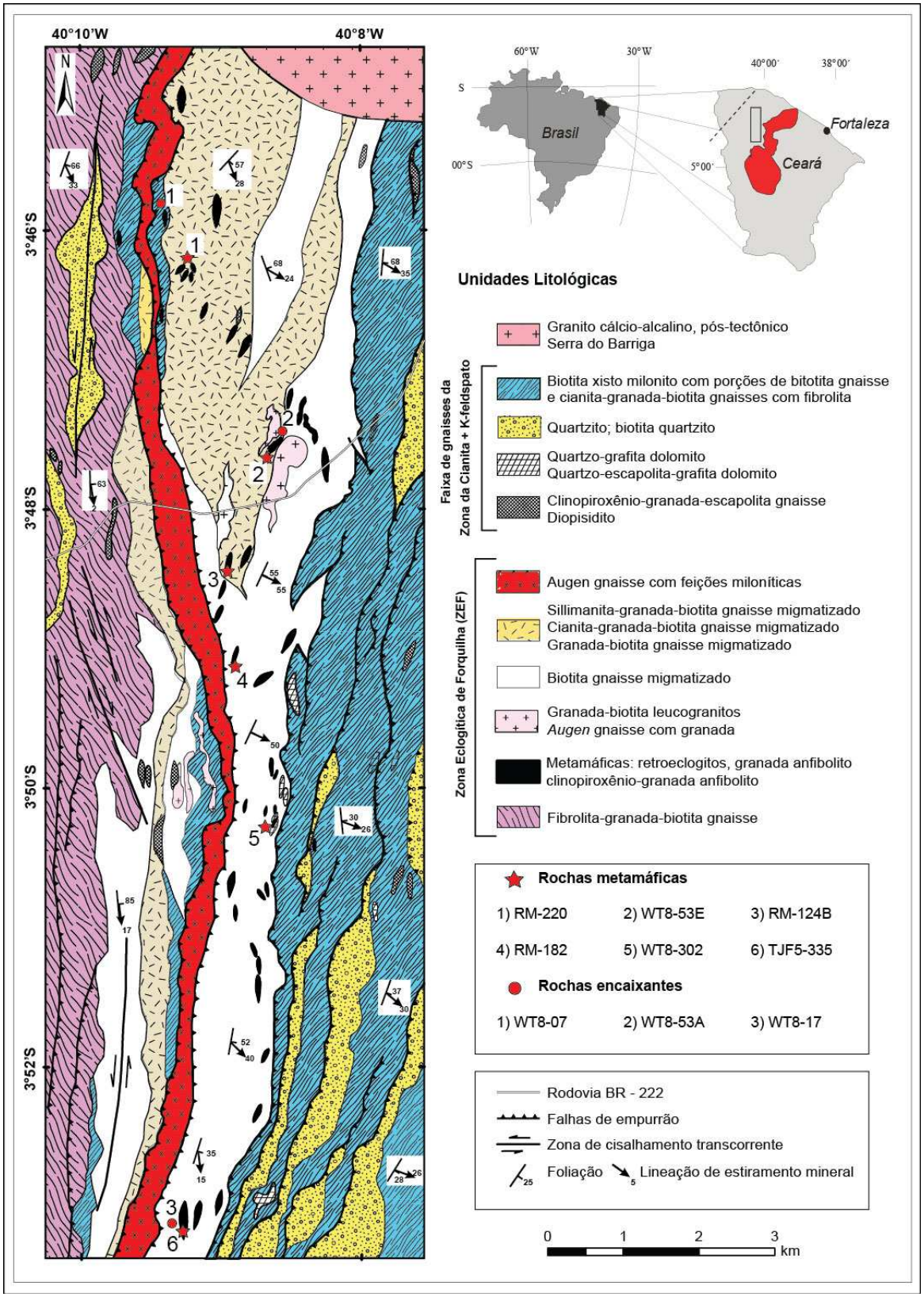

Figura 1: Mapa geológico da Faixa Eclogítica de Forquilha. Com exceção da amostra WT7-25 situada a norte do granito Serra da Barriga, as amostras analisadas nesse estudo estão assinaladas: (X) metamáficas e (I) granulitos encaixantes (adaptado de Ancelmi, 2009).

3. GRANADA
Rochas metamáficas:

A granada presente no clinopiroxênio-granada anfibolito (WT7-25K) apresenta dimensões que variam de 0,3 a 1,5 mm e forma idioblástica a sub-idioblástica. Inclusões são de minerais acessórios, principalmente zircão, apatita, ilmenita e titanita. Granada está sempre em contato com anfibólio ou envolvida por coronas de reação com plagioclásio. As seguintes composições foram determinadas: **Alm** (54.66-65.37%)**, Grs** (26.66-32.74%)**, Prp** (4.57-13.92%)**, Sps** (1.20-2.45%). Os cristais mostram enriquecimento da molécula almandina e espessartita nas bordas, e diminuição em direção ao núcleo. Por outro lado, piropo e grossulária aumentam das bordas para o centro dos minerais analisados.

Nas amostras do setor centro-norte (Figura 1) os cristais de granada variam entre 0,1 e 2 mm e se mostram, via de regra, poiquiloblásticas, com bordas corroídas. As inclusões são predominantemente de quartzo, ilmenita, titanita, rutilo e apatita. Outras inclusões são de minerais incolores de alta cor de birrefringência. Alguns cristais de granada apresentam intenso fraturamento que localmente é preenchido por clorita. Texturas coroníticas formadas por plagioclásio são comuns na maioria dos grãos.

Em termos composicionais a granada da amostra WT8-53E é composta por **Alm** (49.00-59.66%)**, Grs** (21.63-29.45%)**, Prp** (15.43-20.76%)**, Sps** (1.09-2.31%), e mostra enriquecimento na molécula piropo nos núcleos e diminuição nas bordas. A composição das demais amostras do setor central da área investigada está listada na Tabela 1.

Tabela 1: Composição da granada presente nas rochas metamáficas do setor centro-norte.

Amostras	Almandina (%)	Grossulária (%)	Piropo (%)	Espessartita (%)
Amostra RM-124B	52.98-55.39	27.00-29.88	13.65-16.54	1.92-3.63
Amostra RM-182	49.85-57.07	25.95-32.54	13.68-16.99	0.74-2.31
Amostra RM-220	51.24-57.29	25.83-34.75	11.15-17.49	0.92-1.49

3.1. Amostra WT8-302: Retroeclogito (setor centro-sul):

A granada possui dimensões sub-milimétricas e formas sub-idioblásticas, quase sempre orientadas e estiradas segundo a foliação (S_n). Apresenta fraturas bem marcadas e ortogonais à direção de estiramento. Em alguns casos nota-se a disposição de fraturas radiais, preenchidas com quartzo. Zircão, rutilo e apatita são frequentemente encontrados como inclusões. Os cristais estão sempre em contato com o plagioclásio/quartzo, anfibólio e rutilo. Quimicamente é a granada mais magnesiana das rochas analisadas, com os teores de **Prp** (20.44-28.83%)**, Alm** (42.60- 55.37%)**, Grs** (19.37-27.20%)**, Sps** (0.85-2.15%). Os maiores valores da molécula piropo estão sempre nos núcleos dos cristais.

3.2. Amostras TJF5-335, TJF5-335A e TJF5-335B: Granada-clinopiroxênio anfibolito (setor sul):

A granada encontrada nas três amostras TJF5-335, TJF5-335A e TJF5-335B apresenta características petrográficas similares e será descrita de forma conjunta. Possui coloração avermelhada com formas idioblásticas a sub-idioblásticas e dimensões médias variando entre 0,3 a 5 mm. Ocorrem como porfiroblastos, que se distribuem preferencialmente ao longo do plano de foliação (S_n). Os grãos maiores apresentam maior quantidade de fraturas, que se desenvolvem perpendicular à foliação. Nota-se, por vezes, que as fraturas estão preenchidas por anfibólio. Nos cristais menors de granada, o grau de fraturamento é incipiente e o número de inclusões é reduzido, o que sugere uma segunda geração de granada de mais alta temperatura.

Os porfiroblastos geralmente são contornados por ripas isométricas de plagioclásio em forma de corona que, por sua vez, podem também estar circundadas por auréolas de anfibólio azulado rico em sódio (*c.a.* 4,15%).

De maneira geral, a granada é zonada sugerindo mais de uma fase de blastese. O zoneamento é caracterizado pela textura poiquilítica com inclusões concentradas na parte central do grão e bordas mais límpidas sub-idioblásticas. As inclusões são de quartzo e subordinadamente anfibólio, piroxênio, plagioclásio, titanita e rutilo. Em muitos casos as inclusões de quartzo são orientadas, definindo contornos retilíneos que evidenciam linhas de crescimento com desenvolvimento inicial idioblástico para a primeira geração de granada.

No interior de alguns cristais é possível observar inclusões simplectíticas de plagioclásio e clinopiroxênio (Figura 2a). Outros cristais mostram núcleo preservado e uma porção intermediária entre a borda e o centro completamente substituída por simplectitos de clinopiroxênio e plagioclásio, formando "textura em atol" (Figura 2b).

Análises semi-quantitativas (EDS) realizadas por Reginato (2009) em granada da amostra TJF5-335 permitiram estimar uma composição média de **Alm** (46.01-51.44%)**, Grs** (22.98-28.97%)**, Prp** (19.43-24.43%)**, Sps** (0.78-1.69%). Considerando as análises quantitativas (WDS) listadas na Tabela 2, obtidas em microssonda eletrônica, para granada dessa mesma rocha, os valores encontram-se dentro de uma margem de erro aceitável. Deste modo, foi possível avaliar a distribuição das proporções moleculares por meio de perfis longitudinais.

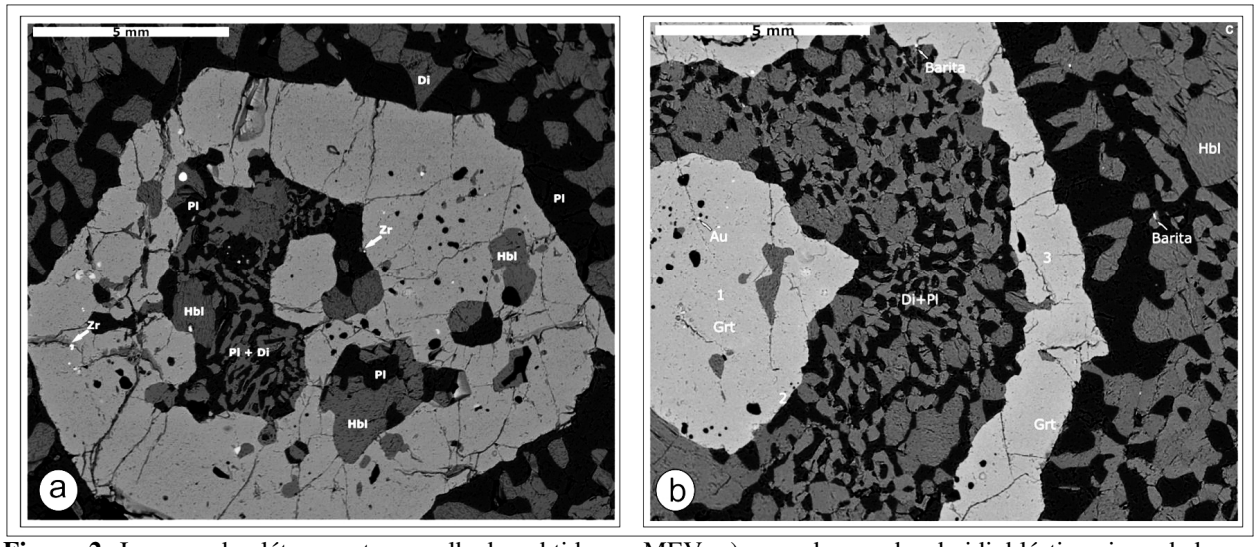

Figura 2: Imagem de elétrons retro-espalhados obtida em MEV: a) granada com borda idioblástica circundada por plagioclásio e clinopiroxênio Este também presente como simplectito na parte central da granada; b) granada parcialmente desestabilizada formando textura em atol, com núcleo envolto por simplectito de clinopiroxênio e plagioclásio. Destaque para uma pequena inclusão de ouro no centro (Amostra TJF5-335).

Constatou-se, a partir da análise do perfil obtido, em cristais de granada das Figuras 3a-b e 4a-b (Reginato, 2009), que há aumento da proporção molecular de piropo em direção as bordas do cristal, que é acompanhado por uma diminuição inversamente proporcional da molécula de almandina e grossulária (Figuras 3a-b e 4a-b).

Os dados adquiridos em microssonda eletrônica confirmam leve enriquecimento da molécula piropo nas bordas dos grãos analisados, sugerindo que a temperatura também é mais elevada nas bordas. Almandina e grossulária mostram tendência de diminuição no sentido das

bordas para o centro, enquanto os conteúdos de espessartita mostraram-se muito inferiores, sendo especulativa qualquer constatação relevante.

Neste sentido, é possível constatar que o núcleo dos cristais preserva composições químicas de mais alta pressão, enquanto as bordas da granada refletem composições químicas de mais alta temperatura.

A Figura 5 mostra os pontos analisados na granada e o perfil composicional a partir da fração molar de almandina, grossulária e piropo (Figura 6). O intervalo médio das proporções de cada membro final obtido em núcleos e bordas de granadas encontra-se sintetizado na Tabela 2.

Tabela 2: Composição dos membros finais da granada do afloramento TJF5-335.

Amostras	Almandina (%)	Grossulária (%)	Piropo (%)	Espessartita (%)
Amostra TJF5-335	53.99-57.74	20.19-25.77	18.61-25.77	0.29-0.78
Amostra TJF5-335A	52.67- 57.10	23.48-31.81	16.14-19.72	0.50-1.28
Amostra TJF5-335B	54.27-61.50	21.33-27.68	13.45-17.10	1.05-2.31

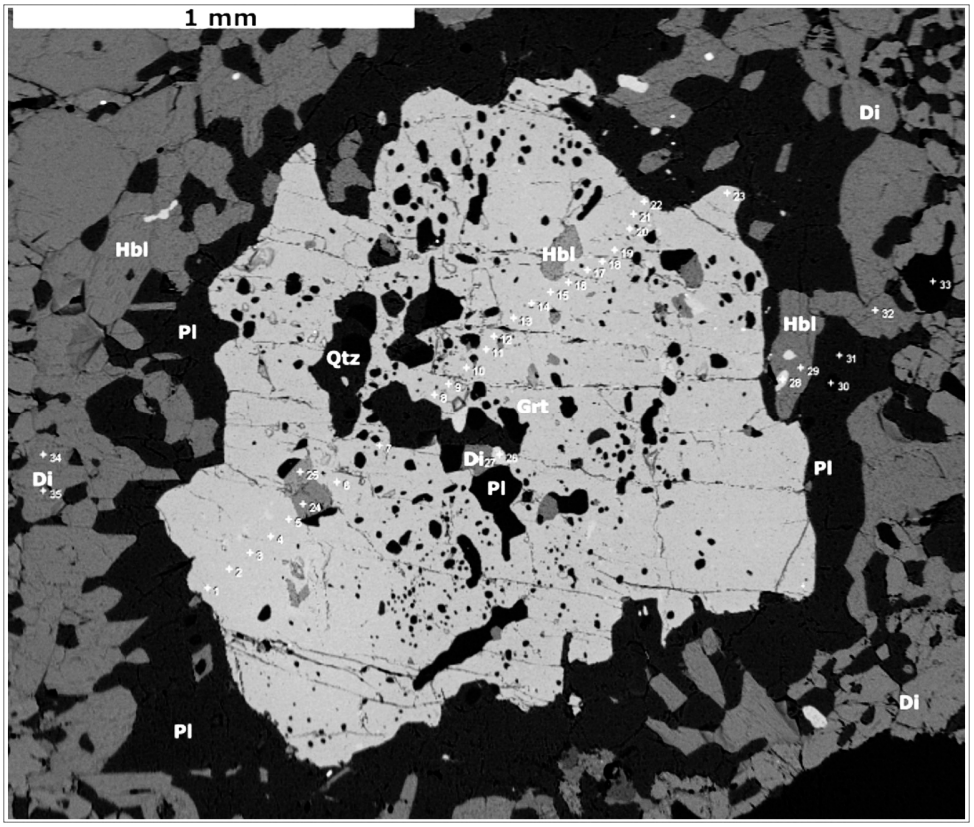

Figura 3a: Imagem de elétrons retro-espalhados mostrando a granada e os respectivos pontos analisados em EDS no MEV (Modificado de Reginato, 2009).

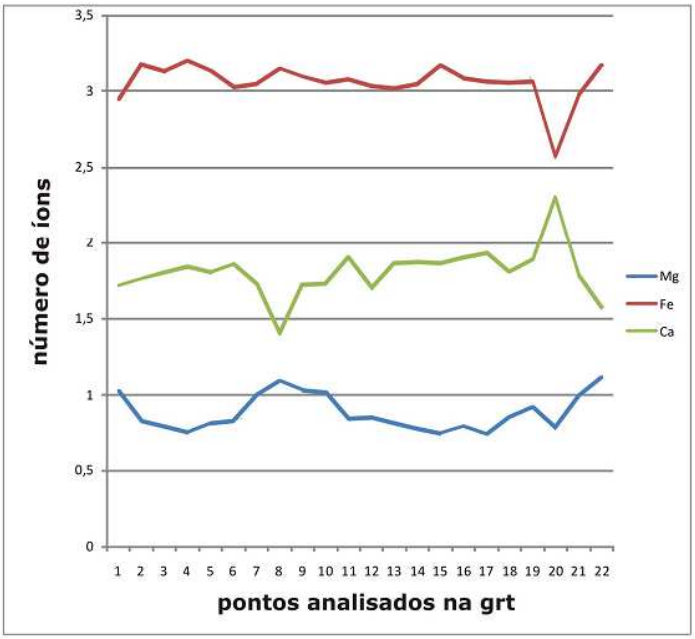

Figura 3b: Gráfico mostrando a distribuição do número de íons de Fe, Ca e Mg para cada ponto analisado na granada pelo método semi-quantitativo. Há tendência ao aumento da molécula piropo em direção as bordas do mineral, ilustrada pelo aumento do número de Mg em detrimento do Fe e do Ca.

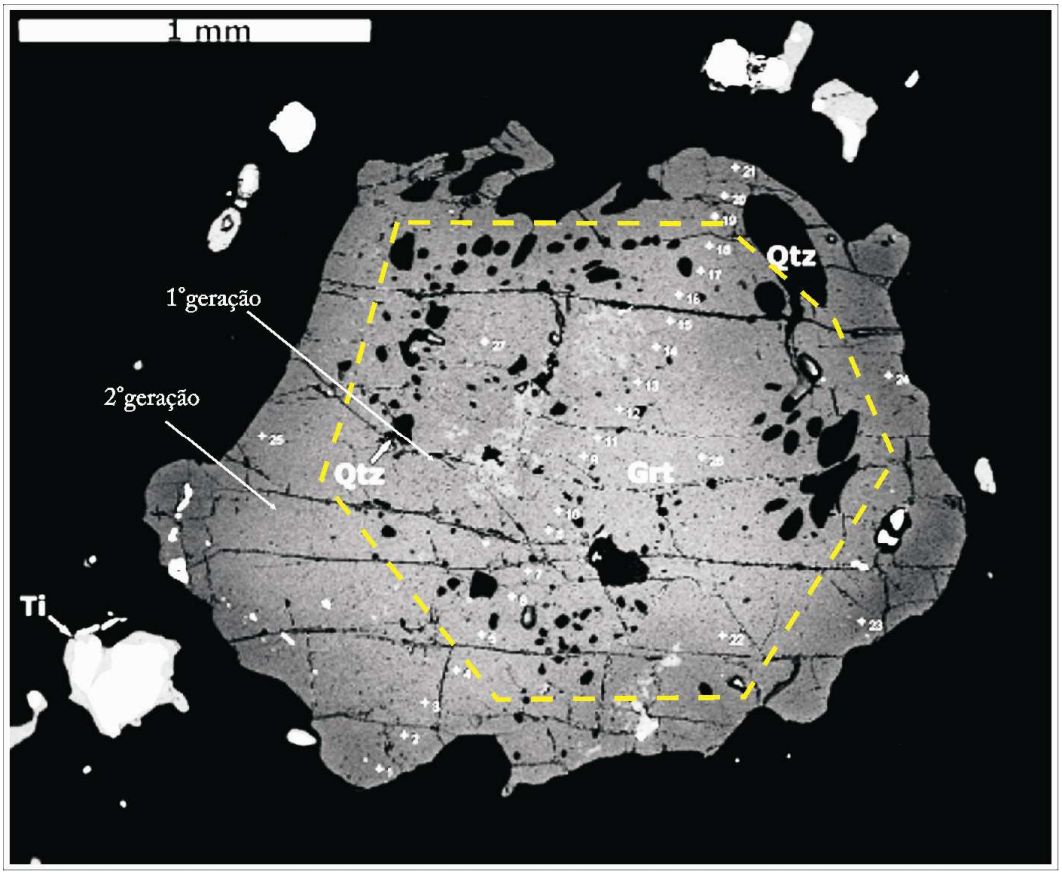

Figura 4a: Imagem de elétrons retro-espalhados obtida em granada com seu respectivo perfil analisado. Notar a presença de quartzo sob a forma de inclusões retilíneas marcando o pseudomorfo (em amarelo) da granada reliquiar da 1° geração (Modificado de Reginato, 2009).

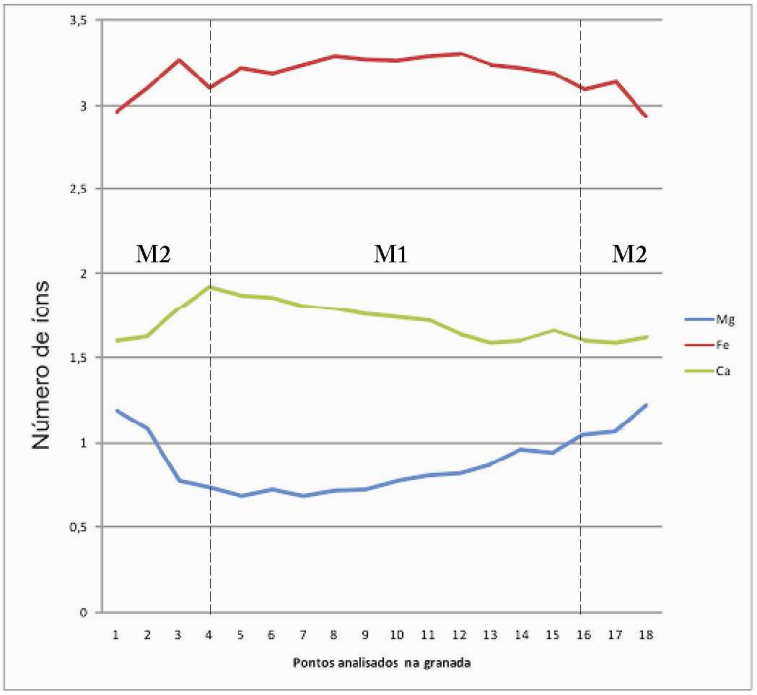

Figura 4b: Gráfico mostrando a distribuição do número de íons de Fe, Ca e Mg para cada ponto analisado na granada pelo método semi-quantitativo. As linhas tracejadas marcam as composições nas bordas da granada.(M1: primeiro evento metamórfico de geração da granada; M2 segundo evento)

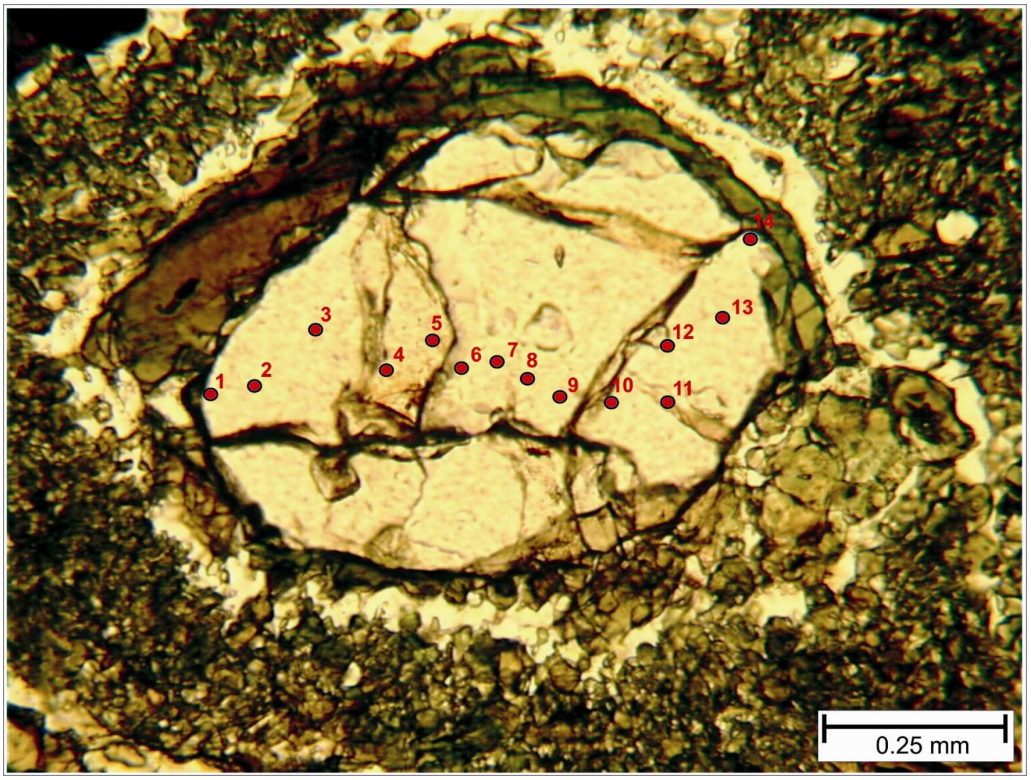

Figura 5: Imagem microscópica de granada (amostra TJF5-335) com os pontos do perfil analisado em microssonda eletrônica. Em grande parte dos cristais de granada observa-se a dupla textura coronítica que envolve os cristais com anfibólio e plagioclásio.

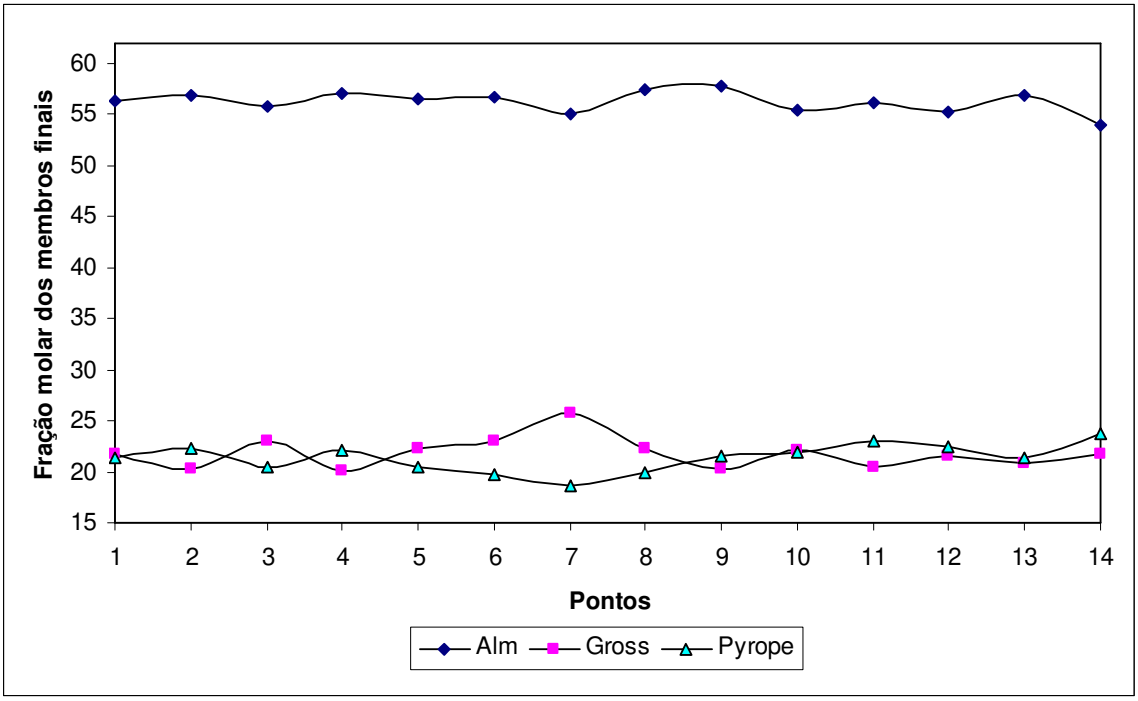

Figura 6: Perfil composicional do porfiroblasto de granada da amostra TJF5-335. Embora a quantidade de pontos seja relativamente pequena, é possível observar a tendência ao aumento da molécula piropo em direção as bordas do mineral.

4. GRANADA

Rochas metassedimentares (encaixantes):

Na amostra WT7-53A (Kinzigito) destaca-se a presença de megacristais de granada com até 3 cm de diâmetro, muitas vezes englobando totalmente cristais de sillimanita e cianita. A granada é xenoblástica e poiquiloblástica, e as inclusões mais frequentes são de quartzo, biotita, cianita, rutilo, illmenita e zircão. Os grãos encontram-se pouco fraturados e estão em contato com biotita, feldspato potássico, quartzo e sillimanita.

As análises químicas foram direcionadas para o núcleo e borda das granadas que estavam em equilíbrio com biotita e feldspato, visando estabelecer as condições de equilíbrio de mais alto grau a partir dos vetores de troca (KNa; FeMg). Destacam-se os elevados conteúdos de piropo, principalmente nos núcleos das granadas- **Prp** (21.61-28.67%). O intervalo das demais composições dos outros membros finais é definido por **Alm** (67.46-73.33%)**, Grs** (1.60-2.24%)**, Sps** (1.80-2.98%).

Na amostra WT8-07 (Cianita gnaisse) a granada ocorre em paragênese com cianita + biotita + feldspato + plagioclásio ± quartzo e apresenta características texturais semelhantes ao kizingito, com exceção do grau de fraturamento. Em termos composicionais é representada por

Alm (71.66- 81.46%)**, Grs** (1.94-3.83%)**, Prp** (15.29-24.60%)**, Sps** (0.53-1.24%). A partir do perfil composicional, observa-se um comportamento inversamente proporcional nos conteúdos de almandina e piropo em diferentes setores do grão, ou seja, discreto enriquecimento de piropo nos núcleos, sugerindo alta temperatura, e leve diminuição em direção as bordas (Figuras 7-8).

A granada presente na amostra WT8-17 (Granada-cianita gnaisse) localizada no extremo sul da área de estudo, ocorre como porfiroblastos com dimensões médias entre 0,1 e 10 mm de diâmetro. Apresenta forma sub-idioblástica com textura poiquilítica e inclusões micrométricas de quartzo, biotita e cianita.

Os cristais analisados apresentam teores de **Alm** (69.43-76.16%) de **Grs** (4.92-8.80%)**, Prp** (17.33-21.63%) e **Sps** (1.02-1.54%). Observa-se discreto aumento no teor de almandina e diminuição no componente piropo nas bordas, tal como verificado na granada do setor centro/norte. Este zoneamento é localizado, restringindo-se espacialmente às porções de borda da granada em contato com biotita.

A granada das amostras WT7-53A e WT8-07 apresenta boa correlação entre almandina e piropo, enquanto a granada da amostra WT8-17 revelou maior concentração de grossulária e diminuição de almandina (Figura 9c-d).

Figura 7: Imagem de granada (amostra WT8-07) com os pontos em perfil analisados em microssonda eletrônica.Destaque para a inclusão com fraturamento radial típica feição de quartzo β

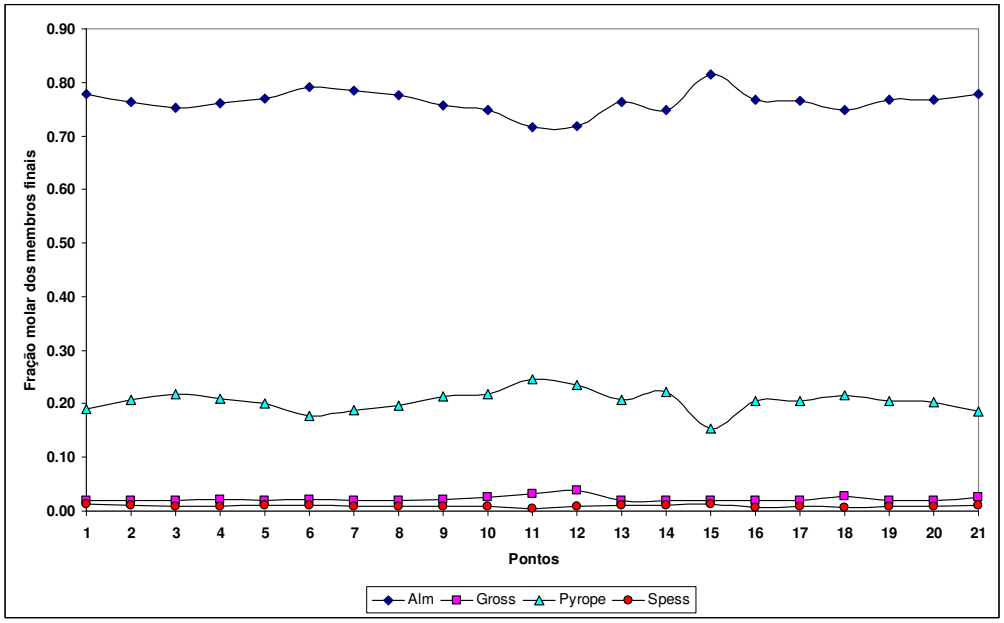

Figura 8: Perfil composicional de granada da amostra WT8-07. É possível observar claramente que as proporções de almandina e piropo são inversamente proporcionais. Os pontos 11 e 12 posicionados na parte central do cristal revelam os maiores teores de piropo, enquanto em direção para as bordas as proporções de piropo diminuem e de almandina tendem a aumentar.

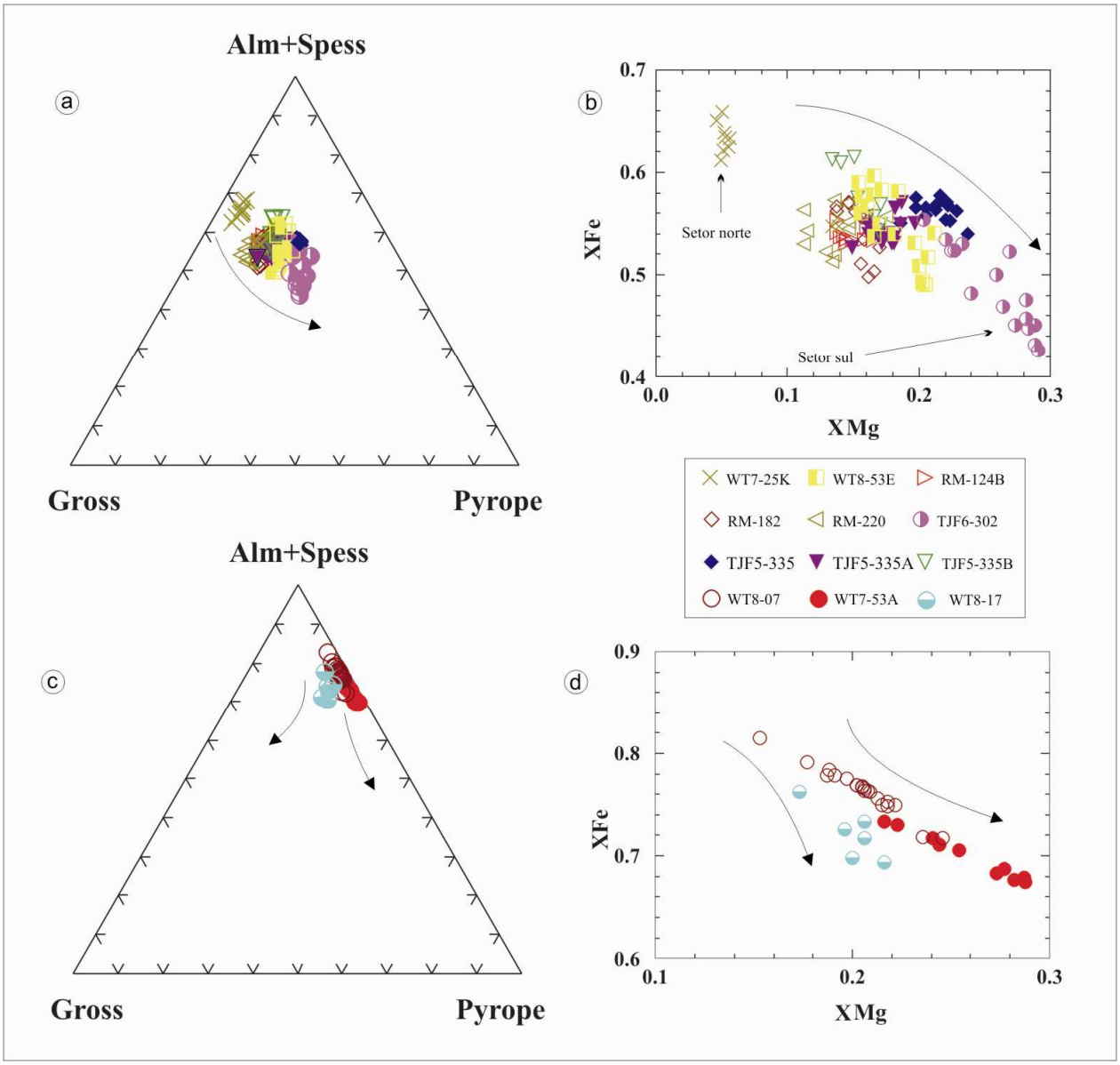

Figura 9: Classificação da granada analisada: a) granada representativa das rochas metamáficas, com tendência de enriquecimento em piropo nas amostras coletadas no sul da área investigada; b) Relação entre XFe *vs.* XMg mostrando a tendência de enriquecimento de Mg em granada das rochas metamáficas na parte sul; c) granada representativa das rochas encaixantes. Notar leve tendência de enriquecimento em grossulária para granada da amostra WT8-07; d) Tendências da correlação XFe *vs.* XMg observada nas rochas encaixantes.

5. PIROXÊNIO

Apenas clinopirôxenio (Cpx) foi identificado nas rochas metamáficas. Apresenta coloração esverdeada pálida, fracamente pleocróica. Ocorre frequentemente intercrescido como simplectitos de plagioclásio ± quartzo ± anfibólios, preenchendo esqueletos de onfacita. Em algumas amostras ocorre como pequenas inclusões em granada ou sob a forma de prismas envolvidos por reações de substituição para anfibólios, tanto nos planos de clivagem do mineral, quanto em reações de borda. Nessa situação, em termos composicionais, o piroxênio apresenta os menores conteúdos de Ca e Mg e maiores em Fe e Al em relação aos demais Cpx.

Com o objetivo de identificar os maiores conteúdos da molécula jadeíta no piroxênio, as análises foram prioritariamente realizadas nas formas vermiculares que constituem os simplectitos, na tentativa de obter as condições próximas ao pico metamórfico dado pela seguinte reação:

Onfacita + quartzo = diopsídio + albita (simplectitos)

Para a classificação dos piroxênios, adotou-se a nomenclatura de Morimoto (1988), que segue as recomendações da IMA (*International Mineralogical Association*). O intervalo de dados das composições químicas dos membros finais encontra-se na Tabela 3.

Os piroxênios analisados constituem-se majoritariamente de Ca, Mg e Fe. No diagrama da Figura 10a, onde estão representados os componentes moleculares wollastonita (Wo), enstatita (En) e ferrossilita (Fs), os piroxênios foram classificados como diopsídio. Apenas uma análise é plotada no campo da augita.

A substituição jadeítica ($NaAl^{VI}Ca_{-1}Mg_{-1}$), que responde à entrada do Na no sítio (M2) dos piroxênios é dependente da pressão, e foi constatada principalmente nas amostras (TJF5-335 e TJF5-335A) que registraram X_{Jd} (0.18) (Figura 10b). Nas demais amostras esses valores ficaram em média X_{Jd} (~0.019).

De maneira análoga ao observado para os grãos de granada em que o componente piropo aumentava nas rochas do setor sul, os piroxênios também mostraram uma tendência de enriquecimento da molécula onfacita (Figuras 10c-d).

Tabela 3: Fórmulas estruturais do clinopiroxênio das amostras analisadas.

WT7-25K	$Na_{(0.04-0.07)}\ Ca_{(0.85-0.93)}\ Mg_{(0.64-0.70)}\ Fe^{2+}_{(0.20-0.25)}\ Fe^{3+}_{(0.05-0.09)}\ Ti_{(0.00-0.01)}\ Al_{(0.04-0.10)}\ Si_{(1.90-1.96)}$
WT8-53E	$Na_{(0.04-0.06)}\ Ca_{(0.73-0.92)}\ Mg_{(0.73-0.77)}\ Fe^{2+}_{(0.04-0.18)}\ Fe^{3+}_{(0.00-0.11)}\ Ti_{(0.00-0.01)}\ Al_{(0.02-0.15)}\ Si_{(1.85-1.98)}$
RM-124B	$Na_{(0.02-0.03)}\ Ca_{(0.90-0.94)}\ Mg_{(0.75-0.78)}\ Fe^{2+}_{(0.14-0.17)}\ Fe^{3+}_{(0.05-0.08)}\ Ti_{(0.00-0.01)}\ Al_{(0.05-0.06)}\ Si_{(1.94-1.95)}$
RM-182	$Na_{(0.03-0.05)}\ Ca_{(0.89-0.92)}\ Mg_{(0.74-0.76)}\ Fe^{2+}_{(0.15-0.19)}\ Fe^{3+}_{(0.02-0.07)}\ Ti_{(0.00-0.00)}\ Al_{(0.03-0.06)}\ Si_{(1.94-1.97)}$
RM-220	$Na_{(0.04-0.05)}\ Ca_{(0.88-0.93)}\ Mg_{(0.66-0.71)}\ Fe^{2+}_{(0.16-0.23)}\ Fe^{3+}_{(0.04-0.09)}\ Ti_{(0.00-0.01)}\ Al_{(0.06-0.10)}\ Si_{(1.88-1.94)}$
WT8-302	$Na_{(0.03-0.07)}\ Ca_{(0.88-0.92)}\ Mg_{(0.76-0.82)}\ Fe^{2+}_{(0.07-0.13)}\ Fe^{3+}_{(0.03-0.10)}\ Ti_{(0.00-0.02)}\ Al_{(0.04-0.11)}\ Si_{(1.89-1.96)}$
TJF5-335	$Na_{(0.09-0.15)}\ Ca_{(0.81-0.86)}\ Mg_{(0.61-0.72)}\ Fe^{2+}_{(0.11-0.14)}\ Fe^{3+}_{(0.06-0.07)}\ Ti_{(0.00-0.00)}\ Al_{(0.06-0.11)}\ Si_{(1.89-1.94)}$
TJF5-335A	$Na_{(0.08-0.18)}\ Ca_{(0.80-0.86)}\ Mg_{(0.63-0.71)}\ Fe^{2+}_{(0.10-0.16)}\ Fe^{3+}_{(0.00-0.10)}\ Ti_{(0.00-0.01)}\ Al_{(0.03-0.12)}\ Si_{(1.88-1.97)}$
TJF5-335B	$Na_{(0.03-0.05)}\ Ca_{(0.86-0.89)}\ Mg_{(0.70-0.72)}\ Fe^{2+}_{(0.19-0.23)}\ Fe^{3+}_{(0.01-0.05)}\ Ti_{(0.00-0.01)}\ Al_{(0.02-0.05)}\ Si_{(1.95-1.98)}$

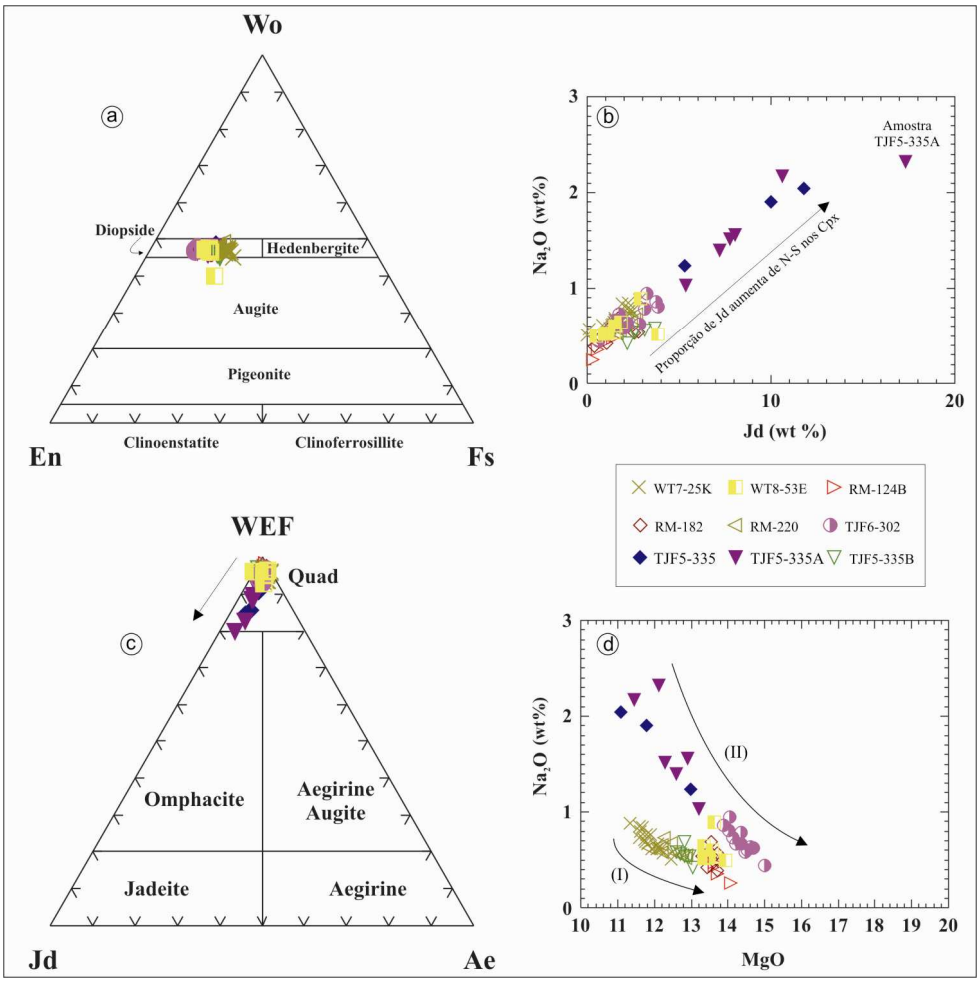

Figura 10: Diagramas de classificação para piroxênio: a) Variação composicional em função dos componentes **Wo** ($Ca_2Si_2O_6$), **En** (Mg_2Si2O_6) e **Fs** ($Fe_2Si_2O_6$), 99% do clinopiroxênio foram classificados como diopsídio (Morimoto *et al.* 1988); b) Diagrama Jd *vs.* Na_2O mostrando o aumento do componente Jd nas amostras do setor sul; c) Diagrama ternário de classificação do piroxênios rico em Na, evidenciando *trend* linear em direção ao campo da onfacita (Morimoto *et al.* 1988); d) Diagrama MgO *vs.* Na_2O onde é possível definir duas tendências (I): para as rochas da porção Norte/Central e (II): para as amostras da região sul (TJF5-335, TJF5-335A, TJF5-335B e TJF6-302).

6. ANFIBÓLIO

O grupo dos anfibólios é de grande importância nas rochas metamáficas. A extensa flexibilidade composicional permite sua ocorrência em diversas rochas e também em um amplo espectro de condições de P-T durante o metamorfismo.

A fórmula geral dos anfibólios é:

$$A_{0-1}\,(M4)_2\,(M1)_2\,(M3)\,(M2)_2\,(T1)_4\,(T2)_4\,O_{22}\,(OH, F, Cl)_2$$

Os principais cátions que ocupam os sítios cristalográficos estão listados na Tabela 4.

Tabela 3: Sítios cristalográficos do anfibólio e seus principais cátions

Sítio Cristalográfico	*Coordenação*	*Principais cátions*
A	XII	Na, K
M4 (B)	VI ou VIII	Na, Li, Ca, Mn, Fe^{2+}, Mg
M1 e M3 (C)	VI	Mn, Fe^{2+}, Mg
M2 (C)	VI	Al, Ti, Fe^{3+}, Mg, Fe^{2+}
T1	IV	Al, Si
T2	IV	Si (Al)

A classificação dos anfibólios é baseada na ocupação do sítio M4, e dividida em quatro grupos:

$(Ca + Na)_{M4} < 1.34$	Grupo dos anfibólios de Fe-Mg-Mn
$(Ca + Na)_{M4} \geq 1.34$ $Na_{M4} \leq 0.67$	Grupo dos anfibólios cálcicos
$(Ca + Na)_{M4} \geq 1.34$ $0.67 \leq Na_{M4} \leq 1.34$	Grupo dos anfibólios sódico-cálcicos
$Na_{M4} \geq 1.34$	Grupo dos anfibólios alcalinos

O nome apropriado para cada anfibólio é baseado na classificação proposta pelo Subcomitê de Anfibólios (Leake, 1978). Sua classificação depende do modo como a fórmula química é calculada. Este cálculo é dificultado pela grande quantidade de sítios cristalográficos,

envolvendo multiplicidades diversas pela vacância nos sítios cristalográficos, pela entrada de água, flúor e cloro na sua estrutura, além da diversidade de elementos em sua estrutura. O cálculo da fórmula estrutural pode ser facilitado por meio de análises via úmida, pelas quais é possível determinar a quantidade de água e a razão Fe^{2+}/Fe^{3+}. Desta maneira, a fórmula estrutural pode ser normalizada a 24 (O, OH, F, Cl). Nas análises efetuadas com microssonda eletrônica, não é possível a determinação do Fe^{3+}, tampouco da água. Neste caso, a normalização para 23 oxigênios (O) é a mais adequada (Robinson *et al.,* 1982).

Nas rochas metamáficas da Zona Eclogítica de Forquilha o anfibólio cálcico predomina. Em alguns casos é indicado tendência de migração para o grupo do anfibólio sódico-cálcico (amostras setor sul). Para o anfibólio cálcico é utilizado o cálculo da fórmula estrutural a 23 (O) normalizados para 13 cátions, com a exclusão de Ca, Na e K. Deste modo, Fe^{2+}, Mg e Mn são excluídos do sítio M4 que será preenchido por Ca e Na.

No caso específico do anfibólio, o programa *Minpet* oferece 5 métodos diferentes de recálculos (*e.g.* Robinson *et al.,* 1982). Optou-se pela média de 15-NK e 13-CNK. A autora do programa (Richard, 1995) considera este método mais apropriado para recálculo dos anfibólios cálcicos (Figura 11a).

O anfibólio está presente em todas as amostras metamáficas estudadas, sempre em proporção modal superior a 20 %. Ocorre, basicamente, sob quatro maneiras: i) envolvendo o piroxênio a partir de reações retrometamórficas; ii) associado com plagioclásio e quartzo em crescimento simplectítico, por vezes orientado segundo uma foliação pouco marcante; iii) como inclusões; e iv) como auréolas envolvendo totalmente a granada. Apresenta cores marrom-esverdeada na matriz e verde azulada nas inclusões e nas auréolas. Os anfibólios do tipo "iii" e "iv" ocorrem somente nas amostras do setor sul. Possuem cores em tonalidades azuladas, são mais aluminosos e apresentam conteúdos de Na_2O de até 4.15 %.

Todos os grãos de anfibólio são cálcicos (Figura 11a-b), entretanto, ocorrem variações composicionais diversas relativas, principalmente, aos conteúdos de Mg e Fe. Para a maioria dos litotipos dos setores norte e central, conforme os parâmetros ($Ca > 1.5$; $(Na + K)_A < 0.5$ e $Ti < 0.5$), os anfibólios foram classificados em magnésio-hornblenda e tschermakita (Figura 11c). Para as demais amostras, de acordo com os parâmetros ($Ca_B > 1.5$; $(Na + K)_A > 0.5$; $Ti < 0.5$ e $Al_C > Fe^{3+}$), os anfibólios ocupam diferentes campos da hornblenda pargasita, pargasita ferrosa e edenita hornblenda (Figura 11d).

Tabela 4: Fórmulas estruturais do anfibólio das amostras analisadas

WT7-25K	$K_{[0.09-0.10]}Na_{[0.44-0.46]}\ (Na_{[0.10-0.12]}Ca_{[1.78-1.82]})_2\ (Fe^{2+}{}_{[1.61-1.81]}Mg_{[2.21-2.41]}Mn_{[0.00-0.01]}Fe^{3+}{}_{[0.29-0.50]}$ $Ti_{[0.11-0.15]}\ Al^{VI}{}_{[0.37-0.47]})_5\ (Al^{IV}{}_{[1.45-1.57]}Si_{[6.43-6.55]})_8\ O_{22}\ (OH, F, Cl)_2$
WT8-53E	$K_{[0.00-0.05]}Na_{[0.32-0.41]}\ (Na_{[0.09-0.18]}Ca_{[1.66-1.83]})_2\ (Fe^{2+}{}_{[0.91-1.32]}Mg_{[2.48-2.85]}Mn_{[0.00-0.01]}Fe^{3+}{}_{[0.27-0.61]}$ $Ti_{[0.10-0.13]}\ Al^{VI}{}_{[0.45-0.88]})_5\ (Al^{IV}{}_{[1.35-1.90]}Si_{[6.10-6.65]})_8\ O_{22}\ (OH, F, Cl)_2$
RM-124B	$K_{[0.00-0.10]}Na_{[0.37-0.44]}\ (Na_{[0.07-0.10]}Ca_{[1.82-1.88]})_2\ (Fe^{2+}{}_{[1.37-1.44]}Mg_{[2.51-2.69]}Mn_{[0.00-0.00]}Fe^{3+}{}_{[0.16-0.20]}$ $Ti_{[0.13-0.16]}\ Al^{VI}{}_{[0.62-0.72]})_5\ (Al^{IV}{}_{[1.40-1.56]}Si_{[6.44-6.60]})_8\ O_{22}\ (OH, F, Cl)_2$
RM-182	$K_{[0.05-0.07]}Na_{[0.33-0.38]}\ (Na_{[0.10-0.12]}Ca_{[1.77-1.81]})_2\ (Fe^{2+}{}_{[1.24-1.31]}Mg_{[2.73-2.81]}Mn_{[0.00-0.01]}Fe^{3+}{}_{[0.26-0.36]}$ $Ti_{[0.10-0.14]}\ Al^{VI}{}_{[0.50-0.56]})_5\ (Al^{IV}{}_{[1.27-1.49]}Si_{[6.51-6.73]})_8\ O_{22}\ (OH, F, Cl)_2$
RM-220	$K_{[0.02-0.04]}Na_{[0.52-0.57]}\ (Na_{[0.07-0.11]}Ca_{[1.79-1.86]})_2\ (Fe^{2+}{}_{[1.50-1.59]}Mg_{[2.34-2.41]}Mn_{[0.00-0.00]}Fe^{3+}{}_{[0.23-0.41]}$ $Ti_{[0.12-0.17]}\ Al^{VI}{}_{[0.53-0.67]})_5\ (Al^{IV}{}_{[1.66-1.74]}Si_{[6.27-6.34]})_8\ O_{22}\ (OH, F, Cl)_2$
WT8-302	$K_{[0.02-0.03]}Na_{[0.45-0.56]}\ (Na_{[0.09-0.15]}Ca_{[1.72-1.84]})_2\ (Fe^{2+}{}_{[0.90-1.15]}Mg_{[2.95-3.17]}Mn_{[0.00-0.00]}Fe^{3+}{}_{[0.15-0.34]}$ $Ti_{[0.12-0.24]}\ Al^{VI}{}_{[0.48-0.59]})_5\ (Al^{IV}{}_{[1.33-1.56]}Si_{[6.44-6.67]})_8\ O_{22}\ (OH, F, Cl)_2$
TJF5-335	$K_{[0.00-0.01]}Na_{[0.83-0.88]}\ (Na_{[0.14-0.18]}Ca_{[1.65-1.74]})_2(Fe^{2+}{}_{[0.93-1.26]}Mg_{[2.52-2.75]}Mn_{[0.00-0.01]}Fe^{3+}{}_{[0.28-0.56]}$ $Ti_{[0.01-0.20]}\ Al^{VI}{}_{[0.51-1.06]})_5\ (Al^{IV}{}_{[1.71-2.16]}Si_{[5.85-6.30]})_8\ O_{22}\ (OH, F, Cl)_2$
TJF5-335A	$K_{[0.00-0.01]}Na_{[0.69-0.97]}\ (Na_{[0.15-0.21]}Ca_{[1.60-1.73]})_2\ (Fe^{2+}{}_{[0.88-1.28]}Mg_{[2.18-2.74]}Mn_{[0.00-0.01]}Fe^{3+}{}_{[0.00-0.53]}$ $Ti_{[0.02-0.18]}\ Al^{VI}{}_{[0.69-1.51]})_5\ (Al^{IV}{}_{[1.47-2.32]}Si_{[5.68-6.53]})_8\ O_{22}\ (OH, F, Cl)_2$
TJF5-335B	$K_{[0.00-0.01]}Na_{[0.21-0.32]}\ (Na_{[0.13-0.15]}Ca_{[1.71-1.76]})_2\ (Fe^{2+}{}_{[1.20-1.37]}Mg_{[2.56-2.74]}Mn_{[0.00-0.01]}Fe^{3+}{}_{[0.31-0.60]}$ $Ti_{[0.11-0.13]}\ Al^{VI}{}_{[0.39-0.60]})_5\ (Al^{IV}{}_{[1.12-1.48]}Si_{[5.52-6.88]})_8\ O_{22}\ (OH, F, Cl)_2$

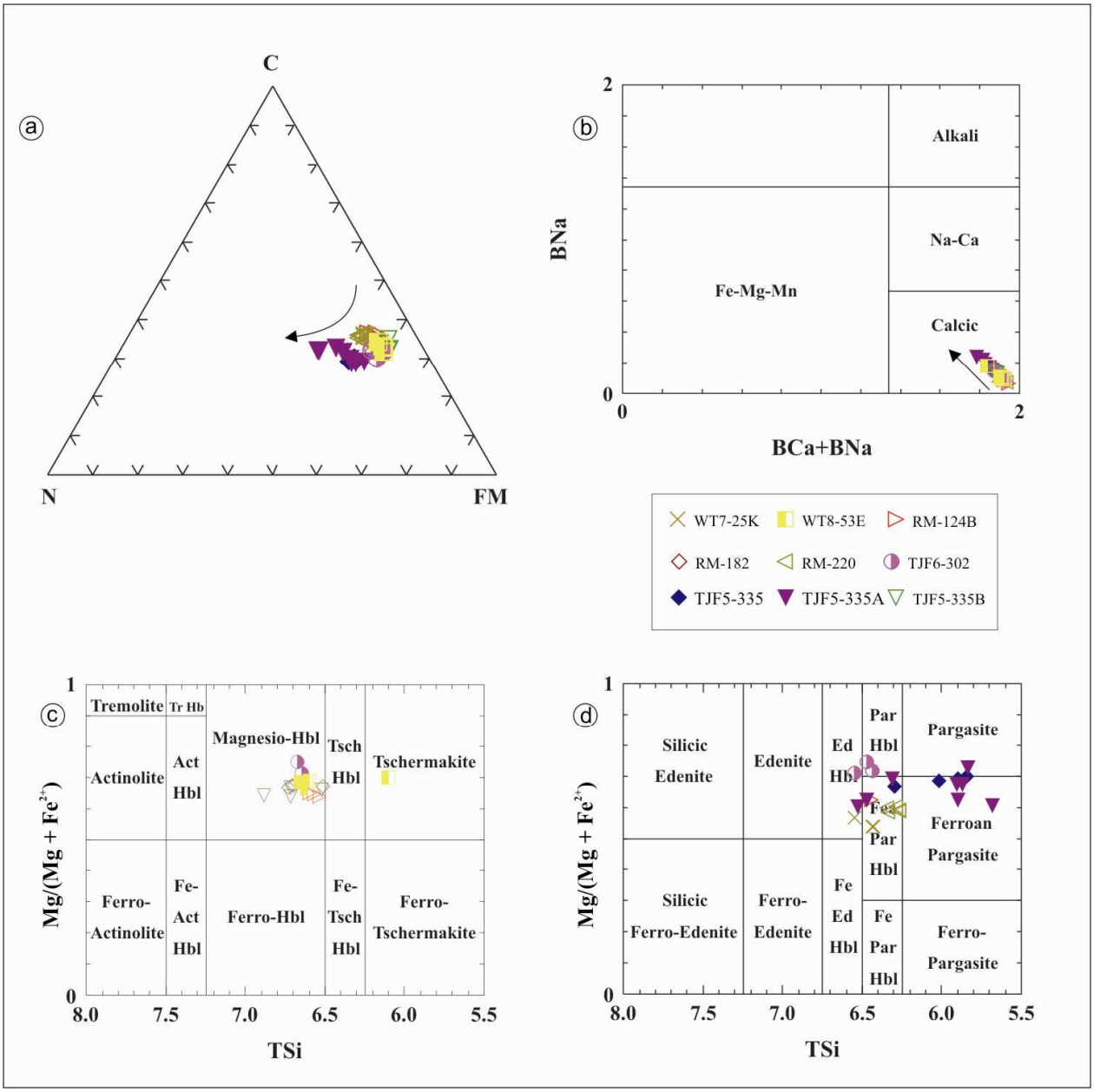

Figura 11: Diagramas classificatórios para anfibólio: a) Classificação em termos de Ca (C), Na (N) e Mn + Fe + Mg (FM) no sítio M4 (Robinson *et al.,* 1982) b) Classificação geral dos quatro principais grupos de anfibólio (Leake *et al.* 1997); c) Classificação segundo (Ca > 1.5; $(Na + K)_A$ < 0.5 e Ti < 0.5); d) Diagrama classificatório (Ca_B > 1.5; $(Na + K)_A$ > 0.5; Ti < 0.5 e $Al_C > Fe^{3+}$).

7. PLAGIOCLÁSIO

O plagioclásio (Pl) predominante nas rochas metamáficas foi classificado no sistema ternário Albita (Ab), Anortita (An) e Ortoclásio (Or), conforme as recomendações de Deer *et al.* (1992) (Figura 12a). Os resultados das microanálises químicas correspondentes aos núcleos e bordas dos grãos estão listados na Tabela 5.

Os cristais de Pl ocorrem dispersos em todas as secções analisadas e estão em contato com as demais fases minerais (anfibólio, quartzo, granada e piroxênio). Compõem principalmente as texturas de simplectitos e coroníticas.

Com o objetivo de estimar condições de P-T próximas ao pico metamórfico, as análises químicas dos plagioclásios priorizaram grãos em contato com piroxênio no núcleo dos pseudomorfos de onfacita. Quando possível, realizou-se análises nas bordas e nos núcleos dos plagioclásios. A zonação é leve ou imperceptível e a variação composicional entre núcleo e borda é pequena, com aumento da molécula de albita em direção às bordas. Oligoclásio e andesina foram os tipos de plagioclásio predominantes nas rochas metamáficas (Figura 12a).

Tabela 5: Fórmulas estruturais do plagioclásio das e conteúdos de Ab nas amostras analisadas

Amostras	***Núcleo***	***Borda***	***Fórmulas estruturais***
WT7-25K	$\mathbf{Ab}_{(71.6)}$	$\mathbf{Ab}_{(77.1)}$	$\mathbf{Na}_{[2.83\text{-}3.12]}\ \mathbf{Ca}_{[0.88\text{-}1.09]}\ \mathbf{Al}_{[4.87\text{-}5.16]}\mathbf{Si}_{[10.83\text{-}11.09]}\ \mathbf{O}_8$
WT8-53E	$\mathbf{Ab}_{(65.0)}$	$\mathbf{Ab}_{(69.1)}$	$\mathbf{Na}_{[2.62\text{-}2.82]}\ \mathbf{Ca}_{[1.25\text{-}1.41]}\ \mathbf{Al}_{[5.23\text{-}5.43]}\mathbf{Si}_{[10.52\text{-}10.72]}\ \mathbf{O}_8$
RM-124B	$\mathbf{Ab}_{(x)}$	$\mathbf{Ab}_{(60.8)}$	$\mathbf{Na}_{[2.32\text{-}2.48]}\ \mathbf{Ca}_{[1.57\text{-}1.67]}\ \mathbf{Al}_{[5.59\text{-}5.79]}\mathbf{Si}_{[10.20\text{-}10.36]}\ \mathbf{O}_8$
RM-182	$\mathbf{Ab}_{(66.6)}$	$\mathbf{Ab}_{(69.7)}$	$\mathbf{Na}_{[2.64\text{-}2.84]}\ \mathbf{Ca}_{[1.20\text{-}1.38]}\ \mathbf{Al}_{[5.23\text{-}5.45]}\mathbf{Si}_{[10.53\text{-}10.75]}\ \mathbf{O}_8$
RM-220	$\mathbf{Ab}_{(67.2)}$	$\mathbf{Ab}_{(51.0)}$	$\mathbf{Na}_{[2.03\text{-}2.74]}\ \mathbf{Ca}_{[1.31\text{-}1.95]}\ \mathbf{Al}_{[5.30\text{-}6.00]}\mathbf{Si}_{[10.01\text{-}10.67]}\ \mathbf{O}_8$
WT8-302	$\mathbf{Ab}_{(75.2)}$	$\mathbf{Ab}_{(75.2)}$	$\mathbf{Na}_{[2.56\text{-}2.93]}\ \mathbf{Ca}_{[1.18\text{-}1.52]}\ \mathbf{Al}_{[5.14\text{-}5.50]}\mathbf{Si}_{[10.43\text{-}10.82]}\ \mathbf{O}_8$
TJF5-335	$\mathbf{Ab}_{(x)}$	$\mathbf{Ab}_{(81.6)}$	$\mathbf{Na}_{[3.25\text{-}3.38]}\ \mathbf{Ca}_{[0.79\text{-}0.91]}\ \mathbf{Al}_{[4.86\text{-}5.05]}\mathbf{Si}_{[10.94\text{-}11.11]}\ \mathbf{O}_8$
TJF5-335A	$\mathbf{Ab}_{(69.6)}$	$\mathbf{Ab}_{(83.3)}$	$\mathbf{Na}_{[1.78\text{-}3.37]}\ \mathbf{Ca}_{[0.67\text{-}2.30]}\ \mathbf{Al}_{[4.72\text{-}6.35]}\mathbf{Si}_{[9.61\text{-}11.26]}\ \mathbf{O}_8$
TJF5-335B	$\mathbf{Ab}_{(x)}$	$\mathbf{Ab}_{(75.3)}$	$\mathbf{Na}_{[2.84\text{-}3.07]}\ \mathbf{Ca}_{[1.01\text{-}1.29]}\ \mathbf{Al}_{[5.09\text{-}5.32]}\mathbf{Si}_{[10.64\text{-}10.89]}\ \mathbf{O}_8$

(x): núcleo não analisado

8. FELDSPATO

O feldspato ocorre exclusivamente nos granulitos aluminosos (rochas metassedimentares encaixantes). Ortoclásio está presente nas amostras WT7-53A e WT8-17 como porfiroblasto com tamanhos médio de 1 cm. Apesar da ausência de zoneamento evidente, alguns grãos apresentam micro-exsoluções em forma de filetes. A composição dominante fica em torno de Or $_{(88.00\text{-}76.60)}$ Ab $_{(23.30\text{-}12.00)}$, não sendo possível determinar a composição das exsoluções. A amostra WT8-07 apresentou somente albita como principal feldspato alcalino Ab $_{(87.80\text{-}86\text{-}40)}$. Verificou-se também que os conteúdos de albita e ortoclásio são levemente maiores em direção às bordas. A composição dos feldspatos é representada por fórmulas estruturais (Tabela 6; Figura 12b).

Tabela 6: Fórmulas estruturais dos feldspatos alcalinos para as rochas encaixantes.

Amostras	***Núcleo***	***Borda***	***Fórmulas estruturais***
WT8-07	$\mathbf{Ab}_{(86.40)}$	$\mathbf{Ab}_{(87.80)}$	$\mathbf{Na}_{[3.49\text{-}3.64]}\ \mathbf{Ca}_{[0.47\text{-}0.53]}\ \mathbf{Al}_{[4.61\text{-}4.70]}\ \mathbf{Si}_{[11.31\text{-}11.37]}\ \mathbf{O}_8$
WT8-53A	$\mathbf{Or}_{(84.00)}$	$\mathbf{Or}_{(88.00)}$	$\mathbf{K}_{[3.21\text{-}3.67]}\ \mathbf{Na}_{[0.49\text{-}0.96]}\ \mathbf{Ca}_{[0.00\text{-}0.07]}\ \mathbf{Al}_{[4.18\text{-}4.27]}\ \mathbf{Si}_{[11.63\text{-}11.78]}\ \mathbf{O}_8$
WT8-17	$\mathbf{Or}_{(83.20)}$	$\mathbf{Or}_{(84.40)}$	$\mathbf{K}_{[3.20\text{-}3.62]}\ \mathbf{Na}_{[0.66\text{-}0.98]}\ \mathbf{Ca}_{[0.01\text{-}0.02]}\ \mathbf{Al}_{[4.19\text{-}4.29]}\ \mathbf{Si}_{[11.73\text{-}11.79]}\ \mathbf{O}_8$

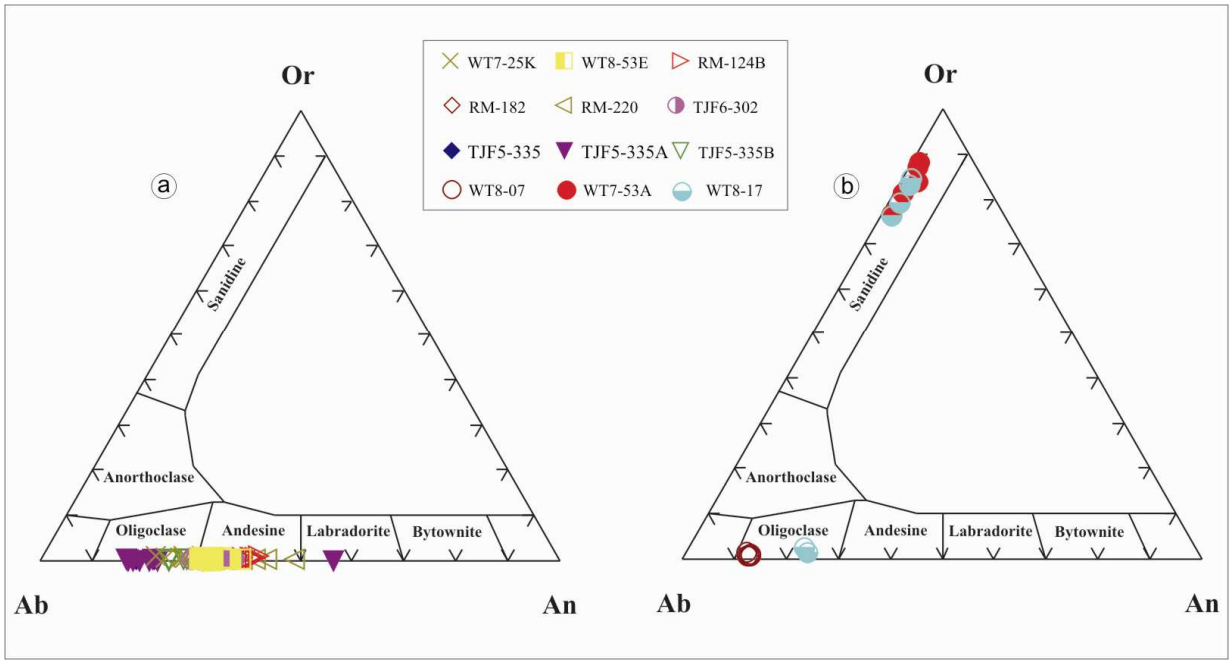

Figura 12: Variação composicional do feldspato, segundo os componentes moleculares albita (Ab), anortita (An) e ortoclásio (Or): a) rochas metamáficas, o plagioclásio ocupa predominantemente os campos do oligoclásio e andesina; b) granulitos aluminosos encaixantes, predomínio de ortoclásio e oligoclásio.

9. BIOTITA

Biotita é encontrada somente nos granulitos aluminosos. Ocorre na forma de palhetas de granulação fina a média e pleocroísmo em tons esverdeado a amarronzado. Em geral, está orientada, acompanhando as sombras de pressão dos porfiroblastos de granada e de feldspato. Apresenta-se também sob a forma lamelar com relevo moderado e forte pleocroísmo castanho-alaranjado. Inclusões de rutilo e zircão com halos pleocróicos são frequentes no interior das lamelas. Finas palhetas presentes na granada marcam foliação pretérita $S_{(n-1)}$.

Considerando os extremos siderofilita-anita-flogopita-eastonita, os grãos analisados mostram uma tendência que se aproxima da flogopita (Figura 13). A biotita avermelhada apresentou maiores teores de TiO_2, enquanto aquelas esverdeadas inclusas em granada mostraram teores mais baixos de TiO_2. As fórmulas estruturais calculadas estão sintetizadas na Tabela 7.

Tabela 7: Fórmulas estruturais da biotita para os granulitos aluminosos.

Amostras	***Fórmulas estruturais***
WT8-07	$\mathbf{K}_{[1.72\text{-}1.86]}\,\mathbf{Na}_{[0.06\text{-}0.15]}\,\mathbf{Ca}_{[0.01]}\,(\mathbf{Mg}_{[2.61\text{-}3.20]}\,\mathbf{Fe}^{2+}_{[1.64\text{-}2.46]}\,\mathbf{Ti}_{[0.02\text{-}0.36]}\,\mathbf{Al}^{\mathbf{VI}}_{[1.02\text{-}1.26]}\,(\mathbf{Al}^{\mathbf{IV}}_{[2.29\text{-}2.43]}\,\mathbf{Si}_{[5.57\text{-}3.69]})\,\mathbf{O_{20}}\,\mathbf{(OH\ F)}$
WT8-53A	$\mathbf{K}_{[1.75\text{-}2.00]}\,\mathbf{Na}_{[0.03\text{-}0.05]}\,\mathbf{Ca}_{[0.01]}\,(\mathbf{Mg}_{[2.75\text{-}3.06]}\,\mathbf{Fe}^{2+}_{[1.58\text{-}2.04]}\,\mathbf{Ti}_{[0.35\text{-}0.57]}\,\mathbf{Al}^{\mathbf{VI}}_{[0.81\text{-}1.28]}\,(\mathbf{Al}^{\mathbf{IV}}_{[2.23\text{-}2.39]}\,\mathbf{Si}_{[5.61\text{-}5.77]})\,\mathbf{O_{20}}\,\mathbf{(OH\ F)}$
WT8-17	$\mathbf{K}_{[1.99\text{-}207]}\,\mathbf{Na}_{[0.03\text{-}0.04]}\,\mathbf{Ca}_{[0.01]}\,(\mathbf{Mg}_{[2.20\text{-}2.56]}\,\mathbf{Fe}^{2+}_{[2.19\text{-}2.28]}\,\mathbf{Ti}_{[0.51\text{-}0.58]}\,\mathbf{Al}^{\mathbf{VI}}_{[0.90\text{-}1.07]}\,(\mathbf{Al}^{\mathbf{IV}}_{[2.38\text{-}2.44]}\,\mathbf{Si}_{[5.56\text{-}5.62]})\,\mathbf{O_{20}}\,\mathbf{(OH\ F)}$

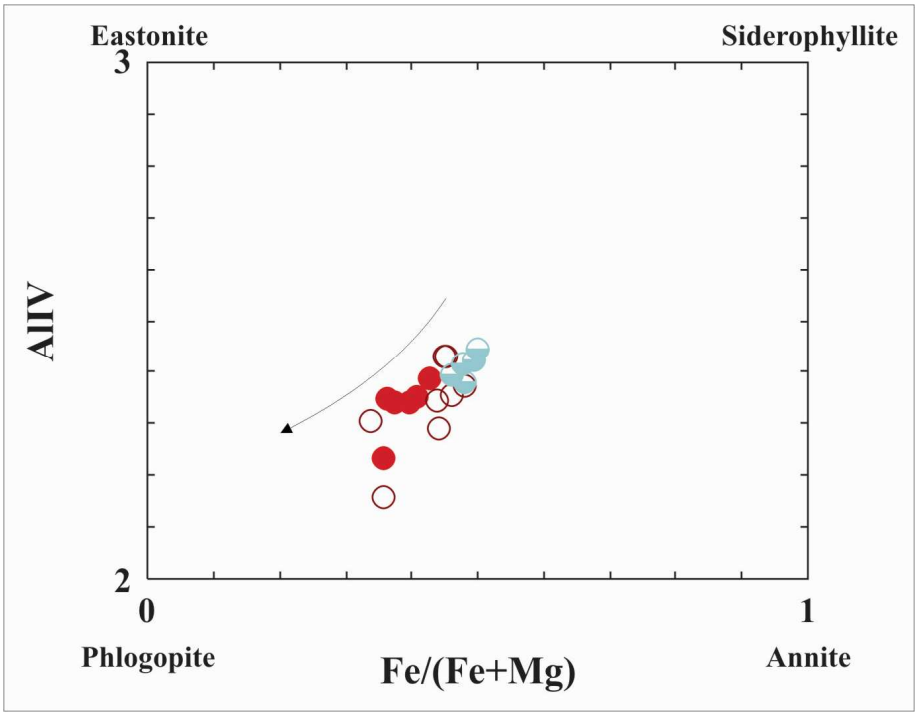

Figura 13: Classificação da biotita dos granulitos aluminosos conforme os extremos da solução sólida anita-flogopita-eastonita-siderofilita, notar a tendência para a composição da flogopita.

10. GEOTERMOBAROMETRIA

Para os cálculos geotermobarométricos foram utilizados três programas de computador clássicos em Termobarometria e os resultados puderam ser comparados entre os diferentes métodos: TWEEQU (*Thermobarometry With Estimation of Equilibrium state*) versões 1.02 (Bermam, 1991), PTMAFIC 2.0 (Soto & Soto, 1995) e THERMOCALC 3.26 (Holland & Powell, 1998). Esse último programa calcula as condições de equilíbrio para cada reação possível, utilizando as atividades dos membros finais das paragêneses em equilíbrio, tendo por base a equação geral do equilíbrio. A abordagem combina todas as informações de um conjunto independente de reações, selecionando as reações em equilíbrio na tentativa de determinar as condições de P-T da rocha. O programa ainda determina erros derivados de incertezas dos cálculos termodinâmicos, sistemáticos (incertezas nos dados termodinâmicos e modelos de atividade) e aleatórios (incertezas analíticas).

As atividades dos membros finais foram obtidas com o programa AX2, que fornece atividades para a utilização de cálculos termobarométricos. Tanto as amostras metamáficas

quanto as metassedimentares foram calculadas no THERMOCALC 3.26. Os resultados médios de P e T estão sintetizados nas Tabelas 9 e 10.

O PTMAFIC cria arquivos ASCII de análises químicas normalizadas para anfibólio, granada, epídoto, ilmenita, piroxênio, olivina, plagioclásio e espinélio. O programa realiza uma ampla gama de cálculos estequiométricos e termodinâmicos para estes minerais. Contém calibrações para treze geotermômetros e doze geobarômetros aplicáveis a rochas máficas e ultramáficas, que cobrem as condições metamórficas que variam da fácies eclogito a fácies xisto verde. Todas as amostras de rochas metamáficas foram também calculadas neste programa.

O TWEEQU (TWQ) calcula os estados de equilíbrio das associações minerais, incluindo o uso de modelos de atividades dependentes de P-T, obtidos a partir de dados experimentais de equilíbrio de fases disponíveis e aplicados às assembléias naturais. Utilizou-se este programa para o cálculo das associações de mais alto grau presentes nas amostras metamáficas do setor sul. As abreviações utilizadas nos gráficos de P-T são referentes aos nomes de fases minerais presentes no banco de dados do TWQ (1.02) indicados na Tabela 8.

Tabela 8: Abreviações de fases minerais segundo o TWQ 1.02.

Hd: hedenbergita	*Tsc: tschermakita*	*Parg: pargasita*	*Alm: almandina*	*Py: piropo*
Gr: grossulária	*Sph: titanita*	*Ilm: ilmenita*	*Rt: rutilo*	*Di: diopsídio*
W: H2O	*Qtz: quartzo*	*Jd: jadeíta*		

Tabela 9: Resultado dos cálculos geotermobarométricos para as rochas metamáficas (THERMOCALC-3.26)

Amostra	Assembléia	Cálculos P-T THERMOCALC								
WT7-25K	Grt+Amp+Cpx+Pl+Qtz	**T °C**	700	750	800	850	900	950	1000	**Av (P)**
		P.cal	12.4	12.7	13.1	13.5	13.9	14.3	14.7	13.50
		sd								0.64
		P	10	11	12	13	14	15	16	**Av (T)**
		T cal	706	706	706	705	705	704	703	705
		sd								
		Av (PT)	**P = 13.2 kbars**				**T = 776°C, sd = 55**			
RM-124B	Grt+Amp+Cpx+Pl+Qtz	**T °C**	750	775	800	825	850	875	900	**Av (P)**
		P.cal	11.8	11.7	11.7	11.6	11.6	11.5	11.5	11.69
		sd	1.06	0.86	0.67	0.53	0.57	0.60	0.85	0.67
		Pfixa	10.0	11.0	12.0	13.0	14.0	-	-	**Av (T)**
		T cal	838	836	834	831	827	-	-	834
		sd	33	31	31	32	32	-	-	31
		Av (PT)	**P = 11.2 kbars, sd = 0.6**				**T = 840°C, sd = 32**			
WT8-53E	Grt+Amp+Cpx+Pl+Qtz	**T °C**	700	725	750	775	800	-	-	**Av (P)**
		P.cal	11.5	11.5	11.5	11.6	11.6	-	-	11.53
		sd	1.49	1.17	0.86	0.61	0.62	-	-	0.86
		Pfixa	10.0	10.5	11.0	11.5	12.0	12.5	13.0	**Av (T)**
		T cal	718	721	725	728	731	735	738	728
		sd	36	36	36	36	36	36	36	36
		Av (PT)	**P = 13.0 kbars, sd = 1.6**				**T = 784°C, sd = 86**			
RM-182	Grt+Amp+Cpx+Pl+Qtz	**T °C**	700	720	740	760	780	800	-	**Av (P)**
		P.cal	11.6	11.7	11.9	12.0	12.2	12.3	-	12.04
		sd	0.53	0.54	0.59	0.79	0.99	1.19	-	0.79
		Pfixa	11.0	11.5	12.0	12.5	13.0	13.5	14.0	**Av (T)**
		T cal	755	762	768	774	781	787	794	774
		sd	49	44	42	43	46	52	59	43
		Av (PT)	**P = 12.3 kbars, sd = 1.1**				**T = 778°C, sd = 51**			
RM-220	Grt+Amp+Cpx+Pl+Qtz	**T °C**	750	775	800	825	850	-	-	**Av (P)**
		P.cal	12.1	12.3	12.4	12.6	12.8	-	-	12.42
		sd	0.58	0.53	0.55	0.67	0.87	-	-	0.55
		Pfixa	11.0	12.0	13.0	14.0	15.0	-	-	**Av (T)**
		T cal	801	804	808	812	816	-	-	808
		sd	61	53	46	42	41	-	-	46
		Av (PT)	**P = 12.4 kbars, sd = 0.9**				**T = 763°C, sd = 43**			
WT8-302	Grt+Amp+Cpx+Pl+Qtz	**T °C**	700	740	780	820	860	900	-	**Av (P)**
		P.cal	13.9	14.0	14.1	14.2	14.3	14.4	-	14.18
		sd	1.73	1.21	0.69	0.57	0.60	0.97	-	0.57
		Pfixa	13.0	13.5	14.0	14.5	15.0	15.5	16.0	**Av (T)**
		T cal	780	798	816	835	-	-	-	835
		sd	53	53	53	53	71	99	127	53
		Av (PT)	**P = 14.8 kbars, sd = 1.1**				**T = 824°C, sd = 57**			
TJF5-335A	Grt+Amp+Cpx+Pl+Qtz	**T °C**	800	825	850	875	900	-	-	**Av (P)**
		P.cal	14.5	14.9	15.4	15.8	16.2	-	-	15.37
		sd	0.64	0.58	0.63	0.80	1.02	-	-	0.63
		Pfixa	14.0	14.5	15.0	15.5	16.0	-	-	**Av (T)**
		T cal	807	817	828	838	848	-	-	828
		sd	24	21	20	21	25	-	-	20
		Av (PT)	**P = 15.0 kbars, sd = 0.8**				**T = 828°C, sd = 28**			

Tabela 10: Resultado dos cálculos geotermobarométricos para as rochas metassedimentares (THERMOCALC-3.26)

Amostra	Assembléia	Cálculos P-T THERMOCALC								
WT7-07	Grt+Bt+ Pl+Ky+Sill+Qtz	**T °C**	700	725	750	775	800	825	850	**Av (P)**
		P.cal	7.7	8.2	8.8	9.3	9.9	10.4	11.0	9.33
		sd	0.13	0.11	0.11	0.11	0.11	0.11	0.11	0.11
		P	8.0	8.5	9.0	9.5	10.0	10.5	11.0	**Av (T)**
		T cal	715	738	761	783	806	828	851	806
		sd	5	5	5	5	5	6	7	5
		Av (PT)	**P = 9.9 kbars, sd = 1.7**				**T = 803 °C, sd = 78**			
WT7-53A	Grt+Bt+fsp+ Sill+Qtz±Ky	**T °C**	-	-	-	-	-	-	-	**Av (P)**
		P.cal	-	-	-	-	-	-	-	
		sd	-	-	-	-	-	-	-	
		Pfixa	-	-	-	-	-	-	-	**Av (T)**
		T cal	-	-	-	-	-	-	-	
		sd	-	-		-	-	-	-	
		Av (PT)	**P = 11.0 kbars, sd = 1.3**				**T = 851°C, sd = 59**			
WT8-17	Grt+Bt+Pl+Ky+Qtz	**T °C**	700	725	750	775	800	825	850	**Av (P)**
		P.cal	9.5	9.9	10.3	10.8	11.2	11.6	12.1	11.20
		sd	0.55	0.57	0.58	0.60	0.61	0.63	0.64	0.86
		Pfixa	10.0	11.0	12.0	13.0	14.0	15.0	16.0	**Av (T)**
		T cal	731	746	762	777	793	808	823	777
		sd	0.2	0.0	0.2	0.3	0.5	0.7	0.9	61
		Av (PT)	**P = 10.1 kbars, sd = 1.5**				**T = 734 °C, sd = 77**			

10.1. Geotermobarometria metamáficas (PTMAFIC 2.0)

Para os cálculos de temperatura foi utilizado o geotermômetro granada-clinopiroxênio (Ellis & Green, 1979; Gangully, 1979) e para pressão o geobarômetro granada-clinopiroxêni-plagioclásio (Powell & Holland, 1988).

Foram calculadas quatro amostras representativas no PTMAFIC 2.0, sendo dois retroeclogitos do setor sul, um do setor central e um clinopiroxênio-granada anfibolito do setor norte. Para uma das amostras do afloramento TJF5-335 (Granada-clinopiroxênio anfibolito) diversas associações entre Cpx + Pl + Grt foram reconhecidas. No entanto, optou-se pelo piroxênio com a maior porcentagem da molécula jadeíta (~18 %) juntamente com o plagioclásio e o núcleo de granada que estavam em contato. Nas demais amostras (TJF5-335A-5spl), (WT8-302-9spl) e (WT7-251K), foi utilizada a composição da borda da granada e os simplectitos de Cpx+Pl na matriz. Os valores de temperatura e pressão estão sintetizados na Tabela 11.

Tabela 11: Resultado dos cálculos geotermobarométricos para as rochas metamáficas (PTMAFIC 2.0)

Geotermômetro (Grt-Cpx)	TJF5-335 Setor Sul	(WT8-302-9spl) Setor Sul	(TJF5-335-5spl) Setor Central	(WT7-251K) Setor Norte
Gangully (1979)	688.89 °C	664.25 °C	624.41 °C	585.02 °C
Ellis & Green (1979)	684.55 °C	652.34 °C	605.29 °C	495.38 °C
Geobarômetro (Grt-Pl-Cpx)	**TJF5-335**	**(WT8-302-9spl)**	**(TJF5-335-5spl)**	**(WT7-251K)**
Powell & Holland (1988)	17.22 ± 0.14 kbar	15.18 ± 1.6 kbar	13.89 ± 2.27 kbar	13.26 ± 3.43 kbar

Os resultados mostram uma boa correlação com o zoneamento do grau metamórfico em termos de pressão. As amostras situadas no setor sul apresentaram pressões mais elevadas com um máximo de 17,22 ± 0,14 kbar, enquanto no setor norte as condições máximas de pressão, embora sem boa precisão, estão na ordem de 13,26 ± 3,43 kbar.

Em relação aos dados de geobarometria calculados pelo THERMOCALC 3.26, os valores da amostra (TJF5-335 do setor sul) foram aproximadamente 2 kbar mais elevados, porém com alta precisão. As demais amostras (TJF5-335-5spl) setor sul, (WT8-302-9spl) e (WT7-25K1) do setor central e norte, respectivamente, apresentaram valores de pressão com boa correlação, bem próximos quando considerado o desvio padrão.

Por outro lado, os resultados da geotermometria apresentaram uma variação bem significativa e são bastante inferiores aos valores obtidos pelo THERMOCALC 3.26.

10.2. Estimativa do "pico metamórfico"

Foram realizados diversos cálculos no TWQ (1.02) com o objetivo de estimar as condições de pressão e temperatura, mais próximas do "pico" do metamorfismo para as rochas metamáficas da Faixa Eclogítica de Forquilha (FEF).

A amostra TJF5-335A que apresentou claramente duas parageneses de equilíbrio: uma representativa das condições de mais alto grau com a associação (i) núcleo de granada ($Py_{29.07\ \%}$) + clinopiroênio ($Jd_{18\%}$) + plagioclásio ($Ab_{83.30\%}$) + rutilo ± quartzo e outra formada pelo início

da quebra do clinopiroxênio e a geração de anfibólio sódico a partir da entrada de fluídos, representada pela associação (ii) núcleo da granada em contato com inclusões de anfibólio sódico + plagioclásio + clinopiroxênio + rutilo + titanita + quartzo.

A atividade de H_2O adotada para os cálculos termobarométricos foi de 0,8 e a atividade de CO_2 que forneceu os melhores valores foi estimada em $XCO_2 = 0,2$. Quando utilizado o *default* do programa, que assume atividade de H_2O e $CO_2 = 1$, as reações apresentam-se desequilibradas com valores de P-T superestimados.

A partir da associação (i) piropo + onfacita (jadeita) + albita + quartzo as condições de pressão e temperatura obtidas foram de 22 kbar e 750 °C (Figura 14 – Diagrama A). Outros cálculos, com variações nas escolhas dos membros finais das soluções sólidas, resultam nos intervalos de 22,9 a 18,5 kbar e 760 a 800 °C.

O início do estágio retrometamórfico é assumido a partir da quebra do clinopiroxênio e a consequente geração de anfibólio, nesta situação formada pela associação (ii) granada + onfacita + tschermakita + albita + rutilo + titanita + quartzo + H_2O o equilíbrio calculado foi de 20,7 kbar e 716 °C (Figura 14 – Diagrama B).

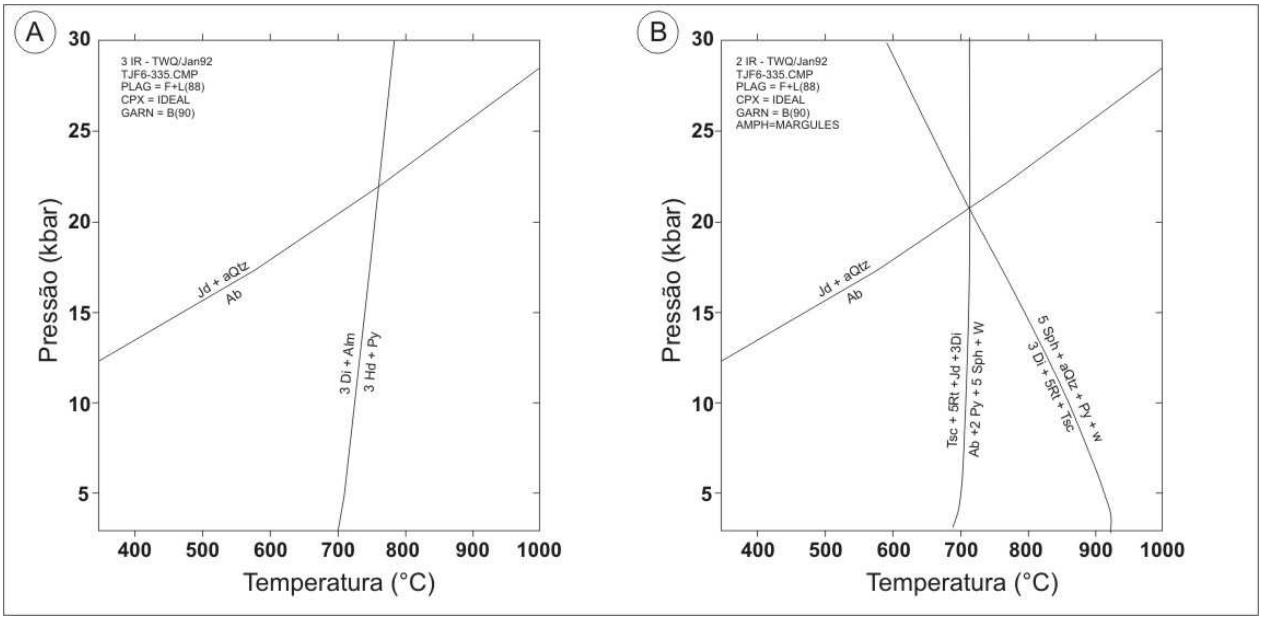

Figura 14: Diagramas P-T obtidos para a amostra TJF5-335 com o programa TWQ (1.02), utilizando as seguintes associações: a) piropo + onfacita (jadeíta) + albita + quartzo; b) granada + onfacita + tschermakita + albita + rutilo + titanita + quartzo, com $X_{H2O} = 0,8$ e $X_{CO2} = 0,2$.

11. DISCUSSÕES E CONCLUSÕES SOBRE A GEOTERMOBAROMETRIA E IMPLICAÇÕES TECTÔNICAS

Na tentativa de estabelecer as condições de P-T próximas ao equilíbrio de mais alto grau metamórfico, os cálculos termobarométricos utilizando diferentes métodos, priorizaram as amostras que apresentaram todas as evidências (campo, petrográficas - texturais, química mineral) de preservação dessas condições.

Cada método aplicado para o cálculo dos resultados revelou alguma diferença entre os valores finais de pressão e temperatura, explicadas pelo uso de diferentes calibrações de barômetros e termômetros embutidos em banco de dados internamente consistentes. Outra explicação remete a escolha de diferentes minerais para o cálculo de paragêneses em equilíbrio. Como ressaltado no início, os simplectitos formados pelo intercrescimento vermiforme de piroxênio e plagioclásio nas rochas metamáficas são extremamente finos, o que dificultou a aquisição de análises pontuais. Assim, um mesmo mineral pode apresentar diferentes teores nos elementos químicos e o posicionamento do feixe de elétrons nem sempre foi possível na borda e no centro de algumas associações.

Uma diferença notável dos dados foi verificada nos resultados de temperatura, principalmente nos cálculos realizados pelo THERMOCALC 3.26 que revelou valores relativamente altos (850 °C), tanto para as rochas metamáficas quanto para as metassedimentares, e os valores calculados pelo PTMAFIC 2.0 que, ao contrário, resultou em valores baixos para diferentes calibrações variando entre 495 e 688°C. Estudos utilizando bancos de dados termodinâmicos internamente consistentes chegam a bons resultados para pressão, no entanto falham na determinação das temperaturas (Zack *et al.,* 2004; Tomkins *et al.,* 2007). Novas alternativas para essas determinações geotermométricas são o geotermômetro de Zr no rutilo e a termometria com isótopos de oxigênio (O´Brien, 2006).

Por outro lado, os valores de temperatura obtidos com o TWQ 1.02 revelaram valores mais consistentes para o equilíbrio em condições da fácies eclogito situados entre 750°C e 800°C. Esses valores de temperatura também são coerentes com aqueles obtidos por Santos *et al.* (2009) em retroeclogitos da mesma região (~770°C) e com metabasitos de alto grau da região de Itatira (~750°C) (Castro, 2004, Garcia *et al.,* 2006).

A geobarometria apresentou pressões com valores muito coerentes entre os diferentes programas de computador utilizados. Os valores obtidos na fase inicial dos estudos permitiram constatar o zoneamento metamórfico de norte para sul ao longo da FEF. Deste modo os resultados obtidos no THERMOCALC, mostraram pressões mínimas de 11,2 kbar e máximas de 15,00 kbar para as rochas metamáficas e 9,9 kbar e 11 kbar para as rochas metassedimentares. Neste caso, deve se ressaltar que o equilíbrio máximo em 15 kbar verificado nas metamáficas foi obtido considerando as seguintes assembléias minerais: granada + clinopiroxênio + plagioclásio + anfibólio, ou seja, esse valor reflete um equilíbrio em condições retrometamórficas com a presença de auréola de anfibólio na granada como descrito nos estudos petrográficos em anexo.

Os valores de pressão calculados para as metamáficas no PTMAFIC 2.0 se mostraram mais realistas. As quatro amostras selecionadas de sul para norte revelaram pressões, respectivamente de 17,22 ± 0,14 kbar, 15,18 ± 1,6 kbar, 13,89 ± 2,27 kbar e 13,26 ± 3,43 kbar. Esses valores coadunam-se com as pressões obtidas por Santos *et al.* (2009) e Castro (2004) em rochas metamáficas de alto grau no DCC.

A partir da análise de uma paragênese formada por relictos de onfacita + albita + piropo ± quartzo, identificada na amostra do retroeclogito TJF5-335A1, pode-se estimar pressões que variam entre 22 e 19 kbar e temperaturas entre 700 e 800 °C. Esses valores foram calculados no TWQ 1.02, embora o número de reações encontradas nesses intervalos seja relativamente pequeno (Figura 14). Diversos outros diagramas foram obtidos com valores similares a esses, quando consideradas as assembléias de alto grau em paragênese.

A identificação de anfibólio verde azulado com altos teores de Na_2O (~4,15 %) como inclusão na granada poderia representar uma fase progressiva do metamorfismo. Entretanto, nenhuma evidência da passagem dos retroeclogitos pela fácies xisto azul foi constatada nos estudos petrográficos. Qualquer registro da evolução progressiva do metamorfismo nessas rochas é especulativo, uma vez que a idade do protólito remete ao Mesoproterozóico (~1,57 Ga) e processos de hidrotermalismo verificados nos estudos de geoquímica (Amaral *et al.,* 2010a) sugerem que essas rochas metamáficas possam ter passado por diversos processos metamórficos. Texturas em atol e mais de uma geração de granada (Figura 2), além de complexas variedades de simplectitos na matriz dos retroeclogitos também reforçam essa hipótese.

Estudos complementares de geotermobarometria com balanços de massa (pseudoseções) para a definição da influência da composição da rocha nos cálculos fazem-se necessários para o refinamento dos dados.

A caracterização de uma zona de sutura no Domínio Ceará Central e a consequente exumação das rochas de alto grau metamórfico não é uma tarefa fácil de ser estabelecida. A ausência de xistos azuis e a superposição do metamorfismo nos retroeclogitos da FEF dificultam ainda mais a definição de quais os mecanismos responsáveis pela exumação das rochas de alta pressão. Entretanto, algumas evidências de campo como ressaltado no início deste capítulo, aliados aos dados de geocronologia obtidos neste estudo, sugerem algumas considerações sobre um possível modelo para explicar a exumação das rochas de alto grau da infra-estrutura.

Trabalhos de mapeamento geológico de detalhe realizados na FEF revelaram que a lineação de estiramento (Lx) definida pelo alinhamento de biotita, sillimanita e cianita, varia progressivamente de leste para oeste. Próximo ao arco magmático de Santa Quitéria, a estruturação é balizada por um sistema de cavalgamentos marcados por planos de empurrão (Sn) de baixo ângulo (25-35°) onde está contida (L_x) com caimento *down dip* para E-ESE. À medida que se avança para oeste, a intensidade do mergulho dos planos de empurrão aumenta, exibindo ângulos de médio (45º) a alto ângulo (65º) de mergulho e (Lx) torna-se oblíqua, com caimento para S-SE.

Indicadores cinemáticos como porfiroblastos de granadas rotacionados, porfiroblastos de álcali-feldspatos, dobras e estruturas S/C observados principalmente nas rochas metassedimentares de alto grau, indicam claramente movimentos de topo para W-NW. Isto sugere que tanto as metamáficas quanto as rochas metassedimentares foram alçadas da infra-estrutura por um sistema de falhas de empurrão ou por falhas reversas que atuaram mais intensamente durante uma provável ruptura da crosta oceânica subductada.

Esta hipótese pode ser explicada pelo mecanismo de *slab breakoff* (Davies & Blanckenburg, 1995) que se encaixa nesta porção do Domínio Ceará Central onde ocorre expressivo volume de magmas com afinidade cálcio-alcalina de alto-K representados em parte por granodioritos, granitóides porfiríticos e migmatitos pertencentes ao arco magmático de Santa Quitéria – AMSQ (Fetter, 1999, Fetter *et al.,* 2003, Costa *et al.,* 2010), o lineamento Transbrasiliano, um potencial marcador da zona de sutura neoproterozóica, as rochas de alto grau

metamórfico que bordejam toda porção oeste do AMSQ, e os granulitos máficos e félsicos de alta pressão contíguos ao lineamento na região de Cariré (Anexo1).

A ruptura da crosta é marcada pelo relaxamento da compressão e pela ascensão da astenosfera, podendo causar distúrbios no manto litosférico e como consequência gerar a fusão parcial e induzir o metamorfismo de alta temperatura (Davies & Blanckenburg, 1995, Ernst *et al.,* 1997, Rolland *et al.,* 2001, Liou *et al.,* 2002, Mahéo *et al.,* 2009).

O metamorfismo da fácies granulito, tanto na região de Cariré quanto na FEF, foi datado em zircão de granulitos máficos em 613 e 615 Ma (Amaral *et al.,* 2008, Amaral *et al.,* 2010b, Amaral *et al.,* 2010c) (Anexos 1 e 3). Arthaud (2008) obteve em monazita de fundidos leucossomáticos de migmatitos da região de Itatira, idades U-Pb concordantes entre 607 e 612 Ma e também interpretou essas idades como o metamorfismo de baixa/média pressão e alta temperatura. Com base nos dados acima, estima-se que a ruptura da crosta oceânica tenha sido contemporânea ao metamorfismo de alta temperatura e a fusão parcial, registrado em granulitos e migmatitos do Domínio Ceará Central.

Zonas de cisalhamento transcorrentes destrais e sinistrais de direção N-S e NNE-SSW, são marcadas por foliação de alto ângulo (S_{n+1}) e lineação de estiramento mineral (L_{x+1}) de caráter direcional a oblíqua, definida por quartzo e muscovita. Por vezes, (S_{n+1}) e (L_{x+1}) obliteram a foliação primária (S_n) o que caracteriza um evento estrutural posterior, porém de natureza progressiva. Estudos geocronológicos mostram que o desenvolvimento das principais zonas de cisalhamento transcorrente, na porção norte da Província Borborema, ocorreu entre 575 e 520 Ma (Vauchez *et al.*, 1995, Monie *et al.,*1997, Fetter, 1999, Cunha, 2007).

Assim, o mecanismo de *slab-breakoff* é apenas um dos processos responsáveis pela exumação das rochas de alto grau da FEF. Estudos mais detalhados da ocorrência e dos tipos das rochas metamáficas e metaultamáficas, aliados a dados de geotermobarometria de maior precisão, com o controle dos distintos estágios metamórficos, utilizando, por exemplo, pseudoseções, mapas composicionais de granada, termometria de zircão (zircônio) em rutilo e principalmente estudos estruturais e microestruturais mais específicos, irão auxiliar na caracterização de um cenário mais preciso da história metamórfica nesta região do Domínio Ceará Central.

12. REFERÊNCIAS BIBLIOGRÁFICAS

Amaral, W.S., Nogueira Neto, J.A., Santos, T.J.S., Fetter, A.H., Arthaud, M.H. 2008. Faixa Granulítica de Cariré, Domínio Ceará Central (DCC): Idades Modelo Sm-Nd, Lu-Hf e U-Pb (zircões) e Contexto Geológico. 44° Congresso Brasileiro de Geologia, Curitiba PR, p. 17.

Amaral, W.S, Santos, T.J.S., Wernick, E. 2010a. Occurrence and geochemistry of metamafic rocks from the Forquilha Eclogite Zone, central Ceará (NE Brazil): Geodynamic implications. *(Special Issue) Geological Journal* (DOI: 10.1002/gj.1224).

Amaral, W. S. ; Santos, T. J. S. ; Wernick, E. ; Nogueira Neto, J. A. ; Matteini, M. ; Dantas, E. L. 2010b. Gênese e evolução dos granulitos de Cariré - NW do Domínio Ceará Central, Província Borborema. 45 Congresso Brasileiro de Geologia, Belém-PA. Anais (CD-ROM).

Amaral, W. S. ; Santos, T. J. S. ; Wernick, E. ; Matteini, M. ; Dantas, E. L. ; Moreto, C. P. N. 2010c. U-Pb, Lu-Hf and Sm-Nd geochronology of rocks from the Forquilha Eclogite Zone, Ceará Central Domain, Borborema Province, NE-Brazil. *VII-SSAGI South American Symposium on Isotope Geology,* Brasília-DF (CD-ROM).

Ancelmi, M.F. 2008. Cartografia de detalhe das rochas metabásicas de alta pressão da região de Forquilha-CE, NW da Província Borborema. Trabalho de conclusão de curso Instituto de Geociências UNICAMP, 62 p.

Arthaud, M.H. 2008. Evolução neoproterozóica do Grupo Ceará (Domínio Ceará Central, NE Brasil): da sedimentação à colisão continental brasiliana. Tese de Doutorado, Instituto de Geociências, Universidade de Brasília, Brasil.

Berman, R.G., 1991. Thermobarometry using multi-equilibrium calculations: a new technique, with petrological applications. The Canadian Mineralogist 29, 833-855

Cawthorn, R. G.; Collerson, K. D. 1974. The recalculation of pyroxene end member parameters and the estimation of ferrous and ferric iron content from electron microprobe analyses. American Mineralogist, Lancaster **59:** 1203-1208

Castro, N.A. 2004. *Evolução geológica proterozóica da região entre Madalena e Taperuaba, domínio tectônico Ceará Central (Província Borborema).* Tese de Doutorado, Universidade de São Paulo, Brasil.

Cunha, F.S.S. 2007. Condicionamento Estrutural das zonas de cislhamento da região de Forquilha, Domínio Ceará Central: uma abordagem integrada de sensoriamento remoto e geologia estrutural. Tese de Doutorado, Centro de Ciências exatas e da Terra, Universidade Federal do Rio Grande do Norte.

Davies, J.H. & Von Blanckenburg, F. 1995. Slab breakoff: a model of lithosphere detachment and its test in the magmatism and deformation of collisional orogens. *Earth Planet. Sci. Lett.*, **129**, 85 102.

Deer, W. A.; Howie, R. A.; Zussman, J. 1992. An introduction to the rock-forming minerals. 2. ed. Harlow, Essex; New York: Longman Scientific & Technical: Wiley, 696 p.

Ellis, D. J., Green, D. H., 1979. An experimental study of the effect of Ca upon garnet-clinopyroxene Fe-Mg exchange equilibria. *Contrib. Mineral. Petrol.* **71: 13-22.**

Ernst, W.G., Maruyama, S., Wallis, S., 1997. Buoyancy-driven, rapid exhumation of ultrahigh-pressure metamorphosed continental crust. *Proceedings of the National Academy of Sciences* **94:** 9532-9537.

Fetter, A.H. 1999. *U–Pb and Sm–Nd Geochronological constraints on the crustal framework and geological history of Ceará State, NW Borborema Province, NE Brazil: implications for the assembly of Gondwana.* Ph.D. Thesis, University of Kansas.

Ganguly, J. 1979. Garnet and clinopyroxene solid solutions, and geothermometry based on Fe-Mg distribution coefficient. *Geoch. Cosm. Acta* **43:** 1021-1029.

Garcia, M.G,M., Arthaud, M.H., Santos, T.J.S., Nogueira Neto, J.A. 2006. Retroeclogitos nas nappes brasilianas do Domínio Ceará Central, Província Borborema: dados texturais e termobarométricos preliminares. 43 Congresso Brasileiro de Geologia, Aracajú-SE Anais p.23.

Holland T.J.B. & Powell R. 1998. An Internally Consistent Thermodynamic Data Set For Phases of Petrological Interest. *Journal of Metamorphic Geology* **16:** 309-343.

Liou, J. G., Zhang, R. Y., Katayama, I., Maruyama, S., Ernst, W. G. 2002. Petrotectonic characterization of the Kokchetav Massif and the Dabie-Sulu terranes ultrahigh-P metamorphism in the so-called forbidden zone: *Western Pacific Earth Sciences*, **2:** 119-148

Mahéo, G., Guillot, S., Blichert-Toft, J., Rolland, Y.Pêcher, A. 2009. Partial Melting of Mantle and Crustal Sources beneath South Karakorum, Pakistan: Implications for the Miocene Geodynamic Evolution of the India–Asia Convergence Zone. Journal of Petrology **50:** 437-449.

Morimoto, N., Ferguson, A.K., Ginzburg, LV., Ross M., Seifert, F.A., Seifert, J. Seifert, Z., Aoki K., Gottardi, G. 1988. Nomenclature of pyroxenes, *American Mineralogist* **73:** 1123-1133.

Monié, P., Caby, R., Arthaud, M.H. 1997. The Neoproterozoic Brasiliano Orogeny in Northeast Brazil: $^{40}Ar/^{39}Ar$ and petrostructural data from Ceará, *Precambrian Research,* **81:** 241-264.

O´Brien, P.J., 2006. Type-locality granulites: high-pressure rocks formed at eclogites-facies conditions. *Mineralogy and Petrology* **86:** 161-175.

Powell, R., Holland, T. J. B. 1988. An internally consistent dataset with uncertainties and correlations: 3. Applications to geobarometry, worked examples and a computer program. *Journal of metamorphic Geology* **6:** 173-204.

Reginato, R.A. 2009. Petrografia das rochas metabásicas de alta pressão do Domínio Ceará Central, Província Borborema, nordeste do Brasil. Trabalho de conclusão de curso – Instituto de Geociências UNICAMP, 74 p.

Richard, L. R.; Clarke, D. 1990. Amphibol: a program for calculating structural formulae and for classifying and plotting analyses of Amphiboles. *American Mineralogist* **75:** 421-423.

Richard, L. R. 1995. Mineralogical and petrological data processing system. Minpet for Windows, version 2.02. MinPet Geological Software, Canada.

Robinson, P.; Spear, F. S.; Schumacher, J. C.; Laird, J.; Klein, C.; Evans, B. W.; Doolan, B. L. 1982. Phase relations of metamorfic amphiboles: natural occurrence and theory. *Reviews in Mineralogy* **9B:** 1-228.

Rolland, Y., Mahéo, G., Guillot, S., Pêcher, A. 2001. Tectonometamorphic evolution of the Karakorum Metamorphic Complex (Dassu-Askole area, NE Pakistan): exhumation of mid-crustal HT-MP gneisses in a convergent context. Journal of Metamorphic Geology **19**: 717-737.

Santos, T.J.S., Garcia, M.G.M., Amaral, W.S., Caby, R., Wernick, E., Arthaud, M.H., Dantas, E.L., Santosh, M. 2009. Relics of eclogite facies assemblages in the Ceará Central Domain, NW Borborema Province, NE Brazil: Implications for the assembly of West Gondwana. *Gondwana Research,* **15:** 454-470.

Soto, J.I, Soto, V.M. 1995. PTMAFIC: Software package for thermometry, barometry, and activity calculations in mafic rocks using an IBM-compatible computer. *Computers & Geosciences* **21:** 619-652.

Tomkins, H.S., Powell, R., Ellis, D.J. 2007. The pressure dependence of the zirconium-in-rutile thermometer. Journal of metamorphic geology **25:** 703-713.

Yoder Jr., H. S.; Tilley, C. E. 1962. Origin of basalt magmas: an experimental study of natural and synthetic rock systems. *Journal of Petrology* **3:** 342-534.

Vauchez, A., Neves, S., Caby, R., Corsini, M., Egydio-Silva, M., Arthaud, M.H., Amaro, V.1995. The Borborema shear zone system, NE Brazil. *Journal of South American Earth Sciences.*8:247-266.

Análises de química mineral

Microssonda eletrônica

Clinopirôxenio, granada, anfibólio, feldspato, biotita

Analyses of clinopyroxene from the Ceará Central high-pressure mafic rocks.

Sample	**RM-124B**	**RM-124B**	**RM-124B**	**RM-124B**	**RM-182**	**RM-182**	**RM-182**	**RM-182**	**RM-182**	**RM-182**	**RM-182**	**RM-182**	**RM-220**	**RM-220**
Location	1spl	3spl	4spl	5spl	1spl	10spl	10spl 2	2cntPlspl	3spl	4cont Pl	7spl	8cont Pl	1spl	2spl
SiO_2	52.70	52.36	52.38	51.98	52.90	52.54	53.02	52.92	52.45	53.02	52.67	52.68	51.44	52.12
TiO_2	0.12	0.04	0.13	0.19	0.11	0.10	0.08	0.07	0.12	0.11	0.04	0.07	0.33	0.37
Al_2O_3	1.84	1.13	1.42	1.94	1.45	1.83	1.77	1.46	2.22	1.81	1.69	1.41	2.43	2.30
FeO	8.89	8.52	8.69	8.30	8.47	8.52	9.21	9.02	8.64	8.83	7.98	9.58	10.78	10.74
Cr_2O_3	0.06	0.06	0.05	0.10	0.04	0.05	0.02	0.05	0.08	0.01	0.12	0.07	0.02	0.02
MnO	0.11	0.18	0.16	0.12	0.12	0.10	0.03	0.13	0.12	0.09	0.08	0.11	0.11	0.11
MgO	13.64	14.08	13.72	13.63	13.75	13.72	13.48	13.43	13.30	13.53	13.61	13.72	12.20	12.21
CaO	23.10	23.77	22.98	22.55	23.36	22.90	22.43	23.17	22.31	22.82	22.60	22.77	22.50	22.17
Na_2O	0.43	0.26	0.36	0.47	0.49	0.57	0.59	0.42	0.53	0.69	0.53	0.39	0.58	0.66
K_2O	0.01	0.01	0.01	0.00	0.00	0.00	0.00	0.00	0.00	0.00	0.00	0.00	0.01	0.00
Total	100.90	100.41	99.90	99.28	100.68	100.32	100.64	100.67	99.76	100.89	99.31	100.81	100.39	100.69
Si	1.94	1.94	1.95	1.94	1.95	1.94	1.96	1.96	1.96	1.95	1.97	1.95	1.92	1.94
Al	0.06	0.05	0.05	0.06	0.05	0.06	0.04	0.04	0.05	0.05	0.03	0.05	0.08	0.06
Ti	0.00	0.00	0.00	0.01	0.00	0.00	0.00	0.00	0.00	0.00	0.00	0.00	0.01	0.01
Fe^{3+}	0.06	0.08	0.05	0.05	0.06	0.07	0.04	0.04	0.02	0.06	0.02	0.06	0.07	0.04
Fe^{2+}	0.17	0.14	0.17	0.16	0.16	0.15	0.18	0.19	0.18	0.16	0.17	0.17	0.21	0.23
Cr	0.00	0.00	0.00	0.00	0.00	0.00	0.00	0.00	0.00	0.00	0.00	0.00	0.00	0.00
Mg	0.75	0.78	0.76	0.76	0.76	0.76	0.74	0.74	0.74	0.74	0.76	0.76	0.68	0.68
Mn	0.00	0.01	0.01	0.00	0.00	0.00	0.00	0.00	0.00	0.00	0.00	0.00	0.00	0.00
Ca	0.91	0.94	0.92	0.90	0.92	0.91	0.89	0.92	0.89	0.90	0.91	0.90	0.90	0.88
Na	0.03	0.02	0.03	0.03	0.04	0.04	0.04	0.03	0.04	0.05	0.04	0.03	0.04	0.05
K	0.00	0.00	0.00	0.00	0.00	0.00	0.00	0.00	0.00	0.00	0.00	0.00	0.00	0.00
Q	1.88	1.90	1.90	1.88	1.88	1.86	1.88	1.90	1.88	1.85	1.89	1.89	1.84	1.85
J	0.06	0.04	0.05	0.07	0.07	0.08	0.09	0.06	0.08	0.10	0.08	0.06	0.08	0.10
WO	47.04	47.40	46.91	46.90	47.48	47.01	46.34	47.29	46.82	46.95	47.26	46.06	46.90	46.55
EN	38.66	39.07	38.97	39.43	38.88	39.18	38.75	38.13	38.83	38.73	39.60	38.63	35.38	35.67
FS	14.30	13.53	14.12	13.67	13.64	13.81	14.91	14.58	14.35	14.32	13.14	15.31	17.72	17.78
WEF	96.81	98.05	97.33	96.48	96.44	95.81	95.68	96.92	96.06	94.98	96.13	97.13	95.64	95.12
JD	0.94	0.00	0.55	1.39	0.73	1.12	2.10	1.07	2.81	1.67	2.55	0.38	1.20	2.38
AE	2.25	1.96	2.12	2.13	2.83	3.07	2.22	2.02	1.13	3.34	1.32	2.50	3.16	2.50

Analyses of clinopyroxene from the Ceará Central high-pressure mafic rocks.

Sample	RM-220	RM-220	RM-220	RM-220	RM-220	RM-220	RM-220	RM-220	TJF5-335	TJF5-335	TJF5-335	TJF5-335A	TJF5-335A	TJF5-335A
Location	3spl	4spl	5spl	6spl	7spl	8spl	9spl	10spl	1spl	11spl	111spl	1spl	2spl	2spl 2
SiO2	51.37	52.34	51.27	50.76	51.80	51.49	51.66	50.90	51.53	52.27	50.99	51.22	51.69	52.72
TiO2	0.22	0.22	0.37	0.46	0.11	0.35	0.19	0.25	0.07	0.16	0.07	0.06	0.11	0.12
Al2O3	2.76	2.46	3.53	4.04	2.40	2.92	2.29	3.93	6.79	3.20	6.24	6.74	5.14	3.93
FeO	9.54	9.48	9.47	9.79	9.20	9.55	9.08	8.96	7.94	8.01	7.49	7.84	7.78	8.08
Cr2O3	0.01	0.07	0.03	0.00	0.00	0.00	0.00	0.00	0.00	0.00	0.01	0.00	0.00	0.01
MnO	0.03	0.06	0.06	0.03	0.05	0.06	0.06	0.07	0.09	0.07	0.04	0.03	0.04	0.09
MgO	12.56	12.87	12.26	11.84	12.77	12.68	12.85	12.46	11.08	12.97	11.78	11.44	12.29	12.60
CaO	22.79	22.94	22.59	23.18	23.36	23.39	22.77	22.56	20.55	21.53	20.31	20.36	21.20	21.49
Na2O	0.57	0.55	0.73	0.63	0.55	0.55	0.52	0.68	2.05	1.24	1.90	2.17	1.51	1.40
K2O	0.00	0.02	0.01	0.02	0.01	0.00	0.01	0.00	0.00	0.01	0.02	0.00	0.00	0.01
Total	99.84	101.01	100.31	100.74	100.24	100.98	99.44	99.82	100.10	99.46	98.85	99.86	99.75	100.45
Si	1.92	1.93	1.91	1.88	1.93	1.90	1.94	1.90	1.89	1.94	1.89	1.88	1.91	1.94
Al	0.08	0.07	0.09	0.12	0.07	0.10	0.06	0.10	0.11	0.06	0.11	0.12	0.09	0.06
Ti	0.01	0.01	0.01	0.01	0.00	0.01	0.01	0.01	0.00	0.00	0.00	0.00	0.00	0.00
Fe3+	0.07	0.05	0.06	0.08	0.08	0.09	0.05	0.07	0.06	0.06	0.07	0.10	0.06	0.05
Fe2+	0.19	0.19	0.19	0.20	0.18	0.18	0.19	0.16	0.14	0.14	0.11	0.10	0.13	0.15
Cr	0.00	0.00	0.00	0.00	0.00	0.00	0.00	0.00	0.00	0.00	0.00	0.00	0.00	0.00
Mg	0.70	0.71	0.68	0.66	0.71	0.70	0.72	0.69	0.61	0.72	0.65	0.63	0.68	0.69
Mn	0.00	0.00	0.00	0.00	0.00	0.00	0.00	0.00	0.00	0.00	0.00	0.00	0.00	0.00
Ca	0.91	0.91	0.90	0.92	0.93	0.93	0.91	0.90	0.81	0.86	0.81	0.80	0.84	0.85
Na	0.04	0.04	0.05	0.05	0.04	0.04	0.04	0.05	0.15	0.09	0.14	0.16	0.11	0.10
K	0.00	0.00	0.00	0.00	0.00	0.00	0.00	0.00	0.00	0.00	0.00	0.00	0.00	0.00
Q	1.84	1.86	1.81	1.80	1.85	1.83	1.86	1.80	1.60	1.76	1.62	1.57	1.69	1.74
J	0.08	0.08	0.11	0.09	0.08	0.08	0.08	0.10	0.29	0.18	0.27	0.31	0.22	0.20
WO	47.75	47.50	47.97	48.98	48.31	48.19	47.65	48.04	48.65	46.92	47.71	47.99	47.74	47.34
EN	36.61	37.08	36.23	34.81	36.75	36.35	37.41	36.94	36.50	39.34	38.49	37.53	38.51	38.61
FS	15.64	15.42	15.80	16.20	14.94	15.46	14.94	15.02	14.84	13.74	13.80	14.48	13.75	14.05
WEF	95.70	95.91	94.50	95.23	95.92	95.91	96.14	94.86	84.62	90.82	85.57	83.60	88.66	89.76
JD	1.62	1.77	2.67	2.11	1.19	1.05	1.58	2.59	11.76	5.28	10.00	10.60	7.75	7.21
AE	2.67	2.32	2.83	2.66	2.89	3.04	2.28	2.55	3.62	3.91	4.43	5.80	3.58	3.03

Analyses of clinopyroxene from the Ceará Central high-pressure mafic rocks.

Sample	**TJF5-335A**	**TJF5-335A**	**TJF5-335A**	**TJF5-335B**	**TJF5-335B**	**TJF5-335B**	**TJF5-335B**	**TJF5-335B**	**TJF5-335B**	**WT7-25K**	**WT7-25K**	**WT7-25K**
Location	2spl 3	4spl	5spl	1spl	2spl	4spl	5spl	6spl	6spl 2	1incl Pl	10spl	11spl
SiO_2	52.72	52.92	52.84	53.06	53.60	53.28	52.36	52.48	52.61	52.23	52.00	50.99
TiO_2	0.13	0.21	0.36	0.16	0.02	0.00	0.05	0.17	0.22	0.11	0.00	0.24
Al_2O_3	2.37	3.57	5.81	1.45	1.24	1.37	1.76	2.16	2.13	1.58	2.09	3.48
FeO	8.08	8.21	5.95	10.07	10.39	10.61	10.42	9.82	9.74	10.94	11.43	12.37
Cr_2O_3	0.04	0.00	0.03	0.00	0.04	0.03	0.00	0.00	0.02	0.02	0.03	0.00
MnO	0.07	0.12	0.03	0.16	0.12	0.12	0.11	0.15	0.13	0.10	0.13	0.11
MgO	13.20	12.90	12.12	12.97	13.05	12.82	12.71	12.81	12.60	12.05	12.10	11.61
CaO	21.57	20.57	18.69	22.12	22.50	22.09	21.40	22.29	22.13	22.56	22.08	21.20
Na_2O	1.04	1.56	2.33	0.54	0.43	0.54	0.56	0.69	0.58	0.61	0.67	0.79
K_2O	0.00	0.00	0.00	0.01	0.00	0.00	0.00	0.00	0.00	0.01	0.00	0.02
Total	99.21	100.04	98.16	100.54	101.38	100.85	99.37	100.57	100.17	100.21	100.53	100.81
Si	1.97	1.95	1.97	1.97	1.98	1.98	1.97	1.95	1.96	1.96	1.94	1.90
Al	0.03	0.05	0.04	0.03	0.02	0.02	0.03	0.05	0.04	0.04	0.06	0.10
Ti	0.00	0.01	0.01	0.00	0.00	0.00	0.00	0.01	0.01	0.00	0.00	0.01
Fe^{3+}	0.03	0.04	0.00	0.02	0.01	0.02	0.02	0.05	0.01	0.05	0.07	0.09
Fe^{2+}	0.16	0.14	0.10	0.22	0.23	0.23	0.22	0.19	0.23	0.24	0.22	0.20
Cr	0.00	0.00	0.00	0.00	0.00	0.00	0.00	0.00	0.00	0.00	0.00	0.00
Mg	0.73	0.71	0.67	0.72	0.72	0.71	0.71	0.71	0.70	0.67	0.67	0.65
Mn	0.00	0.00	0.00	0.01	0.00	0.00	0.00	0.01	0.00	0.00	0.00	0.00
Ca	0.86	0.81	0.75	0.88	0.89	0.88	0.86	0.89	0.89	0.91	0.88	0.85
Na	0.08	0.11	0.17	0.04	0.03	0.04	0.04	0.05	0.04	0.04	0.05	0.06
K	0.00	0.00	0.00	0.00	0.00	0.00	0.00	0.00	0.00	0.00	0.00	0.00
Q	1.82	1.73	1.60	1.89	1.92	1.90	1.89	1.85	1.88	1.87	1.84	1.79
J	0.15	0.22	0.34	0.08	0.06	0.08	0.08	0.10	0.08	0.09	0.10	0.12
WO	46.59	45.69	46.47	45.94	46.06	45.73	45.24	46.54	46.72	47.05	46.06	45.01
EN	39.67	39.87	41.93	37.48	37.16	36.94	37.38	37.21	37.01	34.98	35.11	34.30
FS	13.74	14.45	11.60	16.58	16.78	17.34	17.38	16.25	16.27	17.98	18.84	20.69
WEF	92.40	88.62	82.70	96.03	96.92	96.09	95.88	94.90	95.72	95.48	94.98	93.99
JD	5.34	8.04	17.30	2.60	2.18	2.56	3.09	2.28	3.70	1.50	1.56	2.25
AE	2.26	3.35	0.00	1.37	0.90	1.35	1.03	2.82	0.58	3.03	3.45	3.76

Analyses of clinopyroxene from the Ceará Central high-pressure mafic rocks.

Sample	WT7-25K	WT7-25K	WT7-25K	WT7-25K	WT7-25K	WT7-25K	WT7-25K	WT7-25K	WT7-25K	WT7-25K	WT7-25K	WT7-25K
Location	14	15	16	18rim	19	2incl Pl	matrix	3incl Pl	4incl Pl	5incl Pl	7	7rep
SiO2	52.19	51.98	52.17	51.44	51.54	51.81	51.69	51.83	51.79	51.73	50.82	51.33
TiO2	0.10	0.17	0.04	0.17	0.25	0.13	0.13	0.23	0.11	0.07	0.08	0.20
Al2O3	1.34	1.66	1.60	2.02	2.52	1.84	1.73	1.66	1.88	2.19	2.91	3.19
FeO	11.00	11.36	10.32	10.91	11.23	10.92	10.79	10.57	10.69	11.58	10.62	11.01
Cr2O3	0.03	0.00	0.06	0.02	0.05	0.05	0.33	0.02	0.00	0.00	0.02	0.07
MnO	0.10	0.12	0.10	0.13	0.10	0.14	0.10	0.09	0.11	0.13	0.12	0.09
MgO	12.23	11.92	12.50	11.77	11.68	11.72	11.81	12.11	12.05	11.59	11.32	11.57
CaO	23.25	22.72	22.61	21.72	22.26	22.25	22.40	22.51	22.54	21.89	22.02	22.50
Na2O	0.57	0.61	0.58	0.76	0.84	0.71	0.67	0.63	0.64	0.73	0.88	0.85
K2O	0.02	0.00	0.00	0.00	0.00	0.01	0.02	0.00	0.02	0.01	0.02	0.00
Total	100.84	100.53	99.97	98.94	100.46	99.57	99.68	99.64	99.82	99.91	98.82	100.82
Si	1.94	1.94	1.95	1.95	1.93	1.95	1.95	1.95	1.95	1.95	1.93	1.91
Al	0.06	0.06	0.05	0.05	0.08	0.05	0.05	0.05	0.06	0.05	0.07	0.09
Ti	0.00	0.01	0.00	0.01	0.01	0.00	0.00	0.01	0.00	0.00	0.00	0.01
Fe3+	0.09	0.07	0.06	0.05	0.08	0.05	0.06	0.06	0.07	0.06	0.08	0.09
Fe2+	0.23	0.24	0.22	0.23	0.22	0.25	0.24	0.23	0.23	0.25	0.22	0.21
Cr	0.00	0.00	0.00	0.00	0.00	0.00	0.01	0.00	0.00	0.00	0.00	0.00
Mg	0.68	0.67	0.70	0.67	0.65	0.66	0.66	0.68	0.68	0.65	0.64	0.64
Mn	0.00	0.00	0.00	0.00	0.00	0.00	0.00	0.00	0.00	0.00	0.00	0.00
Ca	0.93	0.91	0.91	0.88	0.89	0.90	0.91	0.91	0.91	0.88	0.89	0.90
Na	0.04	0.05	0.04	0.06	0.06	0.05	0.05	0.05	0.05	0.05	0.07	0.06
K	0.00	0.00	0.00	0.00	0.00	0.00	0.00	0.00	0.00	0.00	0.00	0.00
Q	1.86	1.86	1.87	1.84	1.81	1.85	1.85	1.86	1.85	1.84	1.79	1.79
J	0.08	0.09	0.09	0.11	0.12	0.10	0.10	0.09	0.09	0.11	0.13	0.12
WO	47.52	47.07	46.98	46.49	47.00	47.15	47.32	47.22	47.23	46.42	47.70	47.60
EN	34.78	34.37	36.12	35.06	34.32	34.55	34.72	35.34	35.12	34.20	34.13	34.07
FS	17.71	18.57	16.90	18.45	18.68	18.29	17.96	17.44	17.65	19.38	18.17	18.33
WEF	95.77	95.43	95.66	94.29	93.73	94.69	94.99	95.31	95.20	94.52	93.30	93.61
JD	0.10	0.85	1.22	2.47	1.87	2.11	1.50	1.40	1.42	2.31	2.85	2.21
AE	4.13	3.72	3.12	3.25	4.40	3.19	3.51	3.30	3.39	3.17	3.86	4.17

Analyses of clinopyroxene from the Ceará Central high-pressure mafic rocks.

Sample	WT8-302	WT8-302	WT8-302	WT8-302	WT8-302	WT8-302	WT8-302	WT8-302	WT8-302	WT8-302	WT8-302	WT8-302	WT8-53E	WT8-53E
Location	10spl	11spl	12spl	13spl	2spl	3spl	4spl	5spl	6spl	7spl	8spl	9spl	1spl	1repspl
SiO_2	52.03	53.20	51.46	52.07	53.13	53.37	53.23	52.22	52.49	52.64	51.40	51.82	54.17	52.45
TiO_2	0.23	0.10	0.63	0.13	0.09	0.24	0.21	0.10	0.44	0.36	0.22	0.38	0.31	0.09
Al_2O_3	3.92	1.69	3.89	3.68	1.45	1.91	2.02	2.02	2.63	2.40	3.37	4.11	2.53	1.48
FeO	6.41	6.62	6.59	6.50	6.63	6.80	6.52	6.63	7.16	7.22	7.32	6.65	8.34	8.18
Cr_2O_3	0.13	0.33	0.15	0.09	0.07	0.34	0.25	0.11	0.08	0.12	0.16	0.13	0.09	0.08
MnO	0.05	0.10	0.07	0.08	0.06	0.08	0.06	0.10	0.06	0.09	0.11	0.13	0.04	0.11
MgO	14.02	14.46	14.36	13.89	15.00	14.61	14.70	14.53	14.37	14.22	14.14	14.04	13.34	13.94
CaO	22.43	23.16	21.91	22.53	23.48	22.91	22.62	22.81	22.97	23.20	22.43	22.47	22.53	23.11
Na_2O	0.81	0.58	0.78	0.86	0.44	0.64	0.63	0.60	0.67	0.67	0.73	0.95	0.52	0.50
K_2O	0.00	0.00	0.00	0.00	0.01	0.02	0.02	0.00	0.00	0.00	0.00	0.00	0.02	0.02
Total	100.03	100.24	99.85	99.83	100.35	100.91	100.25	99.12	100.87	100.92	99.87	100.68	101.90	99.95
Si	1.91	1.96	1.90	1.92	1.95	1.95	1.96	1.94	1.92	1.93	1.90	1.89	1.98	1.95
Al	0.09	0.04	0.11	0.08	0.05	0.05	0.04	0.06	0.08	0.07	0.10	0.11	0.02	0.05
Ti	0.01	0.00	0.02	0.00	0.00	0.01	0.01	0.00	0.01	0.01	0.01	0.01	0.01	0.00
Fe^{3+}	0.05	0.04	0.06	0.06	0.06	0.04	0.03	0.07	0.07	0.07	0.10	0.08	0.00	0.07
Fe^{2+}	0.09	0.13	0.07	0.10	0.10	0.12	0.11	0.10	0.10	0.11	0.07	0.07	0.18	0.14
Cr	0.00	0.01	0.00	0.00	0.00	0.01	0.01	0.00	0.00	0.00	0.01	0.00	0.00	0.00
Mg	0.77	0.79	0.79	0.76	0.82	0.80	0.81	0.81	0.78	0.78	0.78	0.76	0.73	0.77
Mn	0.00	0.00	0.00	0.00	0.00	0.00	0.00	0.00	0.00	0.00	0.00	0.00	0.00	0.00
Ca	0.88	0.91	0.87	0.89	0.92	0.90	0.89	0.91	0.90	0.91	0.89	0.88	0.88	0.92
Na	0.06	0.04	0.06	0.06	0.03	0.05	0.05	0.04	0.05	0.05	0.05	0.07	0.04	0.04
K	0.00	0.00	0.00	0.00	0.00	0.00	0.00	0.00	0.00	0.00	0.00	0.00	0.00	0.00
Q	1.80	1.88	1.80	1.80	1.89	1.86	1.87	1.85	1.84	1.84	1.80	1.77	1.86	1.87
J	0.12	0.08	0.11	0.12	0.06	0.09	0.09	0.09	0.10	0.10	0.10	0.13	0.07	0.07
WO	47.75	47.74	46.53	47.95	47.36	47.14	46.93	47.24	47.27	47.65	46.82	47.51	47.30	47.19
EN	41.51	41.45	42.42	41.12	42.10	41.82	42.42	41.88	41.14	40.64	41.07	41.30	38.97	39.60
FS	10.74	10.82	11.05	10.94	10.54	11.05	10.66	10.88	11.59	11.71	12.11	11.20	13.74	13.21
WEF	93.96	95.79	94.15	93.63	96.76	95.36	95.44	95.53	95.07	95.10	94.53	92.97	96.18	96.33
JD	3.85	2.00	3.10	3.74	0.59	2.16	2.82	1.35	1.64	1.51	1.71	3.22	3.82	0.49
AE	2.19	2.20	2.75	2.63	2.65	2.48	1.74	3.13	3.29	3.40	3.76	3.82	0.00	3.18

Analyses of clinopyroxene from the Ceará Central high-pressure mafic rocks.

Sample	**WT8-53E**	**WT8-53E**	**WT8-53E**	**WT8-53E**	**WT8-53E**	**WT8-53E**
Location	2spl	3spl	4spl	5spl	6spl	7spl
SiO_2	51.67	51.83	52.28	52.40	52.35	49.74
TiO_2	0.29	0.01	0.04	0.10	0.13	0.42
Al_2O_3	2.60	1.69	2.19	2.07	2.36	5.36
FeO	8.39	8.86	8.51	8.81	8.74	11.03
Cr_2O_3	0.01	0.02	0.00	0.09	0.09	0.10
MnO	0.11	0.12	0.10	0.12	0.11	0.13
MgO	13.34	13.43	13.42	13.65	13.56	13.64
CaO	22.50	22.52	23.08	22.85	22.73	18.46
Na_2O	0.65	0.52	0.53	0.53	0.60	0.90
K_2O	0.00	0.00	0.00	0.00	0.00	0.09
Total	99.57	99.01	100.13	100.61	100.67	99.88
Si	1.93	1.95	1.94	1.94	1.93	1.85
Al	0.07	0.05	0.06	0.06	0.07	0.15
Ti	0.01	0.00	0.00	0.00	0.00	0.01
Fe^{3+}	0.07	0.07	0.06	0.07	0.07	0.11
Fe^{2+}	0.15	0.16	0.16	0.15	0.15	0.04
Cr	0.00	0.00	0.00	0.00	0.00	0.00
Mg	0.74	0.75	0.74	0.75	0.75	0.76
Mn	0.00	0.00	0.00	0.00	0.00	0.00
Ca	0.90	0.91	0.92	0.90	0.90	0.73
Na	0.05	0.04	0.04	0.04	0.04	0.06
K	0.00	0.00	0.00	0.00	0.00	0.00
Q	1.84	1.87	1.86	1.86	1.85	1.72
J	0.09	0.08	0.08	0.08	0.09	0.13
WO	47.17	46.70	47.62	46.82	46.86	39.99
EN	38.92	38.76	38.51	38.91	38.90	41.13
FS	13.92	14.55	13.87	14.28	14.24	18.89
WEF	95.16	96.11	96.11	96.10	95.57	93.04
JD	1.85	0.92	1.42	1.06	1.48	2.88

Analyses of garnet from the Ceará Central high-pressure metamafic rocks.

Smple	**RM-124B**	**RM-124B**	**RM-124B**	**RM-124B**	**RM-124B**	**RM-124B**	**RM-124B**	**RM-124B**	**RM-124B**	**RM-124B**	**RM-182**	**RM-182**	**RM-182**	**RM-182**
Location	1core	2 rim c-Pl	2 rimAm	2 core	3 core	4 rim c-Pl	4 core	5 rim c-Pl	6 rim c-Pl	7 rim c-Pl	1 rim	1 core	1 rep core	2 rim-Pl
SiO_2	38.64	37.76	38.36	38.09	38.28	38.27	38.17	37.96	38.45	38.21	37.75	38.08	38.57	38.30
TiO_2	0.06	0.07	0.08	0.14	0.01	0.10	0.10	0.00	0.13	0.04	0.01	0.02	0.05	0.06
Al_2O_3	21.52	21.62	21.75	21.38	21.65	21.55	21.61	21.32	21.52	21.46	21.44	21.65	21.59	21.87
FeO	24.12	24.88	24.30	24.10	24.21	23.94	24.87	24.27	23.49	23.95	25.49	23.43	25.43	25.31
MnO	0.86	1.61	1.41	1.22	1.09	1.49	1.09	1.30	0.86	1.21	1.02	0.71	0.87	0.70
MgO	4.20	3.44	3.44	3.68	3.69	3.55	4.09	3.78	3.89	3.50	3.69	4.02	4.02	4.06
CaO	9.98	9.59	10.17	10.61	10.52	9.90	9.60	10.16	9.91	10.30	9.05	11.36	9.54	9.37
Total	99.38	98.97	99.51	99.22	99.44	98.80	99.53	98.80	98.25	98.66	98.46	99.27	100.06	99.67
Si	3.03	3.00	3.02	3.01	3.01	3.03	3.00	3.01	3.06	3.03	3.01	2.99	3.02	3.01
Al^{IV}	0.00	0.00	0.00	0.00	0.00	0.00	0.00	0.00	0.00	0.00	0.00	0.01	0.00	0.00
Al^{VI}	1.99	2.02	2.02	1.99	2.01	2.01	2.00	1.99	2.01	2.01	2.01	1.99	1.99	2.02
Ti	0.00	0.00	0.01	0.01	0.00	0.01	0.01	0.00	0.01	0.00	0.00	0.00	0.00	0.00
Fe^{2+}	1.58	1.65	1.60	1.59	1.59	1.59	1.63	1.61	1.56	1.59	1.70	1.54	1.66	1.66
Mg	0.49	0.41	0.40	0.43	0.43	0.42	0.48	0.45	0.46	0.41	0.44	0.47	0.47	0.48
Mn	0.06	0.11	0.09	0.08	0.07	0.10	0.07	0.09	0.06	0.08	0.07	0.05	0.06	0.05
Ca	0.84	0.82	0.86	0.90	0.89	0.84	0.81	0.86	0.84	0.88	0.77	0.96	0.80	0.79
Alm	53.29	55.39	54.12	52.98	53.38	53.85	54.57	53.52	53.41	53.69	57.03	51.08	55.65	55.92
Gross	28.26	27.34	29.02	29.88	29.71	28.52	27.00	28.71	28.85	29.59	25.95	31.74	26.76	26.52
Pyrope	16.54	13.65	13.67	14.43	14.49	14.24	16.02	14.86	15.77	13.97	14.72	15.60	15.67	16.00
Spess	1.92	3.63	3.19	2.71	2.43	3.39	2.42	2.91	1.98	2.76	2.31	1.57	1.92	1.56

Analyses of garnet from the Ceará Central high-pressure metamafic rocks.

Sample	**RM-182**	**RM-182**	**RM-182**	**RM-182**	**RM-182**	**RM-182**	**RM-182**	**RM-182**	**RM-182**	**RM-220**	**RM-220**	**RM-220**	**RM-220**	**RM-220**
Location	2 core	3 rim c-Pl	3 core	4 rim c-Pl	4 core	5 rim	5 core	6 rim c-Pl	6 core	1 rim	1core/rim	1 core	2 rim	3 rim Cp
SiO_2	38.52	38.16	38.23	38.57	38.36	38.47	38.63	38.49	38.88	38.57	38.30	38.60	38.59	37.73
TiO_2	0.08	0.13	0.07	0.10	0.08	0.13	0.27	0.00	0.22	0.00	0.09	0.10	0.10	0.02
Al_2O_3	21.66	21.58	21.71	21.95	21.72	21.38	21.44	21.77	21.59	21.82	21.90	21.54	21.75	21.25
FeO	22.33	25.31	24.09	24.94	25.06	24.83	23.69	25.72	22.72	24.79	25.93	24.69	23.59	24.83
MnO	0.64	0.86	0.58	0.82	0.33	0.60	0.92	0.87	0.64	0.46	0.41	0.56	0.43	0.54
MgO	4.06	3.43	3.98	3.79	3.43	4.06	4.29	3.72	4.20	4.37	3.45	3.69	3.47	2.94
CaO	11.38	9.63	10.37	9.33	10.25	9.56	9.92	9.24	11.16	8.98	9.96	10.07	11.90	11.83
Total	98.66	99.10	99.02	99.49	99.21	99.03	99.15	99.80	99.39	99.00	100.06	99.27	99.84	99.14
Si	3.04	3.02	3.01	3.03	3.03	3.04	3.04	3.03	3.04	3.04	3.00	3.04	3.02	2.99
Al^{IV}	0.00	0.00	0.00	0.00	0.00	0.00	0.00	0.00	0.00	0.00	0.00	0.00	0.00	0.01
Al^{VI}	2.01	2.01	2.02	2.03	2.02	1.99	1.99	2.01	1.99	2.03	2.02	2.00	2.00	1.97
Ti	0.01	0.01	0.00	0.01	0.01	0.01	0.02	0.00	0.01	0.00	0.01	0.01	0.01	0.00
Fe^{2+}	1.47	1.68	1.59	1.64	1.66	1.64	1.56	1.69	1.49	1.63	1.70	1.63	1.54	1.64
Mg	0.48	0.41	0.47	0.44	0.40	0.48	0.50	0.44	0.49	0.51	0.40	0.43	0.40	0.35
Mn	0.04	0.06	0.04	0.06	0.02	0.04	0.06	0.06	0.04	0.03	0.03	0.04	0.03	0.04
Ca	0.96	0.82	0.88	0.79	0.87	0.81	0.84	0.78	0.94	0.76	0.84	0.85	1.00	1.00
Alm	49.85	56.70	53.47	56.08	56.15	55.26	52.68	57.07	50.33	55.64	57.29	55.18	51.89	54.26
Gross	32.54	27.63	29.48	26.87	29.43	27.26	28.27	26.26	31.66	25.83	28.20	28.84	33.55	33.11
Pyrope	16.15	13.71	15.76	15.18	13.68	16.12	16.99	14.71	16.58	17.49	13.60	14.72	13.60	11.44
Spess	1.46	1.95	1.30	1.87	0.74	1.36	2.07	1.96	1.43	1.04	0.92	1.26	0.97	1.20

Analyses of garnet from the Ceará Central high-pressure metamafic rocks.

Sample	**RM-220**	**RM-220**	**RM-220**	**RM-220**	**RM-220**	**RM-220**	**TJF5-335**	**TJF5-335**	**TJF5-335**	**TJF5-335**	**TJF5-335**	**TJF5-335**	**TJF5-335**
Location	3 core	4 rim c Pl	4 core	6 rim c Pl	6 core	7 rim c Cp	1 rim c Am	10 core	11 core/rim	12 core/rim	13 rim/core	2 rim/core	3 rim/core
SiO_2	38.21	38.58	38.11	38.69	38.40	38.33	38.85	38.86	38.80	38.79	38.56	38.85	38.91
TiO_2	0.01	0.07	0.14	0.00	0.09	0.07	0.01	0.07	0.07	0.09	0.02	0.03	0.23
Al_2O_3	21.67	21.49	21.59	21.32	21.77	21.25	22.07	22.06	22.23	22.03	22.17	22.14	21.86
FeO	24.75	23.62	25.49	24.68	24.56	25.98	25.32	25.34	25.99	25.14	24.35	25.97	25.69
MnO	0.41	0.52	0.52	0.50	0.46	0.68	0.29	0.25	0.16	0.30	0.23	0.35	0.33
MgO	3.98	3.26	3.66	2.92	3.71	2.88	5.37	5.65	5.94	5.71	5.99	5.49	5.30
CaO	9.46	11.91	9.53	12.64	10.50	11.12	7.62	7.89	7.38	7.66	7.68	7.45	8.29
Total	98.48	99.43	99.03	100.76	99.48	100.31	99.53	100.12	100.57	99.71	99.00	100.30	100.60
Si	3.03	3.03	3.02	3.01	3.02	3.01	3.03	3.01	2.99	3.02	3.01	3.01	3.01
Al^{IV}	0.00	0.00	0.00	0.00	0.00	0.00	0.00	0.00	0.01	0.00	0.00	0.00	0.00
Al^{VI}	2.03	1.99	2.01	1.96	2.01	1.96	2.03	2.02	2.01	2.02	2.04	2.02	1.99
Ti	0.00	0.00	0.01	0.00	0.01	0.00	0.00	0.00	0.00	0.01	0.00	0.00	0.01
Fe^{2+}	1.64	1.55	1.69	1.61	1.61	1.71	1.65	1.64	1.68	1.64	1.59	1.69	1.66
Mg	0.47	0.38	0.43	0.34	0.43	0.34	0.63	0.65	0.68	0.66	0.70	0.64	0.61
Mn	0.03	0.03	0.04	0.03	0.03	0.05	0.02	0.02	0.01	0.02	0.02	0.02	0.02
Ca	0.80	1.00	0.81	1.05	0.88	0.94	0.64	0.66	0.61	0.64	0.64	0.62	0.69
Alm	55.78	52.25	56.97	52.98	54.47	56.42	56.32	55.36	56.25	55.34	53.99	56.88	55.74
Gross	27.31	33.75	27.29	34.75	29.84	30.95	21.72	22.07	20.47	21.60	21.82	20.91	23.05
Pyrope	15.99	12.84	14.56	11.18	14.66	11.15	21.29	22.01	22.93	22.40	23.69	21.44	20.50
Spess	0.93	1.16	1.17	1.09	1.02	1.49	0.66	0.56	0.36	0.66	0.51	0.78	0.72

Analyses of garnet from the Ceará Central high-pressure metamafic rocks.

Sample	**TJF5-335**	**TJF5-335**	**TJF5-335**	**TJF5-335**	**TJF5-335**	**TJF5-335**	**TJF5-335**	**TJF5-335A**	**TJF5-335A**	**TJF5-335A**	**TJF5-335A**	**TJF5-335A**	**TJF5-335A**
Location	3 core	4 rim/core	5 rim/core	6 rim/core	7 rim/core	8 rim/core	9 rim/core	1 rim c-Pl	1 core	10 core	12 core c Rt	15 rimAm	2 rim c Pl
SiO_2	39.09	38.75	38.69	38.55	38.46	38.81	38.87	38.34	38.95	38.35	38.85	38.68	38.98
TiO_2	0.07	0.07	0.00	0.13	0.13	0.03	0.07	0.13	0.13	0.02	0.08	0.03	0.00
Al_2O_3	21.52	22.14	22.06	21.95	21.86	22.02	22.12	22.14	21.97	21.59	21.69	21.85	21.88
FeO	25.33	26.21	25.77	25.68	25.42	26.28	26.06	26.62	24.12	25.34	25.03	25.16	24.70
MnO	0.24	0.28	0.28	0.27	0.25	0.19	0.13	0.35	0.32	0.23	0.35	0.25	0.37
MgO	4.80	5.71	5.65	5.23	4.99	5.09	5.47	4.88	4.38	4.26	4.14	4.78	4.68
CaO	9.24	7.24	7.18	7.88	8.05	7.93	7.18	8.55	10.31	10.14	10.09	9.20	10.25
Total	100.29	100.40	99.63	99.69	99.15	100.36	99.90	100.99	100.17	99.93	100.22	99.96	100.86
Si	3.04	3.00	3.02	3.01	3.02	3.01	3.03	2.96	3.03	3.00	3.03	3.01	3.01
Al^{IV}	0.00	0.00	0.00	0.00	0.00	0.00	0.00	0.04	0.00	0.00	0.00	0.00	0.00
Al^{VI}	1.97	2.02	2.03	2.02	2.02	2.01	2.03	1.98	2.01	1.98	1.99	2.01	1.99
Ti	0.00	0.00	0.00	0.01	0.01	0.00	0.00	0.01	0.01	0.00	0.01	0.00	0.00
Fe^{2+}	1.65	1.70	1.68	1.68	1.67	1.71	1.70	1.72	1.57	1.66	1.63	1.64	1.59
Mg	0.56	0.66	0.66	0.61	0.58	0.59	0.64	0.56	0.51	0.50	0.48	0.56	0.54
Mn	0.02	0.02	0.02	0.02	0.02	0.01	0.01	0.02	0.02	0.02	0.02	0.02	0.02
Ca	0.77	0.60	0.60	0.66	0.68	0.66	0.60	0.71	0.86	0.85	0.84	0.77	0.85
Alm	55.11	57.06	56.86	56.62	56.66	57.49	57.74	57.10	53.05	54.90	54.80	55.02	53.06
Gross	25.77	20.19	20.29	22.25	22.98	22.24	20.37	23.48	29.07	28.15	28.28	25.78	28.22
Pyrope	18.61	22.15	22.22	20.53	19.80	19.85	21.61	18.67	17.16	16.46	16.14	18.64	17.90
Spess	0.52	0.61	0.63	0.61	0.56	0.43	0.29	0.75	0.72	0.50	0.78	0.56	0.81

Analyses of garnet from the Ceará Central high-pressure metamafic rocks.

Sample	**TJF5-335A**	**TJF5-335A**	**TJF5-335A**	**TJF5-335A**	**TJF5-335A**	**TJF5-335A**	**TJF5-335A**	**TJF5-335A**	**TJF5-335A**	**TJF5-335B**	**TJF5-335B**	**TJF5-335B**
Location	2 core c Rt	3 core	4 rim c Am	5 rim c Am	6 rim c Am	6 core	7 rim c-Am	9 core	9 core spl	1 core	2 rim cAm	2 core
SiO_2	38.89	37.80	38.87	38.64	38.47	38.65	38.76	38.29	38.70	38.72	38.20	38.81
TiO_2	0.10	0.17	0.10	0.09	0.14	0.08	0.08	0.11	0.05	0.18	0.02	0.11
Al_2O_3	21.90	21.66	21.60	21.74	21.79	21.77	21.91	21.54	21.61	21.70	21.48	21.47
FeO	25.19	24.96	24.08	25.00	24.67	25.18	24.82	25.57	24.73	25.27	26.26	26.44
MnO	0.29	0.33	0.27	0.36	0.55	0.29	0.58	0.30	0.30	0.47	0.65	0.65
MgO	4.62	4.21	4.60	4.72	4.48	4.33	4.28	4.61	4.97	4.42	4.42	4.41
CaO	10.05	10.48	9.96	9.95	10.01	10.26	10.16	8.63	8.59	9.70	8.85	9.74
Total	101.04	99.61	99.47	100.50	100.10	100.55	100.59	99.05	98.94	100.44	99.88	101.64
Si	3.00	2.96	3.04	3.00	3.00	3.00	3.01	3.02	3.04	3.01	2.99	2.99
Al^{IV}	0.00	0.04	0.00	0.01	0.01	0.00	0.00	0.00	0.00	0.00	0.01	0.01
Al^{VI}	1.99	1.96	1.99	1.98	1.99	1.99	2.00	2.00	2.00	1.99	1.98	1.94
Ti	0.01	0.01	0.01	0.01	0.01	0.01	0.01	0.01	0.00	0.01	0.00	0.01
Fe^{2+}	1.63	1.64	1.58	1.62	1.61	1.63	1.61	1.69	1.63	1.64	1.72	1.70
Mg	0.53	0.49	0.54	0.55	0.52	0.50	0.50	0.54	0.58	0.51	0.52	0.51
Mn	0.02	0.02	0.02	0.02	0.04	0.02	0.04	0.02	0.02	0.03	0.04	0.04
Ca	0.83	0.88	0.84	0.83	0.84	0.85	0.84	0.73	0.72	0.81	0.74	0.80
Alm	54.08	54.00	53.13	53.74	53.58	54.35	53.89	56.63	55.09	54.90	56.93	55.75
Gross	27.63	29.04	28.16	27.41	27.86	28.36	28.25	24.49	24.50	26.98	24.58	26.30
Pyrope	17.67	16.24	18.10	18.07	17.35	16.65	16.57	18.20	19.72	17.10	17.07	16.56
Spess	0.62	0.73	0.61	0.79	1.21	0.64	1.28	0.68	0.68	1.03	1.43	1.40

Analyses of garnet from the Ceará Central high-pressure metamafic rocks.

Sample	**TJF5-335B**	**TJF5-335B**	**TJF5-335B**	**TJF5-335B**	**WT7-25K**	**WT7-25K**	**WT7-25K**	**WT7-25K**	**WT7-25K**	**WT7-25K**	**WT7-25K**	**WT7-25K**	**WT7-25K**
Location	3 rim	4 rim c-Pl	5 rim	5 core	1 rim	1 core	2 core	3 rim c-Am	3 core	4 rim c Am	4 core	5 rim c-Pl	7 core
SiO_2	38.17	38.46	37.84	37.83	38.59	38.72	38.58	38.77	38.81	39.17	38.79	38.62	38.75
TiO_2	0.15	0.00	0.03	0.23	0.06	0.19	0.00	0.00	0.07	0.06	0.08	0.04	0.18
Al_2O_3	20.99	21.73	21.24	21.15	21.63	21.45	21.93	21.86	21.62	21.35	21.16	21.41	21.47
FeO	26.71	27.34	28.02	25.20	28.37	27.63	26.71	28.45	26.89	26.33	27.03	25.65	25.44
MnO	0.74	0.89	0.92	0.51	1.18	0.93	0.91	1.05	0.67	0.74	0.88	0.70	0.83
MgO	3.99	3.77	3.61	4.41	1.12	1.31	1.31	1.21	1.34	1.21	1.23	3.57	3.49
CaO	9.28	7.40	8.19	10.03	9.44	9.91	9.95	8.99	9.74	10.29	9.53	10.50	10.96
Total	100.03	99.59	99.85	99.37	100.38	100.15	99.38	100.32	99.15	99.14	98.70	100.49	101.12
Si	3.00	3.04	2.99	2.97	3.07	3.08	3.08	3.08	3.11	3.14	3.13	3.02	3.01
Al^{IV}	0.00	0.00	0.01	0.03	0.00	0.00	0.00	0.00	0.00	0.00	0.00	0.00	0.00
Al^{VI}	1.94	2.02	1.97	1.93	2.03	2.01	2.06	2.05	2.04	2.02	2.01	1.97	1.96
Ti	0.01	0.00	0.00	0.01	0.00	0.01	0.00	0.00	0.00	0.00	0.01	0.00	0.01
Fe^{2+}	1.75	1.81	1.85	1.66	1.89	1.84	1.79	1.89	1.80	1.77	1.82	1.68	1.65
Mg	0.47	0.45	0.43	0.52	0.13	0.16	0.16	0.14	0.16	0.14	0.15	0.42	0.40
Mn	0.05	0.06	0.06	0.03	0.08	0.06	0.06	0.07	0.05	0.05	0.06	0.05	0.06
Ca	0.78	0.63	0.69	0.85	0.80	0.84	0.85	0.77	0.84	0.88	0.82	0.88	0.91
Alm	57.49	61.50	61.06	54.27	65.00	63.37	62.53	65.89	63.37	62.09	63.87	55.55	54.66
Gross	25.58	21.33	22.88	27.68	27.70	29.12	29.85	26.66	29.41	31.08	28.85	29.12	30.17
Pyrope	15.31	15.14	14.04	16.93	4.57	5.36	5.47	4.99	5.62	5.07	5.17	13.78	13.36
Spess	1.61	2.04	2.02	1.12	2.73	2.16	2.16	2.45	1.60	1.77	2.11	1.54	1.81

Analyses of garnet from the Ceará Central high-pressure metamafic rocks.

Sample	**WT7-25K**	**WT8-302**	**WT8-302**	**WT8-302**	**WT8-302**	**WT8-302**	**WT8-302**	**WT8-302**	**WT8-302**	**WT8-302**	**WT8-302**	**WT8-302**	**WT8-302**	**WT8-302**
Location	8 core	1 rim	1 rimc-Pl	1 rim/core	1 core	10 rimAm	10 core	cAm	3 rim	3 core	3 rep core	4 core	5 rim	5 rim/core
SiO_2	38.35	38.97	39.38	39.75	39.48	39.50	39.96	38.97	39.42	39.17	39.23	38.72	39.49	38.28
TiO_2	0.06	0.07	0.00	0.06	0.07	0.00	0.02	0.08	0.05	0.09	0.00	0.00	0.08	0.03
Al_2O_3	21.38	22.14	22.07	22.27	22.34	22.12	22.22	22.31	22.01	22.37	22.16	21.95	22.18	21.74
FeO	25.63	22.45	23.71	21.18	19.57	23.78	19.58	24.31	21.19	23.30	20.51	24.09	21.03	25.33
MnO	0.84	0.64	0.66	0.46	0.49	0.64	0.56	0.80	0.39	0.67	0.50	0.81	0.48	0.90
MgO	3.66	6.28	6.84	7.17	7.50	5.79	7.36	6.00	7.33	6.78	7.31	5.81	7.53	5.25
CaO	10.79	9.62	6.86	9.73	9.75	8.31	9.54	7.82	9.16	8.22	9.28	8.33	9.14	7.93
Total	100.71	100.17	99.51	100.62	99.20	100.13	99.23	100.28	99.54	100.59	98.99	99.72	99.92	99.47
Si	2.99	3.00	3.05	3.02	3.03	3.05	3.07	3.01	3.03	3.00	3.03	3.01	3.02	3.00
Al^{IV}	0.01	0.01	0.00	0.00	0.00	0.00	0.00	0.00	0.00	0.00	0.00	0.00	0.00	0.00
Al^{VI}	1.95	2.00	2.01	1.99	2.02	2.01	2.01	2.03	1.99	2.01	2.01	2.01	2.00	2.00
Ti	0.00	0.00	0.00	0.00	0.00	0.00	0.00	0.01	0.00	0.01	0.00	0.00	0.01	0.00
Fe^{2+}	1.67	1.44	1.54	1.35	1.26	1.54	1.26	1.57	1.36	1.49	1.32	1.57	1.34	1.66
Mg	0.43	0.72	0.79	0.81	0.86	0.67	0.84	0.69	0.84	0.77	0.84	0.67	0.86	0.61
Mn	0.06	0.04	0.04	0.03	0.03	0.04	0.04	0.05	0.03	0.04	0.03	0.05	0.03	0.06
Ca	0.90	0.79	0.57	0.79	0.80	0.69	0.79	0.65	0.75	0.67	0.77	0.69	0.75	0.67
Alm	54.74	48.15	52.27	45.15	42.60	52.39	43.06	53.03	45.68	50.01	44.65	52.43	45.09	55.37
Gross	29.52	26.44	19.37	26.59	27.20	23.46	26.87	21.87	25.31	22.60	25.88	23.24	25.10	22.19
Pyrope	13.92	24.01	26.88	27.26	29.12	22.73	28.83	23.32	28.16	25.94	28.37	22.54	28.79	20.44
Spess	1.82	1.40	1.48	1.00	1.08	1.42	1.25	1.77	0.85	1.46	1.10	1.79	1.03	2.00

Analyses of garnet from the Ceará Central high-pressure metamafic rocks.

Sample	**WT8-302**	**WT8-302**	**WT8-302**	**WT8-53E**	**WT8-53E**	**WT8-53E**	**WT8-53E**	**WT8-53E**	**WT8-53E**	**WT8-53E**	**WT8-53E**	**WT8-53E**	**WT8-53E**	**WT8-53E**
Location	7 rimc-Pl	7 core	8 core Rt	1 rim cPl	1 core	10 rim	11 rim	1 rep rim	2 rimc- Pl	2 core	3 rim c-Pl	3 core	4 rim Pl	4 core
SiO_2	39.28	39.65	39.22	39.06	39.12	38.03	38.51	38.38	39.41	39.41	38.14	39.59	38.68	38.80
TiO_2	0.06	0.09	0.26	0.06	0.06	0.03	0.08	0.07	0.02	0.02	0.00	0.00	0.00	0.06
Al_2O_3	22.26	22.08	22.31	21.67	21.98	21.78	21.96	21.56	22.08	22.08	21.75	22.06	21.77	21.95
FeO	24.82	21.97	21.60	25.72	24.91	27.23	26.35	25.14	22.72	22.72	27.27	23.05	26.10	23.51
MnO	0.98	0.65	0.59	0.77	0.67	0.94	0.87	0.87	0.50	0.50	0.75	0.69	0.80	0.52
MgO	5.73	7.32	6.82	5.66	5.18	4.26	4.22	4.36	5.32	5.32	4.84	5.32	4.09	5.20
CaO	8.11	8.28	9.16	8.56	9.45	7.71	8.46	9.32	10.66	10.66	7.96	10.44	9.70	10.09
Total	101.23	100.04	99.95	101.49	101.36	99.97	100.44	99.70	100.72	100.72	100.70	101.14	101.14	100.12
Si	3.01	3.04	3.01	2.99	3.00	2.99	3.00	3.01	3.03	3.03	2.96	3.03	3.00	3.00
Al^{IV}	0.00	0.00	0.00	0.01	0.00	0.01	0.00	0.00	0.00	0.00	0.04	0.00	0.00	0.00
Al^{VI}	2.01	1.99	2.02	1.95	1.99	2.00	2.02	1.99	2.00	2.00	1.96	1.99	1.98	2.00
Ti	0.00	0.01	0.02	0.00	0.00	0.00	0.01	0.00	0.00	0.00	0.00	0.00	0.00	0.00
Fe^{2+}	1.59	1.41	1.39	1.65	1.60	1.79	1.72	1.65	1.46	1.46	1.77	1.48	1.69	1.52
Mg	0.66	0.84	0.78	0.65	0.59	0.50	0.49	0.51	0.61	0.61	0.56	0.61	0.47	0.60
Mn	0.06	0.04	0.04	0.05	0.04	0.06	0.06	0.06	0.03	0.03	0.05	0.05	0.05	0.03
Ca	0.67	0.68	0.75	0.70	0.78	0.65	0.71	0.78	0.88	0.88	0.66	0.86	0.81	0.84
Alm	53.47	47.47	46.87	54.09	53.09	59.66	57.81	54.98	49.00	49.00	58.22	49.45	55.98	50.84
Gross	22.37	22.92	25.46	23.06	25.80	21.63	23.77	26.10	29.45	29.45	21.76	28.69	26.66	27.97
Pyrope	22.01	28.19	26.37	21.20	19.66	16.64	16.50	16.99	20.47	20.47	18.40	20.36	15.62	20.04
Spess	2.15	1.43	1.30	1.64	1.45	2.08	1.92	1.93	1.09	1.09	1.63	1.50	1.75	1.15

Analyses of garnet from the Ceará Central high-pressure metamafic rocks.

Sample	**WT8-53E**	**WT8-53E**	**WT8-53E**	**WT8-53E**	**WT8-53E**	**WT8-53E**	**WT8-53E**	**WT8-53E**
Location	5 rim Pl	5 core	6 rim cPL	6 core	7 rim cPl	7 core	8 rim	9 rim
SiO_2	38.34	38.25	38.02	38.58	39.05	39.03	38.92	38.96
TiO_2	0.07	0.04	0.06	0.00	0.08	0.08	0.00	0.08
Al_2O_3	21.43	21.77	21.78	21.71	21.80	21.81	21.75	26.15
FeO	27.26	22.56	25.86	26.26	25.06	24.23	24.77	23.04
MnO	0.76	0.53	0.90	0.77	0.70	0.56	0.75	0.89
MgO	4.52	5.25	4.10	4.02	4.74	5.46	4.29	3.38
CaO	8.33	10.57	8.95	8.90	9.53	9.66	10.03	7.11
Total	100.70	98.98	99.68	100.22	100.96	100.82	100.51	99.61
Si	2.99	2.99	2.99	3.02	3.02	3.00	3.02	3.04
Al^{IV}	0.01	0.01	0.01	0.00	0.00	0.00	0.00	0.00
Al^{VI}	1.95	1.99	2.00	2.00	1.98	1.98	1.99	2.40
Ti	0.00	0.00	0.00	0.00	0.01	0.01	0.00	0.01
Fe^{2+}	1.78	1.47	1.70	1.72	1.62	1.56	1.61	1.50
Mg	0.52	0.61	0.48	0.47	0.55	0.63	0.50	0.39
Mn	0.05	0.04	0.06	0.05	0.05	0.04	0.05	0.06
Ca	0.70	0.89	0.75	0.75	0.79	0.80	0.83	0.59
Alm	58.31	49.05	56.77	57.59	53.98	51.66	53.81	58.96
Gross	22.82	29.44	25.16	25.00	26.31	26.38	27.92	23.30
Pyrope	17.22	20.34	16.06	15.71	18.19	20.76	16.63	15.43
Spess	1.65	1.17	2.01	1.71	1.53	1.20	1.64	2.31

Analyses of garnet from the Ceará Central high-pressure metapelitic rocks.

Sample	**WT7-53A**	**WT7-53A**	**WT7-53A**	**WT7-53A**	**WT7-53A**	**WT7-53A**	**WT7-53A**	**WT7-53A**	**WT8-07**	**WT8-07**	**WT8-07**
Location	1rimcSil	2 core	2 core	2 core	3 core	4 rim c-Pl	4 core	7 rim cMic	0 coreBt	1-perfil	10-perf
SiO_2	38.20	38.83	38.00	38.45	38.28	37.68	38.43	38.42	38.22	37.31	37.48
TiO_2	0.00	0.00	0.00	0.00	0.00	0.68	0.01	0.03	0.07	0.00	0.10
Al_2O_3	21.61	22.29	21.84	22.26	22.34	21.88	22.06	21.87	21.76	21.29	21.17
FeO	32.01	31.07	33.18	31.78	31.60	32.63	31.71	32.62	34.25	35.23	35.59
MnO	1.01	0.99	1.25	0.84	0.82	0.96	0.96	1.07	0.44	0.53	0.41
MgO	6.45	7.43	5.69	7.53	7.15	6.15	7.11	6.28	5.70	4.85	5.47
CaO	0.65	0.58	0.66	0.60	0.64	0.72	0.81	0.74	0.69	0.69	0.75
Total	99.93	101.18	100.61	101.47	100.83	100.71	101.10	101.04	101.12	99.90	100.96
Si	3.01	3.00	2.99	2.96	2.97	2.96	2.98	3.00	2.99	2.98	2.95
Al^{IV}	0.00	0.00	0.01	0.04	0.03	0.05	0.02	0.00	0.01	0.02	0.05
Al^{VI}	2.00	2.03	2.01	1.98	2.01	1.98	1.99	2.01	2.00	1.98	1.92
Ti	0.00	0.00	0.00	0.00	0.00	0.04	0.00	0.00	0.00	0.00	0.01
Fe^{2+}	2.11	2.01	2.18	2.05	2.05	2.14	2.06	2.13	2.24	2.35	2.35
Mg	0.76	0.86	0.67	0.87	0.83	0.72	0.82	0.73	0.67	0.58	0.64
Mn	0.07	0.07	0.08	0.06	0.05	0.06	0.06	0.07	0.03	0.04	0.03
Ca	0.06	0.05	0.06	0.05	0.05	0.06	0.07	0.06	0.06	0.06	0.06
Alm	70.55	67.46	73.04	67.86	68.69	71.71	68.34	71.15	74.87	77.78	76.18
Gross	1.83	1.60	1.86	1.65	1.79	2.04	2.24	2.07	1.94	1.94	2.07
Pyrope	25.36	28.77	22.33	28.67	27.72	24.11	27.32	24.42	22.22	19.10	20.87
Spess	2.26	2.17	2.78	1.82	1.80	2.14	2.10	2.37	0.97	1.18	0.89

Analyses of garnet from the Ceará Central high-pressure metapelitic rocks.

Sample	**WT8-07**	**WT8-07**	**WT8-07**	**WT8-07**	**WT8-07**	**WT8-07**	**WT8-07**	**WT8-07**	**WT8-07**	**WT8-07**	**WT8-07**	**WT8-07**	**WT8-07**	**WT8-07**
Location	11-perf	12-perf	2	2-perfil	3	3	3-perfil	4	4-perfil	5	5-perfil	6-perfil	7-perfil	8
SiO_2	37.11	36.79	37.80	37.64	37.74	37.54	37.95	38.05	38.04	37.99	37.84	37.90	38.13	38.31
TiO_2	0.00	0.00	0.00	0.00	0.01	0.00	0.05	0.02	0.00	0.06	0.00	0.00	0.01	0.00
Al_2O_3	21.13	21.00	21.58	21.34	21.64	21.69	21.55	21.86	21.35	21.73	21.39	21.42	21.39	21.84
FeO	35.99	35.38	34.99	35.27	34.46	32.97	34.47	33.24	34.75	32.48	36.32	35.22	34.99	33.88
MnO	0.46	0.49	0.35	0.39	0.40	0.41	0.52	0.24	0.45	0.33	0.55	0.31	0.42	0.28
MgO	5.30	4.45	4.71	5.02	5.44	5.40	5.24	6.40	5.32	5.99	3.82	5.28	5.27	5.47
CaO	0.72	0.73	0.71	0.69	0.80	0.87	0.66	1.16	0.65	1.35	0.70	0.71	0.68	1.02
Total	100.71	98.84	100.13	100.34	100.49	98.87	100.43	100.99	100.57	99.92	100.62	100.84	100.89	100.79
Si	2.94	2.98	3.01	2.99	2.98	3.00	3.00	2.97	3.01	3.00	3.02	2.99	3.01	3.01
Al^{IV}	0.07	0.03	0.00	0.01	0.02	0.00	0.00	0.03	0.00	0.00	0.00	0.01	0.00	0.00
Al^{VI}	1.90	1.98	2.02	1.98	1.99	2.04	2.01	1.97	1.99	2.01	2.01	1.98	1.99	2.02
Ti	0.00	0.00	0.00	0.00	0.00	0.00	0.00	0.00	0.00	0.00	0.00	0.00	0.00	0.00
Fe^{2+}	2.38	2.39	2.33	2.34	2.27	2.21	2.28	2.17	2.30	2.14	2.42	2.32	2.31	2.23
Mg	0.63	0.54	0.56	0.59	0.64	0.64	0.62	0.74	0.63	0.70	0.45	0.62	0.62	0.64
Mn	0.03	0.03	0.02	0.03	0.03	0.03	0.04	0.02	0.03	0.02	0.04	0.02	0.03	0.02
Ca	0.06	0.06	0.06	0.06	0.07	0.07	0.06	0.10	0.06	0.11	0.06	0.06	0.06	0.09
Alm	76.88	79.09	78.38	77.54	75.59	74.73	76.31	71.66	76.31	71.83	81.46	76.80	76.61	74.92
Gross	1.96	2.09	2.03	1.94	2.24	2.52	1.87	3.21	1.84	3.83	2.01	1.98	1.91	2.88
Pyrope	20.18	17.73	18.80	19.66	21.28	21.83	20.66	24.60	20.84	23.60	15.29	20.52	20.56	21.56
Spess	0.98	1.10	0.79	0.86	0.89	0.93	1.16	0.53	1.01	0.75	1.24	0.69	0.93	0.64

Analyses of garnet from the Ceará Central high-pressure metapelitic rocks.

Sample	**WT8-07**	**WT8-07**	**WT8-07**	**WT8-17**	**WT8-17**	**WT8-17**	**WT8-17**	**WT8-17**	**WT8-17**
Location	8-perfil	9	9-perfil	1 rim cBt	1 core	2 rim cBt	3 core	3 core	4 core Bt
SiO_2	37.48	37.34	37.76	38.36	38.31	37.67	38.51	37.17	38.20
TiO_2	0.08	0.04	0.02	0.00	0.00	0.01	0.02	0.06	0.01
Al_2O_3	21.27	21.53	21.24	21.93	21.49	21.92	21.97	21.77	21.54
FeO	35.07	35.51	34.34	32.91	31.81	34.44	32.39	31.95	33.31
MnO	0.35	0.44	0.40	0.62	0.61	0.69	0.50	0.46	0.53
MgO	5.26	4.77	5.07	4.98	5.12	4.40	5.22	5.58	5.25
CaO	0.70	0.89	0.71	2.27	3.13	1.75	2.32	2.85	1.74
Total	100.20	100.53	99.54	101.08	100.47	100.87	100.93	99.84	100.57
Si	2.97	2.96	3.02	3.01	3.01	2.98	3.02	2.94	3.01
Al^{IV}	0.03	0.04	0.00	0.00	0.00	0.03	0.00	0.07	0.00
Al^{VI}	1.96	1.97	2.00	2.02	1.99	2.01	2.03	1.96	2.00
Ti	0.01	0.00	0.00	0.00	0.00	0.00	0.00	0.00	0.00
Fe^{2+}	2.33	2.36	2.29	2.16	2.09	2.27	2.12	2.11	2.19
Mg	0.62	0.56	0.60	0.58	0.60	0.52	0.61	0.66	0.62
Mn	0.02	0.03	0.03	0.04	0.04	0.05	0.03	0.03	0.04
Ca	0.06	0.08	0.06	0.19	0.26	0.15	0.19	0.24	0.15
Alm	76.74	77.87	76.84	72.59	69.81	76.16	71.70	69.43	73.32
Gross	1.97	2.51	2.02	6.43	8.80	4.97	6.57	7.92	4.92
Pyrope	20.52	18.65	20.23	19.59	20.03	17.33	20.61	21.63	20.59
Spess	0.78	0.98	0.91	1.39	1.36	1.54	1.12	1.02	1.18

Analyses of amphibole from the Ceará Central high-pressure mafic rocks.

Sample	**RM-124B**	**RM-124B**	**RM-124B**	**RM-124B**	**RM-182**	**RM-182**	**RM-182**	**RM-182**	**RM-220**	**RM-220**	**RM-220**	**RM-220**	**TJF-335**
Location	1 spl	2 rim c-Pl	2 rim c-Grt	5 rim c-Pl	1 rim c-Pl	2 spl c-cpx	3 rim c-Pl	3 rep	1 matrix	2 rimRt-Cpx	3 rim c-Grt	4 rim cGrt	1 coronal
SiO_2	44.74	44.79	43.66	44.52	44.24	46.40	46.47	46.03	42.48	42.67	43.06	42.70	40.90
TiO_2	1.17	1.25	1.34	1.41	1.27	1.23	1.17	0.92	1.26	1.47	1.04	1.39	0.28
Al_2O_3	11.64	12.14	13.13	12.63	11.62	10.38	10.74	10.78	13.74	12.89	13.27	13.35	17.15
FeO	13.05	13.44	13.63	13.23	13.77	13.69	13.60	13.35	15.67	16.25	15.37	15.25	14.15
MnO	0.12	0.13	0.13	0.12	0.12	0.12	0.04	0.08	0.06	0.07	0.02	0.05	0.04
MgO	12.22	11.99	11.41	11.74	12.45	12.85	13.10	12.88	10.71	10.89	10.96	10.62	12.05
CaO	11.88	11.58	11.64	11.62	11.25	11.63	11.65	11.47	11.48	11.32	11.79	11.50	11.02
Na_2O	1.52	1.69	1.82	1.69	1.76	1.54	1.71	1.72	2.36	2.23	2.17	2.24	3.52
K_2O	0.52	0.54	0.54	0.55	0.38	0.31	0.29	0.37	0.13	0.16	0.17	0.16	0.04
F	0.07	0.00	0.07	0.00	0.04	0.00	0.00	0.00	0.11	0.17	0.00	0.11	0.27
Cl	0.08	0.11	0.08	0.11	0.06	0.03	0.05	0.03	0.00	0.01	0.00	0.00	0.00
Total	97.01	97.65	97.45	97.62	96.95	98.18	98.81	97.64	97.99	98.12	97.84	97.36	99.43
Si	6.60	6.57	6.44	6.53	6.51	6.73	6.69	6.71	6.27	6.29	6.34	6.34	5.90
Al^{IV}	1.40	1.43	1.56	1.47	1.49	1.27	1.31	1.29	1.74	1.71	1.66	1.66	2.10
Al^{VI}	0.62	0.66	0.72	0.72	0.53	0.50	0.51	0.56	0.65	0.53	0.65	0.67	0.81
Ti	0.13	0.14	0.15	0.16	0.14	0.13	0.13	0.10	0.14	0.16	0.12	0.16	0.03
Fe^{3+}	0.16	0.20	0.18	0.16	0.36	0.26	0.28	0.27	0.30	0.41	0.28	0.23	0.56
Fe^{2+}	1.40	1.37	1.44	1.39	1.24	1.31	1.27	1.27	1.55	1.50	1.55	1.59	1.01
Mg	2.69	2.62	2.51	2.57	2.73	2.78	2.81	2.80	2.36	2.40	2.41	2.35	2.59
Mn	0.01	0.01	0.01	0.01	0.01	0.01	0.00	0.01	0.00	0.00	0.00	0.00	0.00
Ca (B)	1.88	1.82	1.84	1.83	1.77	1.81	1.80	1.79	1.81	1.79	1.86	1.83	1.70
Na (B)	0.07	0.10	0.09	0.09	0.12	0.10	0.11	0.11	0.10	0.11	0.07	0.09	0.16
Na (A)	0.37	0.38	0.44	0.39	0.38	0.33	0.37	0.38	0.57	0.53	0.55	0.56	0.83
K	0.10	0.10	0.10	0.10	0.07	0.06	0.05	0.07	0.02	0.03	0.03	0.03	0.01

Analyses of amphibole from the Ceará Central high-pressure mafic rocks.

Sample	**TJF-335**	**TJF-335**	**TJF-335**	**TJF-335A**	**TJF-335A**	**TJF-335A**	**TJF-335A**	**TJF-335A**	**TJF-335A**	**TJF-335A**	**TJF-335B**	**TJF-335B**
Location	2 rim c-Grt	4 rim c-Pl	5 spl c-Cpx	1 rim c-Grt	2 rim c-grt	7 incl-grt	71 rim c-grt	712 incl-grt	8 rim c-Pl	9-spl	0 cont Ap	1 rim c-Pl
SiO_2	41.16	40.60	43.06	39.84	38.65	43.87	42.84	44.49	40.03	39.70	46.13	46.22
TiO_2	0.07	0.10	1.80	0.40	1.65	0.95	0.21	0.85	0.39	0.32	1.10	0.98
Al_2O_3	16.77	18.94	12.87	17.59	19.34	17.51	13.70	16.93	17.28	17.73	9.77	11.00
FeO	13.28	13.06	13.52	14.45	14.17	10.81	13.80	11.78	13.96	12.37	15.24	14.97
MnO	0.06	0.08	0.06	0.06	0.06	0.04	0.06	0.02	0.07	0.08	0.10	0.07
MgO	11.95	11.72	12.63	10.50	9.93	10.11	12.46	10.02	11.32	12.22	12.61	11.95
CaO	10.90	10.72	11.11	10.89	10.95	10.23	10.63	10.19	10.35	10.81	11.30	11.22
Na_2O	3.64	3.74	3.31	3.48	3.53	4.15	3.02	4.14	3.58	3.51	1.47	1.63
K_2O	0.00	0.02	0.04	0.04	0.04	0.01	0.01	0.06	0.02	0.03	0.01	0.02
F	0.07	0.25	0.17	0.13	0.00	0.10	0.30	0.07	0.00	0.24	0.21	0.00
Cl	0.00	0.02	0.00	0.01	0.00	0.02	0.00	0.04	0.01	0.01	0.02	0.01
Total	97.91	99.24	98.58	97.39	98.32	97.79	97.02	98.60	97.00	97.02	97.94	98.07
Si	6.01	5.85	6.30	5.90	5.68	6.47	6.31	6.53	5.91	5.83	6.71	6.71
Al^{IV}	1.99	2.16	1.71	2.10	2.32	1.53	1.69	1.47	2.09	2.17	1.29	1.29
Al^{VI}	0.90	1.06	0.51	0.97	1.02	1.51	0.69	1.45	0.91	0.90	0.39	0.60
Ti	0.01	0.01	0.20	0.05	0.18	0.11	0.02	0.09	0.04	0.04	0.12	0.11
Fe^{3+}	0.42	0.48	0.28	0.38	0.33	0.00	0.48	0.00	0.53	0.51	0.49	0.35
Fe^{2+}	1.07	0.93	1.26	1.28	1.28	1.16	1.07	1.26	1.03	0.88	1.26	1.36
Mg	2.60	2.52	2.75	2.32	2.18	2.22	2.74	2.19	2.49	2.68	2.74	2.59
Mn	0.00	0.01	0.00	0.00	0.00	0.00	0.00	0.00	0.01	0.01	0.01	0.01
Ca (B)	1.71	1.65	1.74	1.73	1.72	1.62	1.68	1.60	1.64	1.70	1.76	1.75
Na (B)	0.16	0.18	0.14	0.15	0.15	0.20	0.17	0.21	0.19	0.16	0.13	0.14
Na (A)	0.88	0.86	0.80	0.86	0.86	0.98	0.69	0.97	0.83	0.84	0.29	0.32
K	0.00	0.00	0.01	0.01	0.01	0.00	0.00	0.01	0.01	0.01	0.00	0.00

Analyses of amphibole from the Ceará Central high-pressure mafic rocks.

Sample	WT7-25K	WT7-25K	WT7-25K	WT8-302	WT8-302	WT8-302	WT8-302	WT8-302	WT8-53E	WT8-53E	WT8-53E	WT8-53E	WT8-53E
Location	1 rim c-Pl	2 rim c-Pl	3 matrix	1 spl	2 spl	3 rim c-Rt	4 spl-Rt	5 spl	1 rim c Cpx	2 rim c-Rt	3 core	4 core	5 core
SiO_2	43.19	43.03	43.90	45.85	45.74	44.04	44.49	44.48	45.40	41.90	44.85	45.86	45.15
TiO_2	1.31	1.26	1.00	1.82	1.06	2.14	2.06	1.47	1.21	0.97	1.11	0.92	0.95
Al_2O_3	11.60	11.26	10.69	10.92	10.52	12.11	11.25	12.35	10.79	16.21	10.69	10.85	11.25
FeO	18.20	18.54	17.81	11.42	10.72	11.27	11.13	11.26	13.17	13.80	13.50	14.21	13.60
MnO	0.08	0.09	0.06	0.05	0.04	0.05	0.06	0.06	0.06	0.10	0.06	0.09	0.08
MgO	9.97	9.89	10.93	13.83	14.55	13.56	13.53	13.87	12.95	11.41	12.98	13.03	12.59
CaO	11.17	11.14	11.23	11.70	11.76	11.48	11.64	11.05	11.41	10.64	11.52	11.74	11.65
Na_2O	2.00	1.96	1.94	1.99	1.91	2.34	2.17	2.35	1.67	1.76	1.69	1.71	1.76
K_2O	0.48	0.51	0.48	0.14	0.11	0.16	0.09	0.13	0.26	0.27	0.25	0.25	0.25
F	0.00	0.00	0.00	0.04	0.00	0.00	0.00	0.04	0.21	0.00	0.00	0.11	0.10
Cl	0.02	0.06	0.02	0.13	0.17	0.18	0.16	0.17	0.01	0.00	0.02	0.02	0.02
Total	98.01	97.73	98.05	97.87	96.57	97.33	96.57	97.23	97.13	97.05	96.66	98.79	97.41
Si	6.43	6.44	6.50	6.65	6.67	6.44	6.55	6.47	6.65	6.10	6.60	6.62	6.61
Al^{IV}	1.57	1.56	1.50	1.35	1.33	1.56	1.45	1.53	1.35	1.90	1.40	1.38	1.39
Al^{VI}	0.47	0.42	0.37	0.51	0.48	0.52	0.50	0.59	0.52	0.88	0.45	0.46	0.55
Ti	0.15	0.14	0.11	0.20	0.12	0.24	0.23	0.16	0.13	0.11	0.12	0.10	0.10
Fe^{3+}	0.38	0.42	0.50	0.18	0.25	0.21	0.15	0.34	0.30	0.61	0.38	0.40	0.27
Fe^{2+}	1.80	1.81	1.61	1.12	0.99	1.07	1.15	0.90	1.22	0.91	1.20	1.23	1.32
Mg	2.21	2.21	2.41	2.99	3.17	2.95	2.97	3.01	2.83	2.48	2.85	2.80	2.75
Mn	0.01	0.01	0.00	0.00	0.00	0.00	0.00	0.00	0.00	0.01	0.00	0.01	0.01
Ca (B)	1.78	1.79	1.78	1.82	1.84	1.80	1.84	1.72	1.79	1.66	1.82	1.81	1.83
Na (B)	0.12	0.11	0.12	0.10	0.09	0.11	0.09	0.15	0.11	0.18	0.10	0.10	0.09
Na (A)	0.46	0.46	0.44	0.46	0.45	0.56	0.53	0.52	0.36	0.32	0.38	0.38	0.41
K	0.09	0.10	0.09	0.03	0.02	0.03	0.02	0.02	0.05	0.05	0.05	0.05	0.05

Analyses of plagioclase from the Ceará Central high-pressure mafic rocks.

Sample	**RM-182**	**RM-182**	**RM-182**	**RM-182**	**RM-182**	**RM-182**	**RM-220**	**RM-220**	**RM-220**	**RM-220**	**RM-220**	**RM-220**	**RM-220**	**RM124B**
Location	1 spl	2 rim c-Am	5 spl	6 c-cpx	6 spl	7 coronal	1 spl	2 rimc-Am	2 spl	3 c-Spl	4 rim c-Cpx	5 rim grt	7 spl	1 spl
SiO_2	60.74	58.84	58.68	59.97	59.24	59.26	60.10	59.11	60.00	57.84	56.88	55.64	57.47	58.07
TiO_2	0.00	0.00	0.05	0.01	0.02	0.00	0.00	0.00	0.00	0.00	0.01	0.00	0.09	0.07
Al_2O_3	25.10	25.70	25.54	25.93	26.04	25.77	25.34	26.03	25.49	26.91	28.05	28.33	27.08	26.55
Fe_2O_3	0.07	0.04	0.14	0.06	0.14	0.08	0.09	0.08	0.16	0.07	0.16	0.08	0.16	0.00
MnO	0.00	0.00	0.01	0.00	0.00	0.01	0.00	0.00	0.00	0.01	0.00	0.00	0.02	0.00
MgO	0.01	0.00	0.02	0.01	0.00	0.01	0.00	0.00	0.00	0.01	0.00	0.00	0.00	0.00
CaO	6.35	6.84	7.17	7.21	7.26	7.01	6.92	7.09	6.90	8.05	9.17	10.10	8.75	8.19
Na_2O	8.29	7.58	7.65	7.80	7.69	7.86	7.96	7.83	7.88	6.99	6.54	5.82	6.87	7.16
K_2O	0.15	0.06	0.14	0.10	0.13	0.11	0.05	0.07	0.05	0.03	0.05	0.02	0.05	0.14
Total	100.69	99.05	99.38	101.10	100.53	100.10	100.45	100.20	100.49	99.91	100.86	99.99	100.48	100.19
Si	10.75	10.59	10.55	10.59	10.53	10.57	10.67	10.53	10.65	10.35	10.13	10.01	10.26	10.38
Al	5.23	5.45	5.41	5.39	5.45	5.41	5.30	5.46	5.33	5.67	5.88	6.00	5.70	5.59
Ti	0.00	0.00	0.01	0.00	0.00	0.00	0.00	0.00	0.00	0.00	0.00	0.00	0.01	0.01
Fe^{3+}	0.01	0.01	0.02	0.01	0.02	0.01	0.01	0.01	0.02	0.01	0.02	0.01	0.02	0.00
Mn	0.00	0.00	0.00	0.00	0.00	0.00	0.00	0.00	0.00	0.00	0.00	0.00	0.00	0.00
Mg	0.00	0.00	0.00	0.00	0.00	0.00	0.00	0.00	0.00	0.00	0.00	0.00	0.00	0.00
Ca	1.20	1.32	1.38	1.36	1.38	1.34	1.32	1.35	1.31	1.54	1.75	1.95	1.67	1.57
Na	2.84	2.64	2.67	2.67	2.65	2.72	2.74	2.70	2.71	2.43	2.26	2.03	2.38	2.48
K	0.03	0.01	0.03	0.02	0.03	0.03	0.01	0.02	0.01	0.01	0.01	0.01	0.01	0.03
Ab	69.70	66.50	65.40	65.80	65.20	66.60	67.40	66.40	67.20	61.00	56.20	51.00	58.50	60.80
An	29.50	33.10	33.90	33.60	34.00	32.80	32.40	33.20	32.50	38.80	43.50	48.90	41.20	38.40
Or	0.80	0.40	0.80	0.50	0.70	0.60	0.30	0.40	0.30	0.20	0.30	0.10	0.30	0.80

Analyses of plagioclase from the Ceará Central high-pressure mafic rocks.

Sample	**RM124B**	**RM124B**	**RM124B**	**RM124B**	**RM124B**	**TJF5-335**	**TJF5-335A**	**TJF5-335A**	**TJF5-335A**	**TJF5-335A**	**TJF5-335A**	**TJF5-335A**
Location	1 spl	2 spl	2 spl-cpx	3 spl	3 rim spl	2 spl	1 spl	1 spl cpx	1 matrix	1 spl	19 coronal	2 spl cpx
SiO_2	56.96	57.46	56.59	58.40	57.41	61.95	62.68	64.72	60.49	64.79	53.04	64.72
TiO_2	0.05	0.05	0.01	0.09	0.00	0.00	0.01	0.00	0.00	0.00	0.06	0.00
Al_2O_3	27.29	27.08	27.25	26.79	26.98	23.02	23.76	23.05	25.35	23.10	29.74	23.05
Fe_2O_3	0.07	0.22	0.10	0.06	0.03	0.16	0.49	0.18	0.08	0.14	0.21	0.18
MnO	0.02	0.00	0.00	0.00	0.02	0.00	0.00	0.02	0.03	0.00	0.00	0.02
MgO	0.00	0.00	0.02	0.00	0.02	0.00	0.12	0.00	0.01	0.00	0.00	0.00
CaO	8.69	8.55	8.54	8.64	8.65	3.96	4.66	3.60	6.47	3.64	11.82	3.60
Na_2O	6.66	6.97	6.95	6.98	6.82	9.71	9.38	9.96	8.20	9.85	5.08	9.96
K_2O	0.16	0.15	0.11	0.11	0.10	0.01	0.04	0.02	0.02	0.00	0.00	0.02
Total	99.89	100.47	99.57	101.07	100.03	98.82	101.14	101.54	100.64	101.51	99.95	101.54
Si	10.23	10.26	10.20	10.36	10.29	11.11	11.01	11.26	10.71	11.27	9.61	11.26
Al	5.77	5.70	5.79	5.60	5.70	4.86	4.91	4.72	5.28	4.73	6.35	4.72
Ti	0.01	0.01	0.00	0.01	0.00	0.00	0.00	0.00	0.00	0.00	0.01	0.00
Fe^{3+}	0.01	0.03	0.01	0.01	0.00	0.02	0.07	0.02	0.01	0.02	0.03	0.02
Mn	0.00	0.00	0.00	0.00	0.00	0.00	0.00	0.00	0.00	0.00	0.00	0.00
Mg	0.00	0.00	0.00	0.00	0.00	0.00	0.03	0.00	0.00	0.00	0.00	0.00
Ca	1.67	1.64	1.65	1.64	1.66	0.76	0.88	0.67	1.23	0.68	2.30	0.67
Na	2.32	2.42	2.43	2.40	2.37	3.38	3.19	3.36	2.81	3.32	1.78	3.36
K	0.04	0.03	0.03	0.03	0.02	0.00	0.01	0.00	0.01	0.00	0.00	0.00
Ab	57.60	59.10	59.20	59.00	58.50	81.60	78.30	83.30	69.60	83.00	43.70	83.30
An	41.50	40.10	40.20	40.40	41.00	18.40	21.50	16.60	30.30	17.00	56.30	16.60
Or	0.90	0.80	0.60	0.60	0.50	0.10	0.20	0.10	0.10	0.00	0.00	0.10

Analyses of plagioclase from the Ceará Central high-pressure mafic rocks.

Sample	**TJF5-335A**	**TJF5-335A**	**TJF5-335A**	**TJF5-335B**	**TJF5-335B**	**TJF5-335B**	**TJF5-335B**	**TJF5-335B**	**WT7-25K**	**WT7-25K**	**WT7-25K**	**WT7-25K**
Location	6 spl	7 spl	8 spl	1 rim c-Am	2 rim c-oxi	5 rim c-Pl	8 rim c-Pl	9 rim-c-grt	1 rim c-Am	3 rim c-Cpx	4 rim c-Pl	9 rim c-Pl
SiO_2	62.68	61.77	63.54	59.47	59.85	60.42	61.57	60.30	62.44	61.53	61.04	63.12
TiO_2	0.00	0.00	0.00	0.01	0.00	0.07	0.07	0.02	0.00	0.00	0.07	0.02
Al_2O_3	22.85	23.85	22.90	25.24	24.50	24.69	24.42	24.95	23.89	24.80	24.52	23.52
Fe_2O_3	0.08	0.27	0.18	0.10	0.18	0.17	0.17	0.21	0.08	0.00	0.24	0.24
MnO	0.04	0.01	0.00	0.02	0.00	0.02	0.00	0.01	0.12	0.00	0.00	0.02
MgO	0.02	0.01	0.01	0.01	0.00	0.02	0.02	0.00	0.00	0.01	0.01	0.00
CaO	4.13	4.90	3.92	6.74	5.97	5.90	5.34	6.09	5.11	5.66	5.70	4.69
Na_2O	9.61	9.33	9.85	8.17	8.19	8.56	8.90	8.52	8.92	8.34	8.56	9.15
K_2O	0.00	0.00	0.00	0.00	0.01	0.03	0.01	0.02	0.15	0.18	0.14	0.19
Total	99.42	100.42	100.39	99.77	98.71	99.87	100.50	100.12	100.72	100.51	100.28	100.95
Si	11.16	10.95	11.20	10.64	10.79	10.77	10.89	10.73	11.01	10.87	10.83	11.09
Al	4.79	4.98	4.75	5.32	5.20	5.18	5.09	5.23	4.96	5.16	5.12	4.87
Ti	0.00	0.00	0.00	0.00	0.00	0.01	0.01	0.00	0.00	0.00	0.01	0.00
Fe^{3+}	0.01	0.04	0.02	0.01	0.03	0.02	0.02	0.03	0.01	0.00	0.03	0.03
Mn	0.01	0.00	0.00	0.00	0.00	0.00	0.00	0.00	0.02	0.00	0.00	0.00
Mg	0.01	0.00	0.00	0.00	0.00	0.00	0.01	0.00	0.00	0.00	0.00	0.00
Ca	0.79	0.93	0.74	1.29	1.15	1.13	1.01	1.16	0.97	1.07	1.08	0.88
Na	3.32	3.21	3.37	2.84	2.86	2.96	3.05	2.94	3.05	2.86	2.94	3.12
K	0.00	0.00	0.00	0.00	0.00	0.01	0.00	0.01	0.03	0.04	0.03	0.04
Ab	80.80	77.50	82.00	68.70	71.20	72.30	75.10	71.60	75.30	72.00	72.50	77.10
An	19.20	22.50	18.00	31.30	28.70	27.60	24.90	28.30	23.90	27.00	26.70	21.80
Or	0.00	0.00	0.00	0.00	0.10	0.10	0.00	0.10	0.80	1.00	0.80	1.10

Analyses of plagioclase from the Ceará Central high-pressure mafic rocks.

Sample	**WT8-302**	**WT8-302**	**WT8-302**	**WT8-302**	**WT8-302**	**WT8-302**	**WT8-302**	**WT8-53E**	**WT8-53E**	**WT8-53E**	**WT8-53E**	**WT8-53E**	**WT8-53E**
Location	1 rim grt	11 spl	2 spl	4 spl	5 spl	7 spl	8 spl	1 spl2	2 coronal	3 rim grt	4 c amp	5 coronal	6 cpx
SiO_2	60.80	61.65	59.92	60.35	60.98	60.58	61.17	58.73	59.27	59.58	60.61	59.80	59.52
TiO_2	0.04	0.00	0.00	0.00	0.06	0.00	0.00	0.04	0.06	0.05	0.04	0.00	0.00
Al_2O_3	25.02	24.85	26.48	24.97	24.97	25.08	24.85	25.53	25.96	25.92	25.11	25.32	25.18
Fe_2O_3	0.20	0.12	0.19	0.28	0.24	0.09	0.21	0.27	0.23	0.36	0.12	0.20	0.19
MnO	0.00	0.00	0.00	0.01	0.00	0.00	0.01	0.00	0.00	0.00	0.00	0.03	0.00
MgO	0.00	0.02	0.02	0.01	0.02	0.00	0.01	0.13	0.01	0.00	0.00	0.00	0.01
CaO	6.34	6.29	7.42	6.42	6.59	6.67	6.22	7.36	7.12	7.36	6.60	7.12	6.49
Na_2O	8.55	8.43	7.60	8.23	8.26	7.89	8.42	7.66	8.03	7.64	8.16	7.95	8.13
K_2O	0.03	0.02	0.06	0.10	0.06	0.04	0.05	0.09	0.00	0.04	0.13	0.09	0.08
Total	100.97	101.38	101.69	100.35	101.19	100.36	100.94	99.80	100.69	100.97	100.76	100.51	99.60
Si	10.74	10.82	10.52	10.72	10.74	10.74	10.79	10.53	10.52	10.55	10.72	10.63	10.66
Al	5.20	5.14	5.47	5.22	5.18	5.24	5.16	5.39	5.43	5.40	5.23	5.30	5.31
Ti	0.01	0.00	0.00	0.00	0.01	0.00	0.00	0.01	0.01	0.01	0.01	0.00	0.00
Fe^{3+}	0.03	0.02	0.02	0.04	0.03	0.01	0.03	0.04	0.03	0.05	0.02	0.03	0.03
Mn	0.00	0.00	0.00	0.00	0.00	0.00	0.00	0.00	0.00	0.00	0.00	0.00	0.00
Mg	0.00	0.01	0.01	0.00	0.01	0.00	0.00	0.03	0.00	0.00	0.00	0.00	0.00
Ca	1.20	1.18	1.40	1.22	1.24	1.27	1.18	1.41	1.36	1.40	1.25	1.36	1.25
Na	2.93	2.87	2.59	2.84	2.82	2.71	2.88	2.66	2.76	2.62	2.80	2.74	2.82
K	0.01	0.01	0.01	0.02	0.01	0.01	0.01	0.02	0.00	0.01	0.03	0.02	0.02
Ab	70.80	70.70	64.70	69.50	69.20	68.00	70.80	65.00	67.10	65.10	68.60	66.60	69.10
An	29.00	29.20	34.90	30.00	30.50	31.80	28.90	34.50	32.90	34.60	30.70	32.90	30.50
Or	0.10	0.10	0.40	0.50	0.30	0.20	0.20	0.50	0.00	0.20	0.70	0.50	0.40

Analyses of plagioclase from the Ceará Central high-pressure metapelitic rocks.

Sample	**WT7-53A**	**WT7-53A**	**WT7-53A**	**WT7-53A**	**WT7-53A**	**WT8-07**	**WT8-07**	**WT8-07**	**WT8-07**	**WT8-07**	**WT8-17**	**WT8-17**	**WT8-17**
Location	2 rim c-Grt	5 rim c-Pl	6 rim c-grt	7 core	8 rim c-Bt	1 core	2 rim c-Bt	2 core c-grt	4 rim	5 rim c-Bt	1 core	3 rim	3 rim cbt
SiO_2	63.03	63.05	61.80	63.03	63.12	64.29	64.23	63.91	63.49	63.86	62.37	61.04	63.10
TiO_2	0.00	0.00	0.00	0.00	0.00	0.06	0.00	0.01	0.01	0.00	0.00	0.00	0.02
Al_2O_3	19.11	19.04	19.27	18.99	19.25	22.17	22.29	22.31	22.39	22.14	19.26	24.37	19.27
Fe_2O_3	0.01	0.09	1.08	0.09	0.02	0.03	0.02	0.00	0.00	0.01	0.01	0.11	0.09
MnO	0.00	0.00	0.00	0.01	0.00	0.01	0.00	0.01	0.00	0.01	0.00	0.00	0.00
MgO	0.01	0.02	0.04	0.00	0.00	0.00	0.00	0.01	0.02	0.00	0.00	0.00	0.00
CaO	0.05	0.00	0.01	0.07	0.09	2.82	2.70	2.67	2.70	2.46	0.11	4.89	0.05
Na_2O	2.13	1.50	1.33	2.15	2.66	10.58	10.16	10.43	10.36	10.44	1.89	9.11	1.82
K_2O	14.16	15.42	14.84	14.36	13.51	0.15	0.13	0.14	0.14	0.16	14.67	0.45	15.26
Total	99.09	99.73	99.12	99.30	99.21	100.11	99.54	99.49	99.11	99.09	98.29	100.05	99.94
Si	11.78	11.77	11.63	11.78	11.76	11.35	11.37	11.34	11.31	11.37	11.73	10.87	11.73
Al	4.20	4.19	4.27	4.18	4.22	4.61	4.65	4.66	4.70	4.64	4.27	5.11	4.22
Ti	0.00	0.00	0.00	0.00	0.00	0.01	0.00	0.00	0.00	0.00	0.00	0.00	0.00
Fe^{3+}	0.00	0.01	0.15	0.01	0.00	0.00	0.00	0.00	0.00	0.00	0.00	0.01	0.01
Mn	0.00	0.00	0.00	0.00	0.00	0.00	0.00	0.00	0.00	0.00	0.00	0.00	0.00
Mg	0.00	0.01	0.01	0.00	0.00	0.00	0.00	0.00	0.00	0.00	0.00	0.00	0.00
Ca	0.01	0.00	0.00	0.01	0.02	0.53	0.51	0.51	0.52	0.47	0.02	0.93	0.01
Na	0.77	0.54	0.49	0.78	0.96	3.62	3.49	3.59	3.58	3.60	0.69	3.15	0.66
K	3.38	3.67	3.56	3.42	3.21	0.04	0.03	0.03	0.03	0.04	3.52	0.10	3.62
Ab	18.60	12.90	12.00	18.50	23.00	86.40	86.60	86.90	86.80	87.70	16.30	75.30	15.30
An	0.20	0.00	0.00	0.30	0.40	12.70	12.70	12.30	12.50	11.40	0.50	22.30	0.20
Or	81.20	87.10	88.00	81.20	76.60	0.80	0.70	0.80	0.80	0.90	83.20	2.40	84.40

Analyses of biotite from the Ceará Central high-pressure metapelitic rocks.

Sample	**WT7-53A**	**WT7-53A**	**WT7-53A**	**WT7-53A**	**WT7-53A**	**WT7-53A**	**WT8-07**	**WT8-07**	**WT8-07**	**WT8-07**	**WT8-07**	**WT8-07**
Location	1 rim c-Grt	1 rim c-Pl	1 rim c-Pl	1 rim c-Sill	2 rim c-Pl	3 rim c-Grt	1 rim c-Grt	2 incl-grt	3 rim c-grt	4 rim c-Ky	5 rim c-Pl	6 rim c-Ky
SiO_2	36.62	36.31	37.58	37.07	36.37	36.82	35.32	35.45	35.94	35.36	35.92	36.17
TiO_2	4.82	4.26	3.76	4.43	2.97	4.90	3.03	2.15	0.19	2.76	1.94	2.90
Al_2O_3	17.98	18.17	19.44	17.62	18.69	17.47	18.72	18.48	19.51	18.61	18.47	18.86
FeO	15.01	15.79	12.29	15.13	13.96	13.59	16.94	18.38	18.71	17.31	17.05	15.65
MnO	0.00	0.00	0.07	0.00	0.04	0.01	0.05	0.04	0.00	0.02	0.02	0.02
MgO	12.20	11.92	12.43	12.97	13.11	13.35	11.48	11.14	12.28	11.92	12.27	11.11
BaO	0.14	0.22	0.04	0.24	0.18	0.10	0.17	0.12	0.09	0.20	0.11	0.10
CaO	0.09	0.00	0.01	0.01	0.03	0.01	0.00	0.03	0.02	0.00	0.00	0.04
Na_2O	0.12	0.12	0.11	0.13	0.16	0.12	0.45	0.33	0.29	0.36	0.20	0.40
K_2O	9.05	10.14	8.93	10.19	9.53	10.16	8.97	8.94	8.58	8.76	9.25	8.71
F	0.64	0.23	0.35	0.54	0.50	0.59	0.00	0.26	0.07	0.20	0.29	0.33
Cl	0.01	0.02	0.06	0.02	0.00	0.04	0.04	0.02	0.06	0.02	0.03	0.03
Total	96.67	97.19	95.05	98.33	95.54	97.14	95.16	95.33	95.71	95.51	95.56	94.30
Si	5.65	5.61	5.77	5.66	5.66	5.65	5.57	5.63	5.65	5.57	5.65	5.71
Al^{IV}	2.35	2.39	2.23	2.34	2.34	2.35	2.43	2.37	2.35	2.43	2.35	2.29
Al^{VI}	0.92	0.92	1.28	0.83	1.08	0.81	1.05	1.08	1.26	1.02	1.08	1.21
Ti	0.56	0.50	0.43	0.51	0.35	0.57	0.36	0.26	0.02	0.33	0.23	0.34
Fe^{2+}	1.94	2.04	1.58	1.93	1.82	1.75	2.23	2.44	2.46	2.28	2.24	2.07
Mn	0.00	0.00	0.01	0.00	0.01	0.00	0.01	0.01	0.00	0.00	0.00	0.00
Mg	2.81	2.75	2.84	2.95	3.04	3.06	2.70	2.64	2.88	2.80	2.88	2.61
Ba	0.01	0.01	0.00	0.01	0.01	0.01	0.01	0.01	0.01	0.01	0.01	0.01
Ca	0.01	0.00	0.00	0.00	0.01	0.00	0.00	0.01	0.00	0.00	0.00	0.01
Na	0.04	0.04	0.03	0.04	0.05	0.03	0.14	0.10	0.09	0.11	0.06	0.12
K	1.78	2.00	1.75	1.98	1.89	1.99	1.81	1.81	1.72	1.76	1.86	1.75

Analyses of biotite from the Ceará Central high-pressure metapelitic rocks.

Sample	**WT8-17**	**WT8-17**	**WT8-17**	**WT8-17**	**WT8-17**	**WT8-17**
Location	0 c-Pl	1 rim c-Pl	1 core-Ms	3 rim c-Pl	5 core	6 core
SiO_2	35.66	35.48	46.56	36.19	35.67	36.12
TiO_2	4.72	4.94	0.05	4.41	4.44	4.35
Al_2O_3	18.43	19.05	37.12	18.24	17.97	18.18
FeO	17.25	16.77	1.29	17.32	17.37	16.86
MnO	0.02	0.03	0.00	0.01	0.00	0.01
MgO	9.91	9.41	0.28	10.55	10.72	11.07
BaO	0.19	0.19	0.16	0.17	0.09	0.23
CaO	0.04	0.00	0.04	0.03	0.00	0.01
Na_2O	0.11	0.12	0.26	0.14	0.12	0.10
K_2O	10.35	10.23	9.74	10.06	10.10	10.22
F	0.36	0.28	0.00	0.30	0.44	0.13
Cl	0.01	0.00	0.01	0.01	0.03	0.01
Total	97.06	96.47	95.50	97.44	96.93	97.28
Si	5.58	5.56	6.42	5.62	5.59	5.60
Al^{IV}	2.42	2.44	1.58	2.38	2.42	2.40
Al^{VI}	0.97	1.07	4.44	0.95	0.90	0.93
Ti	0.56	0.58	0.01	0.52	0.52	0.51
Fe^{2+}	2.26	2.20	0.15	2.25	2.28	2.19
Mn	0.00	0.00	0.00	0.00	0.00	0.00
Mg	2.31	2.20	0.06	2.44	2.50	2.56
Ba	0.01	0.01	0.01	0.01	0.01	0.01
Ca	0.01	0.00	0.01	0.01	0.00	0.00
Na	0.03	0.04	0.07	0.04	0.04	0.03
K	2.07	2.04	1.71	1.99	2.02	2.02

Análises Geocronológicas

Tabelas U-Pb (1-10)

Table 1

Summary of LA-ICP-MS data for sample WT7-25

	Isotopic ratios							Ages							
Spot	**$^{206}Pb/^{204}Pb$**	**$^{207}Pb/^{206}Pb$**	**2σ**	**$^{207}Pb/^{235}U$**	**2σ**	**$^{206}Pb/^{238}U$**	**2σ**	**$^{207}Pb/^{206}Pb$**	**2σ**	**$^{207}Pb/^{235}U$**	**2σ**	**$^{206}Pb/^{238}U$**	**2σ**	**Rho**	**Conc. (%)**
Z3	-	0.09491	1.37829	3.41174	4.91709	0.26071	4.71997	1526.33	25.97	1507.1	28.79	1493.46	39.02	0.96	99.83
Z4	-	0.09707	0.77469	3.73159	2.33671	0.27881	2.20456	1568.58	14.51	1578.17	26.53	1585.36	28.85	0.94	100.11
Z5	-	0.09056	0.77228	2.62104	3.06299	0.20991	2.96403	1437.38	14.73	1306.56	20.06	1228.34	25.49	0.97	98.96
Z6	-	0.09018	1.57943	2.53407	4.90316	0.2038	4.64180	1429.33	30.15	1281.87	21.37	1195.72	31.61	0.95	98.85
Z7	-	0.08687	1.91282	2.26174	5.95525	0.18883	5.63969	1357.59	36.87	1200.45	19.66	1115.05	33.89	0.95	98.86
Z8	-	0.09617	0.77528	3.47138	2.47450	0.26179	2.34992	1551.14	14.56	1520.74	25.10	1498.99	27.99	0.95	99.72
Z9	-	0.09459	0.86757	3.20124	2.92915	0.24547	2.79772	1519.84	16.36	1457.46	24.23	1415.05	28.29	0.96	99.44
Z10	-	0.09579	0.90945	3.44734	3.06238	0.26102	2.92422	1543.63	17.10	1515.26	26.39	1495.05	30.25	0.95	99.74
Z11	-	0.08876	6.04901	2.19519	13.01747	0.17938	11.52666	1398.89	115.95	1179.52	20.70	1063.59	59.01	0.89	98.42
Z12	-	0.07898	2.89506	1.61898	6.60465	0.14868	5.93633	1171.52	57.31	977.59	14.28	893.55	28.67	0.9	98.83
Z13	-	0.09654	0.78889	3.61078	2.35817	0.27127	2.22229	1558.29	14.80	1551.91	25.75	1547.22	28.31	0.94	99.95
Z14	-	0.09658	0.79724	3.56597	2.19111	0.2678	2.04092	1559	14.96	1541.99	24.86	1529.61	27.37	0.93	99.85
Z15	-	0.08141	2.08080	1.79315	5.42187	0.15975	5.00669	1231.32	40.84	1042.97	15.37	955.4	27.03	0.92	98.8
Z16	-	0.09685	0.78843	3.65117	2.24886	0.27343	2.10612	1564.26	14.78	1560.76	25.66	1558.18	28.06	0.94	99.98

Table 2

Summary of LA-ICP-MS data for sample WT8-12F

	Isotopic ratios							Ages							
Spot	**$^{206}Pb/^{204}Pb$**	**$^{207}Pb/^{206}Pb$**	**2σ**	**$^{207}Pb/^{235}U$**	**2σ**	**$^{206}Pb/^{238}U$**	**2σ**	**$^{207}Pb/^{206}Pb$**	**2σ**	**$^{207}Pb/^{235}U$**	**2σ**	**$^{206}Pb/^{238}U$**	**2σ**	**Rho**	**Conc. (%)**
Z2	3629.38	0.09015	6.84952	2.77078	5.45690	0.2229	3.92339	1428.8	125.41	1347.7	40.96	1297.19	46.15	0.72	90.79
Z3	7416.75	0.0914	6.03621	2.79176	4.86033	0.22153	3.48655	1454.98	110.66	1353.33	36.15	1289.93	40.72	0.72	88.66
Z4	10666.09	0.09785	4.35368	3.46049	3.84879	0.2565	1.94938	1583.46	79.28	1518.26	30.20	1471.93	25.64	0.51	92.96
Z6	5259.05	0.09194	4.29224	2.8032	3.54805	0.22113	2.35953	1466.11	79.73	1356.39	26.35	1287.87	27.49	0.67	87.84
Z7	106002.6	0.09661	3.92665	3.82603	3.23769	0.28723	2.18631	1559.62	72.11	1598.24	25.84	1627.69	31.38	0.68	104.36
Z8	17210.72	0.08204	3.47246	1.98768	2.88532	0.17571	1.90086	1246.57	66.53	1111.33	19.44	1043.5	18.31	0.66	83.71
Z9	65401.44	0.08649	3.76442	2.41869	3.02464	0.20283	2.22317	1349.06	70.97	1248.17	21.58	1190.51	24.14	0.74	88.25
Z10	29845.47	0.06652	4.31061	1.15947	3.35420	0.12641	2.69250	822.92	87.50	781.71	18.18	767.35	19.46	0.8	93.25
Z11	4943.28	0.07508	4.13522	1.52232	3.33500	0.14706	2.31712	1070.53	80.93	939.41	20.74	884.48	19.19	0.69	82.62
Z12	1041.7	0.09026	4.43476	3.01013	3.82019	0.24187	2.19531	1431.1	82.35	1410.19	28.94	1396.39	27.53	0.57	97.57
Z13	37672.93	0.07981	7.93399	1.7557	6.17233	0.15956	4.89918	1192.18	149.08	1029.26	39.54	954.32	43.40	0.79	80.05
Z14	110294.4	0.0762	4.93826	1.61958	4.57956	0.15415	1.76793	1100.39	95.74	977.83	28.54	924.16	15.21	0.39	83.98
Z15	26194.67	0.09212	6.94943	3.24491	6.15449	0.25549	2.97817	1469.76	127.26	1467.96	47.28	1466.72	38.97	0.48	99.79
Z16	23746.34	0.09438	5.97488	3.46263	5.20037	0.26609	2.85705	1515.7	109.03	1518.75	40.39	1520.93	38.60	0.55	100.35
Z21	8498.39	0.09004	5.71372	2.68794	4.83500	0.21651	2.92636	1426.43	105.35	1325.14	35.66	1263.39	33.55	0.61	88.57
Z23	3189.21	0.08674	4.96017	2.19367	4.39039	0.18341	2.15871	1354.81	92.76	1179.03	30.67	1085.59	21.57	0.49	80.13
Z24	8086.86	0.09743	5.01806	3.74305	4.18221	0.27864	2.71299	1575.48	91.42	1580.63	33.15	1584.49	38.01	0.65	100.57
Z25	12984.51	0.08608	9.56080	2.54543	7.13510	0.21447	6.25390	1339.9	174.35	1285.13	51.27	1252.61	71.04	0.88	93.49

Table 3

Summary of LA-ICP-MS data for sample WT8-53E.

	Isotopic ratios							Ages							
Spot	**$^{206}Pb/^{204}Pb$**	**$^{207}Pb/^{206}Pb$**	**2σ**	**$^{207}Pb/^{235}U$**	**2σ**	**$^{206}Pb/^{238}U$**	**2σ**	**$^{207}Pb/^{206}Pb$**	**2σ**	**$^{207}Pb/^{235}U$**	**2σ**	**$^{206}Pb/^{238}U$**	**2σ**	**Rho**	**Conc. (%)**
Z4	27720.09	0.09406	1.0203	3.07779	2.31327	0.23731	2.07611	1509.39	19.14	1427.18	17.58	1372.7	25.62	0.83	90.94
Z6	31284.02	0.09392	1.05859	3.46926	2.2239	0.26791	1.95579	1506.47	19.87	1520.26	17.38	1530.18	26.59	0.88	101.57
Z7	16005.73	0.09407	1.0735	3.40143	2.23132	0.26226	1.95612	1509.43	20.14	1504.73	17.36	1501.39	26.15	0.88	99.47
Z9	29406.6	0.09839	0.80961	3.51295	2.4289	0.25896	2.29	1593.81	15.04	1530.13	19.02	1484.5	30.29	0.95	93.14
Z12	11020.15	0.09669	1.88869	3.43155	3.38408	0.25741	2.808	1561.14	35.01	1511.65	26.26	1476.58	36.95	0.71	94.58
Z14	11546.3	0.09628	0.96354	3.58917	1.41314	0.27036	1.03371	1553.31	17.98	1547.14	11.16	1542.63	14.17	0.49	99.31
Z17	9817.15	0.09364	0.81911	2.96772	1.45246	0.22985	1.19946	1500.92	15.41	1399.39	10.97	1333.72	14.43	0.81	88.86
Z18	18150.04	0.09534	0.91182	3.34079	1.27164	0.25413	0.88638	1534.89	17.06	1490.64	9.89	1459.73	11.57	0.56	95.1
Z29	12279.45	0.09128	0.80581	3.01235	1.27371	0.23933	0.98641	1452.55	15.26	1410.75	9.66	1383.23	12.27	0.74	95.23

Table 4

Summary of LA-ICP-MS data for sample WT8-53x

	Isotopic ratios							Ages							
Spot	**$^{206}Pb/^{204}Pb$**	**$^{207}Pb/^{206}Pb$**	**2σ**	**$^{207}Pb/^{235}U$**	**2σ**	**$^{206}Pb/^{238}U$**	**2σ**	**$^{207}Pb/^{206}Pb$**	**2σ**	**$^{207}Pb/^{235}U$**	**2σ**	**$^{206}Pb/^{238}U$**	**2σ**	**Rho**	**Conc. (%)**
z4	-	0.08879	1.17625	2.2286	1.73244	0.18204	1.27192	1399.66	22.38	1190.08	12.07	1078.1	12.61	0.73	77.5
z5	-	0.09715	1.86890	3.35424	2.58077	0.2504	1.77977	1570.18	34.61	1493.78	19.99	1440.54	22.93	0.69	92.82
z6	-	0.09583	1.40843	3.11083	1.98768	0.23545	1.40258	1544.36	26.24	1435.37	15.16	1362.99	17.21	0.71	88.67
z7	-	0.09772	1.97996	3.59397	2.89848	0.26675	2.11682	1581.02	36.59	1548.2	22.77	1524.27	28.67	0.73	97.74
z9	-	0.09646	1.59449	3.31294	2.85527	0.24909	2.36858	1556.82	29.63	1484.1	22.03	1433.76	30.38	0.83	92.28
z11	-	0.08869	2.51096	2.41714	3.14519	0.19767	1.89403	1397.4	47.39	1247.71	22.34	1162.8	20.12	0.6	85.08
z12	-	0.0938	1.62269	2.95772	2.20375	0.2287	1.49110	1504	30.28	1396.83	16.63	1327.7	17.88	0.68	88.28

Table 5

Summary of LA-ICP-MS data for sample TJF6-302

	Isotopic ratios							Ages							
Spot	**$^{206}Pb/^{204}Pb$**	**$^{207}Pb/^{206}Pb$**	**2σ**	**$^{207}Pb/^{235}U$**	**2σ**	**$^{206}Pb/^{238}U$**	**2σ**	**$^{207}Pb/^{206}Pb$**	**2σ**	**$^{207}Pb/^{235}U$**	**2σ**	**$^{206}Pb/^{238}U$**	**2σ**	**Rho**	**Conc. (%)**
Z22	19367.22	0.0794	1.47134	1.86899	1.78296	0.17071	1.007022	1182.23	28.73	1070.17	11.77	1016.03	9.47	0.56	85.94
Z14	0	0.08061	1.15137	1.82516	1.88461	0.16421	1.492014	1211.97	22.47	1054.54	12.30	980.14	13.56	0.62	80.87
Z21	12936.88	0.0802	1.62416	1.86111	2.27950	0.16831	1.599437	1201.88	31.56	1067.38	15.02	1002.78	14.85	0.7	83.43
Z2	15457.53	0.0813	1.41316	1.58023	1.75290	0.14097	1.037120	1228.72	27.41	962.46	10.89	850.14	8.26	0.59	69.19
Z19	31413.04	0.08226	0.91796	1.85648	1.64528	0.16368	1.365398	1251.79	17.83	1065.74	10.82	977.17	12.37	0.83	78.06
Z10	81567.39	0.08295	1.79376	1.91646	3.58365	0.16757	3.102418	1267.98	34.60	1086.84	23.65	998.71	28.64	0.87	78.76
Z13	0	0.08353	2.22139	1.91238	2.45430	0.16605	1.043561	1281.64	42.62	1085.42	16.26	990.29	9.58	0.33	77.27
Z7	20926.15	0.08558	1.40000	1.93503	2.34419	0.16398	1.880216	1328.77	26.80	1093.28	15.62	978.88	17.07	0.8	73.67
Z18	57006.47	0.08616	1.03918	2.3382	1.64548	0.19682	1.275814	1341.79	19.93	1223.97	11.65	1158.22	13.51	0.78	86.32
Z12	0	0.08696	1.05821	2.4292	1.46871	0.20261	1.018479	1359.57	20.25	1251.28	10.52	1189.3	11.05	0.36	87.48
Z11	111751.35	0.08888	0.97994	2.71273	1.42092	0.22137	1.028949	1401.47	18.65	1331.95	10.49	1289.13	12.01	0.72	91.98

Table 6

Summary of LA-ICP-MS data for sample TJF6-335

	Isotopic ratios							Ages							
Spot	**$^{206}Pb/^{204}Pb$**	**$^{207}Pb/^{206}Pb$**	**2σ**	**$^{207}Pb/^{235}U$**	**2σ**	**$^{206}Pb/^{238}U$**	**2σ**	**$^{207}Pb/^{206}Pb$**	**2σ**	**$^{207}Pb/^{235}U$**	**2σ**	**$^{206}Pb/^{238}U$**	**2σ**	**Rho**	**Conc. (%)**
Z3	1104	0.05902	6.94387	0.8399	0.8399	0.10322	6.61966	567.7	151.2	619.1	44.5	633.3	39.9	0.69	102.29
Z10	-188844	0.05954	6.33292	0.9526	0.9526	0.11604	5.12812	586.9	137.4	679.5	40.4	707.7	34.4	0.63	104.16
Z12	-254292	0.05918	3.58504	0.8824	0.8824	0.10814	2.71508	573.7	78.0	642.3	21.4	662	17.1	0.6	103.06
Z19	-483358	0.06474	6.30877	0.9744	0.9744	0.10916	7.36725	765.9	132.9	690.7	48.6	667.9	46.7	0.76	96.69
Z21	-548806	0.05191	6.23081	0.7639	0.7639	0.10673	6.26378	281.6	142.6	576.3	38.9	653.7	38.9	0.71	113.44
Z22	-581529	0.05651	4.90956	0.8546	0.8546	0.10969	5.68858	472.4	108.6	627.2	35.2	671	36.2	0.76	106.98
Z23	-614253	0.06445	5.59719	1.1996	1.1996	0.13498	6.49948	756.6	118.1	800.4	47.5	816.2	49.8	0.76	107.89
Z25	-679701	0.05817	3.34293	0.9495	0.9495	0.1184	2.87201	536	73.2	677.9	21.8	721.3	19.6	0.65	106.41
Z26	-712424	0.06085	4.65287	0.8439	0.8439	0.10058	8.30638	633.9	100.2	621.3	44.2	617.8	48.9	0.87	99.44
Z30	-843319	0.06381	4.05328	0.9448	0.9448	0.10739	5.25908	735.4	85.8	675.4	32.8	657.6	32.9	0.79	97.36
Z31	-876043	0.05929	5.89742	0.7948	0.7948	0.09723	4.72004	577.7	128.2	593.9	34.0	598.1	27.0	0.62	100.71
Z32	-908767	0.06016	2.51935	0.8564	0.8564	0.10323	1.74603	609.5	54.5	628.1	14.4	633.3	10.5	0.57	100.83
Z33	-941491	0.05977	4.31580	0.9128	0.9128	0.11076	3.50246	595.3	93.5	658.6	26.9	677.2	22.5	0.63	102.83
Z35	-1006938	0.06125	5.03457	0.9332	0.9332	0.11051	4.15678	647.9	108.1	669.3	32.0	675.7	26.7	0.64	100.95
Z36	-1039662	0.06036	3.20988	0.8294	0.8294	0.09966	2.65221	616.4	69.3	613.3	19.2	612.4	15.5	0.64	99.86
Z37	-1072386	0.05952	4.92341	0.8203	0.8203	0.09995	2.57622	586.3	106.8	608.2	25.4	614.1	15.1	0.46	100.97
Z38	-1105109	0.06222	4.35348	0.8423	0.8423	0.09818	2.87732	681.8	93.0	620.4	24.2	603.7	16.6	0.55	97.31
Z39	-1137833	0.05973	5.52052	0.8279	0.8279	0.10053	2.74741	593.8	119.6	612.5	28.4	617.5	16.2	0.45	100.83
Z40	-1170557	0.06957	2.24199	1.2597	1.2597	0.13132	3.07448	915.7	46.1	827.8	21.5	795.4	23.0	0.81	86.86

Table 7

Summary of LA-ICP-MS data for sample WT8-53MM.

	Isotopic ratios							Ages							
Spot	$^{206}Pb/^{204}Pb$	$^{207}Pb/^{206}Pb$	**2σ**	$^{207}Pb/^{235}U$	**2σ**	$^{206}Pb/^{238}U$	**2σ**	$^{207}Pb/^{206}Pb$	**2σ**	$^{207}Pb/^{235}U$	**2σ**	$^{206}Pb/^{238}U$	**2σ**	**Rho**	**Conc. (%)**
Z1	9248	0.13406	2.7	4.8475	2.2	0.26225	1.6	2151.9	46	1793.2	18.1	1501.3	20.9	0.67	69.77
Z3	11338	0.13477	2.5	5.452	2	0.2934	1.5	2161	42.8	1893.1	17.2	1658.5	21.3	0.68	76.75
Z4	10478	0.1593	4.2	10.0865	3.3	0.45923	2.6	2448.2	68.9	2442.7	30	2436.2	51.6	0.69	99.51
Z5	6318	0.135	2.5	7.6044	2	0.40852	1.5	2164.1	43.6	2185.4	18	2208.2	28.6	0.74	102.04
Z6	45422	0.12059	2.2	5.1961	1.8	0.31252	1.3	1964.9	38.4	1852	14.9	1753.1	19.7	0.69	89.22
Z7	14232	0.12971	2.4	6.201	1.9	0.34674	1.4	2094	41.3	2004.6	16.7	1919	23.2	0.69	91.64
Z8	27617	0.26648	3.3	21.1335	2.6	0.57518	2.1	3285.4	51.6	3144.7	24.7	2929.1	50.2	0.66	89.15
Z9b	90032	0.12525	2.1	5.7922	1.8	0.3354	1.2	2032.3	37	1945.2	15.2	1864.5	18.7	0.54	91.74
Z9n	99005	0.13636	2.5	6.9629	2	0.37034	1.5	2181.5	43.5	2106.7	17.8	2031	26.6	0.72	93.1
Z10b	10545	0.06088	2.4	0.9286	2	0.11062	1.4	635.1	51.2	666.9	9.7	676.3	8.9	0.66	106.5
Z10n	13541	0.12774	3.8	6.7131	3.1	0.38115	2.2	2067.1	64.8	2074.3	26.6	2081.7	38.8	0.63	100.7
Z11	10820	0.15174	2.2	10.3085	1.8	0.49273	1.2	2365.6	37.2	2462.9	16.7	2582.5	26.4	0.63	109.17
Z12	84044	0.12517	1	6.0611	1.5	0.3512	1.1	2031.2	18.4	1984.7	13.1	1940.3	18.3	0.63	95.53
Z13	18336	0.12555	1.3	5.171	2	0.29872	1.5	2036.5	22.2	1847.9	16.6	1685	22.2	0.72	82.74
Z14	93994	0.13018	1.6	6.7512	2.8	0.37612	2.3	2100.4	28	2079.3	24.5	2058.1	39.9	0.69	97.99
Z15	25634	0.1403	1.2	7.6246	1.7	0.39414	1.2	2231	20.9	2187.8	15.1	2142	21.3	0.52	96.01
Z16n	45471	0.07419	1.7	1.2833	2.2	0.12546	1.4	1046.6	34.2	838.3	12.7	761.9	10.3	0.57	72.8
Z16b	12670	0.06243	1.4	0.8848	2.1	0.10278	1.5	689	30.9	643.6	9.9	630.7	9	0.67	91.54
Z17	22116	0.14181	2	8.5711	2.8	0.43836	2	2249.4	35	2293.5	25.9	2343.3	39.3	0.6	104.17
Z18	11607	0.14096	1.3	8.1441	2	0.41904	1.5	2239	23.3	2247.2	18	2256.1	28	0.7	100.76
Z19	227993	0.12959	1.5	5.447	1.9	0.30485	1.2	2092.4	25.7	1892.3	16.5	1715.3	18.8	0.59	81.98
Z20	23744	0.13664	1.3	7.9519	1.9	0.42207	1.3	2185.1	23.1	2225.6	16.8	2269.9	24.9	0.65	103.88
Z21b	10372	0.09633	2.5	2.0489	3.5	0.15427	2.5	1554.1	46.5	1131.9	24	924.8	21.5	0.59	59.51
Z22	19511	0.12224	1.6	5.6725	2.1	0.33655	1.4	1989.2	29	1927.2	18.5	1870	22.7	0.59	94.01
Z23	9212	0.13268	1.6	6.7571	2.2	0.36938	1.5	2133.7	28.4	2080.1	19.8	2026.5	26.8	0.65	94.98
Z24	17889	0.16233	1.5	9.8479	2	0.43998	1.3	2480.1	25.7	2420.6	18.3	2350.6	25.1	0.58	94.78

Z25n	294328	0.16378	2.2	10.4617	2.8	0.46329	1.8	2495	36.6	2476.5	26.3	2454.1	37.3	0.51	98.36
Z25b	28391	0.12189	1.5	5.3993	2	0.32128	1.4	1984	26.7	1884.8	17.5	1796	21.9	0.64	90.52
Z26	219094	0.15641	1.5	7.6009	2	0.35245	1.3	2417.2	25.9	2185	17.9	1946.3	21.5	0.59	80.52
Z27	23087	0.1455	1.8	6.7892	2.2	0.33842	1.3	2293.7	30.4	2084.3	19.5	1879.1	21.6	0.54	81.92
Z28	39713	0.12907	2.3	6.0598	3.1	0.34052	2.2	2085.3	40	1984.5	27.4	1889.2	35.6	0.52	90.59
Z29b	15784	0.13623	2	6.8905	2.4	0.36684	1.2	2179.8	35.5	2097.4	21.2	2014.5	21.6	0.42	92.42
Z29n	20514	0.14908	1.9	10.188	2.4	0.49563	1.5	2335.4	32	2452	22.4	2595	32.9	0.59	111.11
Z30	20433	0.15279	1.7	8.2979	2.3	0.39388	1.5	2377.4	29.6	2264.1	20.8	2140.8	27.3	0.61	90.05
Z30b	13543	0.06281	2.8	0.8481	3.4	0.09794	1.9	701.6	59.6	623.6	15.9	602.3	11.2	0.47	85.84
Z31	23325	0.11982	1.4	4.3801	2.1	0.26513	1.5	1953.5	25.9	1708.6	17	1516	19.8	0.68	77.61
Z32	5652	0.07043	1.9	0.9654	2.5	0.09941	1.7	940.9	39	686.1	12.6	611	9.6	0.62	64.93
Z33	11170	0.12258	2.1	3.2364	2.5	0.19149	1.4	1994.1	36.8	1465.9	19.2	1129.4	14.1	0.49	56.64
Z34	7407	0.21413	2.6	15.7991	3.8	0.53512	2.7	2937.1	42.8	2864.7	36	2763	60.3	0.59	94.07
Z35n	28466	0.14611	1.7	7.9541	2.2	0.39483	1.4	2300.9	29.9	2225.8	20.2	2145.2	25.7	0.55	93.23
Z35b	66702	0.13304	1.5	6.4899	1.9	0.3538	1.2	2138.5	26.8	2044.5	17	1952.7	19.9	0.51	91.31
Z36	41146	0.12206	1.5	5.6298	2	0.33451	1.3	1986.6	26.3	1920.7	17	1860.2	21	0.6	93.64
Z37	19319	0.13119	2	6.0247	2.9	0.33308	2.1	2113.9	35.1	1979.4	25	1853.3	33.1	0.58	87.67
Z38	17678	0.12314	1.5	3.8112	2	0.22447	1.3	2002.2	26.2	1595.1	16	1305.5	15.8	0.62	65.2
Z39	118172	0.20509	1.4	12.4538	1.8	0.44041	1.2	2867.1	22.7	2639.2	17.2	2352.5	23.4	0.57	82.05
Z40	19942	0.14139	1.6	7.4739	2	0.38338	1.2	2244.3	27.5	2169.9	17.8	2092	21.3	0.51	93.22
Z41	35847	0.15665	1.8	8.6346	2.5	0.39978	1.8	2419.8	29.8	2300.2	22.8	2168	33	0.54	89.6
Z43	14225	0.13513	1.5	6.6729	2.1	0.35816	1.4	2165.6	27	2069	18.5	1973.4	24	0.61	91.12
Z44	17558	0.16607	1.4	10.1135	1.9	0.44169	1.2	2518.4	23.9	2445.2	17.2	2358.2	23.8	0.56	93.64
Z45	8295	0.12699	2.2	6.1447	3.3	0.35095	2.5	2056.7	39.6	1996.6	29.2	1939.1	41.5	0.64	94.28
Z46	6325	0.13633	1.3	6.8203	1.9	0.36285	1.4	2181	23.1	2088.4	16.9	1995.7	23.5	0.68	91.5
Z47	16479	0.14046	1.4	7.569	1.8	0.39082	1.1	2232.9	25	2181.2	16.3	2126.6	19.9	0.52	95.24
Z48	15648	0.1339	1.5	6.5986	1.9	0.35742	1.2	2149.7	25.7	2059.2	16.9	1969.9	20.8	0.57	91.64
Z49	12914	0.1206	2.7	4.9996	3.6	0.30067	2.4	1965.1	47.8	1819.2	30.2	1694.6	35.2	0.54	86.24
Z50	10784	0.13985	2	7.8484	2.3	0.40702	1.3	2225.4	34	2213.8	21	2201.3	23.5	0.45	98.92
Z52	6982	0.14097	1.6	9.4632	2.1	0.48688	1.4	2239.1	28.5	2384	19.7	2557.2	28.9	0.58	114.2
Z53	9325	0.11484	2.1	3.6486	3.3	0.23043	2.5	1877.4	38.6	1560.2	26.2	1336.7	30.1	0.63	71.2
Z54	2618	0.05887	2.4	0.8382	2.8	0.10327	1.4	562.1	52.3	618.1	13	633.5	8.7	0.46	112.7

Table 8
Summary of LA-ICP-MS data for sample WT8-53ML.

	Isotopic ratios							Ages							
Spot	$^{206}Pb/^{204}Pb$	$^{207}Pb/^{206}Pb$	2σ	$^{207}Pb/^{235}U$	2σ	$^{206}Pb/^{238}U$	2σ	$^{207}Pb/^{206}Pb$	2σ	$^{207}Pb/^{235}U$	2σ	$^{206}Pb/^{238}U$	2σ	Rho	Conc. (%)
Z9	16533.29	0.05989	3.95900	0.88346	5.568261	0.10698	3.91559	599.73	83.48	642.85	26.18	655.19	24.35	0.7	109.25
Z10	17470.58	0.05961	4.03404	0.9114	5.983319	0.11089	4.41889	589.36	85.17	657.8	28.56	677.94	28.37	0.74	115.03
Z11	18407.87	0.06025	3.94295	0.86386	6.322258	0.104	4.94208	612.4	82.98	632.23	29.33	637.78	29.94	0.78	104.15
Z12	20282.44	0.06017	4.42083	0.81888	7.402565	0.09871	5.93753	609.65	92.79	607.43	33.29	606.83	34.30	0.8	99.54
Z14	22157.01	0.06099	5.13889	0.85637	6.568211	0.10184	4.09062	638.87	106.85	628.14	30.31	625.16	24.33	0.62	97.85
Mn1	3097.58	0.06106	6.09748	0.7341	5.929448	0.0872	4.70052	641.28	75.77	558.96	25.23	538.95	24.26	0.79	84.04
Mn2	2473.99	0.06105	6.16893	0.73225	6.165975	0.08699	4.56067	641	86.39	557.88	26.35	537.72	23.51	0.74	83.89
Mn3	3411.28	0.06011	8.47561	0.71446	6.677247	0.08621	5.30630	607.47	85.07	547.39	28.00	533.07	27.11	0.79	87.75
Mn4	4348.56	0.06128	6.95358	0.77073	7.220607	0.09122	5.95282	648.97	85.20	580.18	31.56	562.77	32.02	0.82	86.72
Mn5	5285.85	0.06171	6.30376	0.73573	6.370811	0.08647	4.83888	664	86.17	559.91	27.16	534.64	24.79	0.76	80.52
Mn6	6223.14	0.06066	6.29726	0.77212	6.293561	0.09231	4.99591	627.24	80.25	580.98	27.57	569.21	27.17	0.79	90.75
Mn7	7160.42	0.06208	6.92046	0.73399	5.583887	0.08575	4.20172	676.88	76.55	558.89	23.81	530.35	21.37	0.75	78.35

Table 9

Summary of LA-ICP-MS data for sample WT7-21B.

	Isotopic ratios							Ages							
Spot	$^{206}Pb/^{204}Pb$	$^{207}Pb/^{206}Pb$	2σ	$^{207}Pb/^{235}U$	2σ	$^{206}Pb/^{238}U$	2σ	$^{207}Pb/^{206}Pb$	2σ	$^{207}Pb/^{235}U$	2σ	$^{206}Pb/^{238}U$	2σ	Rho	Disc. (%)
z1	-	0.11011	1.39477	1.12771	6.91406	0.07428	6.77191	1801.2	25	766.7	10	461.9	30	1	74.4
z2		0.10726	1.04149	1.44492	6.43967	0.0977	6.35489	1753.4	19	907.8	13	600.9	36	1	65.7
z3		0.11161	1.76738	1.09633	9.07455	0.07125	8.90078	1825.7	32	751.6	10	443.7	38	1	75.7
z4		0.13638	1.21663	6.50144	2.85761	0.34574	2.58568	2181.7	21	2046.1	49	1914.2	43	0.9	12.3
z6		0.10792	1.55614	1.11233	12.57163	0.07475	12.47495	1764.6	28	759.3	10	464.7	56	1	73.7
z7		0.1325	2.12489	5.45419	8.97285	0.29854	8.71762	2131.4	37	1893.4	50	1684.1	129	1	21
z8		0.11555	1.15909	1.05959	2.66961	0.06651	2.40486	1888.5	21	733.6	8	415.1	10	0.9	78
z9		0.1309	1.01908	6.38584	2.93320	0.35382	2.75048	2110.1	18	2030.3	48	1952.8	46	0.9	7.5
z10		0.11191	1.36911	1.69974	6.83188	0.11016	6.69329	1830.7	25	1008.4	15	673.7	43	1	63.2
z11		0.12451	1.42298	3.00189	7.56188	0.17486	7.42679	2021.8	25	1408.1	27	1038.9	71	1	48.6
z12		0.12787	2.36136	3.75882	7.29036	0.2132	6.89735	2068.8	42	1584	34	1245.9	78	0.9	39.8
z13		0.10758	1.31396	1.85045	4.12860	0.12475	3.91393	1758.9	24	1063.6	15	757.8	28	0.9	56.9
z14		0.11949	1.00861	5.59515	5.65760	0.3396	5.56697	1948.7	18	1915.4	48	1884.7	91	1	3.3
z15		0.09075	1.41611	1.66071	2.90109	0.13272	2.53199	1441.4	27	993.6	13	803.4	19	0.9	44.3
z16		0.10043	1.11679	2.748	12.37917	0.19844	12.32869	1632.1	21	1341.5	26	1167	132	1	28.5
z17		0.101	1.29210	2.6006	6.86215	0.18675	6.73940	1642.5	24	1300.8	23	1103.7	68	1	32.8
z18		0.10298	1.18322	2.87288	3.06425	0.20234	2.82659	1678.5	22	1374.8	22	1187.9	31	0.9	29.2
z19		0.12103	1.21489	1.09383	3.55058	0.06555	3.33626	1971.4	22	750.4	9	409.3	13	0.9	79.2
z20		0.12487	1.23804	4.74899	3.02940	0.27583	2.76487	2027	22	1775.9	36	1570.3	39	0.9	22.5
z21		0.13333	1.04385	8.17215	2.74569	0.44453	2.53953	2142.3	18	2250.3	61	2370.9	50	0.9	-10.7
z22		0.11072	2.57715	1.82334	8.58291	0.11944	8.18686	1811.2	47	1053.9	17	727.3	56	1	59.8
z23		0.11985	2.71540	2.07999	9.66272	0.12587	9.27333	1954	48	1142.2	19	764.2	67	1	60.9
z24		0.10197	1.36742	1.81927	5.22200	0.1294	5.03979	1660.3	25	1052.4	16	784.4	37	1	52.8
z25		0.12809	1.85738	1.12568	7.08321	0.06374	6.83535	2071.9	33	765.7	10	398.3	26	1	80.8
z26		0.10656	1.44531	1.19966	4.02331	0.08165	3.75475	1741.4	26	800.4	10	506	18	0.9	70.9
z27		0.12627	1.01517	4.98751	2.80271	0.28646	2.61240	2046.7	18	1817.2	37	1623.8	37	0.9	20.7

z28	0.11003	1.06562	2.1702	4.66934	0.14305	4.54612	1799.9	19	1171.5	18	861.9	37	1	52.1
z29	0.13316	2.09471	1.15757	5.28890	0.06305	4.85641	2140.1	37	780.8	10	394.1	19	0.9	81.6
z30	0.11043	1.76269	1.64786	3.60505	0.10823	3.14472	1806.5	32	988.7	13	662.4	20	0.9	63.3
z31	0.1036	1.16341	0.83156	6.13898	0.05822	6.02773	1689.5	21	614.5	7	364.8	21	1	78.4
z32	0.14329	1.66494	2.44852	3.70446	0.12394	3.30923	2267.3	29	1257	20	753.2	24	0.9	66.8
z33	0.12114	1.58687	0.86219	5.56248	0.05162	5.33133	1973.1	28	631.3	7	324.5	17	1	83.6
z34	0.13674	1.03417	4.01973	8.92349	0.21321	8.86337	2186.3	18	1638.2	37	1245.9	100	1	43
z35	0.11499	1.74831	2.27049	8.39557	0.14321	8.21152	1879.7	32	1203.2	21	862.8	66	1	54.1
z36	0.12745	1.57153	2.91785	17.52428	0.16605	17.45368	2063.1	28	1386.5	28	990.3	160	1	52
z37	0.11746	1.40967	1.54133	7.73794	0.09517	7.60846	1917.9	25	947	14	586	43	1	69.4
z38	0.11327	1.63897	2.30752	9.86732	0.14775	9.73025	1852.5	30	1214.6	21	888.4	81	1	52
z39	0.10355	2.31115	1.21231	4.09927	0.08491	3.38565	1688.7	43	806.3	10	525.4	17	0.8	68.9
z40	0.11187	1.88610	2.02642	4.49219	0.13137	4.07706	1830	34	1124.4	17	795.7	31	0.9	56.5
z41	0.11828	1.74589	3.13452	11.65750	0.1922	11.52602	1930.4	31	1441.2	29	1133.3	120	1	41.3
z42	0.13043	1.22041	6.46616	3.52326	0.35956	3.30514	2103.7	21	2041.3	51	1980.1	56	0.9	5.9
z43	0.11623	2.66807	2.78341	10.87624	0.17368	10.54390	1899.1	48	1351.1	26	1032.4	101	1	45.6
z44	0.14388	2.16351	4.168	5.24482	0.2101	4.77780	2274.4	37	1667.8	36	1229.4	53	0.9	45.9
z45	0.09669	1.32395	0.97574	3.65110	0.07319	3.40260	1561.2	25	691.4	8	455.3	15	0.9	70.8
z46	0.13122	1.33030	6.37793	3.52728	0.35252	3.26680	2114.4	23	2029.2	50	1946.6	55	0.9	7.9
z47	0.13067	1.50542	6.0721	3.27767	0.33702	2.91150	2107	26	1986.2	47	1872.3	47	0.9	11.1
z48	0.13099	1.17370	6.11348	5.63107	0.3385	5.50740	2111.2	21	1992.2	53	1879.5	90	1	11
z49	0.13081	1.14891	6.25481	5.78236	0.34679	5.66707	2108.9	20	2012.1	54	1919.2	94	1	9
z50	0.13577	1.07828	7.1034	5.02601	0.37947	4.90898	2173.9	19	2124.5	60	2073.8	87	1	4.6
z51	0.13814	1.55185	4.44486	11.83468	0.23337	11.73249	2204	27	1720.7	42	1352.1	143	1	38.7
z52	0.13288	1.17037	5.93966	5.19617	0.32418	5.06264	2136.4	20	1967.1	51	1810.1	80	1	15.3
z53	0.13352	1.07094	7.68094	3.14167	0.41724	2.95350	2144.7	19	2194.4	59	2247.9	56	0.9	-4.8
z54	0.15114	1.08449	9.37009	2.55913	0.44963	2.31798	2358.9	19	2374.9	68	2393.6	46	0.9	-1.5
z55	0.12654	1.14411	4.82774	7.46815	0.2767	7.37999	2050.4	20	1789.7	43	1574.7	103	1	23.2
z56	0.12709	1.03873	5.34576	6.04918	0.30506	5.95933	2058.2	18	1876.2	47	1716.3	90	1	16.6

Table 10

Summary of LA-ICP-MS data for sample TJF4-7

Spot	Isotopic ratios							Ages							
	$^{206}Pb/^{204}Pb$	$^{207}Pb/^{206}Pb$	2σ	$^{207}Pb/^{235}U$	2σ	$^{206}Pb/^{238}U$	2σ	$^{207}Pb/^{206}Pb$	2σ	$^{207}Pb/^{235}U$	2σ	$^{206}Pb/^{238}U$	2σ	Rho	Conc. (%)
Z1		0.06118	0.71718	0.85657	2.71628	0.10154	2.61989	645.6	15	628.3	6	623.4	16	1	99.99
Z2		0.06125	1.02011	0.87675	2.72943	0.10382	2.53164	647.9	22	639.2	7	636.8	15	0.9	100.06
Z3		0.06204	1.03686	0.9241	2.74669	0.10802	2.54347	675.6	22	664.5	7	661.3	16	0.9	100.05
Z4		0.12025	0.66296	4.93957	2.67558	0.29793	2.59215	1959.9	12	1809	37	1681.1	38	1	98.09
Z5		0.14684	2.34517	6.55053	7.48666	0.32355	7.10987	2309.4	40	2052.7	59	1807	112	0.9	95.93
Z6		0.10479	1.15099	3.34638	2.80656	0.2316	2.55969	1710.7	21	1491.9	25	1342.9	31	0.9	97.91
Z7		0.08037	3.11206	1.42978	5.01028	0.12902	3.92658	1206.2	61	901.5	12	782.3	29	0.8	98.27
Z8		0.11616	0.85883	4.70991	2.74684	0.29408	2.60913	1897.9	15	1769	35	1661.9	38	0.9	98.43
Z9		0.12728	0.99232	6.43507	3.75476	0.36669	3.62126	2060.7	18	2037.1	52	2013.8	63	1	99.63
Z10		0.1349	0.55882	6.7295	2.75000	0.36181	2.69262	2162.7	10	2076.5	50	1990.7	46	1	98.59
Z11		0.10992	0.89938	3.3051	3.10580	0.21807	2.97273	1798.1	16	1482.3	25	1271.7	34	1	96.98
Z12		0.06172	0.80251	0.88726	2.74874	0.10425	2.62899	664.6	17	644.9	7	639.3	16	1	100.01
Z13		0.06124	1.15200	0.90068	2.77313	0.10667	2.52252	647.6	25	652.1	7	653.4	16	0.9	100.11
Z14		0.06164	0.69998	0.87982	2.64224	0.10352	2.54783	661.7	15	640.9	6	635	15	1	99.97
Z15		0.06141	1.08218	0.85918	2.82591	0.10147	2.61049	653.7	23	629.7	6	623	16	0.9	100.01
Z16		0.12415	0.75900	4.56577	2.73397	0.26672	2.62650	2016.8	13	1743	34	1524.1	36	1	96.71
Z17		0.1316	0.74658	6.82274	2.84637	0.37601	2.74672	2119.4	13	2088.7	51	2057.6	48	1	99.49
Z18		0.12784	0.67130	6.45065	2.80206	0.36595	2.72045	2068.5	12	2039.2	48	2010.3	47	1	99.54
Z19		0.06197	1.06413	0.88369	2.81222	0.10343	2.60312	672.9	23	643	7	634.5	16	0.9	100.06
Z20		0.062	0.85592	0.90183	2.77822	0.10549	2.64309	674.2	18	652.7	7	646.5	16	1	100.02
Z21		0.06123	0.74713	0.92057	2.65512	0.10905	2.54783	647.2	16	662.7	7	667.2	16	1	100.12
Z22		0.06265	1.13163	0.93514	2.86341	0.10826	2.63030	696.4	24	670.3	7	662.6	17	0.9	100.1
Z23		0.06161	0.85283	0.91128	2.67944	0.10727	2.54010	660.7	18	657.7	7	656.9	16	0.9	100.13
Z24		0.13112	0.71103	6.70863	2.70189	0.37108	2.60666	2113	12	2073.8	50	2034.5	45	1	99.36
Z26		0.12874	0.64828	2.46454	3.66402	0.13884	3.60622	2080.9	11	1261.7	20	838.1	28	1	92.79
Z27		0.1325	0.76547	6.03312	5.72240	0.33023	5.67097	2131.4	13	1980.6	52	1839.5	91	1	97.75

Z28	0.10823	2.21499	3.48139	7.48835	0.2333	7.15326	1769.8	40	1523	31	1351.8	87	1	97.57
Z29	0.13056	0.87273	6.12325	3.73279	0.34016	3.62934	2105.5	15	1993.6	49	1887.4	59	1	98.31
Z30	0.06185	0.77777	0.8748	2.75035	0.10258	2.63809	668.9	17	638.2	7	629.5	16	1	99.97
Z31	0.13294	0.70664	6.17817	3.32767	0.33705	3.25178	2137.2	12	2001.4	48	1872.5	53	1	97.94
Z32	0.06195	0.73801	0.90663	2.73252	0.10614	2.63097	672.4	16	655.3	7	650.3	16	1	99.98
Z33	0.06101	0.75459	0.889	2.65498	0.10569	2.54549	639.4	16	645.8	7	647.7	16	1	100.08
Z34	0.15335	0.67228	8.9491	2.63506	0.42326	2.54785	2383.6	11	2332.8	66	2275.2	49	1	98.92
Z35	0.06164	0.78056	0.90519	2.63627	0.10651	2.51806	661.5	17	654.5	7	652.5	16	1	100.01
Z36	0.12566	0.63956	4.82071	2.67232	0.27823	2.59466	2038.1	11	1788.5	36	1582.5	36	1	96.88
Z37	0.06132	0.67482	0.90616	2.68877	0.10717	2.60271	650.5	14	655	7	656.3	16	1	100.06
Z38	0.11481	1.00075	3.31538	2.92153	0.20944	2.74478	1876.9	18	1484.7	25	1225.8	31	0.9	96.18
Z39	0.06135	0.78681	0.90076	2.67126	0.10649	2.55275	651.5	17	652.1	7	652.3	16	1	100.1
Z41	0.12455	0.89551	6.04745	3.04955	0.35214	2.91510	2022.5	16	1982.7	46	1944.8	49	1	99.42
Z42	0.06102	0.69799	0.87981	2.63187	0.10458	2.53762	639.9	15	640.9	6	641.2	15	1	100.05
Z43	0.12703	0.89845	4.3106	4.34054	0.24611	4.24654	2057.3	16	1695.4	36	1418.4	54	1	95.8
Z44	0.06115	0.77917	0.89336	2.71564	0.10595	2.60146	644.7	17	648.2	7	649.2	16	1	100.08
Z45	0.06079	0.63701	0.88598	2.69760	0.10571	2.62132	631.7	14	644.2	7	647.8	16	1	100.09
Z47	0.06143	0.71514	0.92705	2.68607	0.10945	2.58912	654.3	15	666.1	7	669.6	16	1	100.12
Z48	0.13272	0.70479	5.59221	2.91832	0.3056	2.83194	2134.3	12	1914.9	42	1719	43	1	96.93
Z49	0.06272	1.21300	0.92749	2.87154	0.10726	2.60276	698.6	26	666.3	7	656.8	16	0.9	99.9
Z50	0.1205	1.12074	4.21554	3.15799	0.25373	2.95243	1963.6	20	1677.1	33	1457.7	39	0.9	96.74
Z51	0.06214	0.91274	0.92269	2.75279	0.10769	2.59706	679.1	20	663.8	7	659.3	16	0.9	100.08
Z53	0.13462	0.89908	6.83357	3.65146	0.36816	3.53904	2159.1	16	2090.1	54	2020.7	61	1	98.85
Z54	0.15244	2.85323	7.08144	4.28375	0.33692	3.19524	2373.4	49	2121.7	58	1871.9	52	0.7	95.75
z56	0.12916	0.58754	6.84448	2.96614	0.38433	2.90737	2086.6	10	2091.5	52	2096.5	52	1	100.09